

On Improving Data Rates of Users in LTE HetNets

A Thesis Submitted to
Indian Institute of Technology Hyderabad
In Partial Fulfillment of the Requirements for
The Degree of Doctor of Philosophy



Department of Computer Science and Engineering
Indian Institute of Technology Hyderabad

July 2016

Declaration

I declare that this written submission represents my ideas in my own words, and where ideas or words of others have been included, I have adequately cited and referenced the original sources. I also declare that I have adhered to all principles of academic honesty and integrity and have not misrepresented or fabricated or falsified any idea/data/fact/source in my submission. I understand that any violation of the above will be a cause for disciplinary action by the Institute and can also evoke penal action from the sources that have thus not been properly cited, or from whom proper permission has not been taken when needed.

Vanli Sathya

(Signature)

VANLIN SATHYA

(R Vanlin Sathya)

CS11P1003

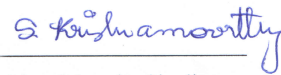
(Roll No.)

Approval Sheet

This thesis entitled **On Improving Data Rates of Users in LTE HetNets** by **R. Vanlin Sathya** is approved for the degree of Doctor of Philosophy from IIT Hyderabad.



Dr. Abhay Karandikar
IIT Bombay
External Examiner



Dr. Krishna Moorthy Sivalingam
IIT Madras
External Examiner



Dr. Bheemarjuna Reddy Tamma
IIT Hyderabad
Adviser



Dr. Antony Franklin
IIT Hyderabad
Internal Examiner



Dr. Kiran Kumar Kuchi
IIT Hyderabad
Chairman

Acknowledgements

I would like to thank everyone who supported and assisted me during my doctoral program at IIT Hyderabad. First and foremost, I would like to thank my research advisor, Dr. Bheemarjuna Reddy Tamma, for accepting me as his student, and then for his constant encouragement, guidance, and support during my Ph.D. program. He allowed me to pursue my own research interests, and was always available to discuss various problems and provided feedback. His attentive and approachable attitude towards students and the countless hours of discussion, guidance, revision, and following up of research ideas have helped several students including myself. I really enjoyed working with him. I have to admit that I was so lucky to be part of his research group since he was so concerned about his students.

Despite being at a relatively young institute, there is nothing I needed that I could not have gotten by just asking. I would like to thank Dr. C. Krishna Mohan who was the Head of Department, CSE, at the time of my admission and Dr. Bheemarjuna Reddy Tamma, the present Head of the Department, CSE, for providing excellent facilities in our department. I consider it as a blessing to be a part of the robust research atmosphere they established.

Rome was not built in a day and neither in any thesis. My work would not have materialized if not for the useful suggestions and constructive criticism offered by my Doctoral Committee members, Dr. M. V. Panduranga Rao, Dr. Subrahmanyam Kalyanasundaram, Dr. Mohammed Zafar Ali Khan and Dr. Kiran Kuchi. I also owe an intellectual debt to Prof. David Koilpillai, Dr. Naveen Sivadasan, Dr. Rajalakshmi, and Dr. Antony Franklin from whom I learned many technical concepts during my time here.

I am also grateful to the former and present members of the Networked Wireless Systems Lab (NeWS), namely, Mukesh Kumar Giluka, Anil Kumar, Thomas Valerian Pasca, Baswade Anand, Malikarjun, Naveen, Nitish Rajoria, Harsha Vardhan, Hemanth, Bala, Madhuri, Sachin Rathod, Hatim, Manas Kala, Aishwarya, Goutham Pilla, Praveen and Sarath. Their technical support was vital to my research work and their social companionship made my long stays at the lab enjoyable.

In particular, I must specially thank Mukesh Kumar Giluka, Thomas Valerian Pasca, and Arun Ramamurthy for their help in my research work. A note of extreme gratitude to Arun Ramamurthy for his patient explanations and helpful advice on technical matters. I cannot stress enough that I have never seen a more humble and helpful friend in all my research work. And additionally, would like to thank staff members in the Administrative block, Cyber Physical Systems lab (CPS) and

Network Operations Center (NOC), Jaya (CPS), Mr. Baswaraj (CPS), Mr. Raguram (NOC), Mr. Vijay Chakri (NOC) for their cheerful assistance.

And I owe immense gratitude to the people who helped me start my adventure at IITH. I did like to thank Nelson Rosario, Dinesh Kumar, Leo Prabhu, Ganesh and Rajesh Pandian (alumnus of Velammal Engineering College (Anna University)) for encouraging me to go ahead with my interests and pursue a Ph.D. at IIT Hyderabad.

I also express my thanks to my project guide, Mr. Vijaya Kumar, and Head of the department (Dr. B. Venkatalakshmi) during M.E. program at Velammal Engineering College (Anna University), for encouraging me to pursue doctoral program. It was Dr. B. Venkatalakshmi who gave me permission to attend the written test and Ph.D. interview at IIT Hyderabad and I am thankful for that.

The biggest highlight of my research here was my trip to ICNC 2015 conference at Anaheim, CA, USA. I deeply thank Prof. U.B. Desai, current director of IIT Hyderabad for providing me the necessary financial support to attend the same. It was my first visit to another country and a highly enriching one. The international research exposure that by the conference I got was unmatched and increased my vigor.

The community at IIT Hyderabad is simply unforgettable. I had the best years of my life and that is surely no understatement. My social, management and language skills have improved many folds since I joined in 2011.

I was the Ph.D. Representative of the IITH Student Gymkhana 2014-15. It was a roller coaster ride from campaigning to listening to everyone's opinions and pushing for change at the institute level. My people and organization skills improved and a sense of responsibility for the community sprouted greatly in my heart. Research Scholar Day 2014, which I helped organize during my position, was an enlivening experience both technically and socially. I would like to thank my fellow batch mates and Gymkhana members for showing me that there is so much to learn and gain when you work together as a community and for the community. I must express my gratitude to Dr. Tamma once again for permitting me to contest in the elections.

Another fantastic experience was at the 50th Inter-IIT Sports Meet 2014 at IIT Bombay. It was an honor representing my institute at the Weightlifting competition. And plus, listening to one of my biggest idols, Sachin Tendulkar, at the 50th Inter IIT meet was a fulfilling experience.

I stayed in 500 series ODF hostel for more than four years have dreaded the day I will vacate it. I'm particularly attached to the gym room, where I went almost every day. I wish to thank Vimal prabhu, Prabu anna, Aravind anna, Karthick

anna, Josh anna, Thomas, Srivathsan, Vignesh, Arun Balaji, Sandeep, Brince Paul, Jithin Mathew, Murali Krishna, Sunil Mallireddy, Surya and Chandra sekar for their friendship and hospitality. From birthday parties to late night hangouts to Tamil New Year celebrations, I had a blast here at Yeddumailaram. I hope to keep in touch with everyone throughout my life.

I would like to thank staff members at the Hostel office and Mess, Mr. Vel Murugan (Hostel office), Mr. Prabhu (SGR Mess), Mr. Logu (Shakthi Mess) for their true service and also for their special assistance during my time in the Gymkhana.

I would like to thank Viswanath, Arun Balaji, Arun Ramamurthy, Manas Kala, Mukesh Kumar Giluka and Arasu Arun for helping me to improve my writing and presentation skills through constant interactions with them.

And finally, I want to thank all my family members, and in particular, my father V. Robinson, my mother P. Latha Let, my sister R. Roselin Kiruba, my brother-in-law Benny Ebinezar, and my church brother Amirtharaj anna and Hachumi brother for simply everything. This entire journey, from research interests to my extra curricular activities, would not have been meaningful without their constant support and companionship.

I did like to end with my favorite Thirukkural. It teaches that anyone who strives hard and puts forth all his effort will surely meet with good fortune. On the other hand, laziness will bring only despair.

R. Vanlin Sathya

Dedication

To Almighty God & my Parents

Abstract

The proliferation of smartphones and tablets has led to huge demand for data services over cellular networks. Cisco VNI mobile forecast (2014-2019) tells that although only 3.9% of mobile connections were Long Term Evolution (LTE) based they accounted for 40% of the mobile traffic and this will rise to 51% by 2019, by which the mobile data usage will grow 11 fold to over 15 Exabytes per month. Reports by Cisco and Huawei tell that 70% of the traffic is generated in indoor environments such as homes, enterprise buildings and hotspots. Hence, it is very important for mobile operators to improve coverage and capacity of indoor environments. Indoor data demand is partly met by intensifying the deployment of Macro Base Stations (MBSs/eNodeBs) in LTE cellular networks. Owing to many obstacles in the communication path between MBS and users inside the building, radio signals attenuate at a faster rate as the distance increases. Thus, Indoor User Equipments (*IUEs*) receive still low signal strength (*i.e.*, Signal-to-Noise Ratio, SNR) compared to Outdoor User Equipments (*OUEs*). To address this problem, one can deploy a large number of Low Power Nodes (LPNs) a.k.a. small cells (*e.g.*, Picos and Femtos) under an umbrella MBS coverage and thereby form an LTE Heterogeneous Network (HetNet). Small cells are mainly being deployed in homes, enterprise buildings and hotspots like shopping malls and airports to improve indoor coverage and data rates. This is a win-win situation as telecom operators also benefit by reduction in their CAPEX and OPEX.

Though the deployment of Femtocells improves indoor data rates, the resulting LTE HetNet may face a host of problems like co-tier and cross-tier interference (due to frequency reuse one in LTE) and frequent handovers (due to short coverage areas of Femtocells). Deployment of Femtos inside a building can lead to signal leakage at the edges/corners of the buildings. This causes cross-tier interference and degrades the performance of *OUEs* in High Interference Zone (HIZone) around the building area, which are connected to one of the MBSs in the LTE HetNet. Arbitrary placement of Femtos can lead to high co-channel cross-tier interference among Femtos and Macro BSs and coverage holes inside buildings. If Femtos are placed without power control, this leads to high power consumption and high inter-cell interference in large scale deployments. Our goal is to address these problems by developing efficient architecture, Femto placement and power control schemes in LTE HetNets.

Random or unplanned placement of the Femtos leads to poor SNR and hence affects achievable data rates of *IUEs*. Hence, placement of Femtos is important for the cellular operators to perform planned deployment of minimum number of Femtos

with no coverage holes and guarantee a good signal quality with no co-tier interference. Once the placement of Femtos is done optimally in enterprise environments, operators need to ensure that traffic load is evenly distributed among neighboring Femtos for improving Quality of Service (QoS) of *IUEs* by efficiently utilizing the network resources. In traditional cellular networks, the uplink access and downlink access of UEs are *coupled* to the same (Femto) cell. Suppose a Femto is fully loaded when compared to its neighboring Femtos, the traditional offloading or load balancing algorithms will try offloading some of the UEs for both their uplink and downlink access from the loaded cell to one of less loaded neighboring cells (*i.e.*, target cell) provided that these UEs could get connected to the chosen target cell. This type of offloading is a forced handover to reduce traffic imbalance and trigger for handover is not based on better signal strength from the target cell. But, the offloaded UEs are connected for both their uplink and downlink access to the same target cell. Since UEs are most likely separated by walls and floors from their connected cells in enterprise environments, these offloaded UEs now have to transmit with higher transmit power in the uplink and thereby affects their battery lives. In order to reduce the battery drain for the offloaded UEs while maintaining their QoS, we employ the *Decoupled* Uplink and Downlink (DUD) access method in such a way that, the uplink of UE is connected to the closest Femto while the downlink is connected to a less loaded neighboring Femto.

To maximize the utilization of the limited operating spectrum and provide higher data rate for *IUEs*, operators can configure Femtos in open access mode with *frequency reuse one* (*i.e.*, all Femtos and MBSs operates on a same frequency) in LTE HetNets. However, this leads to high co-tier interference and cross-tier interference. Another problem in enterprise buildings having Femtos is frequent handovers, that happens when *IUEs* move from one room/floor to another room/floor inside the building. This leads to degradation of network performance in terms of increased signaling overhead and low throughputs. In order to reduce this kind of unnecessary handovers in enterprise buildings, Femtos should be placed optimally with handover constraints. Hence, we obtain the optimal coordinates from the OptHO model by adding handover constraints to the Minimize Number of Femtos (MinNF) model which guarantees threshold Signal-to-Interference plus Noise Ratio (SINR) of -2 dB for all *IUEs* inside the building. Such optimized deployment of Femtos reduces the number of handovers while guaranteeing good SINR to all *IUEs*.

In LTE HetNets, even though planned deployment of Femtos in open access mode boosts the *IUEs* performance, the power leakage from indoor Femtos create interfer-

ence to the *OUEs* in the *HIZone* in the buildings surrounding areas. We propose an efficient placement and power control SON (Self organizing Network) algorithm which optimally places Femtos and dynamically adjusts the transmit power of Femtos based on the occupancy of Macro connected *OUEs* in the *HIZone*. To do this, we use the same MinNF model to place the Femtos optimally and solve Optimal Femto Power (OptFP) allocation problem (Mixed Integer Linear Programming (MILP)) which guarantees threshold SINR of -4 dB for *IUEs* with the Macro users SINR degradation as lesser than 2 dB. In the OptFP model, Femto's transmit power is tuned dynamically according to the occupancy of *OUEs* in the *HIZone*. But the presence of even a single *OUE* in the *HIZone* decreases SINR of numerous *IUEs*, which is not fair to *IUEs*. In order to address this issue, we propose two solutions a) On improving SINR in LTE HetNets with D2D relays and b) A novel resource allocation and power control mechanism for Hybrid Access Femtos in LTE HetNets, which we describe in the following two paragraphs.

To guarantee certain minimum SINR and fairness to both *IUEs* and *OUEs* in *HIZone*, we consider a system model by applying the concept of Device-to-Device (D2D) communication wherein free/idle *IUEs* connected to Femto act like UE-relays (*i.e.*, UE-like BS, forwarding downlink data plane traffic for some of the *HIZone* users connected to MBS). We formulate a Mixed-Integer Linear Programming (MILP) optimization model which efficiently establishes D2D pairs between free/idle cell-edge *IUEs* and *HIZone* users by guaranteeing certain $SINR_{Th}$ for both *IUEs* and *HIZone* users. As D2D MILP model takes more computation time, it is not usable in real-world scenarios for establishing D2D pairs on the fly. Hence, we propose a two-step D2D heuristic algorithm for establishing D2D pairs.

In above works, we assume that Femtos are configured in open access mode. But Hybrid Access Femtocells (HAFs) are favored by the operators because they ensure the paid Subscribed Group (SG) users certain QoS and then try to maximize the system capacity by serving near-by Non Subscribed Group (NSG) users in a best-effort manner. To reap in the benefits of HAFs, the operators need to employ effective resource sharing and scheduling mechanisms to contain co-tier and cross-tier interference arising out of reuse one in the HetNet system. Towards this, we address various challenges in terms of deployment and operation of HAFs in indoor environments. We propose an *Optimal Placement of hybrid access Femtos* (OPF) model which ensures a certain $SINR_{Th}$ inside the building and a certain $SINR_{Th}$ in the *HIZone* of the building. Unlike in previous optimization models, in this model, users in *HIZone* are connected to *HAFs* deployed inside the building. Also we propose a decentralized

Dynamic Bandwidth Allocation (BWA) mechanism which divides the available HAF bandwidth between the two sets of user groups: SG and NSG. In order to mitigate co-tier and cross-tier interference, we then propose a dynamic *Optimal Power Control* (OPC) mechanism which adjusts the transmit powers of HAFs whenever the users in the *HIZone* cannot be served by the HAFs. In such a case, HIZone users connect to an MBS instead. Since the OPC problem is hard to solve in polynomial time, we also present a Sub-Optimal Power Control (SOPC) mechanism. To maintain fair resource allocation between SG and NSG users, we propose an Enhanced Priority (EP) scheduling mechanism which employs two schedulers which are based on the Proportional Fair (PF) and the Priority Set (PS) scheduling mechanisms.

In above works, placement of Femtos is optimized to reduce co-channel co-tier interference among neighboring Femtos and transmit power of Femtos is optimized to reduce cross-tier interference between MBSs and Femtos. But, for arbitrary deployed Femtos, Inter Cell Interference Coordination (ICIC) techniques could be employed to address co-tier interference problem among Femtos which are connected with each other over X2 interface. Hence, in this work, we propose an ICIC technique, Variable Radius (VR) algorithm which dynamically increases or decreases the cell edge/non-cell edge regions of Femtos and efficiently allocates radio resources among cell edge/non-cell edge regions of Femtos so that the interference between neighboring Femtos can be avoided. We implement the proposed VR algorithm on top of PF scheduler in NS-3 simulator and find that it significantly improves average network throughput when compared to existing techniques in the literature.

Contents

Acknowledgements	iv
Abstract	viii
Nomenclature	xvi
Abbreviations	10
1 Introduction	12
1.1 Evolution of Cellular Networks	12
1.2 Overview of LTE	14
1.2.1 LTE Frame Format	19
1.2.2 Radio Resource Management	21
1.3 LTE Femtocell Networks	22
1.3.1 Architecture of Indoor LTE Femtocells	23
1.3.2 Access Modes in Femto	24
1.3.3 Handover Mechanism	25
1.4 Issues, Existing Solutions and Associated Challenges	26
1.5 Objectives and Scope of the Thesis	31
1.6 Organization of the Thesis	31
2 On Femto Placement and <i>Decoupled</i> Access for Downlink and Up- link in Enterprise Environments	33
2.1 Introduction	33
2.1.1 Organization of this Chapter	35
2.2 Related Work	36
2.3 Optimal Femto Placement in Enterprise Environments	37
2.3.1 Building Model	38
2.3.2 System Model	39
2.3.3 Formulation of Femto Placement Model	40

2.4	<i>Decoupled</i> Uplink and Downlink (DUD) Access for Efficient Offloading in Femtocell Networks	46
2.4.1	Downlink Offloading Algorithm for DUD Access System	48
2.4.2	Time Complexity of the Offloading Algorithm	50
2.5	Experimental Setup and Performance Results	50
2.5.1	Optimal Femto Placement	51
2.5.2	Comparison of Coupled and Decoupled Access Systems in Uniform Traffic Scenario	54
2.5.3	Comparison of Coupled and Decoupled Access Systems in Non-uniform Traffic Scenario	63
2.6	Summary	63
3	Handover and SINR Optimized deployment of LTE Femtocells	65
3.1	Introduction	65
3.1.1	Organization of this chapter	66
3.2	Related Work	66
3.2.1	Contribution of this Chapter	67
3.3	Proposed Work	68
3.3.1	System Model	68
3.3.2	Channel Model	69
3.3.3	<i>MinNF</i> Placement Model	70
3.4	Experimental Setup and Numerical Results	72
3.4.1	Building Setup	72
3.4.2	Other Placement Schemes for Comparison	72
3.4.3	Performance of Placement Schemes	73
3.4.4	Motivation for Optimal Placement Models	77
3.4.5	Connectivity Region of Femtos inside the building	78
3.5	Handover Optimized Femto Placement Model	78
3.5.1	User Mobility Model	79
3.5.2	OptHO Placement Model	80
3.6	Experimental Setup and Numerical Results	80
3.6.1	Setup for OptHO Placement Model	80
3.6.2	Performance of OptHO Placement Model	81
3.7	Summary	86

4	On Placement and Dynamic Power Control of Femtocells in LTE HetNets	88
4.1	Introduction	88
4.1.1	Organization of this Chapter	89
4.2	Related Work	89
4.3	Proposed Work	90
4.3.1	LTE SON and System Model	90
4.3.2	Building Model	90
4.3.3	Proposed Efficient Placement and Power Control Algorithm	91
4.4	Experimental Setup and Numerical Results	96
4.4.1	Scenario 1: No Macro Users in HIZone	97
4.4.2	Scenario 2: Macro Users in HIZone	98
4.5	Summary	100
5	Energy-efficient Femtocell Placement in LTE Networks	101
5.1	Introduction	101
5.1.1	Organization of this Chapter	102
5.2	Related Work	102
5.3	Proposed Work	103
5.3.1	System Model	103
5.3.2	Uplink Power Control	103
5.3.3	Optimization Problem Formulations	104
5.4	Experimental Setup and Numerical Results	109
5.4.1	Performance Results in Downlink	109
5.4.2	Performance Results in Uplink	111
5.5	Summary	114
6	On improving SINR in LTE HetNets with D2D Relays	115
6.1	Introduction	115
6.1.1	Organization of this Chapter	116
6.2	Related Work	116
6.2.1	Our Contributions	117
6.3	Proposed LTE HetNet System with D2D Relays	118
6.3.1	HetNet Architecture with D2D Relays	118
6.3.2	System Model	120
6.4	Femto Placement and D2D Pair Selection Models in LTE HetNets	121
6.4.1	D2D MILP Model	122

6.4.2	D2D Heuristic Algorithm	125
6.4.3	Time Complexity	128
6.4.4	Optimal Femto Transmit Power (OptFP) MILP Model	128
6.4.5	Joint D2D Heuristic and OptFP (JDHO) Algorithm	129
6.4.6	Cost Analysis	130
6.5	Performance Results	131
6.5.1	MinNF Model: Performance Results	132
6.5.2	Performance Results of D2D MILP Model and D2D Heuristic Algorithm	133
6.5.3	Comparison between D2D MILP Model and D2D Heuristic Algorithm	139
6.5.4	Cost Analysis	142
6.5.5	JDHO Performance Analysis	143
6.6	Summary	145
7	A Novel Resource Allocation and Power Control Mechanism for Hybrid Access Femtos in LTE HetNet	146
7.1	Introduction	146
7.1.1	Organization of this Chapter	148
7.2	Related Work	149
7.2.1	Our Contributions	152
7.3	Preliminaries and Assumptions	153
7.3.1	System Model	153
7.4	Proposed Work	155
7.4.1	Optimal Placement of Femtos (OPF) Model	155
7.4.2	Optimal Power Control (OPC) Model	157
7.4.3	Sub-Optimal Power Control (SOPC) Mechanism	160
7.4.4	Analysis of Occupant Locations	166
7.5	Simulation Setup and Performance Results	168
7.5.1	Simulation Environment	168
7.5.2	Performance Analysis	170
7.6	Summary	188
8	Comparison of Proposed Solutions	189
8.1	Scheduling Algorithms	190
8.2	Experimental Setup and Comparison Results	192
8.2.1	Throughput Comparison	192

8.2.2	Operators' Revenue: An estimate	195
9	Enhanced Distributed Resource Allocation and Interference Management in LTE Femtocell Networks	197
9.1	Introduction	197
9.1.1	Organization of this Chapter	197
9.2	Related Work	198
9.3	Proposed VR Algorithm	199
9.3.1	Interference Scenario 1	199
9.3.2	Interference Scenario 2	203
9.4	Simulation Setup and Performance Results	204
9.4.1	Throughput Results	206
9.4.2	Area Spectrum Efficiency Results	207
9.5	Summary	207
10	Conclusions and Future Work	209
10.1	Conclusions	209
10.2	Future Research Directions	210
	List of Publications	211
	References	213

List of Plots

1.1	Typical example of D2D communication	15
1.2	LTE Heterogeneous Network	17
1.3	Architecture of LTE Network	18
1.4	Frequency and time division duplex in LTE	20
1.5	LTE Frame Format	21
1.6	Resource Block (RB)	21
1.7	SNR variation inside the building. Z-axis is used to list out SNR values in dB scale at various sub-regions (X, Y) inside the building. Owing to the walls inside the building, <i>IUEs</i> on average receive low SNR (e.g., -8 dB, -9 dB) compared to <i>OUEs</i> (e.g., 4, 2, 0, -1 dB) due to poor indoor signal strength	23
1.8	Architecture of LTE HetNet with Femtocells	24
1.9	Femto Handover Mechanism	25
1.10	Co-tier and Cross-tier Interference in LTE Small Cell Network	26
1.11	Load Balance in Enterprise Building	28
1.12	Arbitrary Placement of Femtocells	29
1.13	An Example Scenario Showing Ping-pong Handovers in Femtocells	30
2.1	<i>Coupled</i> Access System before offloading U_t to $Femto_1$	34
2.2	<i>Coupled</i> Access System after offloading U_t to $Femto_1$ from $Femto_2$	34
2.3	<i>Decoupled</i> Access System after offloading only downlink of U_t to $Femto_1$ from $Femto_2$	35
2.4	Top view of a floor in the building	38
2.5	Numbering of rooms in a two-storey building and calculation of number of walls between Femto and sub-region	38
2.6	Top view of sub-regions in the building	39
2.7	Numbering of sub-regions on floor #1 and floor #2	39
2.8	Upper and lower bounds for x_f and y_f	40

2.9	$minRB_{u_f}$ matrix of UEs in Femtocell Network	48
2.10	Two-storey Building	51
2.11	SNR distribution and Femto locations given by MILP model for uniform UE distribution on the floor #1	51
2.12	SNR distribution and Femto locations given by MILP model for uniform UE distribution on the floor #2	51
2.13	Femto Connectivity Region for uniform UE distribution on the floor #1	52
2.14	Femto Connectivity Region for uniform UE distribution on the floor #2	52
2.15	A building's floor with non-uniform UE distribution	53
2.16	Femto connectivity region for non-uniform UE distribution given in Figure 2.15	53
2.17	SNR distribution and Femto locations given by optimal Femto placement model for non-uniform UE distribution given in Figure 2.15	54
2.18	UE Distribution on floor #1 for uniform traffic pattern	55
2.19	UE Distribution on floor #2 for uniform traffic pattern	55
2.20	UE Connectivity before and after Offloading on floor #1 for uniform traffic pattern	56
2.21	UE Connectivity before and after Offloading on floor #2 for uniform traffic pattern	56
2.22	$TotDemand_f$ of each Femto before and after offloading on floor #1 for uniform traffic pattern	57
2.23	$TotDemand_f$ of each Femto before and after offloading on floor #2 for uniform traffic pattern	57
2.24	Downlink user count in each Femto before and after offloading on floor #1 for uniform traffic pattern	57
2.25	Downlink user count in each Femto before and after offloading on floor #2 for uniform traffic pattern	57
2.26	Maximum Achieved Uplink SNR in <i>coupled</i> and <i>decoupled</i> access systems on floor #1 for uniform traffic pattern	58
2.27	Maximum Achieved Uplink SNR in <i>coupled</i> and <i>decoupled</i> access systems on floor #2 for uniform traffic pattern	58
2.28	Power emitted by UE in <i>coupled</i> and <i>decoupled</i> access systems on floor #1 for uniform traffic pattern	58
2.29	Power emitted by UE in <i>coupled</i> and <i>decoupled</i> access systems on floor #2 for uniform traffic pattern	58

2.30	CDF of the maximum Achievable Uplink SNR in <i>coupled</i> and <i>decoupled access systems</i>	59
2.31	% Decrease in the maximum achievable Uplink SNR in <i>coupled system</i> when compared to <i>decoupled system</i> for Different Data Demands . . .	59
2.32	UE Connectivity before and after Offloading on floor #1 for non-uniform traffic pattern	60
2.33	UE Connectivity before and after Offloading on floor #2 for non-uniform traffic pattern	60
2.34	$TotDemand_f$ of each Femto before and after offloading on floor #1 and floor #2 for non-uniform traffic pattern	60
2.35	User count in each Femto before and after offloading on floor #1 and floor #2 for non-uniform traffic pattern	61
2.36	Maximum Achieved Uplink SNR in <i>coupled</i> and <i>decoupled</i> access systems on floor #1 and floor #2 for non-uniform traffic pattern	61
2.37	Power emitted by UE in <i>coupled</i> and <i>decoupled</i> access systems on floor #1 and floor #2 for non-uniform traffic pattern	62
3.1	An example of enterprise building with rooms, corridors and entry/exit points	68
3.2	Sub-region index and dimensions of the enterprise building	70
3.3	REM for CKM Placement	73
3.4	REM for MinNF Placement	74
3.5	Modulation Schemes in CKM placement	75
3.6	Modulation Schemes in MinNF placement	75
3.7	SINR CDF	75
3.8	% of UEs in Employing Different Modulation Schemes	76
3.9	Number of Clusters (k) Vs Minimum $SINR_{Th}$	76
3.10	Connectivity of Sub-regions in CKM placement	77
3.11	Connectivity of Sub-regions in MinNF placement	77
3.12	Building Scenario with Simple Flow	79
3.13	REM of OptHO Placement	82
3.14	Modulation Schemes in OptHO Placement	82
3.15	Connectivity of Sub-regions in OptHO Placement	82
3.16	Number of Handovers vs UE Density in 0.2 m/s Mobility Case	83
3.17	Number of Handovers vs UE Density in 0.5 m/s Mobility Case	84
3.18	Number of Handovers vs UE Density in 1 m/s Mobility Case	84

3.19	Average Throughput of Users vs UE Density in 0.2 m/s Mobility Case	85
3.20	Average Throughput of Users vs UE Density in 0.5 m/s Mobility Case	86
3.21	Average Throughput of Users vs UE Density in 1 m/s Mobility Case	86
4.1	Bird-eye view of floor area inside and outside a single-floor building	92
4.2	REM across sub-regions for MinNF	96
4.3	REM across sub-regions for OptFP	96
4.4	Femtos sub-region association for MinNF	97
4.5	Femtos sub-region association for OptFP	97
4.6	GAMS Running Time	97
5.1	CDF of UE uplink power.	102
5.2	Uplink Interference Scenario in Indoor Building	108
5.3	Femto sub-region association for CKM Placement	110
5.4	DSINR (in dB) for CKM Placement of Femtos	110
5.5	Femto sub-region association for MFUTP placement	111
5.6	DSINR (in dB) for MFUTP Placement of Femto	111
5.7	Uplink power (in Watts) for CKM-RPC Placement of Femto.	112
5.8	Uplink Power (in Watts) for (MFUTP, USTP) Placement of Femto.	112
5.9	Uplink SINR (in dB) interms of users	112
5.10	Uplink Power interms of users	112
5.11	Variation of Uplink $SINR_{Th}$ (-2 to 1) dB across sub-regions in (MFUTP, USTP) placement	113
5.12	Variation of Uplink Power (in Watts) based on $SINR_{Th}$ in (MFUTP, USTP) placement	113
6.1	Architecture of Proposed HetNet System with D2D based Relays	119
6.2	Call flow diagram for D2D based communication in proposed HetNet system	120
6.3	REM plot of sub-regions inside building after placing Femtos by using MinNF	132
6.4	$hDPRA$ D2D links in instance #1	133
6.5	$hDPRA$ D2D links in instance #2	134
6.6	$hDPRA$ D2D links in instance #3	134
6.7	SINR CDF of $IUEs$ using Heuristic Algorithm	135
6.8	SINR CDF of $HIZUEs$ using Heuristic Algorithm	135
6.9	Average SINR CDF of $IUEs$ for various schemes in 500 topologies	138

6.10	Average SINR CDF of <i>HIZUEs</i> for various schemes in 500 topologies	138
6.11	MILP D2D links in instance #1	138
6.12	MILP D2D links in instance #2	138
6.13	MILP D2D links in instance #3	139
6.14	SINR CDF of <i>IUEs</i> using MILP Model	139
6.15	UE distribution in Topology 1	140
6.16	UE distribution in Topology 2	140
6.17	UE distribution in Topology 3	140
6.18	UE distribution in Topology 4	140
6.19	UE distribution in Topology 5	140
6.20	UE distribution in Topology 6	141
6.21	UE distribution in Topology 7	141
6.22	Average SINR of <i>IUEs</i>	142
6.23	Running Time of D2D MILP and heuristic algorithm	142
6.24	D2D Average Transmission Power	143
6.25	<i>hDPRA</i> D2D links in instance #1	144
6.26	<i>hDPRA</i> D2D links in instance #2	144
6.27	<i>hDPRA</i> D2D links in instance #3	144
6.28	<i>hDPRA</i> D2D links in instance #4	144
6.29	SINR CDF of <i>IUEs</i> using JDHO algorithm	145
6.30	SINR CDF of <i>HIZUEs</i> using JDHO algorithm	145
7.1	An example of LTE HetNet with MBS, OAF, CAF, and HAF Cells	147
7.2	HAF based LTE HetNet System Model	154
7.3	Flowchart of the proposed SOPC mechanism	161
7.4	REM across sub-regions for HAFs at P_{max}	170
7.5	Connectivity of sub-regions to HAFs, where same coloured sub-regions are connected to a single HAF, HAF_i	171
7.6	Scenario I: Building with SG users in indoor sub-regions and NSG users in HIzone sub-regions	172
7.7	Average throughput per user in each HAF using a legacy PF scheduler	172
7.8	Average throughput per user in each HAF using a legacy PS scheduler	172
7.9	Average throughput per user in each HAF using EP scheduler	173
7.10	Average throughput per user connected to HAF as a function of NSG users in the HIZone	175

7.11	Scenario II: Building with SG in indoor sub-regions and NSG in HIZone sub-regions	176
7.12	CDF plot for Scenario II; <i>Case</i> ₁ : When the HIZone users are connected to the MBS and there are no HAFs in the building, <i>Case</i> ₂ : When the HIZone users are connected to HAFs operating at P_{max} , <i>Case</i> ₃ : When the HIZone users connect to MBS after the HAFs tune their transmit power to P' , <i>Case</i> ₄ : When the HIZone users connect to MBS with the HAFs operating at P_{max} in closed access mode for the HIZone users .	176
7.13	Connectivity of sub-regions to HAFs, where same colored sub-regions are connected to a single HAF, HAF_i	178
7.14	Average throughput per user in each HAF after power control in SOPC mechanism	179
7.15	Average throughput per user in each HAF without power control . .	179
7.16	Scenario IV: Building with SG and NSG users in indoor as well as HIZone sub-regions	181
7.17	CDF plot for Scenario IV; <i>Case</i> ₁ : When the HIZone users are connected to the MBS and there are no HAFs in the building, <i>Case</i> ₂ : When the HIZone users are connected to HAFs operating at P_{max} , <i>Case</i> ₃ : When the HIZone users connect to MBS after the HAFs tune their transmit power to P' , <i>Case</i> ₄ : When the HIZone users connect to MBS with the HAFs operating at P_{max} in closed access mode	181
7.18	REM across sub-regions for HAFs after power control	182
7.19	Connectivity of sub-regions to HAFs, where same colored sub-regions are connected to a single HAF, HAF_i	182
7.20	Average throughput per user in each HAF after power control in SOPC mechanism	183
7.21	Average throughput per user in each HAF without power control . .	183
7.22	Average throughput plot for users connected to the MBS for video sessions	186
7.23	Average throughput plot for users connected to the MBS for voice sessions	186
8.1	CDF of <i>IUEs</i> Throughput in Different Solutions	193
8.2	CDF of <i>HIZUEs</i> Throughput in Different Solutions	193
9.1	Regions inside Femto coverage area	199
9.2	Initial inner regions of Femtos	201

9.3	Reducing the inner regions of Femtos	202
9.4	Calculating Avg CQI value in the strip	202
9.5	Increasing the Inner regions of Femtos	203
9.6	Positions of six Femtos and 90 UEs inside a building	204
9.7	REM for Femto Locations	205
9.8	CDF of throughput of UEs: Static, 60 UEs	205
9.9	CDF of throughput of UEs: Static, 90 UEs	205
9.10	CDF of throughput of UEs: Mobile, 60 UEs	205
9.11	CDF of throughput of UEs: Mobile, 90 UEs	205
9.12	Area Spectrum Efficiency of Femtos with 60 static UEs	206
9.13	Area Spectrum Efficiency of Femtos with 90 static UEs	206
9.14	Area Spectrum Efficiency of Femtos with 60 mobile UEs	207
9.15	Area Spectrum Efficiency of Femtos with 90 mobile UEs	207

List of Tables

1.1	Comparison of LTE and LTE-Advanced Networks	13
1.2	Characteristics of heterogeneous cells in LTE	16
1.3	LTE parameters	20
2.1	Glossary of MILP Model	37
2.2	Simulation Parameters	50
3.1	Glossary of MinNF ILP Model	69
3.2	Variation of No. of Femtos with $SINR_{Th}$ in MinNF	77
3.3	NS-3 Simulation Parameters	81
4.1	Glossary of OptFP MILP Model	91
4.2	Simulation Parameters	96
4.3	Optimal Femto Transmission Power	99
5.1	Glossary of MFUTP MILP Model	104
5.2	Simulation Parameters	109
6.1	Glossary of D2D MILP Model	122
6.2	Simulation Parameters	131
6.3	$SINR_{Th}$ vs $IUEs$ SINR	136
6.4	Number of $FIUEs$ vs Average D2D transmission power	137
6.5	Topologies having varying distribution of $HIZUEs$ in HIZone	141
7.1	List of notations used in the problem formulations	156
7.2	Truth table showing combinations of user occupant locations	167
7.3	Simulation Parameters	169
7.4	New transmit power values after power control	177
7.5	New transmit power values after power control	182
7.6	Radio resource requirement in each HAF before power control	183
7.7	Radio resource requirement in each HAF after power control	184

8.1	Characteristic of Proposed Solutions	191
8.2	$SINR_{Th}$ vs Average D2D Transmission Power	194
8.3	Comparison of different solutions	195
9.1	Simulation Parameters	204

Abbreviation	Expanded
<i>ACK</i>	- Acknowledgement
<i>ABS</i>	- Almost Blank Sub-frame
<i>BS</i>	- Base Station
<i>BWA</i>	- Bandwidth Allocation
<i>CAPEX</i>	- Capital Expenditure
<i>C/DPlane</i>	- Control/Data Plane
<i>CDF</i>	- Cumulative Distribution Function
<i>DUD</i>	- Decoupled Uplink and Downlink access
<i>D2D</i>	- Device-to-Device
<i>eNB</i>	- Evolved Node B
<i>eICIC</i>	- enhanced Inter-Cell Interference Co-ordination
<i>EPScheduler</i>	- Enhanced Priority Scheduler
<i>F – GW</i>	- Femto Gateway
<i>FDPS</i>	- Frequency Division Packet Scheduler
<i>HO</i>	- Handover
<i>hDPA</i>	- Heuristic D2D Power Allocation
<i>HIZone</i>	- High Interference Zone
<i>HIZUE</i>	- <i>OUE</i> in <i>HIZone</i>
<i>HAF</i>	- Hybrid Access Femto
<i>HetNet</i>	- Heterogeneous Network
<i>HeNB</i>	- Home evolved Node B
<i>IUE</i>	- Indoor UE
<i>IAT</i>	- Instantaneous Average Throughput
<i>IP</i>	- Integer Programming
<i>LAI</i>	- Last Average Throughput
<i>LP</i>	- Linear Programming
<i>LTE</i>	- Long Term Evolution
<i>LPN</i>	- Low Power Node
<i>MBS</i>	- Macro Base Station
<i>MAC</i>	- Medium Access Control
<i>MinNF</i>	- Minimize the Number of Femtos
<i>MINLP</i>	- Mixed Integer Non-Linear Programming
<i>MILP</i>	- Mixed Integer Linear Programming
<i>MME</i>	- Mobility Management Entity

<i>NSG</i>	- Non-Subscriber Group
<i>OFDMA</i>	- Orthogonal Frequency Division Multiple Access
<i>OPC</i>	- Optimal Power Control
<i>OPEX</i>	- Operational Expenditure
<i>OPF</i>	- Optimal Placement of Femtocells
<i>OptFP</i>	- Optimal Femto Transmission Power
<i>OptHO</i>	- Optimal Handover
<i>OptFP</i>	- Optimal Femto Transmission Power
<i>PC</i>	- Power Control
<i>P – GW</i>	- Packet Gateway
<i>PL</i>	- Path Loss
<i>PF</i>	- Proportional Fair
<i>PRS</i>	- Position Reference Signal
<i>PS</i>	- Priority Set Scheduler
<i>QoS</i>	- Quality of Service
<i>RA</i>	- Resource Allocation
<i>RB</i>	- Resource Block
<i>REM</i>	- Radio Environmental Map
<i>RR</i>	- Round Robin
<i>S – GW</i>	- Serving Gateway
<i>SON</i>	- Self Organizing Network
<i>SOPC</i>	- Sub-optimal Power Control
<i>SG</i>	- Subscriber Group
<i>SINR</i>	- Signal-to-Interference plus Noise Ratio
<i>SINR_{Th}</i>	- Threshold SINR
<i>TTI</i>	- Transmission Time Interval
<i>UE</i>	- User Equipment
<i>VR</i>	- Variable Radius
<i>W2L</i>	- Win to Loss Ratio

Chapter 1

Introduction

1.1 Evolution of Cellular Networks

The history of mobile networks or cellular networks is four decades old. It began with the introduction of first generation mobile networks (1G) in late 1970s which were using analog communication schemes and designed to deliver voice services. Some of the first generation systems were Advanced Mobile Phone Service (AMPS), Extended Total Access Communication Systems (ETACS) and Narrowband Total Access Communication Systems (NTACS). The era of second generation mobile networks (2G) came in early 1990s where mode of communication is switched from analog to digital. The adoption of digital communication improved cellular systems in terms of enhanced system capacity, improved voice quality by using efficient speech codecs, lesser battery consumption, enhanced security, facilitation of digital data services such as Short Message Service (SMS) and Internet access. Some of the examples of 2G digital cellular systems are Global System for Mobile Communications (GSM), IS-95 Code Division Multiple Access (CDMA), IS-136 Time Division Multiple Access (TDMA). Later in mid 1990s, in order to achieve higher data rates, General Packet Radio Service (GPRS) was introduced. GPRS is based on packet switching where data is sent in the form of packets unlike in 1G and 2G systems where circuit switch was employed. Advantage of packet switching over circuit switching can be well understood from the fact that, in circuit switching, resources are reserved for the whole voice or data session and released only after end of the session. Packet switching got more importance with the evolution of Internet and Internet Protocol (IP). Enhanced Data for Global Evolution (EDGE) or enhanced GPRS is an example of 2.75G cellular technology. Although, EDGE network was providing voice as well as data service, specially Internet access, it was unable to fulfill user demands because

of increasing number of mobile phone users and their increasing urge for data. As a solution, 3G technologies [1] came into existence in late 1990s with the objective of providing high data rates and better Quality of Service (QoS) to various data applications such as web browsing, online gaming and streaming multimedia applications. CDMA was the key enabler of 3G technologies. Examples of 3G technologies are W-CDMA and CDMA2000. CDMA does not scale well for higher bandwidths (*i.e.*, beyond 5 MHz). In case of higher carrier bandwidth, data transmission rate will be higher and hence, transmission step will be shorter which will increase the impact of multipath fading on received signal. With the progress of time, demand for high data rates is increasing which motivated research communities come up with new technologies that efficiently work at highest bandwidths. As a solution, Orthogonal Frequency Division Multiplexing (OFDM) technology was conceptualized in which data signal is split into multiple data streams and each stream is sent over a narrowband carrier. In this case, transmission step will be longer and hence, multipath fading will have lesser impact on received signal. With this approach, it was possible to scale cellular systems for higher bandwidths just by increasing the number of narrowband carriers. Further, Multiple Input Multiple Output (MIMO) technology enhanced the data throughput even under adverse environments such as interference and multipath fading. In MIMO, multiple transmitting antenna are kept at sender side and multiple receiving antennas are kept at receiver side. Using MIMO techniques, multiple data streams can simultaneously be sent over the same carrier. Both OFDM and MIMO were the key enablers of 4G cellular systems [2, 3]. Third Generation Partnership

Table 1.1: Comparison of LTE and LTE-Advanced Networks

Parameter	LTE	LTE-Advanced
Downlink peak data rate	300 Mbps	1 Gbps
Uplink peak data rate	75 Mbps	500 Mbps
Downlink bandwidth	20 MHz	100 MHz
Uplink bandwidth	20 MHz	40 MHz
Bandwidth scalability	1.4, 3, 5, 10, 15 & 20 MHz	20, 40, 60, 80 & 100 MHz

Project (3GPP) developed standards and specifications for 3G mobile systems based on evolved GSM technologies. 3GPP standards are structured in the form of 'releases'. The scope of 3GPP includes development and maintenance of GSM and its related standards such as GPRS and EDGE, UMTS and its related standard such as HSPA, LTE and its related standards such as LTE-A. LTE is abbreviation of Long Term Evolution. LTE standards were introduced by 3GPP in Release 8 [4]. LTE has

several advantages such as enhanced system capacity and coverage, better Quality of Experience (QoE), backward compatibility with existing systems viz., 2G and 3G and reduced operating costs. LTE-A meets requirements of 4G specified by International Mobile Telecommunications-Advanced (IMT-Advanced). Release 10 and all further advancements for LTE are called as LTE-A.

1.2 Overview of LTE

Table 1.1 shows the comparison of LTE and LTE-A networks. Following are some of advancements in LTE-A in summarized form:

1. **Carrier Aggregation:** It was introduced in Release 10 [5]. In this concept, multiple carriers are aggregated to achieve higher system bandwidth. The maximum bandwidth that can be achieved is 100 MHz. Using carrier aggregation, peak data rate reaches up to 1 Gbps in downlink and 500 Mbps in uplink. Apart from higher data rates, several other advantages are associated with carrier aggregation which include QoS differentiation, carrier load balancing, interference management and efficient deployment of heterogeneous LTE network. Depending upon the availability of the spectrum, there are three aggregation scenarios, viz., contiguous aggregation in a single radio band, non-contiguous aggregation in single radio band and non-contiguous aggregation in multiple radio bands.
2. **Co-ordinated Multi-point Transmission and Reception (COMP):** It was introduced in Release 11 [6, 7]. In COMP, users in the overlapping region of multiple BSs are jointly scheduled by allocating the same radio resources from the multiple neighboring base stations, thereby improving the throughput of cell edge users. COMP also enables the dynamic coordination of transmission and reception over a variety of different base stations within the network. This concept can be applied to both homogeneous (*i.e.*, all the base stations belong to the same type and power class) and heterogeneous networks (*i.e.*, the base stations could belong to different type or power classes).
3. **Device to Device (D2D) Communication:** In traditional cellular networks, during communication between two users (devices), both control plane (C-Plane) and data plane (D-Plane) are under the control of base stations. In D2D communication, only C-Plane is handled by base stations while data exchange between two devices is done directly without involving base stations.

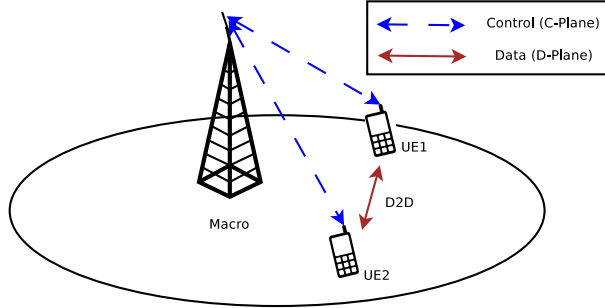


Figure 1.1: Typical example of D2D communication

The base stations control and optimize the use of shared radio resources for regular and D2D sessions. Figure 1.1 shows a typical example of D2D communication. D2D is standardized by 3GPP in Release 12 for proximity-based services [8]. Some of the challenges in D2D include interference management, resource allocation, power control, session management, mobility management, security, location estimation and multi-hop D2D.

4. **Dual Connectivity:** Release 12 from 3GPP brought the concept of dual connectivity [9]. In this case, a UE can be connected to both Macro evolved NodeB (eNB) and small cell eNB, and both C-plane & D-plane happen through both of them. This in turn boosts the throughput of UEs which reside in the cell edge or coverage region of both Macro and small cell eNBs. In this thesis, user, device or UE are used interchangeably.
5. **Interworking of LTE with Wi-Fi:** It is introduced in Release 9 [10]. As Wi-Fi, which operates on unlicensed bands, has the ability to boost the capacity for indoor environments, telecom operators consider this for offloading mobile data from cellular networks. This cellular/Wi-Fi interworking not only improves QoS of flows but also maximizes the network utilization. Currently in Release 13, LTE-Wi-Fi aggregation (LWA) is being standardized for efficient LTE/Wi-Fi interworking at UE/eNB protocol stack level.
6. **Machine-to-Machine (M2M) Communication:** In M2M communication, a large number of low power, low cost, low data requirement and resource constrained Internet of Things (IoT) devices communicate with a distant server mostly in uplink. Characteristics of M2M communication are different from traditional H2H (Human-to-Human) communication in terms of nature of traffic, types of devices, number of devices, delay tolerance and scope. Hence,

its associated challenges are also different from H2H communication such as, excess signaling due to large number of devices, support for devices having long sleeping cycles, power efficient communication and support for small data transmission. Existing cellular networks were designed for H2H communication. In Release 11 [11], 3GPP introduced M2M communication where solutions for RAN overload control (one of the challenges due to excess signaling) have been discussed. Later, in Release 12 and Release 13, some more advancements have been achieved in terms of small data transmission, low power and low cost device specifications.

Table 1.2: Characteristics of heterogeneous cells in LTE

Technology	Placement	Transmit Power	Backhaul Characteristic	Number of Users
Macro BS	Outdoor	46 dBm	Dedicated wireline	1000-2000
Pico or Micro cell	Outdoor	30 dBm	Dedicated wireline	100-200
RRH	Outdoor or indoor	30-35 dBm	Dedicated wireline	100-200
Relay	Outdoor or indoor	30-35 dBm	Wireless out-of-band or in-band	60-100
Femtocell	Indoor	20-23 dBm	Residential or enterprise broadband	10-30

7. Heterogeneous Networks (HetNets): Presently, cellular network users are not only those which generate mostly downlink traffic (*i.e.*, web browsing, downloading) but also combination of users generating symmetric (both uplink (UL) and downlink (DL)) traffic (*i.e.*, social networking, gaming) and users generating uplink traffic (*i.e.*, M2M/IoT). In order to provide better connectivity and high data rates to these users, low power network nodes, called as small cells, are being deployed. Presence of such diverse traffic generating users and small cells with different transmit powers and sizes, has turned cellular networks from homogeneous to heterogeneous in nature. A heterogeneous network (HetNet) consists of a Macro cell augmented with various types of small cells to address the challenge of enhancing system capacity and coverage. Examples of small cells are micro cell, pico cell, relay, Remote Radio Head (RRH) and Femtocell. Table 1.2 shows characteristics of various types of cells. Figure 1.2 shows a typical example of LTE heterogeneous network. The description of various types of small cells are as follows.

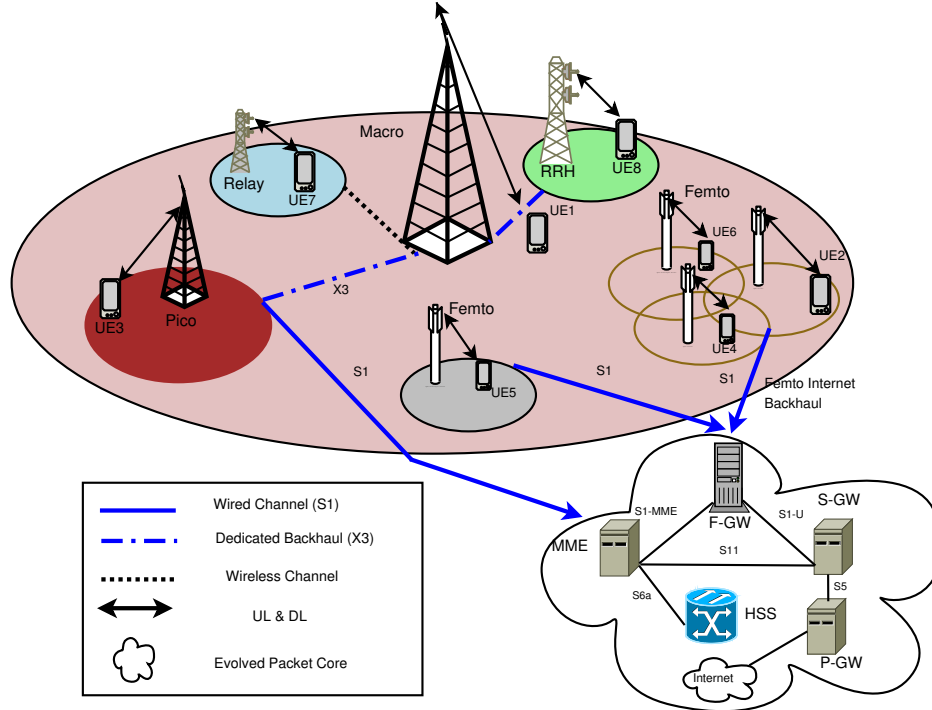


Figure 1.2: LTE Heterogeneous Network

- **Pico or Micro BS:** These are deployed in outdoor environment to cover a radius up to 300 m. The transmission power of the pico BS (*i.e.*, 30 dBm) is smaller than that of Macro BS. Pico BS has a dedicated X3 backhaul connection to the Macro BS for co-ordination as shown in Figure 1.2.
- **Relay:** Relay BS acts as a repeater. It receives the data/signal from the Macro BS and transmits/boosts the data to the relay connected users. The link between the relay and Macro BS is also wireless. Normally the relay BS(s) are the preferred choice of operators in order to extend the coverage region (for e.g., Hilly region, rural areas) of the Macro BS.
- **RRH:** Unlike traditional BS, RRH is a radio transceiver component which performs only the transmission and reception of In-phase Quadrature (IQ) samples. The remaining BS processing is done at a centralized cloud data center by Baseband Unit (BBU) pool. By performing centralized processing, the cost of the BS will come down, which directly reduces CAPEX and OPEX.

The advantage of HetNets are as follows.

1. *Cell range expansion (CRE):* Increasing or decreasing the transmit power (or

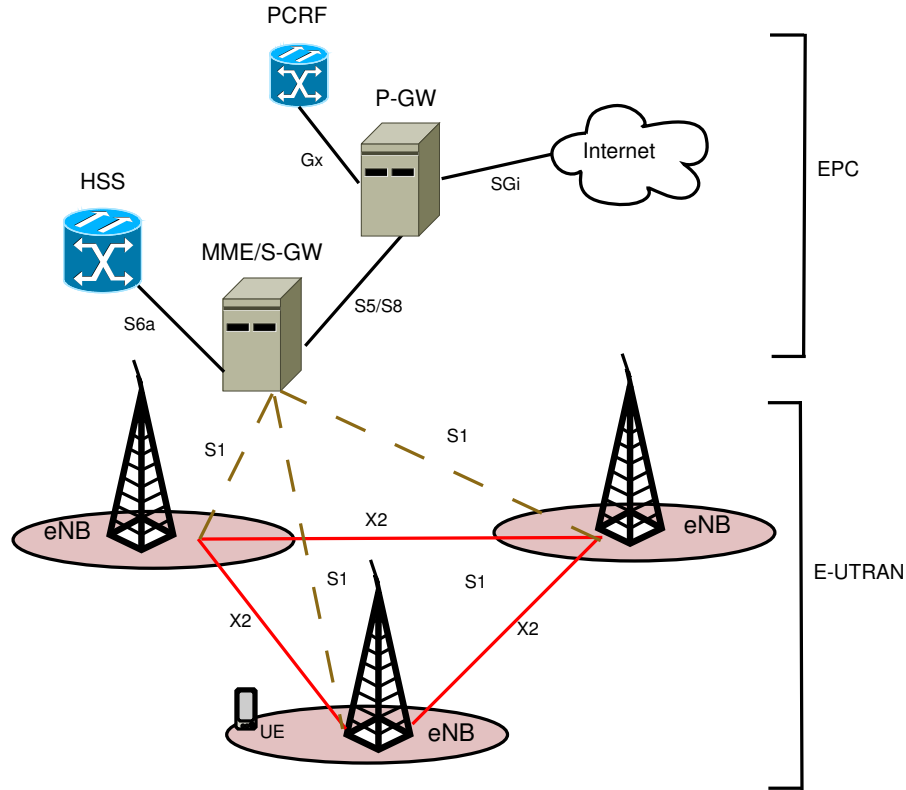


Figure 1.3: Architecture of LTE Network

coverage region) based on the load in small cells will boost the overall system throughput.

2. *Integrating Macro and small cells:* Improving user throughput by dual connectivity (*i.e.*, Macro and one small cell).
3. *Self organizing network (SON):* In HetNets, small cells are deployed in huge number. Each small cell can be provided with SON features, which aims to configure and optimize the network automatically thereby reducing the human effort. It plays a key role in improving OAM (operation, administration, management).

As discussed in above paragraphs, OFDM and MIMO helped in evolution from 3G technologies and this evolution is called as long term evolution or LTE. Along with evolution in technologies, the overall 3GPP network architecture is also being evolved. This evolution is termed as System Architecture Evolution (SAE). The SAE can also be termed as LTE network architecture. SAE consists of both core network, called as Evolved Packet Core (EPC) and radio access network called as Evolved

UMTS Terrestrial Radio Access Network (E-UTRAN). Figure 1.3 shows LTE network architecture. Components of EPC are described as follows:

- **MME:** Mobility Management Entity (MME) is responsible for handover, authentication, paging, security, UE identity and establishment and release of connection. MME connects to base station through S1 interface as shown in Figure 1.3.
- **Serving GW:** Serving Gateway (S-GW) is responsible for data plane (*i.e.*, D-plane), bearer establishment and also routes the packets during handovers.
- **Packet GW:** Packet Gateway (P-GW) is responsible for enforcing policy control and charging rules. The P-GW acts as a mediator between EPC and external networks (*e.g.*, Internet).
- **Home Subscriber Server (HSS):** It is a central repository containing all the operator's subscriber information. This functionality has evolved from GSM and 3G networks. This constitutes a Home Location Register (HLR) part and Authentication Center (AuC) part. HLR part of HSS takes care of database management of user subscription information whereas AuC part utilizes the user identity keys to generate security information and this security information is communicated to other components in the network.

Components of E-UTRAN are described as follows:

- **UE:** This is the user terminal which connects to the eNB as specified in the 3GPP standards.
- **E-Node B:** E-Node B stands for *evolved node B* or *eNB* or *eNodeB*. It is the evolution of Node B from UMTS technology (*i.e.*, 3G). It is responsible for processing the request (from the UEs), resource allocation, handover, interference management, load balance, etc. Hence, eNB plays a key role in LTE.

1.2.1 LTE Frame Format

LTE supports both Time Division Duplexing (TDD) and Frequency Division Duplexing (FDD). In FDD, uplink and downlink transmissions are performed in different frequency bands separated sufficiently while in TDD, these are performed in the same frequency band but in different time slots. LTE also supports half-duplex FDD at UE side. In half-duplex FDD, sending and receiving at a UE are separated in both time

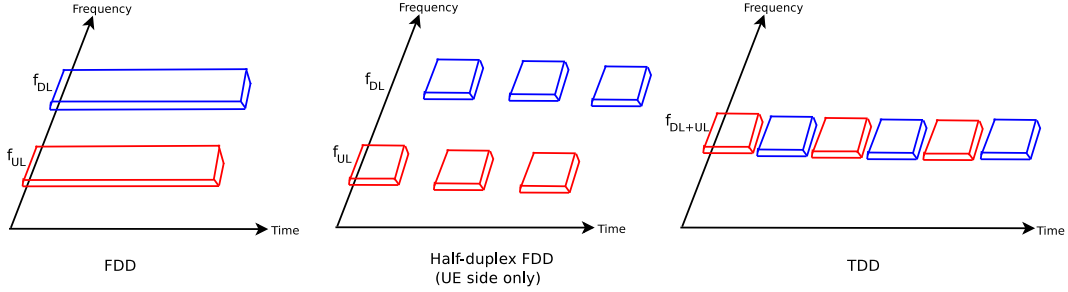


Figure 1.4: Frequency and time division duplex in LTE

and frequency domain because of which duplex filters are not required and hence, terminal complexity is reduced. Figure 1.4 shows examples of FDD, half-duplex FDD and TDD modes of operation. In both TDD and FDD modes, the higher level frame structure is same. Each frame is divided into ten sub-frames. Each subframe has 2 slots with a total duration of 1 ms, making 20 slots in a frame as shown in Figure 1.5. In each subframe, the scheduler running inside the base station allocates to UEs radio resources in terms of Resource Blocks (RBs) for both uplink and downlink transmissions.

Table 1.3 shows the LTE parameters. As shown in Figure 1.6, RB is the smallest unit of radio resources which can be allocated to a UE. If the scheduler allocates one RB to a UE, it means that 180 KHz bandwidth has been allocated to that UE for the next TTI. Each RB of 180 KHz bandwidth will contain 12 sub-carriers, each with 7 OFDM symbols. Hence, it constitutes 84 resource elements. Depending upon the modulation and coding schemes (QPSK, 16-QAM, 64-QAM), each symbol or resource element in the RB carries 2, 4 or 6 bits per symbol, respectively. In an LTE system with 20 MHz bandwidth, there will be 100 RBs available for downlink/uplink scheduling.

Table 1.3: LTE parameters

Parameter	Value
Uplink scheme	Single carrier-FDMA (SC-FDMA)
Downlink scheme	OFDMA
Possible bandwidth	1.4, 3, 5, 10, 15, 20 MHz
Minimum scheduling time (TTI)	1 ms
Sub-carrier spacing	15 kHz
Modulation schemes	QPSK, 16-QAM, 64-QAM

In uplink, SC-FDMA is used as the multiple access scheme to reduce Peak Average

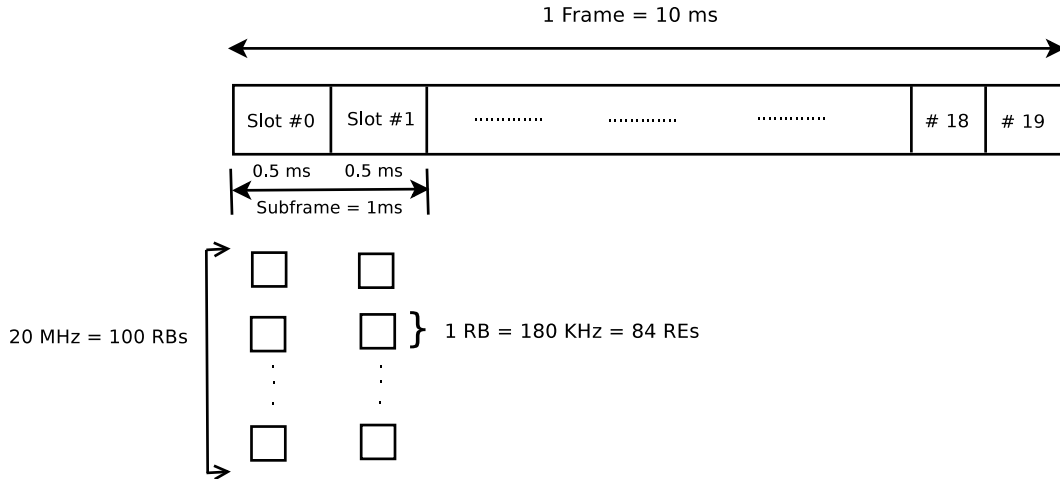


Figure 1.5: LTE Frame Format

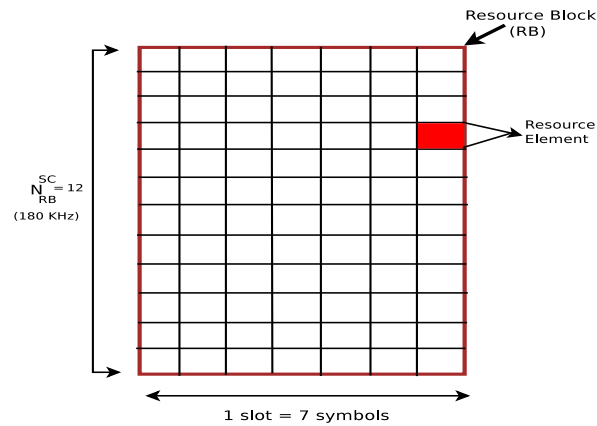


Figure 1.6: Resource Block (RB)

Power Ratio (PAPR) and for uplink transmission, Physical Uplink Control Channel (PUCCH) and Physical Uplink Shared Channel (PUSCH) are used for communication. UEs provide their Channel Quality Indicator (CQI) values as feedback to their attached eNB through PUCCH channel. In downlink, OFDMA is used as the multiple access scheme and Physical Downlink Control Channel (PDCCH) and Physical Downlink Shared Channel (PDSCH) are used for communication.

1.2.2 Radio Resource Management

Scheduling of radio resources to the users is done using various schemes depending upon the objective of the operator. These scheduling schemes include channel unaware, channel-aware/QoS-unaware, channel-aware/QoS-aware, semi-persistent and

energy aware schemes. In this thesis, we have used the well known scheduling algorithm, Proportional-Fair (PF) scheduling [12]. The PF scheduling is a channel aware-QoS unaware scheme which is the combination of Blind Equal Throughput (BET) scheduling (channel-unaware scheduling) and Maximum Throughput (MT) scheduling (channel-aware/QoS-unaware scheduling). The BET scheduling provides fairness to users in terms of throughput. In this case, users in the cell edge may get more RBs to have same throughput as that of non cell edge users. The MT scheduling tries to maximize the spectral efficiency by assigning RBs only to those users which have best Signal to Interference Plus Noise Ratio (SINR). By considering both BET and MT, the PF scheduling provides fairness as well as improves spectral efficiency.

1.3 LTE Femtocell Networks

The existing Macro Base Stations (MBS) are unable to satisfy mobile users because of the very huge data demand and indoor locality of most of the users. Reports by Cisco [13] tell that 70% of the traffic is generated in indoor environments such as homes, enterprise buildings and hotspots. Hence, it is very important for mobile operators to improve coverage and capacity of indoor environments. But the basic problem with the existing MBS (or outdoor small cells with shorter coverage) is that they can only boost data rates of Outdoor User Equipments (*OUEs*). But, they are not able to do the same for Indoor User Equipments (*IUEs*), because it is difficult for electromagnetic signals to penetrate through walls and floors. Owing to many obstacles in the communication path between MBS and *IUEs* inside the building, radio signals attenuate at a faster rate with increase in the distance. Thus, *IUEs* receive low signal strength (*i.e.*, Signal-to-Noise Ratio, SNR) compared to outdoor users. To demonstrate this, we consider a single-floor building with a single MBS (interchangeably used as MBS, Macro and eNodeB in rest of this thesis) situated at a distance of 350 meters from the building on its south-west side. By taking into account path loss due to walls and floors from the MBS, SNR variation inside the building is shown in Figure 1.7. Hence, it is very important for mobile operators to improve coverage and capacity in indoor environments.

As a solution, Femtocells are being deployed by both operators and end customers. Femtocell is a low-cost, low-power consuming cellular base station which operates only in licensed spectrum and designed for both outdoor and indoor communication. The range of Femtocell is 100-150 meters for enterprise environments consuming 100 mW power. A home based Femto (HeNB) can serve 4-5 users whereas an office based

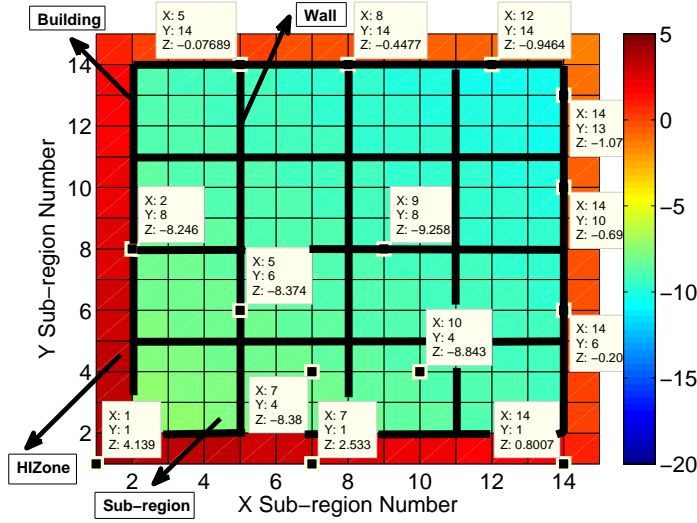


Figure 1.7: SNR variation inside the building. Z-axis is used to list out SNR values in dB scale at various sub-regions (X, Y) inside the building. Owing to the walls inside the building, *IUEs* on average receive low SNR (e.g., -8 dB, -9 dB) compared to *OUEs* (e.g., 4, 2, 0, -1 dB) due to poor indoor signal strength

Femto can serve maximum of 64 users [14]. Each Femto requires a backhaul connection to EPC. Advantages of using Femtos are described as follows:

Operator Advantages :

- The network capacity can be increased.
- OPEX and CAPEX can be reduced.
- Backhaul cost can be reduced.
- Traffic overload on MBSs can be reduced.

User Advantages :

- Improved QoE.
- Improved energy efficiency/battery life.

1.3.1 Architecture of Indoor LTE Femtocells

Figure 1.8 shows the architecture of LTE HetNet system, where Femtos are deployed inside the building and are connected to a Femto Gateway (F-GW) over S1 interface.

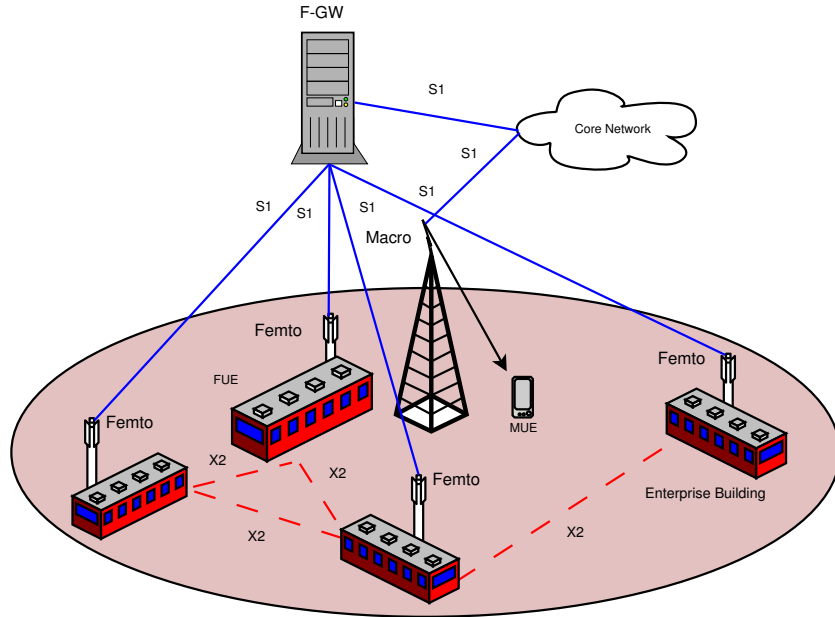


Figure 1.8: Architecture of LTE HetNet with Femtocells

F-GW is mainly used to reduce the load on MME. It acts as a virtual core network to Femtos. The F-GW gets assigned with a eNB ID and thus F-GW is considered as yet another eNB by the MME. The X2 interface is introduced between Femtos of enterprise Femtocell networks to avoid inter cell interference and directly route the data and signaling messages among Femtos, thereby reducing the load on LTE core network and offering better co-ordination among Femtos.

1.3.2 Access Modes in Femto

Since Femtos are deployed for offering high data rates to indoor (paid) users in enterprise and residential buildings, each Femto is configured with a list of subscribers called Subscriber Group (SG) such that only the users in the SG can access the Femto. The users not belonging to this list are called Non-SG (NSG) and they may not served by the Femto even when they are in close proximity to the Femto. Following access modes are defined for Femtos:

- **Open access:** The open access mode allows all users (*i.e.*, SG & NSG) to access the Femto without any restriction.
- **Closed access:** The closed access mode permits only authorized users (*i.e.*, SG) to access the Femto.

- **Hybrid access:** The hybrid access is the combination of both open and closed access. It allows all users (*i.e.*, *SG* & *NSG*) by providing preferential access for *SG* users over *NSG* users.

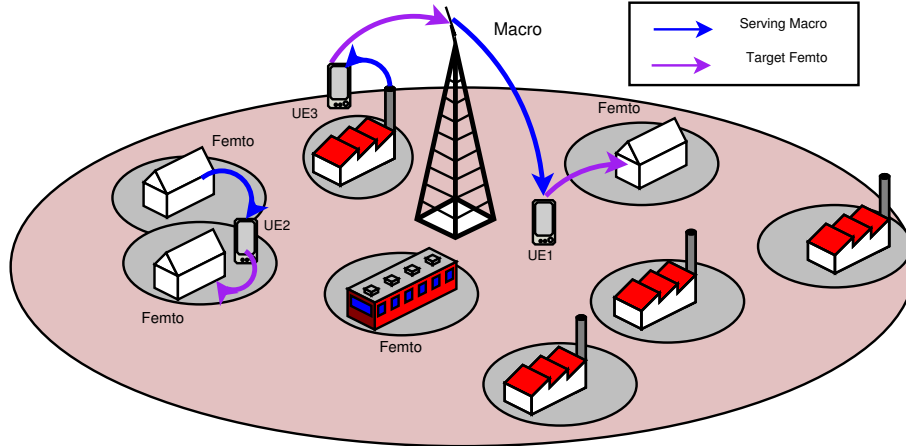


Figure 1.9: Femto Handover Mechanism

1.3.3 Handover Mechanism

In enterprise building with large deployment of Femtocells, as users keep moving from place to place inside the building this triggers many handovers compared to the traditional Macro to Macro handovers due to shorter coverage area of Femtocells. There are three different types of handovers between Femto and Macro BSs.

- **In-Bound:** Figure 1.9 shows handover of UE1 from Macro BS to Femto BS when it enters inside the building where one Femto is deployed. The UE automatically detects Femto by its unique physical cell ID and connects to it. This handover is complex because of the presence of large number of Femtos in indoor. Macro BS has to decide the Femto to which handover must be made.
- **Out-bound:** Figure 1.9 shows handover of UE3 from Femto BS to Macro BS when it comes out of the building.
- **Femto-to-Femto Handover:** The principle used in Macro-to-Macro handover is also applied in the case of Femto-to-Femto handover. But, here F-GW handles handovers. Figure 1.9 shows an example of handover of UE2 between two Femto BSs.

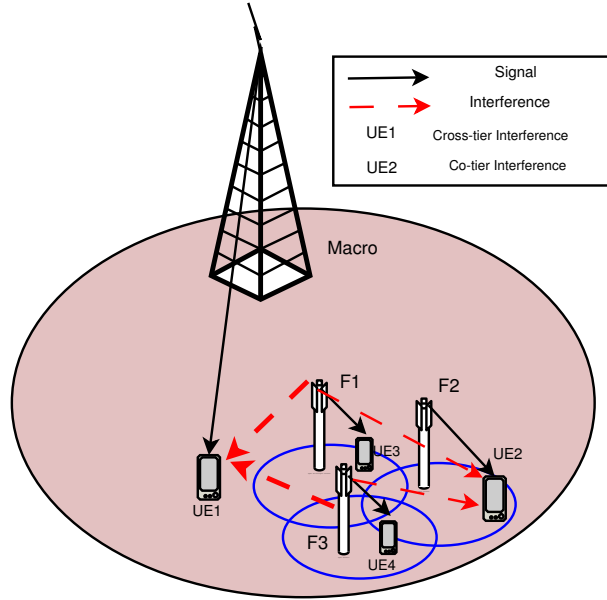


Figure 1.10: Co-tier and Cross-tier Interference in LTE Small Cell Network

1.4 Issues, Existing Solutions and Associated Challenges

In this section, we discuss various issues and challenges while deploying small cells in LTE HetNets. Also, we discuss the existing solutions to address these issues and challenges. Some of the important challenges are discussed below:

1. Interference in HetNet Scenarios

In HetNet systems, the major factor that affects the network throughput is the interference (between Femtos and between Macro and Femtos). There are two types of interference possible in the HetNet systems:

- (a) **Co-tier Interference:** Due to reuse one usage of spectrum, interference from the neighboring small cells is called as co-tier interference. For example, in Figure 1.10, UE2 is getting served by the Femto BS (F2) but it is receiving interference from the neighboring Femto BSs (F1 & F3). The traditional solution to avoid co-tier interference among BSs is the Inter Cell Interference Coordination (ICIC) [15–18]. In ICIC scheme, all BSs cooperatively communicate using X2 interface as shown in Figure 1.8 and allocate RBs efficiently to the cell edge users, but on the other hand, this increases the signaling messages.

(b) **Cross-tier Interference:** The interference between Macro BS and small cell is called as cross-tier interference. For example, in Figure 1.10, UE1 is getting served by the Macro BS but it is receiving interference from small cells (*i.e.*, Femtocells F1, F3). The traditional solution to avoid cross-tier interference is enhanced ICIC (eICIC) [19, 20]. In eICIC scheme, the interference between MBS and Femto BS (FBS) is avoided by muting some sub-frames (Almost Blank Sub-frame) in MBS during FBSs transmissions. This in turn reduces the interference and increases the capacity in HetNet systems.

Though the spectrum efficiency and system capacity could increase due to spatial reuse of the same spectrum in LTE HetNets, SINR (and hence, network throughput) may get affected because of cross-tier inference among MBS(s) and small cells and co-tier interference among small cells and obstacles inside buildings. Also, the signal leaks at the edges/corners of the buildings which in turn causes cross-tier interference and degrades the performance of *OUEs* in the High Interference Zone (HIZone) around the building area, which are connected to one of the Macro BSs in LTE HetNet. To the best of our knowledge, none of the existing works addressed the cross-tier interference issue to HIZone UEs (*HIZUEs*) in a dynamic fashion based on their occupancy levels in the HIZone. In this thesis, in chapter 6, we propose a dynamic power control scheme which is employed at the Femtos in order to reduce cross-tier interference to *HIZUEs* in the HIZone.

2. Load Balancing

The other varying parameter that affects the data rates in cellular networks is the traffic load. This happens due to non-uniform UE traffic distribution in indoor. In traditional cellular networks, the uplink access and downlink access are *coupled* to the same BS as shown in Figure 1.11. The user U_t uses *Femto* F2 for both uplink and downlink communication due to high signal strength from *Femto* F2 than *Femto* F1. Suppose a particular Femto is fully loaded when compared to its neighboring Femtos. Then the traditional offloading or load balancing algorithms [21, 22] will shift some of the UEs for both uplink and downlink from the over loaded cell to one of less loaded cells (target cells) provided that these UEs still could get connected to the target cell. This type of offloading is a forced handover based on the load but not based on sig-

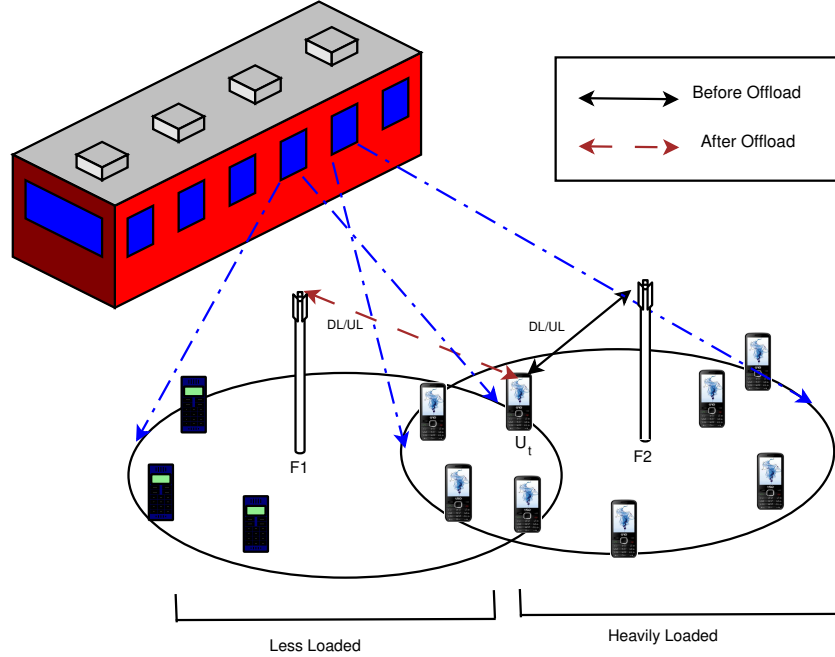


Figure 1.11: Load Balance in Enterprise Building

nal strength, because the signal strength when connected to the initial serving Femto was high compared to the target Femto. For example in Figure 1.11, we observe that *Femto* F2 is heavily loaded, so the user U_t can be offloaded to the neighboring Femto *i.e.*, *FemtoBS1*. In a *coupled* access system, as shown in Figure 1.11, after offloading, U_t uses *Femto* F1 for both uplink and downlink communication. But this could increase the uplink transmission power of UE as it is now connected to the cell which is not the closest one. This in turn drains the battery of UE at faster rate. In order to address this issue, in chapter 2, we adopt downlink/uplink decoupling (DUD) based approach [23,24] in which UEs connect in the uplink to the shortest path loss Femto and in the downlink to one of less loaded Femtos.

3. Placement

Due to large scale deployment of Femtocells in enterprise/office environments and many practical constraints (*e.g.*, lack of space and power), operators will go for arbitrary deployment. Arbitrary deployment of Femtos will lead to the issues such as coverage holes, and increased number of Femtos (increased OPEX and CAPEX) as shown in Figure 1.12. In order to address these issues, placement of Femtos need to be optimal. Optimal placement of Femtos ensures good SINR

and thereby improves overall system capacity. But, in some scenarios, operators may need to go for sub-optimal or arbitrary deployment (due to physical constraints) which will lead to deployment of more number of Femtos than that in the optimal model to ensure that there are no coverage holes inside the building. In this thesis, in chapter 6, we propose an optimal model for placing Femtos in large scale enterprise scenarios.

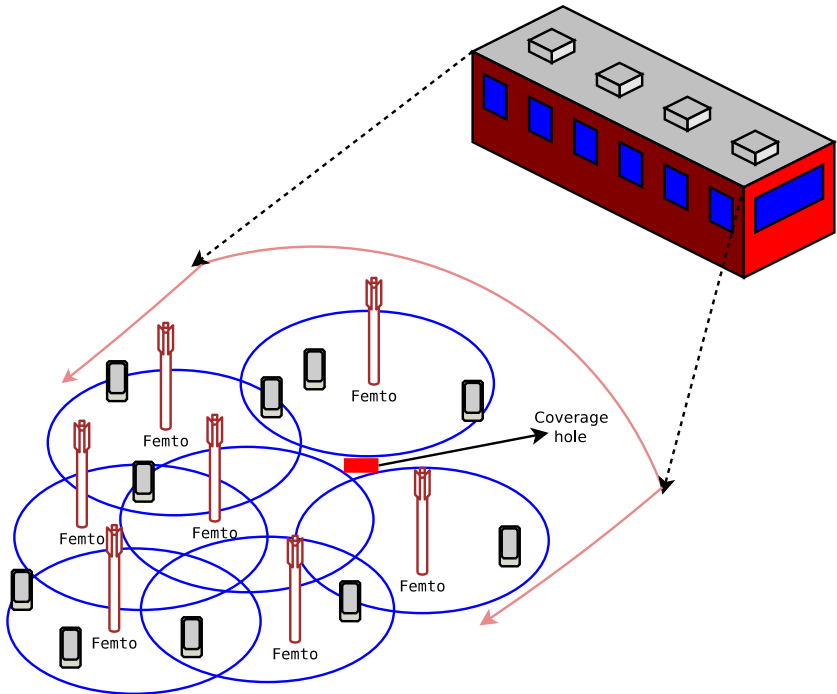


Figure 1.12: Arbitrary Placement of Femtocells

4. Mobility

Another major issue in enterprise Femto building deployments is frequent or unnecessary handovers (*i.e.*, ping-pong effect), which may happen when UE moves from one room to another room or within the same room and similarly in the corridors of the building. For example, in Figure 1.13, the UE1 will experience unnecessary handovers due to signal strength variation from neighboring Femtos when it moves within the building. This leads to degradation of performance like service interruption during signaling overhead, decrease in throughput and increase in number of handovers. Existing works [25,26] focus on the hysteresis margin, signal strength and load aware handovers. But, above approaches lead to more signaling overhead and ping-pong effects as they have

not considered placement aware handover decisions. In this thesis, in chapter 3, we propose a handover and SINR optimized deployment of Femtocells in enterprise environments which prevents unnecessary handovers (*i.e.*, handovers happening within the same room or in corridors) and reduced signaling in enterprise building, by placing the Femtos with additional handover constraint.

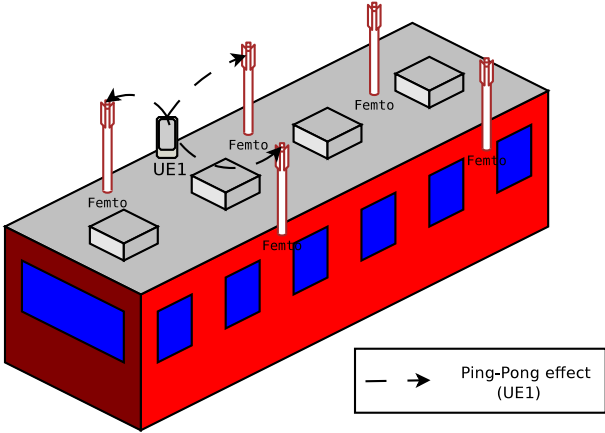


Figure 1.13: An Example Scenario Showing Ping-pong Handovers in Femtocells

5. Scheduling

Femtos that are configured in open access mode do not distinguish between SG users and non-SG users and hence, they may fail to ensure QoS for SG users especially during peak traffic loads. Hybrid Access Femtocells (HAFs) are favored by telecom operators as they can ensure QoS for SG users by giving them preferential access to radio resources over NSG users and also improve the capacity of LTE HetNet by serving nearby NSG users. Challenges here are optimal HAF deployment and efficient splitting of radio resources between SG and NSG users of HAFs in indoor environments. To the best of our knowledge, none of the existing works discussed about the fair allocation of radio resources among SG and NSG users. In this thesis, in chapter 7, we propose a dynamic bandwidth allocation method which divides the available bandwidth between the SG and NSG users and also an efficient power control and fair resource allocation method which allocates the radio resources between SG and NSG users.

1.5 Objectives and Scope of the Thesis

The main objective of this thesis is to propose efficient solutions to improve data rates of users in LTE HetNets. The scope of the work is summarized below.

- To develop efficient Femto placement schemes for enterprise environments which boost SINR of indoor UEs.
- To develop dynamic power control algorithms at Femtos (deployed in buildings) for optimally tuning the transmit power based on presence of outdoor users in the *HIZone* of the building.
- To make use of free/idle *IUEs* as D2D relays for improving data rates of Macro users who are present in the *HIZone* of the building.
- To modify the traditional radio resource allocation (*i.e.*, scheduling) for efficiently supporting SG & NSG users of Hybrid access Femtos in LTE HetNets.
- To develop a Decoupled Uplink and Downlink (DUD) access scheme such that users connect in the uplink to the shortest path loss Femtocell and to one of less loaded Femtocells in downlink in order to efficiently manage user offloading and reduce uplink transmit power.
- Handover and SINR optimized deployment of Femtocells in enterprise environments.
- To design efficient distributed resource allocation and interference management scheme for arbitrary deployed Femtocell environments.

1.6 Organization of the Thesis

In this chapter, we described the outline and contributions of the thesis. Rest of the thesis is organized as follows. In chapter 2, we describe the advantages of *decoupled* access for downlink and uplink in the enterprise Femtocell environments. Then, we propose an efficient downlink offloading algorithm and study the performance of the proposed system in both uniform and non-uniform traffic load scenarios.

In chapter 3, to reduce the unnecessary handovers or ping-pong effect in enterprise building environments, we propose a handover and SINR optimized deployment of LTE Femtocells and study the performance in terms of throughput by comparing it with arbitrary and center placement schemes. In chapter 4, we design a efficient

power control algorithm to reduce the impact of cross-tier interference to *OUEs* and in chapter 5, we consider both uplink and downlink interference while Femto planning. Also we ensure that energy consumption in Green HetNet (uplink) building is less when compare to center placement. In chapter 6, to improve the SINR in LTE HetNet system, we adopt the *D2D based relay* concept to propose a D2D pair selection algorithm and compare the SINR performance with that of a D2D Mixed Integer Linear Programming (MILP) model.

In chapter 7, a novel resource allocation and power control mechanism for HAFs is proposed. Also, we have shown the trade off between the closed access and hybrid access Femtocell. In chapter 8, we compare the above proposed solutions (described in chapters 6, 7 and 8) in terms of throughput and operator revenues. In chapter 9, we propose a distributed resource allocation and interference management algorithm for LTE Femtocells which dynamically increases or decreases the radius of inner regions to avoid co-tier interference among Femto BSs. Finally, we summarize the contributions of the thesis and discuss the possible future extensions in chapter 10.

Chapter 2

On Femto Placement and *Decoupled* Access for Downlink and Uplink in Enterprise Environments

2.1 Introduction

Dense deployment of Femtos in enterprise environments [27] necessitates the need for their optimal placement to guarantee good signal strength to all indoor UEs and to minimize coverage holes. In this work, we formulate a Mixed Integer Linear Programming (MILP) model for the optimal placement of Femtos. In a typical indoor scenario with Femtocells, the uplink load of a cell would more or less be the same in the entire building, but the downlink load would vary widely from one Femto to other depending on the number of UEs being served [28,29] and their traffic demands. In traditional cellular networks (*i.e.*, coupled access systems), the uplink access and downlink access are *coupled* to the same cell as shown in Figure 2.1. Here, the user u_t uses *Femto*₂ for both uplink and downlink communication because the signal strength from *Femto*₂ is higher than that of *Femto*₁. Suppose a Femto is fully loaded when compared to its neighboring Femtos, the traditional offloading or load balancing algorithms [30,31] will shift some of the UEs for both uplink and downlink from the over loaded cell to one of less loaded cells (target cells) provided that these UEs still could get connected to the target cell. This type of offloading is a forced handover based on the load but not based on signal strength, because the signal strength when

connected to the initial serving Femto will be high compared to the target Femto. For example in Figure 2.1, we observe that $Femto_2$ is more loaded (by assuming more traffic load when there are more UEs in a cell) hence the user u_t can be offloaded to the neighboring Femto *i.e.*, $Femto_1$. In a *coupled* access system, as shown in Figure 2.2, after offloading, u_t uses $Femto_1$ for both uplink and downlink communication. Since u_t and $Femto_1$ are separated by a wall, u_t has to transmit with higher power to achieve good UL SNR in $Femto_1$ compared to when it was connected to $Femto_2$. By doing this kind of offloading, the overall system throughput will increase but the uplink power of the shifted UEs would increase and thereby drain their batteries faster.

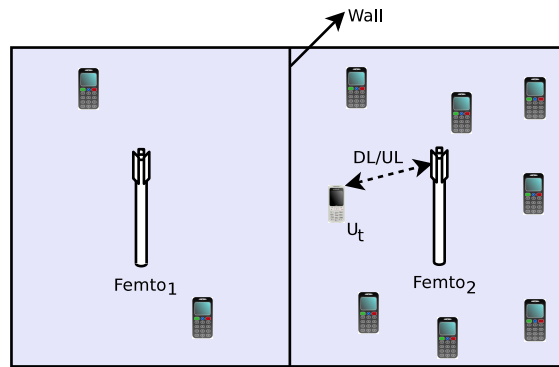


Figure 2.1: *Coupled* Access System before offloading U_t to $Femto_1$

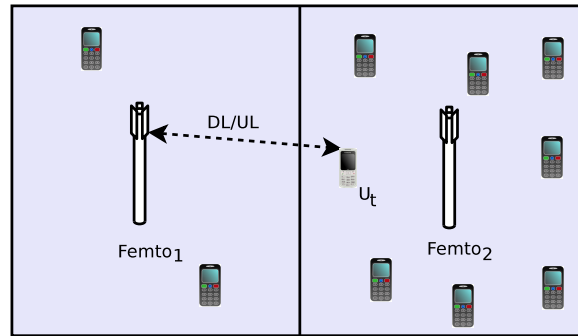


Figure 2.2: *Coupled* Access System after offloading U_t to $Femto_1$ from $Femto_2$

In order to reduce the battery drain from UEs and to improve the downlink data rate, one could use the *Decoupled* Uplink and Downlink (DUD) access method [23] *i.e.*, uplink connected to the closest Femto and downlink to a less loaded Femto. For example in Figure 2.3, we observe that user u_t connects to $Femto_1$ for downlink and

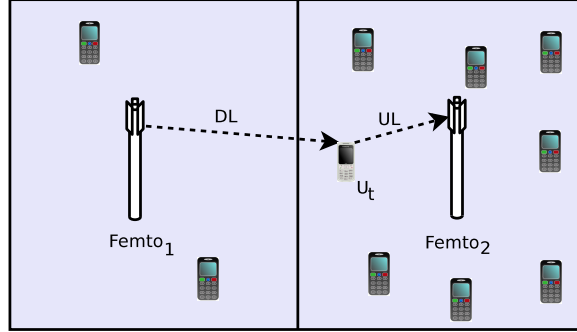


Figure 2.3: *Decoupled* Access System after offloading only downlink of U_t to $Femto_1$ from $Femto_2$

$Femto_2$ for uplink communication. Before doing this, the placement of Femtos should be optimal inside the building to attain a desirable SNR for indoor UEs.

In the present work, we look into the problem of optimal Femto placement in indoor environments to obtain a desirable SNR at each location inside the building with out any coverage holes. Two major parameters that determine the optimal Femto locations include (i) distance between Femto and the farthest point inside the building and (ii) the minimum SNR needed by each UE. Solving for optimal placement of Femtos by considering the above parameters results in a non-convex optimization problem [32]. We further simplify this non-convex problem to fit into MILP model and solve it using GAMS tool [33]. After Femtos are placed optimally, to increase the downlink throughput and reduce battery drain, we propose an offloading algorithm in DUD access system.

2.1.1 Organization of this Chapter

The rest of the chapter is organized as follows. Section 2.2 presents related work on Femto placement and *decoupled* access systems. Section 2.3 describes the proposed Femto placement model. Section 2.4 presents the proposed efficient offloading algorithm for *DUD* access systems. In Section 2.5, we show the performance results of the proposed Femto placement model and offloading algorithm in a two-storey enterprise building scenario. Finally, Section 2.6 summarizes the work.

2.2 Related Work

Right from its incorporation, extensive research has been carried out to address Femto placement problem considering various issues like frequent hand-offs, interference and Physical Cell ID (PCID) [27]. An effective algorithm for the optimal placement of Femtos depends on the distance between the first Femto deployed inside the building and the Macro BS, as given in [34, 35], which reduces the CAPEX and energy consumption of the cellular network. Works on optimal relay node placement in tunnels [36], sensor placement [37, 38] in terrain regions and optimal placement of Wi-Fi APs [39] exist in literature. The algorithm for optimal Femto placement provided in [32, 40] is of limited practical value since it ignores walls inside the buildings while determining Femto locations. Appending to the above work, we constrained the problem to be similar to realistic enterprise buildings by considering the path loss due to walls inside the building. The resulting non-convex optimization model is solved by approximating it as an MILP.

After placing the Femtos optimally to guarantee good signal strength at the farthest points inside the sub-region of the building, the other problem that arises is load-imbalance across Femtos. Lot of existing literature discuss about the load balancing in LTE systems by varying the handover hysteresis margin, dynamic BS power control [41] and centralized load balance using Software Defined Network (SDN) approaches. In [30] authors proposed a solution framework that considers QoS-guaranteed scheduling and call admission control. Also this work analyzed the complexity of the proposed algorithm and proves that it can be adaptable in practical environments. In [31, 42] authors proposed a multi-objective problem with the objective of load balance by meeting QoS requirements and the network utility of services like voice, video and online gaming, but the running time of the proposed optimization problem is very high. Hence, they proposed a practical algorithm which considers QoS guaranteed hybrid scheduling, handover of users with and without QoS requirements and call admission control.

All these traditional load balancing techniques increase the battery power consumption of the UE which is being offloaded from the heavily loaded Femto to a lightly loaded Femto since the distance for the uplink access is high in *coupled* access systems. In order to save energy, *decoupling* is the efficient solution without degrading the performance of the UE. Along these lines, in the first work [24, 43], authors proposed a way in which the uplink connects to one of less path loss small cells and the downlink connects to a Macro BS, causing a reduction in the uplink power. But

it also decreases the downlink throughput due to path losses encountered in reaching the UE indoors. But demand in the downlink is more than uplink in indoors so dual connectivity from small cells in downlink connection plays a key role. In [44], the authors discussed about dual connectivity with uncoordinated power control in uplink between Macro and small cells, but, this may reduce the battery life of UEs and increase the burden on the backhaul. In [45], authors considered joint ICIC and forced cooperative downlink packet scheduling. Practical deployment of this solution is challenging due to spectrum sharing issues. This solution also limits secondary cell resource usage due to forced scheduling by primary cell.

In this chapter, we consider obstacles and shadowing effects by walls and include them in the system model. We develop a Linear Programming Problem (LPP) model to place Femtos optimally inside the building by converting convex constraints into linear ones and solve it using GAMS tool. Also, we extend the work by proposing an efficient offloading algorithm in DUD access system for addressing load imbalance in Femtocells.

2.3 Optimal Femto Placement in Enterprise Environments

In this section, we present Femto placement in enterprise building environments as an optimization problem. Table 2.1 shows the notation used in MILP formulation.

Table 2.1: Glossary of MILP Model

Notation	Definition
d_{ijk}^f	Farthest distance between Femto f and sub-region (i, j, k)
$ F $	Number of Femtos
x_f, y_f, z_f	x, y and z are the co-ordinates of Femto f
π_{ijk}^f	1 if Femto f is placed at sub-region (i, j, k) , zero otherwise
ρ^f	Represents the room number of Femto f
ρ_{ijk}	Represents the room number of sub-region (i, j, k)
N	Total number of rooms in the building
h_m	Average height of the UE
P_f	Femto transmit power
P_N	Noise power
α	Path-loss exponent

2.3.1 Building Model

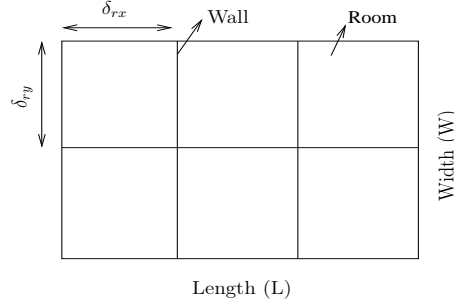


Figure 2.4: Top view of a floor in the building

The enterprise building is considered to be of length L and width W . Let, the height of each floor be h . Each floor is further partitioned into rooms of equal dimensions as illustrated in Figure 2.4. The length and width of each room are δ_{rx} and δ_{ry} , respectively. Each room is numbered ρ_{zxy} , also be denoted as $\rho_z\rho_x\rho_y$. The first digit in three digit numerical scheme signifies the floor number, second digit varies along X - axis and the third digit varies along Y -axis as shown in Figure 2.5. If the room number is referred to as ρ_x , it implies that the room number is varied along the X - axis only. For example, if $\rho_{zxy} = 122$ and if $\rho_x + 1$ operation is applied, then $\rho_{zxy} = 132$.

We assume that $|F|$ Femtos are available to cover the entire building area and they are to be placed only on the ceiling of the rooms. ρ_f denotes the room number of f^{th} Femto. We further divide each room into sub-regions as shown in Figure 2.6. The sub-regions are formed to reduce complex calculations. The length and width of each sub-region are δ_x and δ_y , respectively. The sub-regions are numbered with indices (i, j, k) . The first index in the adopted triplet scheme (i, j, k) , varies along the

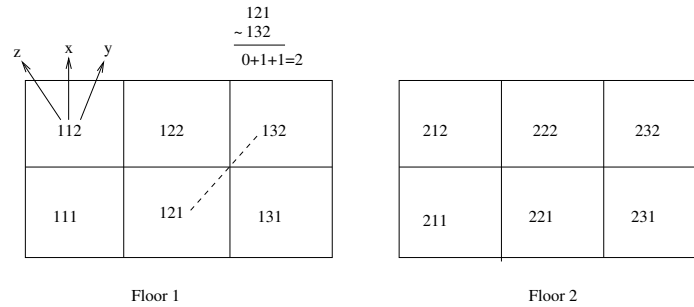


Figure 2.5: Numbering of rooms in a two-storey building and calculation of number of walls between Femto and sub-region

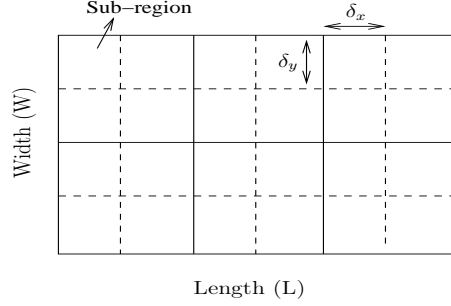


Figure 2.6: Top view of sub-regions in the building

X – axis, the second index varies along the Y – axis and the third index designates the floor number as shown in Figure 2.7.

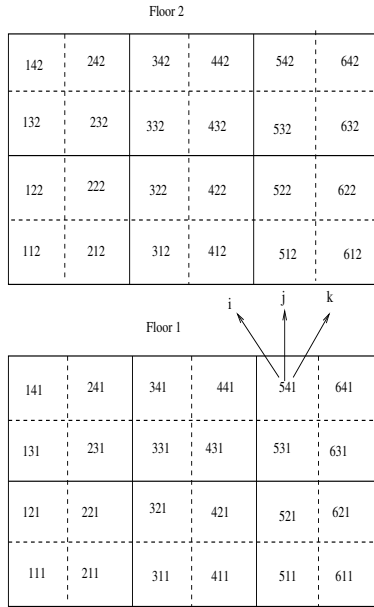


Figure 2.7: Numbering of sub-regions on floor #1 and floor #2

2.3.2 System Model

In this chapter, we consider an LTE Femtocell network where Femtos are deployed by network providers, each operating on a different frequency, *i.e.*, no co-tier interference. Also the cross-tier interference between Macro BS and Femtos is ignored. We relax these assumptions later in chapters 6 onwards where we should be studying placement problem in LTE HetNets with frequency reuse one. We also assume that Femtos are configured in open access so that all UEs of the network provider are authorized to

connect with any of the Femtos.

2.3.3 Formulation of Femto Placement Model

Let us suppose that a given Femto f has the co-ordinates x_f , y_f and z_f . Then, the distance from the Femto to the farthest point in a sub-region defined by (i, j, k) is given by d_{ijk}^f (from reference [32], Figure 2).

$$(d_{ijk}^f)^2 = (|x_f - (i - \frac{1}{2})\delta_x| + \frac{1}{2}\delta_x)^2 + (|y_f - (j - \frac{1}{2})\delta_y| + \frac{1}{2}\delta_y)^2 + ((z_f - k + 1)h - h_m)^2 \quad (2.1)$$

We define a binary variable $\lambda_{f\rho}$ as 1 if the f^{th} Femto is in room ρ , and 0 otherwise. z_f co-ordinate of a Femto is an integer indicating the Femto's residing floor number and is given by,

$$z_f = \sum_{\rho=1}^N \rho_z \lambda_{f\rho} \quad (2.2)$$

where N is the number of rooms in the building. Let us assume that f^{th} Femto is residing in the room number ρ_{zxy} . The x and y co-ordinates of the Femto are constrained to be within the bounds of the room in which it is contained as shown in Figure 2.8.

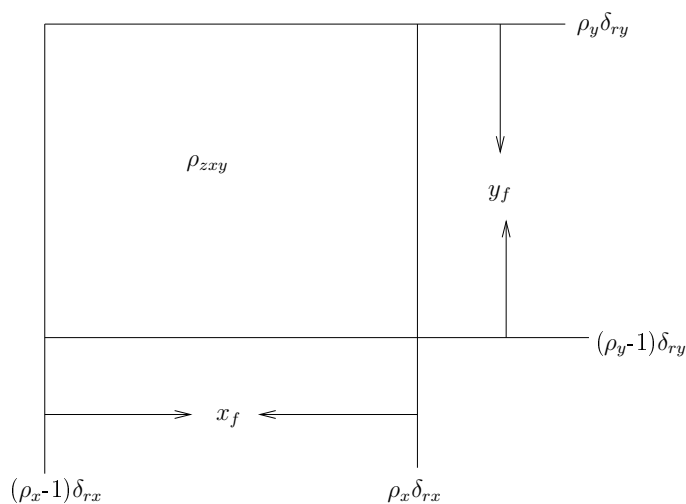


Figure 2.8: Upper and lower bounds for x_f and y_f

Equations (2.3) and (2.4) give that the x co-ordinate of the Femto should have the value greater than the left wall and less than the right wall, respectively.

$$x_f \geq \sum_{\rho_x=1}^N (\rho_x - 1) \delta_{rx} \lambda_{f\rho} \quad (2.3)$$

$$x_f \leq \sum_{\rho_x=1}^N \rho_x \delta_{rx} \lambda_{f\rho} \quad (2.4)$$

Similarly, equations (2.5) and (2.6) give that the y co-ordinate of the Femto should have the value greater than the lower wall and less than upper wall, respectively.

$$y_f \geq \sum_{\rho_y=1}^N (\rho_y - 1) \delta_{ry} \lambda_{f\rho} \quad (2.5)$$

$$y_f \leq \sum_{\rho_y=1}^N \rho_y \delta_{ry} \lambda_{f\rho} \quad (2.6)$$

To ensure that a sub-region is served by only one Femto, we have the following constraint,

$$\sum_{f=1}^{|F|} \pi_{ijk}^f = 1 \quad (2.7)$$

The efficiency of a Femto in serving the UEs in a sub-region depends on the SNR in that sub-region. We set a constraint that the SNR at the farthest point of the sub-region should be higher than the threshold SNR, γ_{min} . This would imply that every point in the sub-region would receive SNR greater than γ_{min} , since SNR decreases with increasing distance from the Femto. The SNR in the sub-region (i, j, k) , γ_{ijk} is given by

$$\gamma_{ijk} = \frac{P_f}{L_{r_{ref}} \left(\frac{d_{ijk}}{r_{ref}} \right)^\alpha P_N} \quad (2.8)$$

Here d_{ijk} is the distance between the sub-region (i, j, k) and the serving Femto, $L_{r_{ref}}$ is the path loss at the reference distance r_{ref} in linear scale and α is the path-loss exponent. SNR in dB scale is given by,

$$\gamma_{ijk}^* = P_f^* - L_{r_{ref}}^* - 10\alpha \log_{10}\left(\frac{d_{ijk}}{r_{ref}}\right) - P_N^*$$

where, γ_{ijk}^* , P_f^* , P_N^* and $L_{r_{ref}}^*$ are all in dB scale. Considering the attenuation factors, the total attenuation is given by,

$$L_{TAF}^* = L_{FAF}^* + L_{WAF}^* \quad (2.9)$$

where, L_{TAF}^* is total attenuation factor and L_{FAF}^* and L_{WAF}^* are the losses due to floor attenuation and wall attenuation, respectively. SNR in dB scale considering wall and floor losses is given by,

$$\gamma_{ijk}^* = P_f^* - L_{r_{ref}}^* - 10\alpha \log_{10}\left(\frac{d_{ijk}}{r_{ref}}\right) - P_N^* - L_{TAF}^* \quad (2.10)$$

We assume two more variables for the reciprocal of SNR values. Let,

$$\gamma'_{ijk} = \frac{1}{\gamma_{ijk}} \quad (2.11)$$

γ_{min} is the threshold value of SNR and its reciprocal is γ'_{min} .

$$\gamma'_{min} = \frac{1}{\gamma_{min}} \quad (2.12)$$

Now equation (2.8) can be rewritten as [32]:

$$(d_{ijk})^\alpha G(\rho) \Delta^{\rho_f \sim \rho_{ijk}} - \gamma'_{ijk} = 0 \quad (2.13)$$

$F(\rho)$ is a function defined by,

$$F(\rho) = \begin{cases} K_0 = \frac{C_0 P_n L_{r_{ref}}}{P_f r_{ref}^\alpha}, & \text{if } \rho_f \neq \rho_{ijk} \\ K_1 = \frac{C_1 P_n L_{r_{ref}}}{P_f r_{ref}^\alpha}, & \text{if } \rho_f = \rho_{ijk} \end{cases} \quad (2.14)$$

Here C_0 and C_1 are constants depending on the environment. Δ is also a constant depending on the environment and $\rho_f \sim \rho_{ijk}$ is calculated in such a way that it gives the number of obstructions (walls or floors) between the sub-region (i, j, k) and the f^{th} Femto. This special difference (\sim) is the absolute value of the digit wise difference between ρ_f and ρ_{ijk} as shown in Figure 2.5. Few examples are given below.

Example 1) consider $\rho_f = 121$ and $\rho_{ijk} = 132$.

$\rho_f \sim \rho_{ijk} = 121 \sim 132 = |1 - 1|\beta_1 + (|2 - 3| + |1 - 2|)\beta_2 = 2\beta_2$. Here, $\beta_1 = T_{FAF}$,

$\beta_2 = T_{WAF}$. Hence, the rooms 121 and 132 are separated by two walls.

Example 2) consider $\rho_f = 121$ and $\rho_{ijk} = 231$.

$\rho_f \sim \rho_{ijk} = 121 \sim 231 = |1 - 2|\beta_1 + (|2 - 3| + |1 - 1|)\beta_2 = \beta_1 + \beta_2$. The co-efficient of β indicates the number of floors separating the f^{th} Femto and the sub-region (i, j, k) . The co-efficient of β_2 indicates the number of walls separating the f^{th} Femto and sub-region (i, j, k) . Hence, the rooms 121 and 231 are separated by one floor and one wall.

Since the SNR received in any sub-region should be greater than the threshold SNR, we have the following constraint,

$$\gamma'_{ijk} \leq \gamma'_{min} \quad (2.15)$$

The above constraint is ensured for all the sub-regions whose user occupant probability is greater than zero (*i.e.*, $p_{ijk} > 0$). If p_{ijk} is the expected peak user density in sub-region (i, j, k) , then the placement of Femtos should be in such a way that the product, $p_{ijk}\gamma_{ijk}$ should be the maximum for all the sub-regions. Alternately, the product $p_{ijk}\gamma'_{ijk}$ should be minimum. Hence, our objective is

$$\min \sum_{ijk} p_{ijk} \gamma'_{ijk}$$

subject to (2.1), (2.2), (2.3), (2.4), (2.5), (2.6), (2.7), (2.13) and (2.15).

But equations (2.1) and (2.13) are non-convex equations which cannot be solved by the available tools [46]. Hence, these equations are first converted to convex equations and then to linear equations.

Linearization of Equation (2.1):

Let,

$$R_{ijk}^f = (d_{ijk}^f)^2 \quad (2.16)$$

$$X_{fi} = |x_f - (i - \frac{1}{2}\delta_x)| \quad (2.17)$$

$$Y_{fj} = |y_f - (j - \frac{1}{2}\delta_y)| \quad (2.18)$$

Without loss of generality, we can convert the equality in the equations into inequalities with the help of Lemma 1 [32] as follows,

Lemma 1. *The constraints in Equation (2.1) can be equivalently replaced by,*

$$(X_{fi} + \frac{1}{2}\delta_x)^2 + (Y_{fj} + \frac{1}{2}\delta_y)^2 + (hz_f - ((k-1)h + h_m))^2 - R_{ijk}^f \leq 0 \quad (2.19)$$

Moreover, the inequality in equation (2.19) holds as equality to the optimal solution.

Equations (2.17) and (2.18) are expanded as,

$$x_f - X_{fi} \leq (i - \frac{1}{2})\delta_x \quad (2.20)$$

$$x_f + X_{fi} \geq (i - \frac{1}{2})\delta_x \quad (2.21)$$

$$y_f - Y_{fj} \leq (j - \frac{1}{2})\delta_y \quad (2.22)$$

$$y_f + Y_{fj} \geq (j - \frac{1}{2})\delta_y \quad (2.23)$$

Let,

$$X_{fi}^2 = B_{fi}, Y_{fj}^2 = D_{fj}, z_f^2 = E_f$$

The above equations can be written as, (with the help of Lemma 1)

$$X_{fi}^2 - B_{fi} \leq 0 \quad (2.24)$$

$$Y_{fj}^2 - D_{fj} \leq 0 \quad (2.25)$$

$$z_f^2 - E_f \leq 0 \quad (2.26)$$

Accordingly, equation (2.19) becomes,

$$B_{fi} + D_{fj} + h^2 E_f + \delta_x X_{fi} + \delta_y Y_{fj} - 2h((k-1)h + h_m)z_f - R_{ijk}^f \leq -\frac{1}{4}\delta_x^2 - \frac{1}{4}\delta_y^2 - ((k-1)h + h_m)^2 \quad (2.27)$$

Using Piece-wise Linear Approximation (PLAP) [47], the convex constraints (2.24), (2.25) and (2.26) are transformed into linear constraints, which steers the deduction of the following equations,

$$\sum_{S=1}^{S_X} w_1^X (X_S)^2 \leq B, \sum_{S=1}^{S_X} w_1^X (X_S) = X, \sum_{S=1}^{S_X} w_1^X = 1 \quad (2.28)$$

$$\sum_{S=1}^{S_Y} w_2^Y (Y_S)^2 \leq D, \sum_{S=1}^{S_Y} w_2^Y (Y_S) = Y, \sum_{S=1}^{S_Y} w_2^Y = 1 \quad (2.29)$$

$$\sum_{S=1}^{S_Z} w_3^Z (Z_S)^2 \leq E, \sum_{S=1}^{S_Z} w_3^Z (Z_S) = z, \sum_{S=1}^{S_Z} w_3^Z = 1 \quad (2.30)$$

where, w_1^X , w_2^Y and w_3^Z are the positive weights between 0 and 1. The X_S , Y_S and Z_S are the S pieces in their respective domains.

Linearization of Equation (2.13):

Let,

$$\nu_{ijk}^f = (R_{ijk}^f)^{\frac{\alpha}{2}} \quad (2.31)$$

The above equation can be written (with the help of Lemma 1 [32]) as,

$$\nu_{ijk}^f \geq (R_{ijk}^f)^{\frac{\alpha}{2}} \quad (2.32)$$

Let,

$$g_{ijk}^{f\rho} = \nu_{ijk}^f \lambda_{f\rho} \quad (2.33)$$

Then equation (2.13) can be written as

$$K_1 \sum_{\rho, \rho \neq \rho_f}^N ((\Delta^{\rho \sim \rho_f}) g_{ijk}^{f\rho}) + K_0 g_{ijk}^{f\rho} - (1 - \pi_{ijk}^f) \Gamma_{ijk}^f - \gamma'_{ijk} \leq 0 \quad (2.34)$$

Here, Γ_{ijk}^f is the upper bound of $(d_{ijk})^\alpha F(\rho) \Delta^{\rho \sim \rho_{ijk}}$. $\bar{\nu}_{ijk}^f$ is the upper bound for ν_{ijk}^f . The bilinear equation (2.33) holds good within the bound $0 \leq \nu_{ijk}^f \leq \bar{\nu}_{ijk}^f$ if and only if (from reference [32]):

$$g_{ijk}^{f\rho} \geq 0 \quad (2.35)$$

$$g_{ijk}^{f\rho} - \bar{\nu}_{ijk}^f \leq 0 \quad (2.36)$$

$$\sum_{\rho}^N g_{ijk}^{f\rho} - \nu_{ijk}^f = 0 \quad (2.37)$$

We linearize the convex constraint given in equation (2.32) by PLAP and then obtain

$$\sum_{S=1}^{S_R} w_s (R_S)^{\frac{\alpha}{2}} - \nu \leq 0, \sum_{S=1}^{S_R} w_s (R_S) = R, \sum_{S=1}^{S_R} w_s = 1 \quad (2.38)$$

where, w_s are the positive weights between 0 and 1. R_S (contain S pieces) are also positive weights to do piece wise linear approximation and they also used as a decision variable in our optimization.

MILP Model

The optimal Femto placement model can be stated as,

$$\min \sum_{ijk} p_{ijk} \gamma'_{ijk} \quad (2.39)$$

Subject to

- a) Femto placement constraints: Equations (2.2), (2.3), (2.4), (2.5), (2.6), (2.7), (2.15)
- b) Linear equations equivalent to Equation (2.1): Equations (2.20), (2.21), (2.22), (2.23), (2.27), (2.28), (2.29), (2.30)
- c) Linear equations equivalent to Equation (2.13): Equations (2.34), (2.35), (2.36), (2.37), (2.38)

2.4 *Decoupled* Uplink and Downlink (DUD) Access for Efficient Offloading in Femtocell Networks

The proposed offloading algorithm in DUD access system will be running in a centralized Femto-GW to address offloading problem in Femtocells. The SON feature in Femto-GW can automate the offloading algorithm efficiently. Optimal Femto place-

Algorithm 1 Offloading Algorithm

Input 1 : F : Set of all Femtos

Input 2 : \bar{R} : Total no. of RBs in a Femto over n TTI

Input 3 : u_f : Set of all UEs connected to Femto f

Input 4 : $minRB$ matrix

Input 5 : $TotDemand_f$: Total RB demand in each Femto

Input 6 : TED^0 : Initial total excess demand

Initialization:

Iteration Count \leftarrow 1;

- 1: Arrange the Femtos in non-ascending order of $TotDemand$ values
 - 2: **for** $f = 1 : |F|$ **do**
 - 3: **while** $TotDemand_f > \bar{R}$ **do**
 - 4: Using $minRB$ matrix find a pair (u^*, f^*) such that $u^* \in u_f$, $f^* \in F - \{f\}$ and $minRB$ is the minimum
 - 5: **if** $(TotDemand_{f^*} + minRB_{u^*f^*}) \leq \bar{R}$ **then**
 - 6: **if** $minRB$ is ∞ **then**
 - 7: Continue; {Go to step 2 to select next Femto for offloading}
 - 8: **end if**
 - 9: $TotDemand_{f^*} = TotDemand_{f^*} + minRB_{u^*f^*}$
 - 10: $TotDemand_f = TotDemand_f - minRB_{u^*f}$
 - 11: $u_f = u_f - \{u^*\}$
 - 12: $u_{f^*} = u_{f^*} \cup \{u^*\}$
 - 13: **else**
 - 14: $minRB_{u^*f^*} \leftarrow \infty$ {Avoid (u^*f^*) pair getting selected again}
 - 15: **end if**
 - 16: **end while**
 - 17: **end for**
 - 18: Update TED^{Count} (using Equation (2.42)).
 - 19: **if** $(TED^{Count} == TED^{Count-1}$ or $TED^{Count} == 0)$ **then**
 - 20: Exit {Load in the network (*i.e.*, Femto f) is balanced}
 - 21: **else**
 - 22: Count \leftarrow Count + 1;
 - 23: Goto Step 1 {Look for offloading some more UEs to achieve load balancing}
 - 24: **end if**
-

ment model (refer Equation (2.39)) presented in the previous section ensures that there is no coverage hole inside the building and each sub-region $> \gamma_{min}$. However, the next challenge after deploying the Femtos inside the building is load balancing. In reality, all the Femtos will not be fully loaded at all the times. In order to balance the load, some UEs which are in the cell edge region are offloaded from the heavily loaded Femtos to one of less loaded neighboring Femtos. In traditional *coupled* access systems, the uplink power of offloaded UEs might increase because the *target* Femto after offloading is typically far from the UE than the *serving* Femto. But DUD access helps the offloaded UE to get the downlink access from the *target* Femto while the uplink access is still from the same *serving* Femto, thereby decreasing the battery depletion at UE.

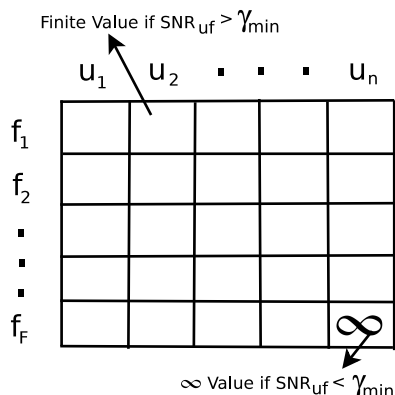


Figure 2.9: $minRB_{uf}$ matrix of UEs in Femtocell Network

2.4.1 Downlink Offloading Algorithm for DUD Access System

The offloading algorithm runs at the Femto-GW every n Transmission Time Intervals (TTIs). We assume that the channel gain remains static for the next n TTIs. Using the channel gain, the Femto-GW can calculate SNR of a UE from each Femto. We use SNR_{uf} to denote SNR of UE u from Femto f . Using SNR_{uf} , Femto-GW can calculate the amount of data [48] that can be sent in one Resource Block (RB) in DL to UE u . Based on this information, the minimum number of RBs required to guarantee the minimum data rate to UE u can be calculated. Let $minRB_{uf}$ be the minimum number of RBs required from the *serving* Femto f to maintain the minimum

data rate for UE u . Then,

$$\text{minRB}_{uf} = \frac{\text{Data Demand}_u}{\text{Data sent in one RB}} \quad (2.40)$$

Where, Data Demand_u is the minimum data demand of user u (*i.e.*, product of required data rate and time period (nTTIs)) and $\text{Data sent in one RB}$ can be calculated using SNR_{uf} . minRB_{uf} matrix can be constructed using minRB_{uf} values as shown in Figure 2.9.

Before running the offloading algorithm, initially every UE is attached to some *-serving* Femto. TotDemand_f is the total RB demand in Femto f from its UEs and it can be calculated as,

$$\text{TotDemand}_f = \sum_{u \in u_f} \text{minRB}_{uf} \quad (2.41)$$

Where, u_f is the set of UEs connected to Femto f . A cell is heavily loaded if the TotDemand of the cell is more than \bar{R} , where, \bar{R} is the total number of available RBs in a Femto over n TTIs. We also define another variable, TED, which is used to calculate the total excess demand in the system.

$$\text{TED} = \sum_{f=1}^{|F|} \max(\text{TotDemand}_f - \bar{R}, 0) \quad (2.42)$$

The proposed offloading algorithm is given in Algorithm 1. The Femtos are arranged in decreasing order based on their TotDemand_f values. If TotDemand_f is more than \bar{R} for a Femto f , then the Femto is picked for offloading some of its UEs. From the minRB matrix find (u^*, f^*) such that $u^* \in u_f, f^* \in F - \{f\}$ and $\text{minRB}_{u^*f^*}$ is minimum. Now check if the total RB demand of Femto f^* exceeds \bar{R} if the user u^* is offloaded to f^* . If it does not exceed \bar{R} , then handover the UE u^* to Femto f^* and update TotDemand_{f^*} and TotDemand_f . If it exceeds \bar{R} , then assign a large value (*e.g.*, ∞) to $\text{minRB}_{u^*f^*}$ so that the (UE, Femto) pair is not chosen again. Now choose the next best (u^*, f^*) pair and proceed. After transferring a UE if the updated TotDemand_f is less than \bar{R} , select the next Femto. After traversing across all the Femtos, calculate the TED value. Stop the Algorithm 1 if $\text{TED} = 0$ *i.e.*, every Femto has sufficient RBs to satisfy the user demand. If $\text{TED} \neq 0$, go to step one to repeat Algorithm 1. Stop Algorithm 1 if the TED value remains the same for two successive iterations.

Table 2.2: Simulation Parameters

Parameter	Value
Building dimensions	120 m \times 80 m \times 6m
Sub-region dimensions	5 m \times 5m \times 3m
Number of Sub-regions	384
Number of floors in building	Two
Indoor path loss (α)	3.5
Number of rooms	48
Femto Transmit Power	20 dBm
Downlink SNR threshold (γ_{min})	-2 dB
UEs distribution in building	Uniform
LTE mode	FDD
Femto Bandwidth	5 MHz (25 RBs)
Simulation time	100 s

2.4.2 Time Complexity of the Offloading Algorithm

The time complexity of the proposed offloading algorithm is as follows:

Time taken to compute $minRB$ matrix is $O(N * |F|)$, where, N is the total number of users. Number of users who have to be compared for offloading is $O(N^2)$ and the number of comparisons (with neighboring Femtos) that have to be made for each user is $O(|F|^2)$. Hence, the total time complexity of the offloading algorithm is $O(N^2 * |F|^2)$.

2.5 Experimental Setup and Performance Results

The system model described in Section 2.3 has been simulated using MATLAB. Table 2.2 shows the simulation parameters used in this experimental setup. The optimal Femto co-ordinates are obtained by solving the proposed MILP model (Equation (2.39)) with GAMS tool which uses CPLEX solver [33]. The GAMS CPLEX solver is a high-level modeling system for optimization and utilizes branch and bound framework for solving MILP based optimization problems. This MILP optimizer has the capability to solve large and numerically difficult MILP models with features including settable priorities on integer variables, choice of different branching, and node selection strategies. Thus the CPLEX solver in GAMS is ideal for our purpose of solving a large MILP model with many equations and variables.

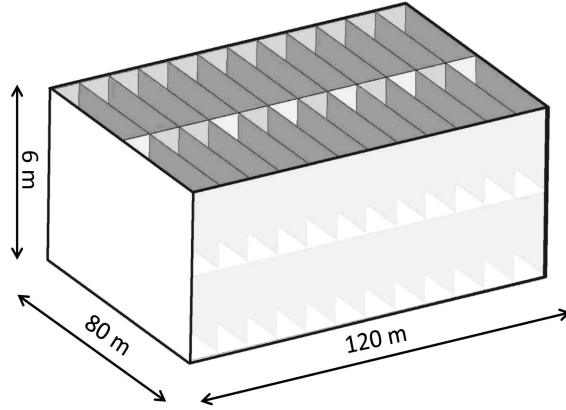


Figure 2.10: Two-storey Building

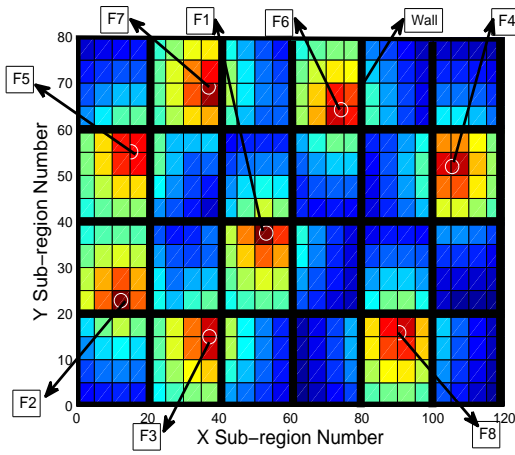


Figure 2.11: SNR distribution and Femto locations given by MILP model for uniform UE distribution on the floor #1

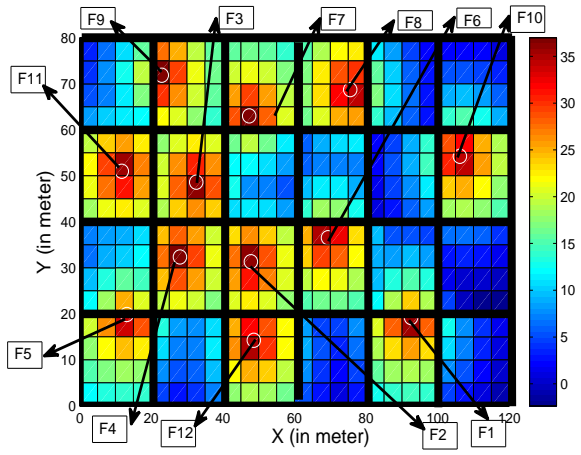


Figure 2.12: SNR distribution and Femto locations given by MILP model for uniform UE distribution on the floor #2

2.5.1 Optimal Femto Placement

To represent an enterprise scenario, we have considered a two-storey building of dimensions $(120 \text{ m} \times 80 \text{ m} \times 6 \text{ m})$ with walls as shown in Figure 2.10. Each of its sub-regions are of dimensions $(5 \text{ m} \times 5 \text{ m} \times 3 \text{ m})$. We present placement results for both uniform and non-uniform UE distributions inside the building. As UE density (*i.e.*, p_{ijk}) is factored into the proposed optimal Femto placement model, non-uniform UE distribution case could lead to cover holes inside the building.

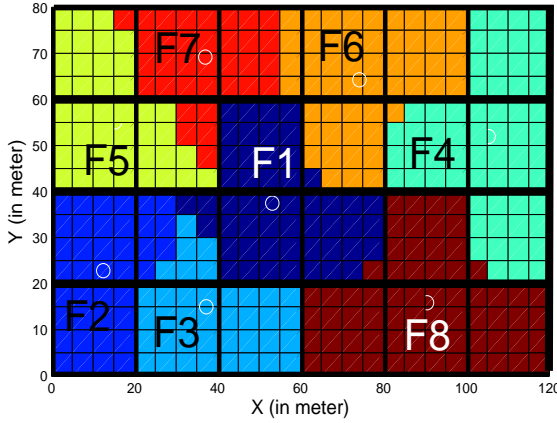


Figure 2.13: Femto Connectivity Region for uniform UE distribution on the floor #1

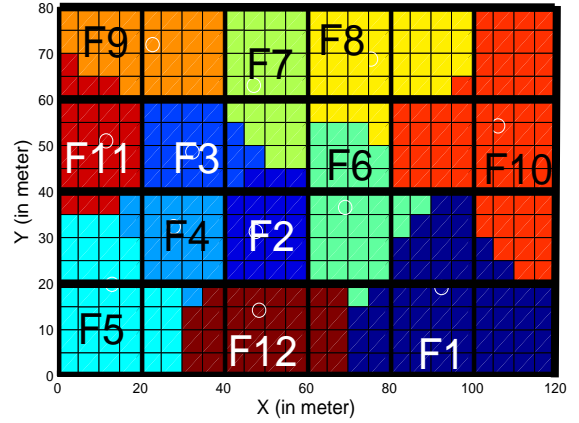


Figure 2.14: Femto Connectivity Region for uniform UE distribution on the floor #2

A. Uniform UE Distribution

For this case, the average user density on the floor #1 of the building is 1.2 UEs per sub-region and on the floor #2 is 1.9 UEs per sub-region. The reason for having different average UE density on different floors is to analyze the performance of our offloading algorithm. Proposed MILP placement model has given 20 Femtos as optimal to cover both the floors *i.e.*, 8 Femtos to cover the entire floor #1 ($|F| = 8$ *i.e.*, $F1, F2, \dots, F8$) as shown in Figure 2.11 and 12 Femtos to cover the floor #2 ($|F| = 12$ *i.e.*, $F1, F2, \dots, F12$) as shown in Figure 2.12. Figure 2.11 also shows SNR heat map on the floor #1 along with Femtos locations. The darker regions in SNR heat map represent the Femto locations with high SNR. In Figure 2.11, the Femtos $F1$ and $F2$ are deployed very close to the walls. For users within the boundaries of the four walls in which the Femto is present, a good SNR in the range of 15 to 35 dB can be guaranteed. But, when the signal has to cross a wall to reach the user, the range of SNR that can be guaranteed decreases drastically to -2 to 15 dB. This is because the signal attenuates faster and degrades the signal strength in the presence of walls. As the distance increases from the Femto, most of the sub-regions on the floor #1, get only 0 to 5 dB. Similar trend can be observed on the floor #2, refer Figure 2.12.

Figure 2.13 shows the connectivity region of each of the Femtos on the floor #1. The same colored sub-regions are connected to the same Femto *i.e.*, UEs in these sub-regions get connected to the same Femto when we consider high SNR as the criteria

for association to a Femto. The average number of sub-regions served by a Femto on floor #1 is more when compare to floor #2, which is due to the large deployment of Femtos in the latter. Similarly, the connectivity region of the floor #2 is shown in Figure 2.14.

B. Non-uniform UE Distribution

If the density of UEs is non-uniform (e.g., random), the proposed MILP model for Femto placement still works and provides placement, however, it may lead to coverage holes inside the building. To demonstrate this, we took non-uniform distribution of UEs as shown in Figure 2.15. Here we assumed that there are no UEs in the center region of a floor in the building (represented by blue color in Figure 2.15). Based on this UE density, Figure 2.16 shows the total number of Femtos required (*i.e.*, $|F|=8$) as per the proposed Femto placement model and their connectivity regions. Figure 2.17 shows SNR distribution across sub-regions inside the building. The darker regions in SNR heat map represent the Femto locations with high SNR values. The SNR observed in the center region of the building is < -5 dB (*i.e.*, coverage hole). Because our placement model has not considered those sub-regions (*i.e.*, center), it does not deploy Femtos in center region to guarantee minimum SNR.

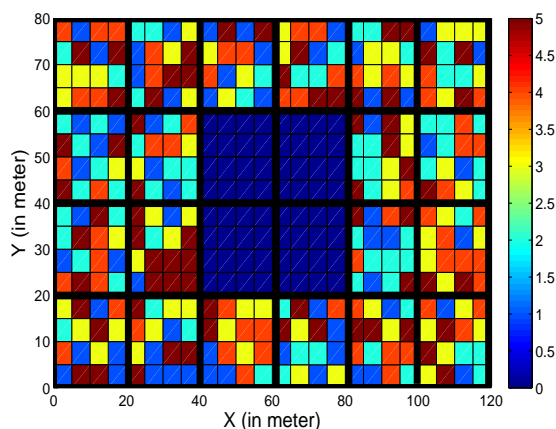


Figure 2.15: A building's floor with non-uniform UE distribution

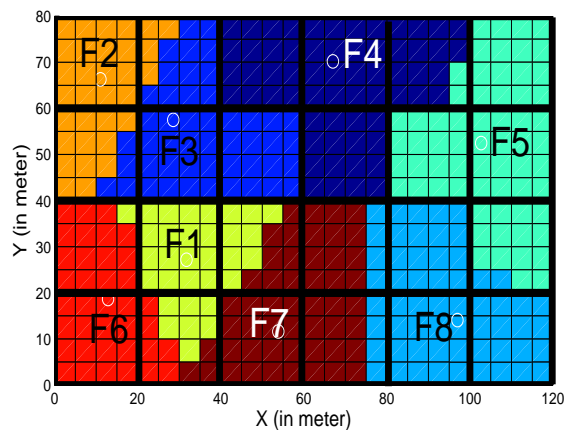


Figure 2.16: Femto connectivity region for non-uniform UE distribution given in Figure 2.15

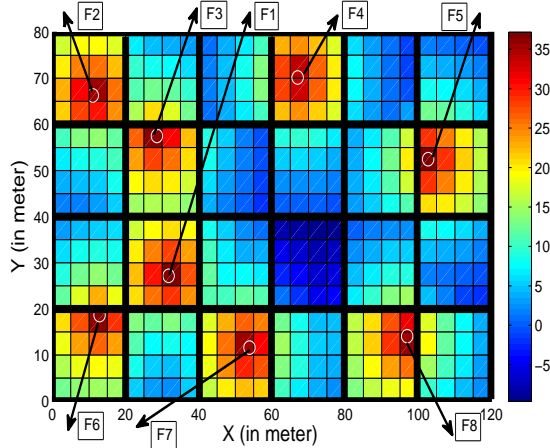


Figure 2.17: SNR distribution and Femto locations given by optimal Femto placement model for non-uniform UE distribution given in Figure 2.15

2.5.2 Comparison of Coupled and Decoupled Access Systems in Uniform Traffic Scenario

In the following, we consider Femto deployment by assuming uniform UE distribution to avoid coverage holes inside the building and study the performance of the coupled and decoupled systems in the case of uniform UE traffic demand in the network.

A. Performance of the Proposed Offloading Algorithm

In order to analyze the performance of our proposed offloading algorithm we have considered the UE distribution as shown in Figures 2.18 and 2.19 for floor #1 and floor #2, respectively. The placement of Femtos which is based on a uniform distribution of UEs having same data demand implies that the load across all Femtos is uniform. To evaluate the efficiency of our proposed offloading algorithm, the assumptions of a uniform UE distribution and an equivalent data demand cannot be employed. To show the potential of proposed offloading algorithm, we assumed non-uniform UE distribution with fixed traffic demand (*i.e.*, 400 Kbps) per UE.

(a) UE Connectivity Before and After Offloading

Figure 2.20 shows the user downlink connection before and after offloading on floor #1. The red lines show the offloaded UEs and their corresponding *target* Femtos after offloading. The Femtos $F1$, $F3$, $F4$, $F5$ and $F7$ are lightly loaded with lesser user

count, but the other Femtos ($F2$, $F6$ and $F8$) are heavily loaded. Proposed offloading algorithm chooses an efficient and closest downlink pair (u^* , f^*) by checking the load of all the users from the overlapping neighboring Femtos in such a way that the throughput and load are well balanced. The reason for the offloading algorithm to choose the shortest downlink attachment is due to efficient usage of RBs. Otherwise, it requires more bandwidth (RBs) from the neighboring Femtos due to less SNR. For example, the Femto $F2$ is heavily loaded but the neighboring Femtos ($F3$ and $F5$) are lightly loaded. Our offloading algorithm offloads 5 UEs ($u1$, $u2$, $u3$, $u4$ and $u5$) to Femtos $F3$ and $F5$. Similarly, $F1$ chooses one cell edge UE ($u6$) from $F8$ for offloading by the neighboring Femtos. Hence, in this example (*i.e.*, Figure 2.20), the total number of offloaded downlink user-Femto pair is represented as $U1$, $U2$, \dots , $U7$ respectively.

Figure 2.21 shows the downlink offloading on floor #2. Here, most of the Femtos ($F1$, $F7$, $F9$, $F10$, $F12$) are heavily loaded due to large number of UEs. Observations similar to the ones made for floor #1 scenario can be made in this case as well.

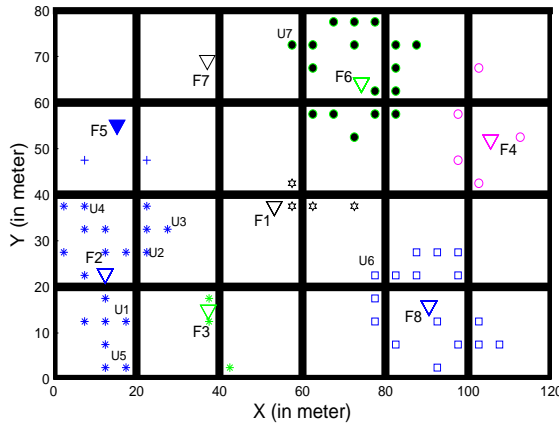


Figure 2.18: UE Distribution on floor #1 for uniform traffic pattern

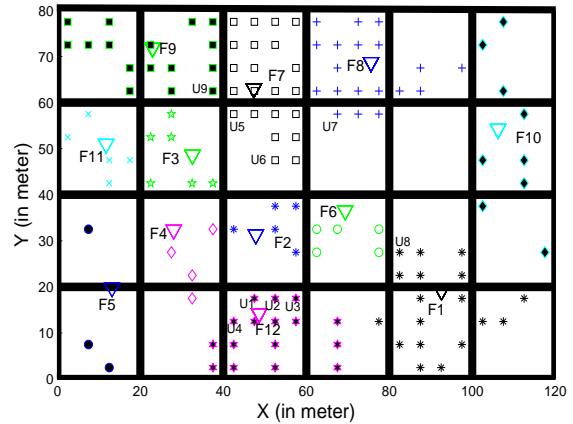


Figure 2.19: UE Distribution on floor #2 for uniform traffic pattern

(b) Required RBs in each Femto

Figure 2.22 shows the required RBs for each Femto ($TotDemand_f$) on floor #1 before and after offloading. Before offloading, Femtos $F2$, $F6$ and $F8$ require excess number of RBs (*i.e.*, 3400000 RBs which is greater than the limit¹ \bar{R} , 2500000 RBs)

¹The limit depends on spectrum bandwidth allotted for each Femto by the network operator. In our scenario the total amount of bandwidth is 5 MHz (*i.e.*, 25 RBs). Simulation is done for 100 s. Hence, the total no. of available RBs is 2500000 RB.

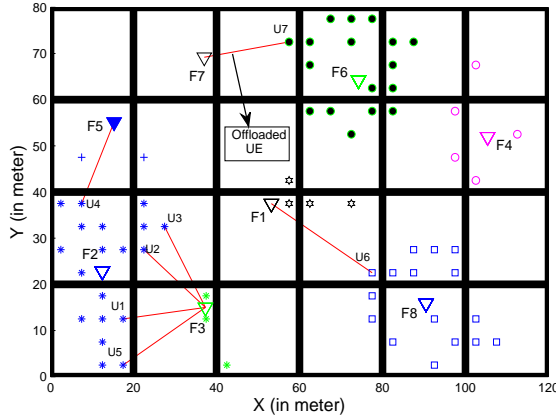


Figure 2.20: UE Connectivity before and after Offloading on floor #1 for uniform traffic pattern

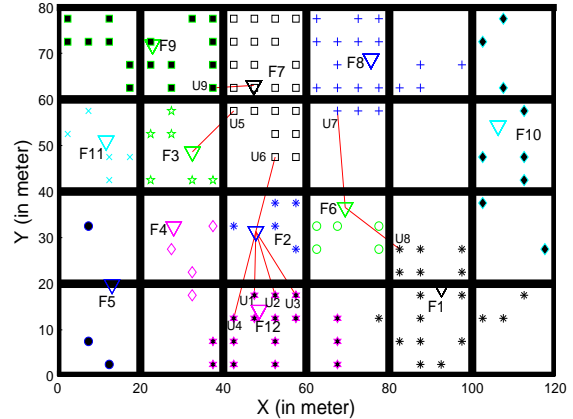


Figure 2.21: UE Connectivity before and after Offloading on floor #2 for uniform traffic pattern

due to heavy load and less DL SNR. Femto $F2$ has two overlapping *target* Femtos (*i.e.*, $F3$ and $F5$) as shown in Figure 2.20. But, the Femtos $F3$ and $F5$ are lightly loaded and require only 400000 RBs and 200000 RBs, respectively, which is lesser than the limit, 2500000 RBs. Hence, the *target* Femtos can share the RBs with the heavily loaded *serving* Femto $F2$ which brings down $F2$'s requirement to 2200000 RBs. Similarly, $F6$ also needs excess RBs due to heavy load (refer Figure 2.20). The overlapping Femto $F7$ can balance the load by sharing their RBs. Hence, minimum data rate (*i.e.*, 400 Kbps) is maintained for all users in each Femto. Further, to guarantee more than the minimum data rate and to ensure fairness among all UEs, the operator should incorporate scheduling algorithm like proportional fair during offloading. Similar pattern can be observed on floor #2 for Femtos $F12$, $F7$ and $F8$ (Figure 2.23).

(c) Downlink User Count

Figure 2.24 shows the user count on floor #1 for different Femtos before and after offloading. If we observe Figure 2.24, the number of users in Femto $F2$ is very high before offloading. After offloading with *target* Femtos $F3$ and $F5$, five users have been offloaded. This reduces the load in the overloaded Femto $F2$ and the QoS demand for the remaining connected users in Femto $F2$ is guaranteed.

Similarly, Figure 2.25 shows the user count on floor #2 for different Femtos before and after offloading. The load on Femtos $F1$, $F7$, $F9$, $F10$ and $F12$ is high due to higher number of users. Since $F2$ is closer, more number of users from $F12$ got offloaded to $F2$.

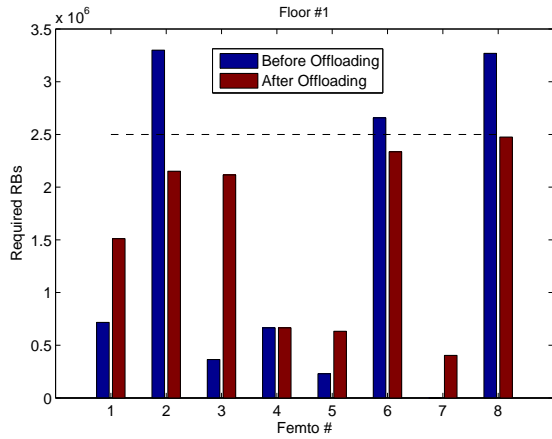


Figure 2.22: $TotDemand_f$ of each Femto before and after offloading on floor #1 for uniform traffic pattern

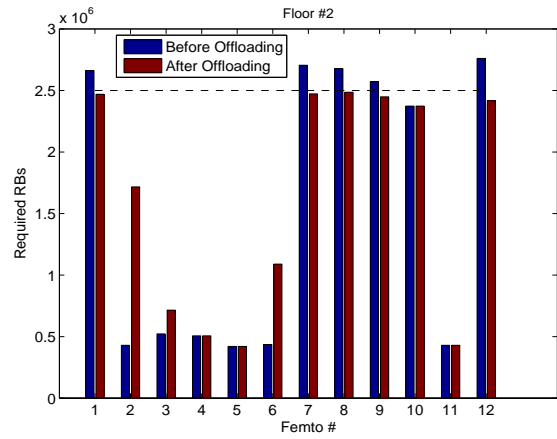


Figure 2.23: $TotDemand_f$ of each Femto before and after offloading on floor #2 for uniform traffic pattern

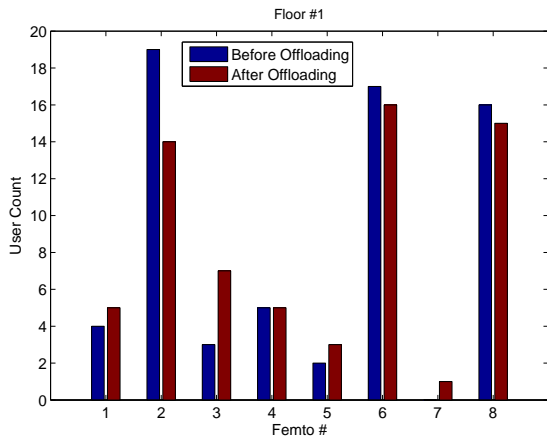


Figure 2.24: Downlink user count in each Femto before and after offloading on floor #1 for uniform traffic pattern

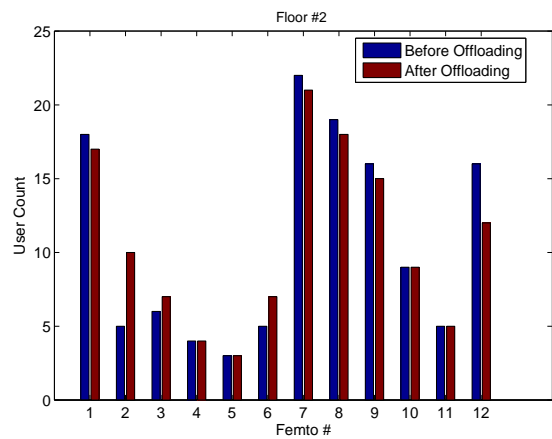


Figure 2.25: Downlink user count in each Femto before and after offloading on floor #2 for uniform traffic pattern

B. Comparison between Coupled and Decoupled Access Systems

We show uplink SNR of the offloaded UEs when they transmit with full power in *coupled* and *decoupled* access systems. For the fixed uplink SNR, we also show the advantages in terms of the transmission power when UEs are in *coupled* and *decoupled*

access systems.

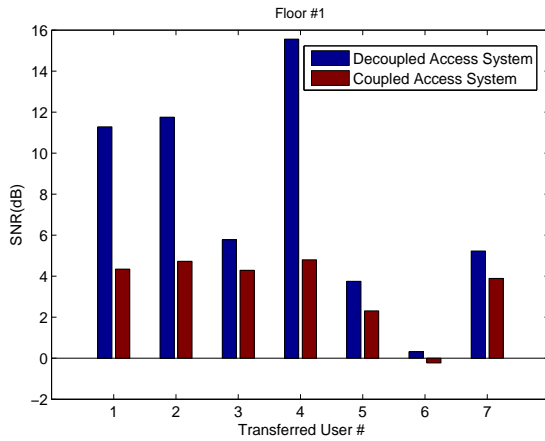


Figure 2.26: Maximum Achieved Uplink SNR in *coupled* and *decoupled* access systems on floor #1 for uniform traffic pattern

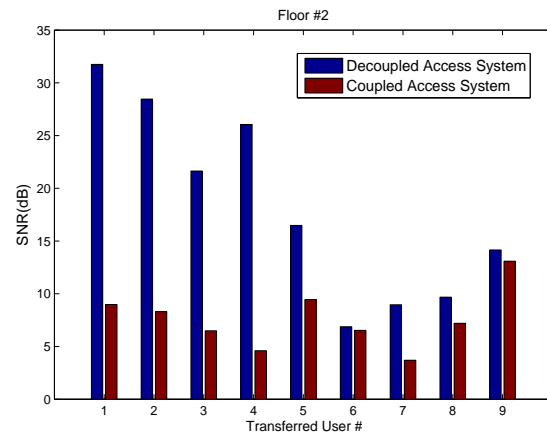


Figure 2.27: Maximum Achieved Uplink SNR in *coupled* and *decoupled* access systems on floor #2 for uniform traffic pattern

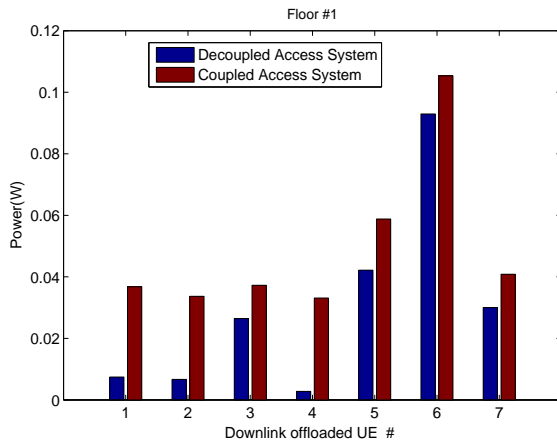


Figure 2.28: Power emitted by UE in *coupled* and *decoupled* access systems on floor #1 for uniform traffic pattern

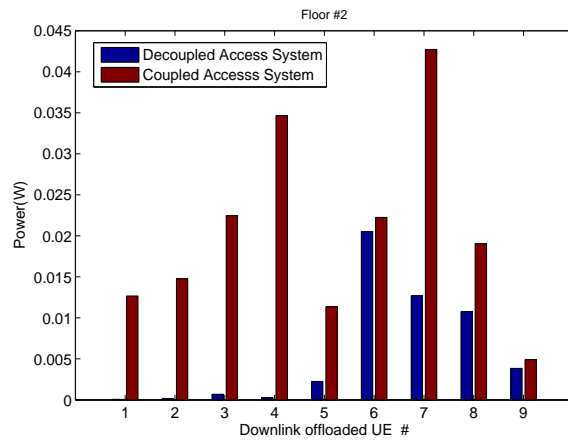


Figure 2.29: Power emitted by UE in *coupled* and *decoupled* access systems on floor #2 for uniform traffic pattern

(a) *Maximum Achieved Uplink SNR*

Figure 2.26 shows the maximum SNR that the UEs can achieve in full power transmission mode on floor #1 for coupled and decoupled (DUD) systems. Due to heavy load in $F8$, the user ($u6$) got offloaded to $F1$. The user $u6$ receives roughly +1 dB SNR during uplink from *-serving* Femto $F8$ because it has to cross 2 walls. Thus

for the same uplink transmission power, when it gets connected to the *target* Femto, it receives very less *i.e.*, roughly -1 dB SNR because it is located in the cell edge of Femto *F1*.

Figure 2.27 shows the maximum SNR achieved on floor #2. As the Femtos are densely deployed on floor #2, the inter distance between the Femtos is less (refer Figure 2.21). This assists most of the users to achieve better SNR when compared to users on floor #1. Even after offloading 9 users, all of them are able to achieve decent SNR values. Compared to *decoupled* access system, uplink SNR has decreased by 52% in *coupled* access system.

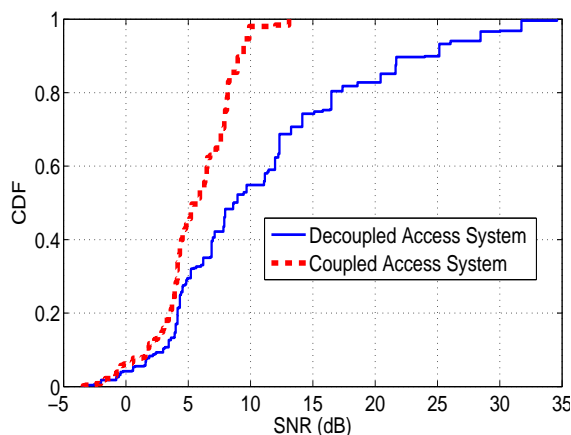


Figure 2.30: CDF of the maximum Achievable Uplink SNR in *coupled* and *decoupled* access systems

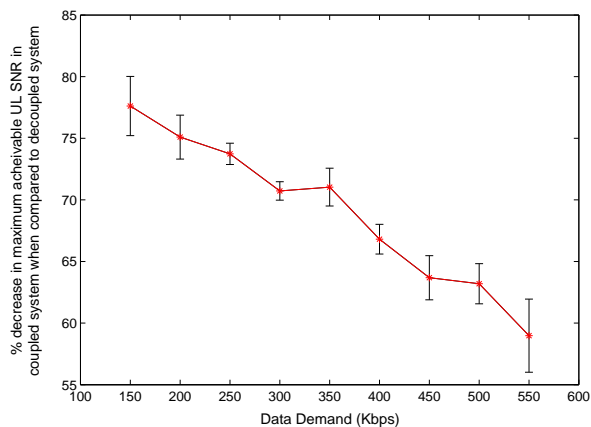


Figure 2.31: % Decrease in the maximum achievable Uplink SNR in *coupled* system when compared to *decoupled* system for Different Data Demands

(b) Uplink Power to maintain 0 dB SNR

Figure 2.28 shows the uplink power emitted by the downlink offloaded UEs to maintain *SNR* of 0 dB on floor #1. In this scenario, the *-serving* Femto always allows UEs to transmit with less power due to shorter distance. For example, to maintain *SNR* = 0 dB, the UE *u6* transmits at 0.09 W to the *-serving* Femto. If the same UE wants to connect with the *target* Femto, it has to transmit with power > 0.1 W. However, according to 3GPP standard, the user cannot transmit > 0.1 W. Hence, user cannot maintain communication with the *target* Femto. To maintain communication with the *target* Femto, the user has to tune its *SNR* threshold to less than 0 dB.

Figure 2.29 shows the uplink power emitted by the downlink offloaded UEs to maintain *SNR* of 0 dB on floor #2. Due to dense deployment of Femtos and less

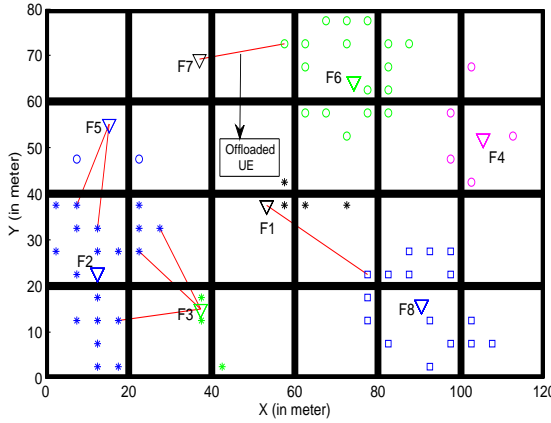


Figure 2.32: UE Connectivity before and after Offloading on floor #1 for non-uniform traffic pattern

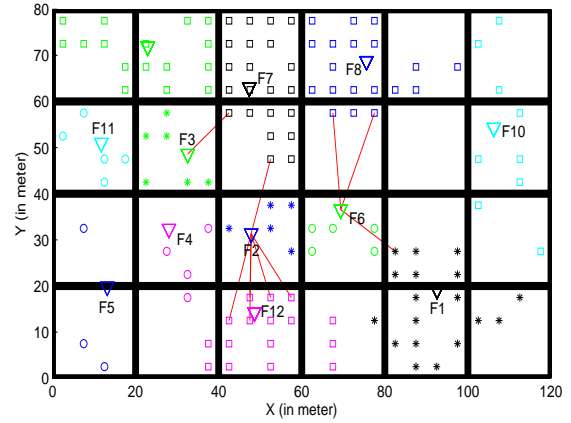


Figure 2.33: UE Connectivity before and after Offloading on floor #2 for non-uniform traffic pattern

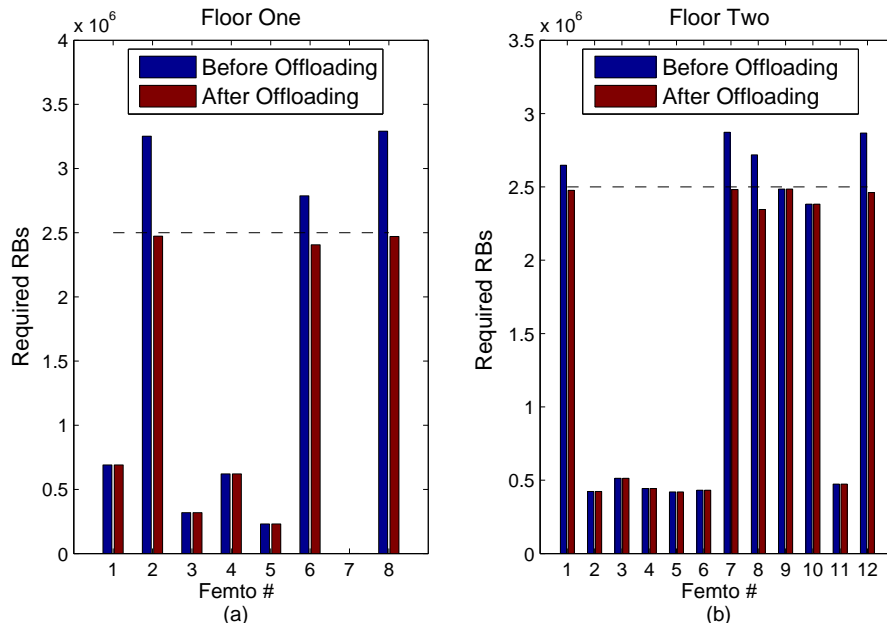


Figure 2.34: $TotDemand_f$ of each Femto before and after offloading on floor #1 and floor #2 for non-uniform traffic pattern

inter distance between them, the uplink power is reduced drastically when compared to floor #1. For example, most of the UEs are allowed to transmit with less power (*i.e.*, 0.025 W) in closer Femto. As the UE battery power plays an important role in wireless communication, we allow the UEs to communicate in uplink to the closer Femto. Thus DUD access system helps in saving power of UEs. Compared to *coupled* access system in uplink power has reduced by 56% in DUD access system.

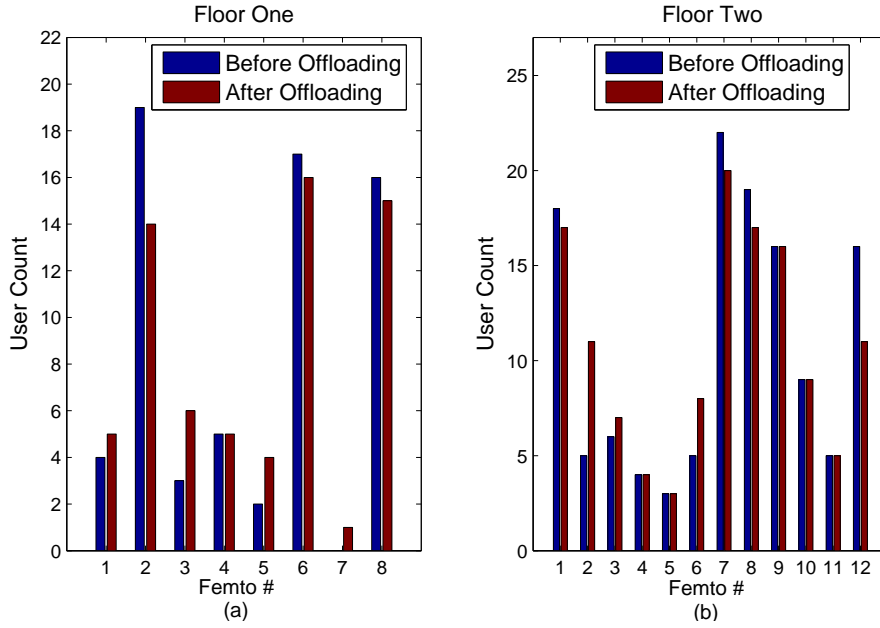


Figure 2.35: User count in each Femto before and after offloading on floor #1 and floor #2 for non-uniform traffic pattern

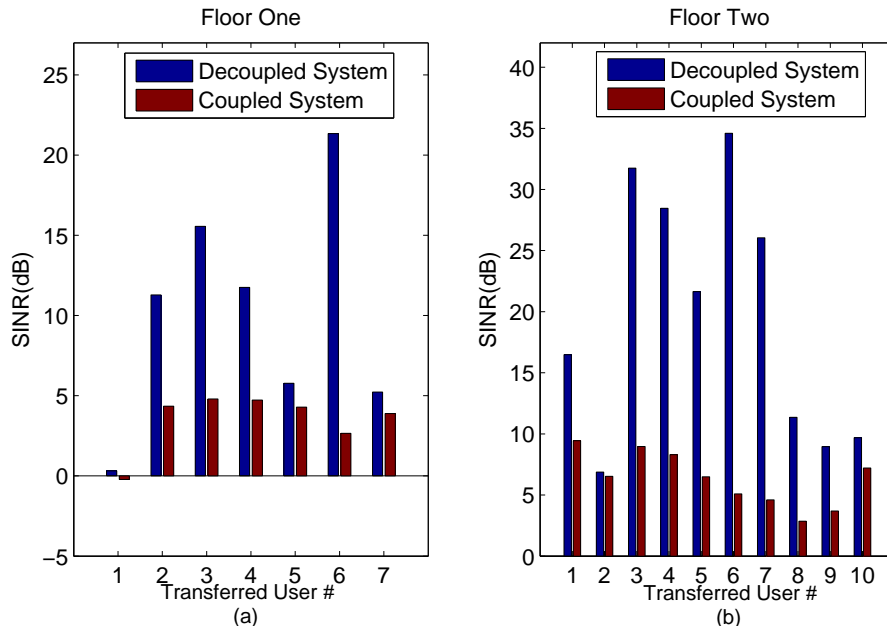


Figure 2.36: Maximum Achieved Uplink SINR in *coupled* and *decoupled* access systems on floor #1 and floor #2 for non-uniform traffic pattern

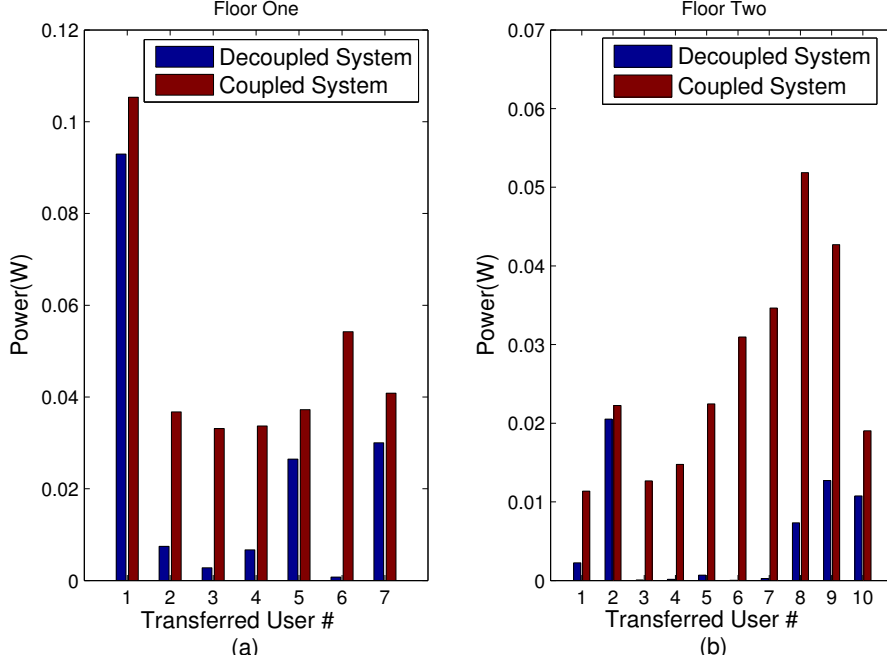


Figure 2.37: Power emitted by UE in *coupled* and *decoupled* access systems on floor #1 and floor #2 for non-uniform traffic pattern

C. Average Performance of the Proposed System

We performed simulations for 30 different scenarios (*i.e.*, UE distribution is varied arbitrarily by changing seed values) by keeping minimum data rate as 400 Kbps and the following are the results.

Figure 2.30 shows the CDF of the maximum uplink SNR achieved in full power transmission mode by the transferred UEs in the *DUD access system* and the *coupled access system*. On an average, compared to *DUD access system*, the maximum achievable uplink SNR has decreased by 64% in *coupled access system*. For a fixed uplink SNR threshold (*i.e.*, 0 dB), on an average, the UE transmission power has reduced by 70% in *DUD access system* when compared to the *coupled access system*.

We then vary minimum traffic rate from 150 Kbps to 550 Kbps in the steps of 50 Kbps in 9 experiments in such a way that all UEs in any given experiment generate fixed traffic in the above interval of (150 Kbps to 550 Kbps). Each experiment was ran for 30 seeds. In Figure 2.31, X-axis shows the variation in traffic demand and Y-axis shows the percentage decrease in achievable uplink SNR in *coupled access system* when compared to the proposed *DUD access system*. It is plotted with 95% confidence intervals.

2.5.3 Comparison of Coupled and Decoupled Access Systems in Non-uniform Traffic Scenario

In the following, we consider Femto deployment given by uniform UE distribution and compare the performance of the DUD system with coupled system in the case of non-uniform UE traffic demand *i.e.*, 300 to 500 Kbps.

As in Section 2.5.2, the same optimal placement model is used with the assumption of uniform UE distribution. The UE distribution on floors #1 and #2 is same as shown in Figures 2.18 and 2.19. We assumed that the traffic rates are varied from 300 Kbps to 500 Kbps in the steps of 10 Kbps. That means UEs arbitrarily select some traffic rates in the interval of (300 Kbps to 500 Kbps). Figure 2.32 shows the user downlink connection before and after offloading on floor #1. Similarly, Figure 2.33 shows the user downlink connection before and after offloading on floor #2. Note that all the observations are similar to what had been reported for the uniform UE distribution and only the offloading UEs will differ based on the traffic load (*i.e.*, traffic pattern).

Figure 2.34 (a) and Figure 2.34 (b) show the required RBs for different Femtos ($TotDemand_f$) on floor #1 and floor #2, respectively before and after offloading. Figure 2.35 (a) and Figure 2.35 (b) show the user count on floor #1 and floor #2, respectively for different Femtos before and after offloading. We show the SNR of the offloaded UEs when they transmit with full power in *coupled* and DUD access systems. For the given fixed uplink SNR, we also show the advantages in terms of the transmission power when UEs are in *coupled* and *decoupled* access systems. Figure 2.36 (a) and Figure 2.36 (b) show the maximum SNR of the transferred UEs can achieve in full power transmission mode. Similarly, Figure 2.37 (a) and Figure 2.37 (b) show the uplink power emitted by the transferred UEs to maintain $SNR = 0$ dB for floor #1 and floor #2.

2.6 Summary

In this chapter, considering realistic constraints, we have provided an MILP model for the optimal placement of Femtos based on user occupant probabilities inside an enterprise building scenario to achieve desirable signal strength for all the users. We established DuD connections based on the shortest-path loss Femto for the uplink

access and a less loaded neighboring Femtos for the downlink access. We conducted extensive experiments in MATLAB based LTE system simulator to demonstrate the benefits of proposed optimal placement model. On average we observed 70% energy savings in *decoupled* access system when compared to the traditional *coupled* access system.

Chapter 3

Handover and SINR Optimized deployment of LTE Femtocells

3.1 Introduction

In the previous chapter, we proposed an optimal Femto placement model which did not consider the impact of co-tier and cross-tier interference. Also we assumed the users are static in nature. In this chapter, we consider co-tier interference among neighboring Femtos but no cross-tier interference (*i.e.*, Macro and Femtos are assumed operating in different frequency bands) and formulate two ILP optimization models for Femto placement: first, Minimize the Number of Femtos (MinNF) model and second, Optimal Handover (OptHO) model. MinNF model guarantees a certain minimum SINR for each region inside the building while minimizing the number of Femtos needed for coverage of the entire enterprise building.

A major issue in enterprise building is frequent or unnecessary handovers (*i.e.*, ping pong effect [49]), which may happen when user moves from one room to another room or within the same room and similarly in the corridors of the building. This leads to degradation of performance like service interruption during signaling overhead [50], decrease in throughput and increase in number of handovers [51]. Hence, in order to avoid the unnecessary handovers (*i.e.*, handovers happening within the same room or in corridors) in enterprise buildings, Femtos should be placed by considering an additional constraint. Hence, we add Handover (HO) constraint to the MinNF model which reduces the number of handovers and at the same time guarantees good SINR to all UEs inside the building. This MinNF model along with HO constraint is referred as OptHO model in this chapter.

3.1.1 Organization of this chapter

Rest of the chapter has been organized as follows. Section 3.2 describes the notable research literature relevant to our study. Section 3.3 discusses the system model and proposed ILP formulation for MinNF. Section 3.4 presents experimental setup and numerical results for MinNF. Section 3.5 explains the user mobility model and proposed ILP formulation for OptHO. Section 3.6 demonstrates the experimental setup and numerical results for OptHO. Finally, Section 3.7 summarizes the work.

3.2 Related Work

Considering MBS and Femto-to-Femto interference plays a key role in small cell planning, in [52], Femtos are placed in a multi-storey enterprise building by not considering co-tier and cross-tier interferences. Authors of [34,53], considered the interference among MBSs to achieve better throughput in the system. In [32], the authors investigated a joint Femto placement and power control optimization problem in enterprise buildings with the aim to prolong UEs' battery life. They proposed a novel two-step reformulation approach to convert the original Mixed Integer Non-Convex Problem (MINCP) into a MILP and then devised a global optimization algorithm by utilizing the MILP. But their system model did not consider co-tier and cross-tier interferences. In [53], the locations of the pico cells are moved iteratively. This way they reduce the interference to maximize the network throughput of the users in outdoor and indoor environments. However, in that work the placement of pico cells in indoor environments and the traffic pattern are not considered. In [34,35], Guo et. al. suggested an automated small cell deployment model which attempts to find the optimal location of a new cell, subject to knowledge about the locations of existing cells, UEs and the building environment. A closed-form equation is given for the new cell's deployment location which is a function of transmit power, transmission scheme and path loss parameters.

In [54], the transmission power of randomly placed Femtos is optimized. This is to avoid interference and guarantee certain minimum SINR threshold for indoor UEs. But as the available bandwidth gets split into three parts (*i.e.*, because the reuse factor is three), there could be inefficient usage of the spectrum. And because Femtos are placed randomly, the number of Femtos to obtain threshold SINR may not be minimal. Path loss factors such as obstructions (walls) inside the building are also not considered in the model while solving the optimization problem.

In [55], a joint Femto placement and power control model was proposed for guaranteeing SINR threshold depending on varying user occupancy in each region inside the building. The efficiency of the spectrum usage is improved by considering reuse factor one and the number of Femto needed for enterprise deployments also got reduced, which would reduce the overall cost. User density, interference among Femtos and MBSs and building obstructions are also given as inputs to the system model. Then authors studied the joint optimal placement and power control of Femtos to maintain a certain minimum downlink $SINR_{Th}$. The joint placement and power control will help to reduce the energy/power by Femtos and minimize the Femto count. However, doing so decreases SINR of indoors when compared to the case wherein Femtos are transmitting at the maximum power.

Large scale deployment of Femtos in enterprise environments could lead to unnecessary handovers, [26,51] which decrease the network throughput [56], increase signal overhead [50,57] and cause delay [56]. Our current literature survey includes various unnecessary handover reducing mechanisms [58–60]. The authors in [58], proposed an optimized handover algorithm based on UE mobility state for reducing unnecessary handovers and also to improve the performance of LTE femtocell network. The authors in [59], proposed a dynamic handover hysteresis margin calculation based on the UE position within cell coverage region. In [60], the authors proposed a Fuzzy Logic Controller (FLC) that adaptively modifies handover hysteresis margins for reducing handovers. The authors in [50] proposed a simplified handover algorithm based on UE mobility state for reducing unnecessary handovers and signaling overhead in two-tier LTE femtocell network. In [57], a mobility management scheme is proposed where the control point of mobility in user plane is shifted from the S-GW to the Femto-GW so that it will make the handover decision between Femtos. In high density of Femtos and two-tier LTE HeNB network, UE mobility will produce lot of signaling overhead.

In [56], a SON [61] model was proposed to mitigate unnecessary handovers inside enterprise environments with the help of building information and estimated user position information. In [62], the handover decision at FBS is based on energy efficiency and knowledge of interference. Thus handover plays a major role in enterprise buildings.

3.2.1 Contribution of this Chapter

Suggesting power saving by Femtos is not an appreciable contribution to the research community. Moreover, it also leads to decrease in average indoor SINR. We place

the Femtos optimally with all the constraints as mentioned in the system model (explained later) for MinNF and the Femtos are transmitting at full power to boost the average indoor SINR. We extend this MinNF model to bring in HO constraint thereby minimizing unnecessary handovers and boosting the throughput of the users in the building even while they are moving. To our knowledge, this is the first work that endeavors at reducing the number of handovers by placing the HO constraint as one of the input factors for the problem of placement of Femtos.

3.3 Proposed Work

In this section, we present the system model and channel model, and then describe the proposed MinNF ILP formulation to guarantee $SINR_{Th}$ to all regions inside the building.

3.3.1 System Model

This chapter considers an LTE HetNet system comprising of MBSs deployed in outdoor environment and FBSs deployed inside the enterprise building. The users inside the building are assumed to be mobile. We also assume that the location of the UE is known inside the building and the layout of the building is available to the telecom operator. The FBS and MBS are assumed to operate in the same frequency band (*i.e.*, reuse one) in LTE HetNet and therefore may experience high cross-channel interference. Table 3.1 shows the set of notations and abbreviations used in this chapter.

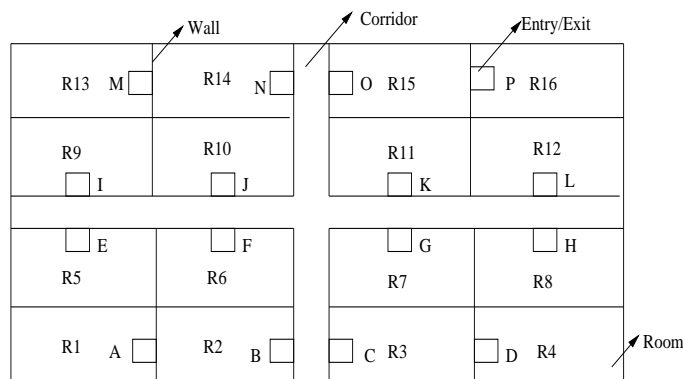


Figure 3.1: An example of enterprise building with rooms, corridors and entry/exit points

Table 3.1: Glossary of MinNF ILP Model

Notation	Definition
S	Set of all sub-regions inside the building
z_a	1 if Femto is placed at sub-region a , zero otherwise
α_{ja}	1 if j^{th} sub-region of the building is associated with the Femto located at sub-region a , zero otherwise
γ_{ja}	Channel gain between sub-regions j and a
M	Set of all Macro BSs

Let us consider a building having dimensions of $L \times W \times H$, where L , W and H are the length, breadth and height of the building, respectively. Each floor of the building is divided by walls into several rooms (for *e.g.*, R_1, R_2, \dots, R_n) and corridor as shown in Figure 3.1. Every *IUE* is allowed to move freely in the corridor. Every room has an entry/exit. For the purpose of the study, rooms and corridor are further divided logically into smaller sub-regions of length δ_x and width δ_y , which have been indexed as shown in Figure 3.2. Walls have been depicted by thick lines and sub-regions by the small squares in the building grid. Since the size of sub-region is much smaller compared to the room size, it is assumed that inside every sub-region, the SINR remains constant.

3.3.2 Channel Model

The path loss (PL) between MBS and Indoor UE (*IUE*) is given by,

$$PL_{MBS} = 40 \log_{10} \frac{d_{pl}}{1000} + 30 \log_{10} f + 49 + n\phi \quad (3.1)$$

where, d_{pl} is the distance (in meters) between the sub-region of *IUE* and MBS and the distance between the centers of two sub-regions is taken as the propagation distance, n is the number of walls in between MBS and *IUE*, f is the center frequency of MBS in MHz, ν is the number of floors and ϕ is the penetration loss.

The PL between Femto and *IUE* is given by [54]:

$$PL_{FBS} = 37 + 30 \log_{10} d_{pl} + 18.3\nu^{\frac{(\nu+2)}{(\nu+1)-0.46}} + n\phi \quad (3.2)$$

These two PL models are used in this chapter for calculating the channel gain [54] between users and various BSs by considering the effects of antenna gain for Macro and Femtos as 20 dBi and 2 dBi, respectively. The same PL models are used in rest

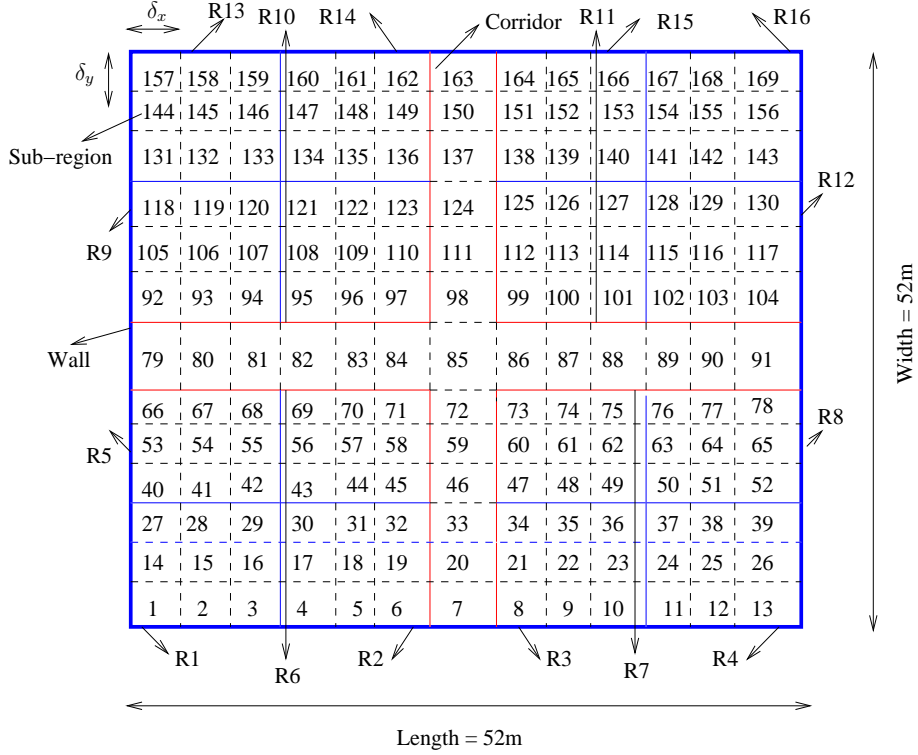


Figure 3.2: Sub-region index and dimensions of the enterprise building

of the thesis.

3.3.3 *MinNF* Placement Model

To address the optimal Femto placement problem, an optimization ILP model is formulated. By solving the ILP model, one can determine the following:

- The minimum number of Femtos needed to maintain $SINR_{Th}$ in each sub-region of the building.
- Optimal Femto locations inside the building.
- Femto to which each sub-region (*i.e.*, UEs present at those sub-regions) is associated.

Each Femto operates at the maximum transmit power (P_{max}) in order to provide good signal strength to *IUEs*. Our goal is to minimize the total number of Femtos

deployed, which is expressed by Equation (4.1).

$$\min \sum_{a \in S} z_a \quad (3.3)$$

Assuming that each sub-region is allowed to associate with only one FBS (refer Equation (3.4)) inside the building, we get:

$$\sum_{a \in S} \alpha_{ja} = 1 \quad \forall j \in S \quad (3.4)$$

$$\alpha_{ja} - z_a \leq 0 \quad \forall j, a \in S \quad (3.5)$$

Above two constraints ensure that every sub-region is connected to only one FBS. Another constraint is needed on SINR.

In this ILP model, MinNF, certain minimum $SINR_{Th}(\lambda)$ is guaranteed for all sub-regions of the building. SINR received by a particular sub-region j from the Femto located at sub-region a , is given by the L.H.S. of Equation (3.6). It guarantees coverage by maintaining a predefined $SINR$ threshold λ in each sub-region.

$$\frac{Inf * (1 - \alpha_{ja}) + \gamma_{ja} P_{max} z_a}{N_o + \sum_{b \in S \setminus a} \gamma_{jb} P_{max} z_b + \sum_{e \in M} \gamma'_{je} P_{macro}} \geq \lambda \quad \forall j, a \in S \quad (3.6)$$

In Equation (3.6), Inf is a virtual infinite value [54] (a very large value like 10^6). The reason for using $Inf * (1 - \alpha_{ja})$ is that if $\alpha_{ja} = 0$ then $Inf * (1 - \alpha_{ja})$ becomes a large value and the expression can be ignored safely. Without the virtual infinite value, Equation (3.6) tries to ensure that all the Femtos meet $SINR_{Th}$ constraint for each sub-region. But just a single Femto is enough to give $SINR_{Th}$ for any given sub-region. The ILP will always be infeasible if the virtual infinite value is not used, as not all Femtos can meet $SINR_{Th}$ constraint for a particular sub-region. Equation (3.6) can be rewritten as follows:

$$Inf * (1 - \alpha_{ja}) + \gamma_{ja} P_{max} z_a \geq (\lambda N_o + \sum_{b \in S \setminus a} \gamma_{jb} P_{max} z_b \lambda + \sum_{e \in M} \gamma'_{je} P_{macro} \lambda) \quad \forall j, a \in S \quad (3.7)$$

γ'_{je} and γ_{ja} are the channel gain from Macro and Femto, respectively. The channel gain can be estimated by using Equation (3.1) and Equation (3.2) and P_{macro} is the

power of Macro. Finally, the MinNF model is formulated as follows,

$$\min \sum_{a \in S} z_a, \text{ subject to (3.4), (3.5), (3.7).} \quad (3.8)$$

The above MinNF ILP model is solved using CPLEX solver to obtain the optimal co-ordinates of the Femtos for deploying indoors. This model is also used in many of the chapters later for efficient Femto placement.

3.4 Experimental Setup and Numerical Results

3.4.1 Building Setup

In experimental setup, we consider a single floor building within the coverage region of one MBS. In order to verify the improvement in system's throughput, we have chosen the network simulator NS-3, to create a building of dimension 52 m \times 52 m \times 4 m with 16 rooms of dimension 12 m \times 12 m \times 4 m each and two corridors of dimensions 4 m \times 52 m \times 4 m and 52 m \times 4 m \times 4 m running through the center of the building. The entire building is divided into 169 sub-regions of dimension 4 m \times 4 m \times 4 m¹ each as shown in Figure 3.2. The users in the building are served by Femtos with the transmission power of 20 dBm. In order to consider the effect of cross-channel interference, a Macro BS with transmission power of 46 dBm at a height 36 meters is placed at an euclidean distance of 300 m [14] (diagonally from the center of sub-region 1). Femtos are allowed to be fixed only to the ceilings of the rooms at a height of 4 meters. The minimum number of Femtos and corresponding sub-region indices are given by GAMS CPLEX solver [33].

3.4.2 Other Placement Schemes for Comparison

The proposed placement model is compared with the following Femto placement schemes:

- Random Placement: Femtos are placed randomly inside the building.

¹In our work, location of the center of each sub-region is given as input to the ILP CPLEX solver to find the optimal Femto location. If size of the sub-region is small, SINR remains the same throughout the sub-region but at the cost of increased time in solving ILP with large number of sub-regions. If it is large, SINR may not remain the same throughout the building even though ILP problem could be solved very easily. Hence, after some initial studies, we have taken the sub-region dimensions as 4m \times 4m \times 4m in our work.

- Center k -Means (CKM) Placement: The co-ordinates of the exact mean locations of every sub-region are given as input to k -Means clustering scheme [63] to form five clusters. These mean locations happen to be the centers of the sub-regions. The Femtos are then placed at the centroid of each cluster.

3.4.3 Performance of Placement Schemes

The metrics that we use to compare the performance of Random, CKM and MinNF based Femto placement schemes are:

- SINR: The signal strength distribution inside the building.
- Femto connectivity: The collection of sub-regions of the building served by each Femto.
- Modulation scheme: The modulation scheme used by each UE for its transmission based on observed downlink SINR value.

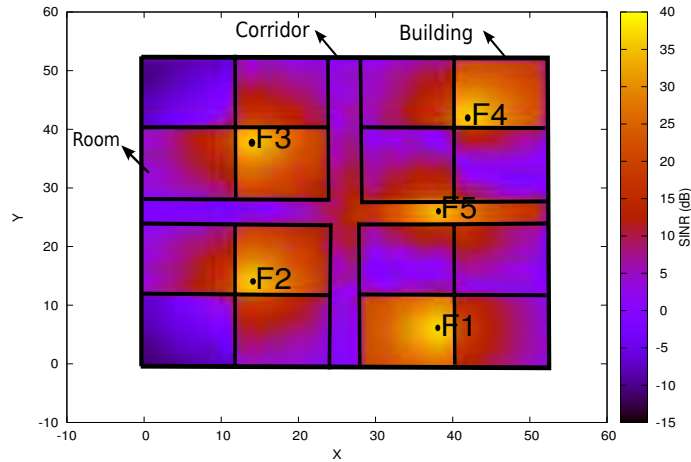


Figure 3.3: REM for CKM Placement

Radio Environmental/Heat Map for CKM and MinNF schemes

MinNF model has given five as the minimum count of the Femtos to achieve $SINR_{Th}$ (-2 dB) in each sub-region for the building considered. To have a fair comparison, we took the same count of Femtos ($F=5$) for CKM placement. Figures 3.3 and 3.4 show REM plots of the CKM placement and MinNF placement, respectively. They give the SINR distribution across the building and the dark yellow regions represent the Femto locations. The users located in those sub-regions enjoy the

highest SINR. In such a setup, as expected CKM placement of Femtos does not guarantee a $SINR_{Th}$ to all regions inside the building. As a result, certain parts of the building have coverage holes *i.e.*, SINR dropped to as low as -10 dB as shown in Figure 3.3. Moreover, in the CKM placement, UEs can experience a fluctuation in connectivity due to co-channel interference between Femtos. These issues are overcome by placing the Femtos optimally in MinNF based placement scheme. The minimum $SINR_{Th}$ is set as -2 dB in MinNF model to obtain the optimal sub-regions for Femto placement. Now, no coverage holes are present in the case of MinNF, as shown in Figure 3.4.

Modulation Scheme for CKM and MinNF:

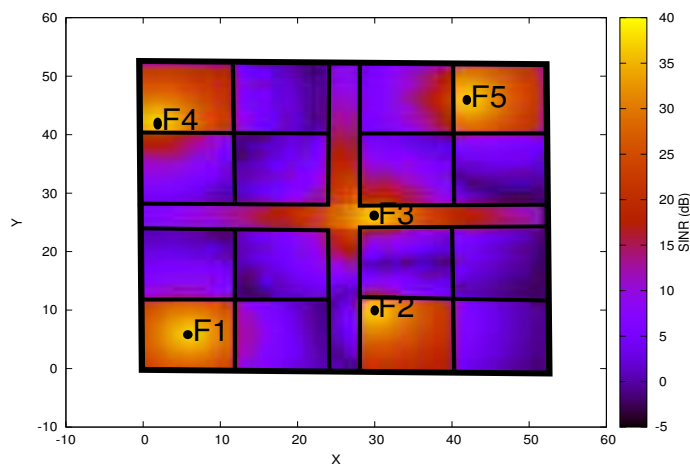


Figure 3.4: REM for MinNF Placement

Figures 3.5 and 3.6 show the modulation schemes that will be used by UEs located at different locations inside building based on the SINR values. In the CKM placement (Figure 3.5), 64-QAM modulation scheme is used near the Femto positions, as shown by the yellow regions. As the distance from the Femto BS increases, the modulation scheme used changes from 64-QAM to 16-QAM and 16-QAM to QPSK as depicted by the blue regions and the green regions, respectively. This is due to the wall penetration loss and interference between the neighboring Femtos inside the building. Also, from the given Figure 3.3 it is evident that some portions of the building get a very poor SINR which is as low as -10 dB leading to no-data regions (coverage holes). This is depicted by red colored regions. The users in these regions completely lose their connectivity to the network. Figure 3.6 shows the modulation scheme used at different points inside the building based on the SINR from MinNF placement scheme. In Figure 3.6, it is observed that a good SINR is maintained in

regions surrounding the Femtos and a reasonable SINR is maintained at other regions throughout the building, thus guaranteeing a minimum $SINR_{Th}$ of -2 dB. Thus, there are no coverage holes and there is no possible loss of connectivity to the users inside the building.

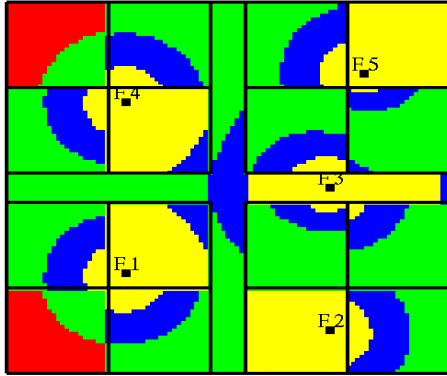


Figure 3.5: Modulation Schemes in CKM placement

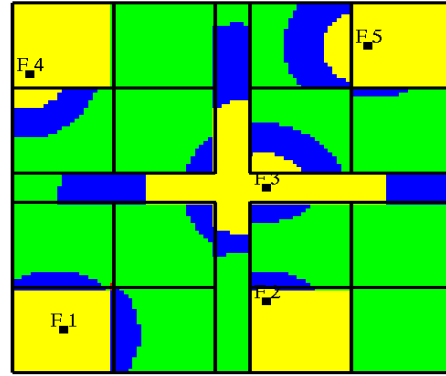


Figure 3.6: Modulation Schemes in MinNF placement

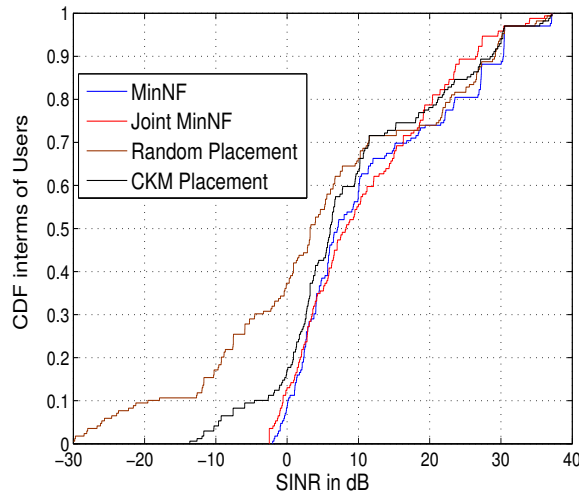


Figure 3.7: SINR CDF

SINR CDF of Various Placement Models

Figure 3.7 shows the SINR CDF of users for various placement schemes. Compared to random placement scheme, CKM placement provides better average SINR and the improvement is 87%. Compared to CKM placement, MinNF placement provides better average SINR and the improvement is 28%. We compared the SINR

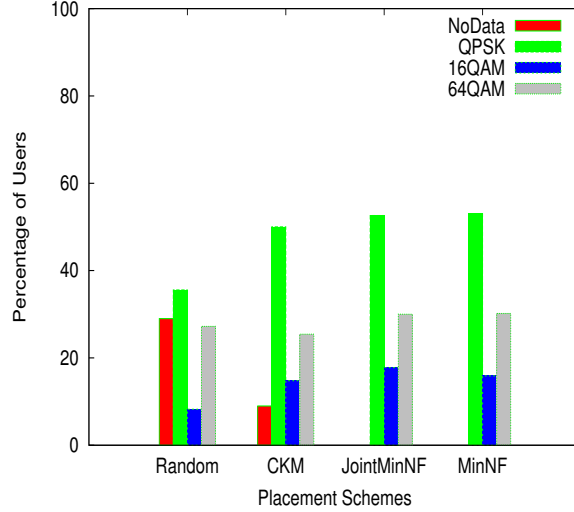


Figure 3.8: % of UEs in Employing Different Modulation Schemes

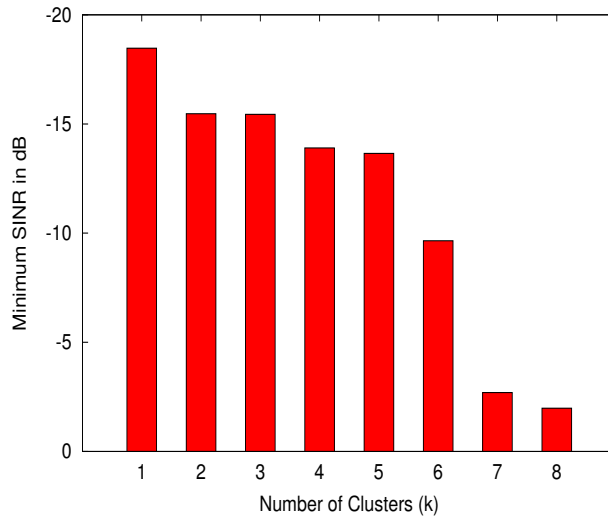


Figure 3.9: Number of Clusters (k) Vs Minimum $SINR_{Th}$

performance with our Joint Femto placement and power control model [55] (referred as Joint MinNF) and observed that MinNF performs 8% better than Joint MinNF. Joint MinNF does not perform better due to less Femto transmission power.

Figure 3.8 represents the percentage of sub-regions using each modulation scheme, based on SINR mapping to modulation scheme as given by 3GPP [64]. In random and CKM placements, some percentage of sub-regions have SINR less than -5 dB as shown in Figure 3.7, and hence they will not be able to transmit any data as shown in Figure 3.8. Hence, proposed MinNF model is better than these two schemes.

Table 3.2: Variation of No. of Femtos with $SINR_{Th}$ in MinNF

$SINR_{Th}$	Number of Femtos Required
-2 dB	5
-1 dB	5
0 dB	6
1 dB	7
2 dB	8
2 dB	8

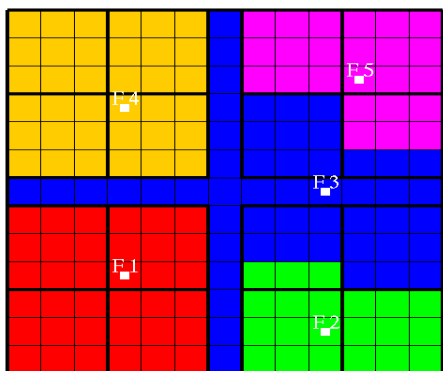


Figure 3.10: Connectivity of Sub-regions in CKM placement

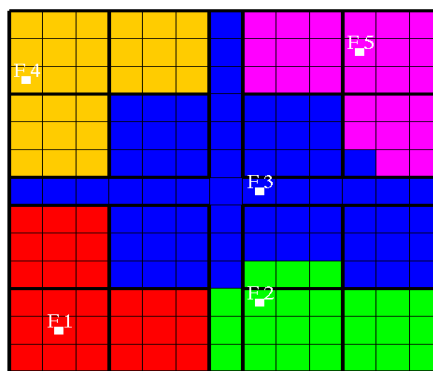


Figure 3.11: Connectivity of Sub-regions in MinNF placement

23% of users employ 64-QAM modulation in MinNF for their data transmission. Table 3.2 shows the variation in Femto count as $SINR_{Th}$ increases in MinNF model. As expected, the Femto count increases with increase in $SINR_{Th}$.

3.4.4 Motivation for Optimal Placement Models

Without Joint MinNF and MinNF models, the next best way for placement of Femtos, in our opinion, is CKM placement scheme. In the CKM scheme, as we do not know how many clusters/Femtos are required to guarantee minimum $SINR_{Th}$, we have to start with an initial guess value for the number of Femtos to be deployed and check if that count is sufficient for maintaining minimum $SINR_{Th}$ in every sub-region of the building. If the $SINR_{Th}$ is not met for all sub-regions, then the count of Femtos has to be increased.

In CKM, as shown in Figure 3.9, to maintain a minimum threshold (- 2 dB) for all sub-regions as in the case of MinNF model we require 7 Femtos (clusters) for the deployment. Hence, this motivates us to go for optimization techniques (*e.g.*, MinNF) to place Femtos.

3.4.5 Connectivity Region of Femtos inside the building

Figures 3.10 and 3.11 show the connectivity diagrams for CKM and MinNF placement schemes, respectively. The connectivity diagram is plotted by comparing the RSRP or SINR (reference signal received power) values offered to each sub-region by all the Femtos and connecting it to the Femto that offers the largest value. The sub-regions that are served by the same Femto are shown using the same color. In the connectivity diagram for the CKM placement (shown in Figure 3.10), it can be verified that the different sub-regions within the same room are being served by different Femtos. The sub-regions I_{47} , I_{48} and I_{49} in room #R7 (in Figure 3.2) are served by a Femto while I_{60} , I_{61} , I_{62} , I_{73} , I_{74} and I_{75} are served by another (for sub-region numbering refer Figure 3.2). Similarly, in room #R12, the sub-regions I_{128} , I_{129} and I_{130} are served by one Femto while I_{102} , I_{103} and I_{104} are served by another. This increases the number of handovers even when the user is walking a bit inside the same room. Though it was previously observed in Figure 3.6 that a good SINR was guaranteed by the optimal placement of Femtos, it can be seen from Figure 3.11 that the sub-regions I_7 , I_{20} and I_{33} of the corridor are served by a different Femto from that of the other sub-regions of the corridor. Also more than one Femto serve the rooms #R7 and #R12 leading to more number of handovers for movement within the rooms. Therefore this optimal placement leads to more number of handovers than CKM placement although it guarantees a minimum $SINR_{Th}$ to all the users unlike CKM placement. This motivates us to look into the handover optimization problem because it is severe in enterprise office buildings where a large scale deployment of Femtos is necessary.

3.5 Handover Optimized Femto Placement Model

In the previous section, it is seen that users of the same room connecting to the different Femtos. This causes ping pong effect which leads to decrease in throughput and increase in number of handovers. Such handovers are severe in irregular shaped buildings with corridors. In order to avoid such handovers inside rooms and corridors, we formulate an optimization model, OptHO (by adding handover constraint to MinNF model) Femto placement model. Before explaining the formulation in the subsequent section, we discuss about the user mobility model which is important in realizing the formulation.

3.5.1 User Mobility Model

A user mobility model is considered based on the entry/exit points of the rooms which are indexed as (A-P) in Figure 3.12 and the walls emulate realistic indoor movement of UEs. The UE movement is constrained by these walls and entry/exit (doors) points. Free movement (human walk) of the UEs is assumed inside the rooms. Depending upon the starting point (source) and ending point (destination), the human walk behavior model is incorporated [65]. This model replicates the real human mobility in indoor environments. An indoor building mobility model has been simulated by taking into account the presence of walls and entry/exit points. The existing NS-3 Building Mobility Model has been modified to make the UEs move along the shortest distance between the rooms and also according to the entry/exit points. When there are no direct connecting entry/exit between two rooms, the UE reaches its destination room by moving to the corridor that is reachable at the nearest distance from the starting position, and then it moves along the corridor to reach the position which is nearest to the destination room, from there it directly moves into the destination room.

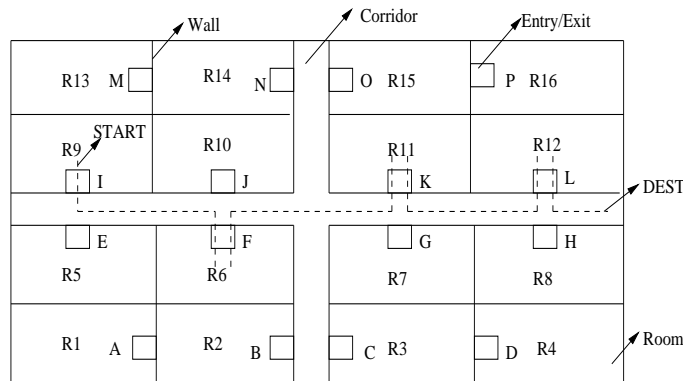


Figure 3.12: Building Scenario with Simple Flow

Handover Algorithm

Existing A3 handover algorithm of NS-3 [66] is used to perform handovers. A3 algorithm signifies the event where the serving cell's RSRP goes below the threshold of -3 dB. This information is carried out as a measurement report by UE for every 80 ms to the serving eNB.

3.5.2 OptHO Placement Model

Our goal is to reduce the number of unnecessary handovers inside the building by using the existing A3 handover algorithm. Once the Femtos are placed optimally by MinNF model inside the building, $SINR_{Th}$ is guaranteed. But the handover constraint is not given in MinNF, thus leading to a possibility of large number of handovers because of free movement of UEs. Our aim is to make sure that there are no handovers when a user moves from sub-region b to sub-region c *i.e.*, to reduce the number of unnecessary handovers inside the same room and along the corridor. The constraint to achieve this is given below.

$$\alpha_{ab} = \alpha_{ac} \quad b, c \in H \text{ and } a \in S \quad (3.9)$$

Where H is the set of all sub-regions which belong to the same room or corridor (*i.e.*, mostly connected to the same Femto with in the same room). In Equation (3.9) the constraint is made in such a way that if the sub-region b is connected to the Femto a then the sub-region c should also get connected to the Femto a , such that when a UE moves from sub-region b to sub-region c there is no handover. The SINR and placement constraints are similar to MinNF. Finally, the OptHO model is formulated as follows,

$$\min \sum_{a \in S} z_a, \text{ subject to (3.4), (3.5), (3.7), (3.9).}$$

Like MinNF model, the above OptHO ILP model is solved using CPLEX solver to obtain the optimal Femto co-ordinates.

3.6 Experimental Setup and Numerical Results

The experimental scenario given in section 3.5 is created in NS-3 and proportional fair is set as the scheduler to analyze the performance in terms of throughput and number of handovers.

3.6.1 Setup for OptHO Placement Model

NS-3 simulation parameters are given in Table 3.3. During simulations, the number of users placed randomly within the building (same randomness is maintained in MinNF and OptHO model) are increased from 3 to 30. The destination point to

Table 3.3: NS-3 Simulation Parameters

Parameter	Value
Number of Users	30
Application	TCP (Bulk Sender)
Scheduling Algorithm	Proportional Fair
Simulated traffic	Video using TCP
Simulation Time	300s
Number of seeds	10
$SINR_{Th}$	-2 dB
Femto Bandwidth	5 MHz (25 RBs)
LTE Mode	FDD
Packet Size	512 Bytes
Mobility	0.2, 0.5, 1m/s
Operating Frequency of BS	2.6 GHz
Mobility Model	Building Mobility Model

which each UE is moving to is also selected using a random function. For instance, if a user from room #R9 (source) wants to reach room #R15 (destination), the path traveled will be (#R9 \rightarrow corridor \rightarrow #R15) as shown in Figure 3.12. In the defined mobility model, the users move continuously throughout the simulation by selecting a new random destination on reaching the previously chosen destination well within the simulation time.

Density of UE: In our experiment, the density of UE represents the number of mobile users inside the building. Simulations are run for numerous UE densities in multiples of three(*i.e.*, 3, 6, 9 till 30).

3.6.2 Performance of OptHO Placement Model

The metrics that we use to analyze the performance of OptHO placement scheme are:

- Number of Handovers: The number of handovers triggered compared against the density of UEs for all the placement schemes (CKM, MinNF and OptHO).
- Throughput: Increase in throughput is compared against the density of UEs for all the placement schemes (CKM, MinNF and OptHO).

Radio Environmental/Heat Map for OptHO: After solving the OptHO model in GAMS solver, we obtain the same count of Femtos (F=5) as in MinNF. But for different handover constraints, it may be difficult to maintain the same Femto count

as in MinNF. We observe that there is no coverage hole in the building as shown in Figure 3.13.

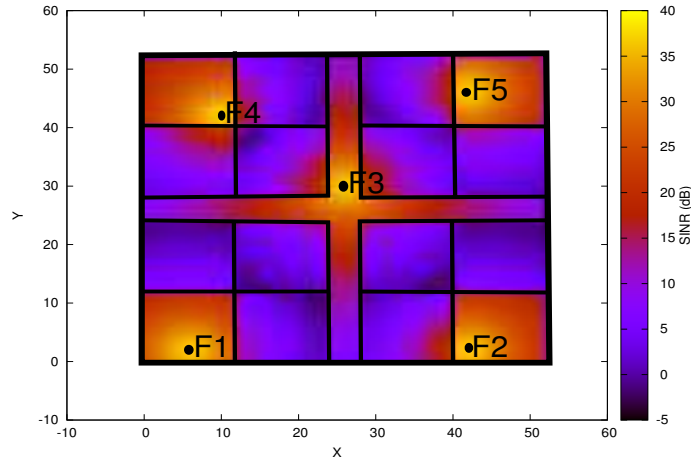


Figure 3.13: REM of OptHO Placement

Modulation Schemes in OptHO: Similar to MinNF, in Figure 3.14, it is observed that good SINR is maintained in regions surrounding the Femtos and a reasonable SINR is maintained at other regions throughout the building thus guaranteeing SINR threshold of -2 dB. Thus, there are no coverage holes and there is no possible loss of connectivity.

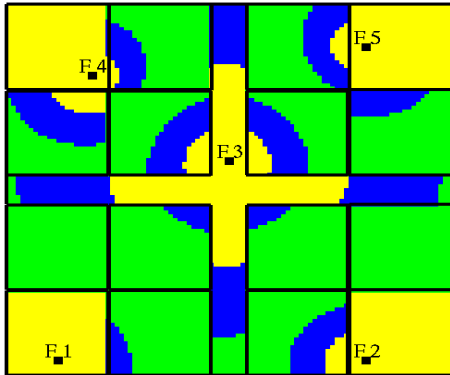


Figure 3.14: Modulation Schemes in OptHO Placement

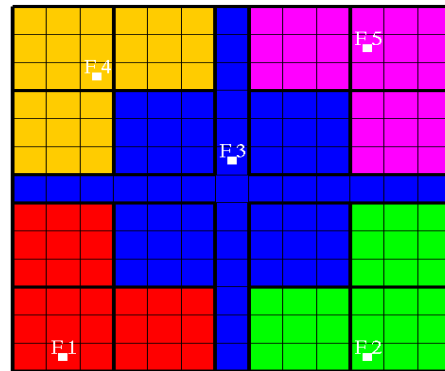


Figure 3.15: Connectivity of Sub-regions in OptHO Placement

Connectivity Region of Femtos in OptHO: Figure 3.15 shows the Femto connectivity of regions in OptHO model. In this connectivity diagram, it can be observed that no more than one Femto serves any room and the entire corridor is served by a single Femto. This placement guarantees that there are no coverage holes and a minimum $SINR_{Th}$ value is given to all the users along with reduction in the number

of handovers. Thus this provides a better throughput than the CKM and MinNF placement models.

In CKM placement, the rooms #R1, #R2, #R5 and #R6 (refer Figures 3.10 and 3.12) are connected to Femto F1 and the rooms #R9, #R10, #R13 and #R14 are connected to Femto F4. The entire corridor, the rooms #R8 and #R11 and parts of the rooms #R7 and #R12 are connected to Femto F3. The rooms #R15, #R16 and parts of the room #R12 are connected to Femto F5 and the rooms #R3 and #R4 and parts of the room #R7 are connected to Femto F2. While there are no handovers for users moving in the corridors, there is a good chance of handovers within rooms #R7 and #R12. Also, in MinNF placement, the rooms #R6, #R7, #R10 and #R11 are not connected to the same Femto as that of the corridors thereby, leading to more number of handovers.

Consider the flow marked by start point START and end point DEST as shown in Figure 3.12 for all the three placements (CKM, MinNF, OptHO). Then the user's travel path will be #R9 → corridor → #R6 → corridor → #R11 → corridor → #R12. In CKM placement, the handovers are expected to happen when moving out of room #R9, while entering and exiting rooms #R6 and #R11, and while entering and exiting room #R12. In addition to this, handovers will happen inside room #R12 as sub-regions within the room are connected to different Femtos. For the same flow, in the case of OptHO, handovers are expected to happen only while exiting room #R9 and while entering and exiting room #R12. Therefore, the number of handovers decrease when compared to the CKM placement model.

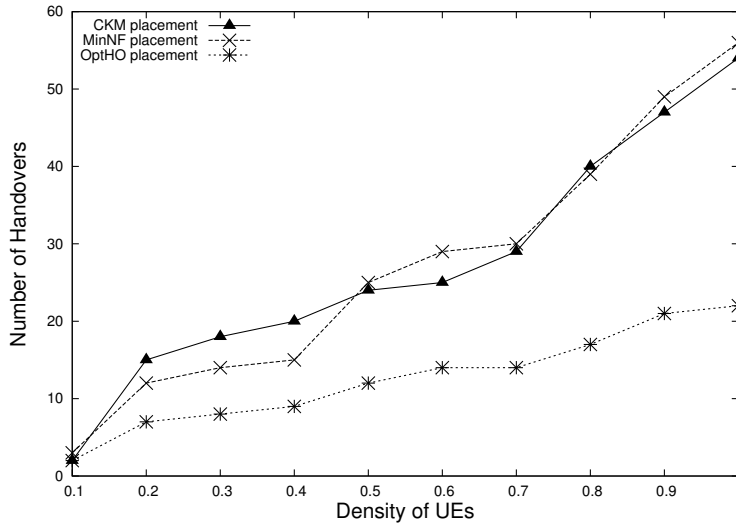


Figure 3.16: Number of Handovers vs UE Density in 0.2 m/s Mobility Case

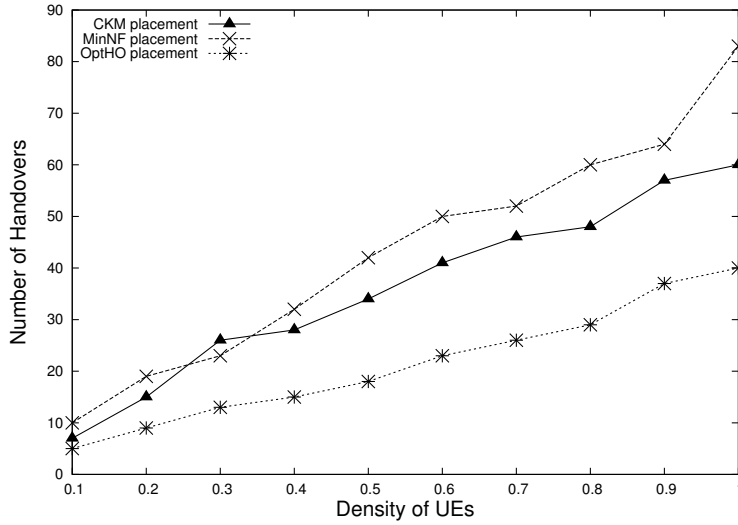


Figure 3.17: Number of Handovers vs UE Density in 0.5 m/s Mobility Case

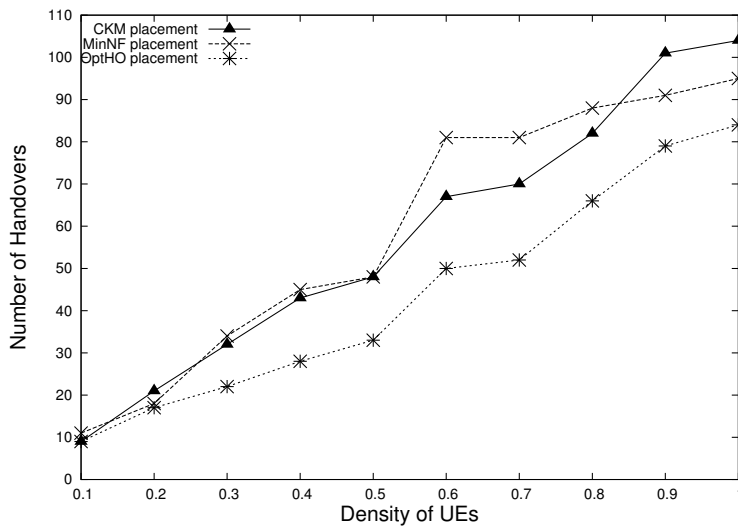


Figure 3.18: Number of Handovers vs UE Density in 1 m/s Mobility Case

Number of Handovers vs Density of UEs: The number of handovers for different density of UEs with mobility 0.2 m/s for all the three placement models is shown in Figure 3.16. In Figure 3.16, X-axis represents the density of UEs with a scaling factor by 30 and Y-axis represents number of handovers. It can be observed that the number of handovers is more for CKM and MinNF without handover constraint. This is because, even though the neighboring rooms are served by the same Femto in CKM and MinNF, due to the presence of walls the UE mobility is constrained. Generally, there is a high possibility of UE movement in the corridors or within the

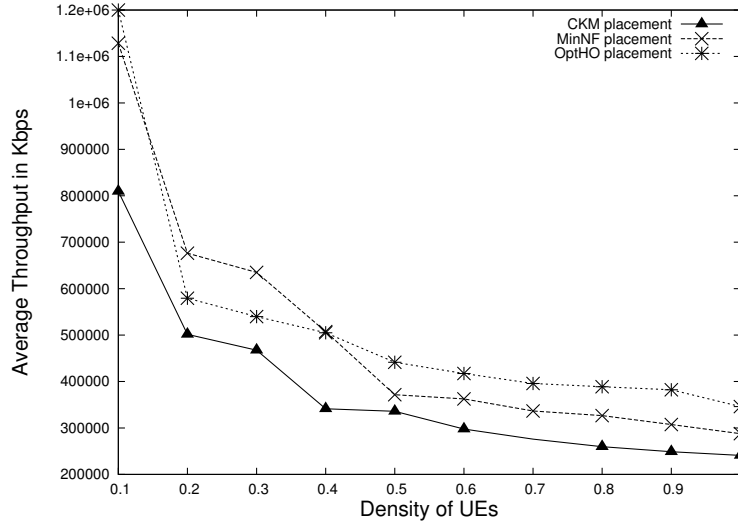


Figure 3.19: Average Throughput of Users vs UE Density in 0.2 m/s Mobility Case

rooms and it is essential to reduce the handovers in such scenarios. This is not taken into account in the CKM and MinNF. Whereas in the case of OptHO placement model, these handover constraints are taken into the system model while placing the Femtos, which leads to decrease in number of handovers up to 30%. In case of 0.5 m/s and 1 m/s user mobility, the number of handover decreased compare to MinNF by 22% and 16%, respectively. Similarly, the number of handovers for CKM and MinNF increases as the mobility increases in the order of 0.2, 0.5 and 1 m/s as shown in Figures 3.16, 3.17 and 3.18, respectively because the frequency of handover increases with mobility.

Throughput Vs Density of UEs: Figures 3.19, 3.20 and 3.21 show the average throughput plotted against the density of UEs with mobility 0.2, 0.5, 1 m/s for all the three placement models. As it can be seen from the modulation and coding scheme diagram shown in Figure 3.5, the no-data (red spot) regions in the CKM placement lead to decrease in throughput. Moreover, a lot of handovers happen in order to maintain connectivity which reduces the throughput. In optimal placement, a good $SINR_{Th}$ leverages the throughput. Even though the number of handovers is more or less the same as CKM placement, due to usage of comparatively better modulation schemes as shown in Figure 3.6, higher throughput is achieved. For 0.2 m/s mobility, OptHO placement performs 27% better than MinNF placement in terms of throughput as it combines the advantage of having an optimal placement and reduced handover scenario. Similarly, there is 14% and 20% improvement in throughput for mobility 0.5 m/s and 1 m/s in OptHO placement, when compared to CKM and MinNF place-

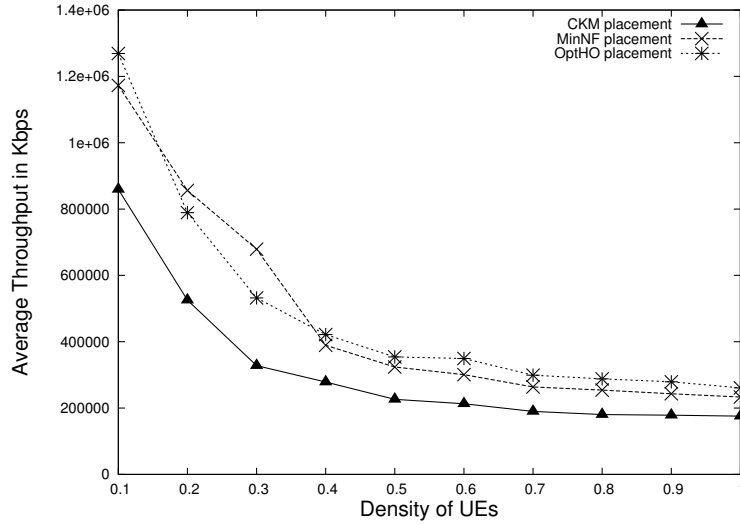


Figure 3.20: Average Throughput of Users vs UE Density in 0.5 m/s Mobility Case

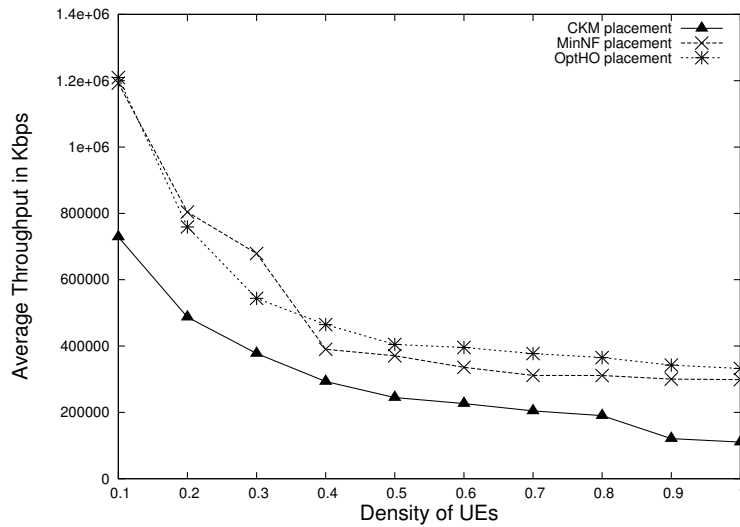


Figure 3.21: Average Throughput of Users vs UE Density in 1 m/s Mobility Case

ments, respectively.

3.7 Summary

In this chapter, we formulated two ILP optimization models: MinNF and OptHO to minimize the required number of Femtos and guarantee a threshold SINR for all users inside enterprise office buildings. This in turn increases the overall system

capacity and reduces the deployment cost. Our OptHO model reduces the number of unnecessary handovers in enterprise building environments. When compared to K-means clustering based placement scheme, proposed MinNF results in average SINR improvement of 28%. By adding handover constraint in MinNF, OptHO reduces 30% of unnecessary handovers in enterprise building environments.

Chapter 4

On Placement and Dynamic Power Control of Femtocells in LTE HetNets

4.1 Introduction

In previous chapters, we placed the Femtos optimally inside buildings to boost the data rates of Indoor UEs (*IUEs*) but so far we have not analysed the impact on outdoor UEs (*OUEs*) due to indoor Femtocell deployment. In this chapter, we consider both co-tier and cross-tier interference and apply the same MinNF model (presented in chapter 3) to determine the optimal count and the optimal placement of Femtos for reducing operator's CAPEX and OPEX. Hence, we expect that large scale enterprises could benefit from MinNF model based deployment. However, in some scenarios, operator may need to go for sub-optimal or arbitrary deployment (due to physical constraints) which will lead to deployment of more number of Femtos than that in MinNF to ensure that there are no coverage holes. Even optimal placement of Femtos inside a building leads to power leakage at the edges/corners of the building. This degrades the performance of the *OUEs* (*i.e.*, Macro connected) in High Interference Zone (*HIZone*) around the building area because both Macros and Femtos operate on the same frequency due to reuse one in LTE HetNets. Setting the Femto transmission at optimal/low power could solve this problem. But in a real-world scenario, the Macro users may not always be there in the surroundings of the building, such as at nights. Thus, Femtos need not always transmit at low power as indoor enterprise users could benefit from the maximum transmission power of Femtos. Our

goal is to address this problem and come up with a solution which dynamically adjusts transmit power based on the occupancy of Macro users around the building. In this chapter, we specifically refer the *OUEs* in *HIZone* as *HIZUEs*.

Hence, in this chapter, we dynamically adjust the transmit powers of Femtos in two steps. In the first step, MinNF model (refer Equation 3.8 in chapter 3) guarantees certain $SINR_{Th}$ for each sub-region inside the building with minimum number of Femtos and in the second step, Optimal Femto power (OptFP) model guarantees threshold SINR of -4 dB for *IUEs* with the Macro users SINR degradation as lesser than 2 dB. In the OptFP model, Femto's transmit power is tuned dynamically according to the occupancy of *OUEs* in the *HIZone*.

4.1.1 Organization of this Chapter

Rest of the chapter is organized as follows. Section 4.2 describes the related works. Proposed efficient placement and power control algorithm is presented in Section 4.3. Performance results are explained in Section 4.4. Finally, Section 4.5 summarizes the work.

4.2 Related Work

Many approaches to placing Femtos have been discussed in literature with sufficient insight, keeping in mind various parameters such as building dimensions, interference from Macro BSs and other Femto BSs. In [67], small cell locations are optimized in an airport environment depending upon the traffic demand. Authors in [54] proposed an algorithm which gives the optimal transmission power of each of the Femtos deployed in a HetNet scenario by guaranteeing $SINR_{Th}$ for *IUEs* and lesser degradation for *HIZUEs*. However, Femto power adaptation has not factored in occupancy level of *HIZUEs* outside the building.

In [55], an optimization problem is formulated for Femtos deployment which guarantees $SINR_{Th}$ inside the building by considering co-tier interference, cross-tier interference and impedance caused by walls. The $SINR_{Th}$ also varied depending on average user density in each region inside the building. This resulted in improving spectral efficiency of Femtos deployed in indoors. However, *HIZUEs* suffered degradation in SINR due to cross-tier interference between Macros and Femtos. In this chapter, optimal placement of Femtos and dynamic control of their transmit powers are studied by solving two optimization models, namely MinNF and OptFP. MinNF

determines the minimum number of Femtos and their respective co-ordinates to guarantee a minimum $SINR_{Th}$ of 0 dB for all indoor regions, assuming full transmission power of the Femtos. Configuration of Femtos at the full transmission power degrades SINR values of *HIZUEs*. To address this issue, OptFP model is used to find the optimal power of the Femtos to reduce degradation in SINR for the *HIZUEs*. The maximum fall in SINR for *HIZUEs* is limited to 2 dB after the deployment of Femtos. Since Femto power is reduced, $SINR_{Th}$ of *IUEs* is also reduced to -2 dB. This optimal power dynamically changes according to the occupancy of *HIZUEs* in the *HIZone*.

4.3 Proposed Work

In this section, we present architecture of LTE SON, system model, building model and efficient placement and power control algorithm.

4.3.1 LTE SON and System Model

We planned to design self organization network (SON) function that dynamically adjusts the Femto power (In our case, we assume a uniform transmission power across sub-channels) and optimizes the mobile radio access networks and also self heal itself (but it is out of scope of this thesis). In this chapter, we consider a LTE HetNet system comprising of Macro BSs in outdoor environment, to which the outdoor users are associated with and Femto BSs inside an enterprise office building. All these Femtos are connected to Femto-GW over S1 interface and SON features are integrated in the Femto-GW to automate the system. We have considered the case where the Femtos and Macro BSs operate on same frequencies (to enable reuse of the spectrum) and hence, experience high cross-tier co-channel interference. This affects the performance in *HIZone* *i.e.*, the region around the building in which, the Macro users experience high interference from Femtocells and leads to degradation in performance. In this work, we propose a solution to avoid high interference in *HIZone*. Table 4.1 shows the notations used in this chapter.

4.3.2 Building Model

Consider the dimensions of a building to be $L \times W \times H$, where L , W and H are respectively the length, width and height. Each floor is divided by walls into several rooms as shown in Figure 6.1. Each room is further logically divided into

Table 4.1: Glossary of OptFP MILP Model

Notation	Definition
S_i	Set of all inner sub-regions
S_o	Set of all outer sub-regions
w_a	1 if Femto is placed at inner sub-region a , zero otherwise
y_{ja}	1 if j^{th} inner sub-region of the building is associated with the Femto located at inner sub-region a , zero otherwise
g_{ja}	Channel gain between inner sub-regions j and a
b_j	1 if user is located at outer sub-region j , 0 otherwise
M	Set of all Macro BSs
p_a	Normalized transmit power of Femto BS a , $0 \leq p_a \leq 1$

smaller inner sub-regions, S_i s. For example, a building which is divided logically into $(I_1, I_2, \dots, I_{144})$ is shown in Figure 4.1. The thick lines represent the walls of the rooms and the small squares are the sub-regions. Similarly, the HIZone region outside the building is divided into outer sub-regions, S_o s. In the example, they are O_1, O_2, \dots, O_{52} . As the size of sub-region is much smaller compared to the building/room size, we can safely assume that within every sub-region, the average SINR value is almost constant. The PL model given in chapter 3 is used for this work.

4.3.3 Proposed Efficient Placement and Power Control Algorithm

In this chapter, we propose an efficient placement and power control SON algorithm which dynamically adjusts the power of Femtos by employing two optimization models:- MinNF and OptFP. In the MinNF model, we estimate the minimum number of Femtos required for placement, so as to provide a $SINR_{Th}$ to every inner sub-region (-2 dB). Here, we assume that the Femtos transmit at maximum power owing to which SINR degradation for *OUEs* in *HIZone* is high. In the OptFP model, using the solution of the MinNF optimization problem as the input setup their Femto power is optimally chosen to make sure that the difference in the SINR for *HIZUEs* before and after placement is less than 2 dB. And also a $SINR_{Th}$ value (-4 dB) is maintained for every inner sub-region. The Femto power changes dynamically (using SON module) depending upon the user pattern in the outer sub-regions S_o .

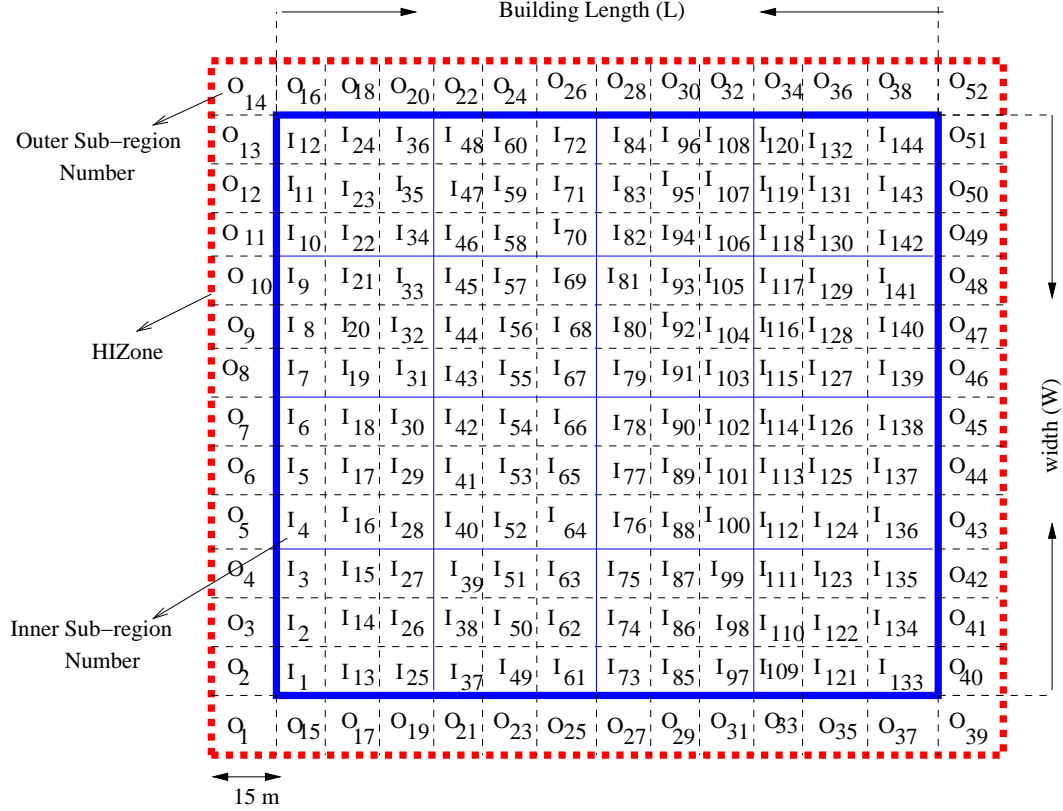


Figure 4.1: Bird-eye view of floor area inside and outside a single-floor building

(a) Minimize the number of Femtos (MinNF)

The MinNF formulation (refer Equation (3.8) in chapter 3) guarantees that all the users inside the building will get a certain $SINR_{Th}$ with minimum number of Femtos. It is a reasonable approach to boost the SINR in indoor regions when no *OUEs* in the surrounding of the building. But if the *OUEs* present in *HIZone* of the building, this method won't work as the Femtos transmit with maximum transmission power. Since Femtos and Macros operate on the same spectrum, interference can occur between the Macro and Femto users which in turn would degrade the signal strengths of the *OUEs* in *HIZone*. To overcome these shortcomings, we propose another optimization problem, described below, which optimally reduces the Femto transmit power.

(b) Dynamic transmit power for each Femto (OptFP)

In this scheme, we assume that the *OUEs* are in the surroundings of the building and obtain the optimal NF_{min} using MinNF model. We try to guarantee minimum $SINR_{Th}$ for *IUEs* and reduce the SINR degradation of *OUEs*, by minimizing the power of the Femtos in such a way that it reduces the interference with the *HIZUEs*. The formulation of the OptFP model is described below.

Problem Formulation for OptFP:

The objective of the proposed optimization scheme is to reduce the *HIZUEs* SINR degradation. By formulating this MILP, we will:

- Determine the power required by each Femto for maintaining the $SINR_{Th}$ in each of the inner sub-regions and maintain the SINR degradation at less than 2 dB in HIZone.
- Determine the Femto to which the users in any given inner sub-region have to be associated with.

The Femtos cannot operate at the highest power because if they do so, the *HIZUEs* will experience higher SINR degradation. We can safely assume that if we maximize the sum of all the transmission powers of Femtos, the transmission powers of individual Femtos will also be maximized (considering that the Femto BSs are "greedy" to keep their transmission power as high as possible) as the power values are obviously positive.

$$\max \sum_{a \in S_i} p_a \quad (4.1)$$

$$p_a \leq w_a \quad \forall a \in S_i \quad (4.2)$$

Let p_{max} be the maximum power of the Femto BS. The normalized power p_a value ranges from 0 to 1 and is 0 if w_a is 0. If Femto is not located at a given location a , w_a is set to 0. Once the model is solved, the actual power of Femto BS at location a is determined by $p_a * p_{max}$. Assuming that each inner sub-region corresponds to a user, any user is allowed to associate with only one Femto BS:

$$\sum_{a \in S_i} y_{ja} = 1 \quad \forall j \in S_i \quad (4.3)$$

$$y_{ja} - w_a \leq 0 \quad \forall j, a \in S_i \quad (4.4)$$

The two constraints mentioned above ensure that every sub-region is connected to one and only one Femto. To maintain the minimum SINR threshold for each inner sub-region, we add the following constraint:

$$Inf * (1 - y_{ja}) + g_{ja} P_{max} w_a \geq (\lambda N_o + \sum_{b \in S_i \setminus a} g_{jb} P_{max} w_b \lambda + \sum_{e \in M} g'_{je} P_{Macro} \lambda) \quad \forall j, a \in S_i \quad (4.5)$$

Another major concern is minimizing the cross-tier interference from Femtocell network on the *OUEs* in *HIZone*, who are connected to Macro BSs. To meet this requirement, we restrict the SINR degradation at each outer sub region (S_o) to be equal to or lesser than 2 dB:

$$\max_{e \in M} (g'_{je} P_{Macro}) + Inf * (1 - b_j) \geq (\zeta_j N_o + \sum_{e \in M'} g'_{je} P_{Macro} \zeta_j + \sum_{a \in S_i} g_{ja} P_{max} p_a \zeta_j) \quad \forall j \in S_o \quad (4.6)$$

$$M' \equiv M \setminus \arg \max_{e \in M} (g'_{je} P_{Macro}), \quad \forall j \in S_o$$

ζ_j is the minimum $SINR_{Th}$ at outer sub-region j . After the deployment of Femto, the precomputed ζ_j would be 2dB lesser than the original SINR. Note that outer sub region j is assumed to be attached to macro BS $\arg \max_{e \in M} (g'_{je} P_{Macro})$. Finally, the OptFP model is formulated as follows,

$$\max \sum_{a \in S_i} p_a \quad s.t., (4.2), (4.3), (4.4), (4.5), (4.6). \quad (4.7)$$

The above OptFP formulation guarantees a certain minimum $SINR_{Th}$ for *IUEs* with less degradation in SINR of *HIZUES*. This method is good when *HIZUES* are present in the outer sub-regions but it could be a waste of resources because the *IUEs* could benefit from the peak power of Femtos but they are actually receiving reduced power, even when no *HIZUES* is present outside the building. To overcome the above drawback, the OptFP model is adopted only when *HIZUES* is present

within 15 m range outside the building (*HIZone*), the users, SINR degradation is under 2 dB.

Algorithm 2 Efficient Placement and Power Control SON

```

1: Part 1:
2: Input:  $S_i$  and  $S_o$  (Sets of inner and outer sub-regions)
3: Run MinNF model;
4: Output: Obtain optimal no. of Femtos (Equation (3.8)) and their co-ordinates
5: Part 2:
6: Input:  $S_u \subset S_o$ , where  $S_u$  is set of outer HIZone sub-regions having Macro UEs
7: while true do
8:   Occupancy of Macro UEs (HIZUEs) in  $S_o$  as given by  $S_u$ ;
9:   if SON.DB contains ( $S_u$ ) then
10:    Retrieve Femtos Tx power settings from SON.DB;
11:   else
12:    Run OptFP model;
13:    SON.DB.Add( $S_u$ , Femto Tx Powers);
14:   end if
15:   Output: Configure Femtos with Optimal Tx power settings.
16:   Sleep ( $t_o$ )
17: end while

```

(c) SON Module in Proposed Power Control Algorithm:

A practical way to implement the proposed algorithm (refer Algorithm 2) would be to use the SON module dynamically such that whenever a *OUEs* is nearby, the Femto will reduce its transmission power and increase the transmission power when there are no *OUEs* nearby. Depending upon the user mobility, position reference signal (PRS) and scheduling information, Femto-GW will decide which side of the Femto should reduce or increase its transmission power (in worst case it might be all the Femtos). This, in turn, will boost the signal strength for both indoor and outdoor user devices because increase/decrease of Femto transmission power will guarantee good SINR and these power values of that pattern are stored in a database. The process is repeated for most of possible occupancy pattern of users in the outdoor sub regions and the data patterns are stored. If, in future an old occupancy pattern matches, instead of running the GAMS tool, we fetch the power values from the database. Otherwise, it is given as an input to the GAMS tool [33]. The new resultant output data pattern may also be stored.

Table 4.2: Simulation Parameters

Parameter	Value
Building dimensions	48 m \times 48 m \times 3 m
Number of Rooms	16
Room dimensions	12m \times 12m \times 3m
Number of inner Sub-region	144
Number of outer Sub-region	52
Inner Sub-region dimension	4 m \times 4m \times 3m
Number of Floors	One
Floor and Wall penetration losses	8 and 10 dB
Femto transmit Power	20 dBm (0.1w)
Macro transmit Power	46 dBm
Macro BS Height	30 m

4.4 Experimental Setup and Numerical Results

The system model described in Section 4.3.1 is simulated using MATLAB and the simulation parameters are given in Table 4.2. We have considered a single floor building and the shortest distance between the building and Macro is 350 m (diagonally from the center of inner sub-region I_1). Femtos are allowed to be placed only to the ceiling of the building and the minimum number of Femtos with their optimal coordinates and corresponding sub-region indices are obtained by solving MinNF ILP model using GAMS CPLEX solver [33]. The output (optimal co-ordinates of Femtos) of GAMS solver is then given as the input to MATLAB based system model. In the following, we analyze two extreme scenarios: without Macro users and with Macro users in HIZone.

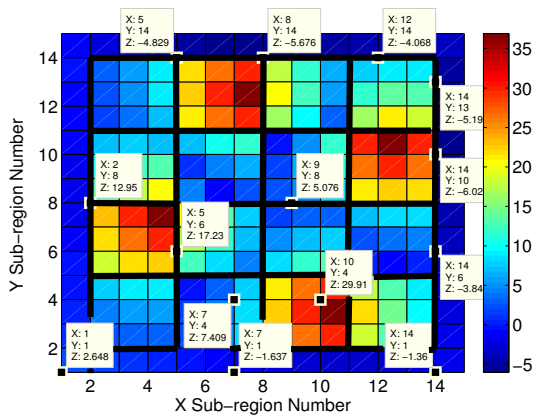


Figure 4.2: REM across sub-regions for MinNF

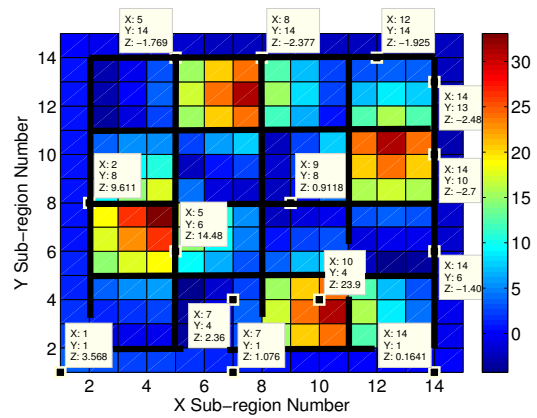


Figure 4.3: REM across sub-regions for OptFP

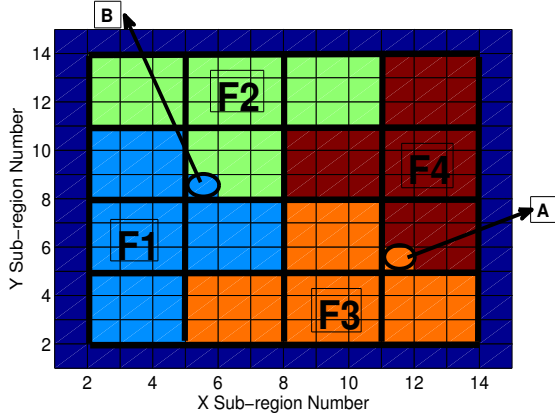


Figure 4.4: Fentoms sub-region association for MinNF

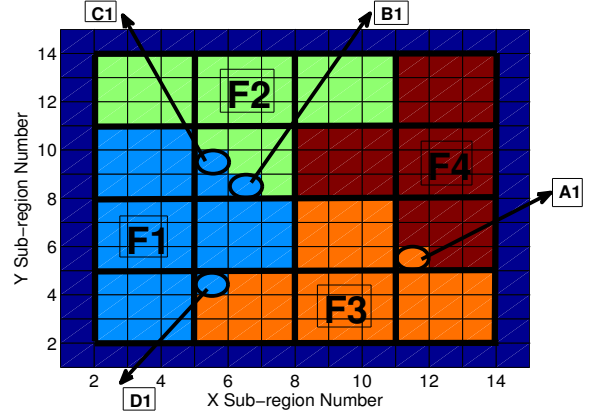


Figure 4.5: Fentoms sub-region association for OptFP

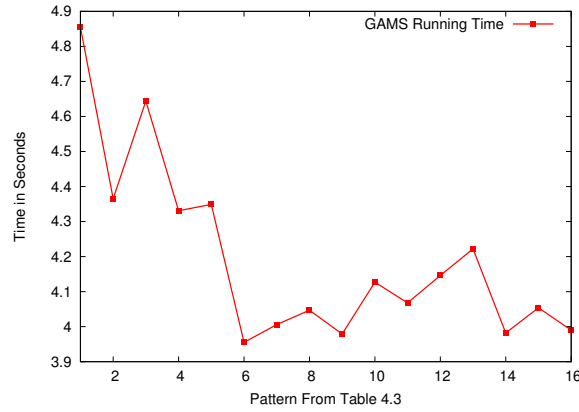


Figure 4.6: GAMS Running Time

4.4.1 Scenario 1: No Macro Users in HIZone

The MinNF model provides the optimal NF_{min} for four Femtos with corresponding sub-region indices and they are placed in dark brown region inside the building at those sub-regions I_{30} , I_{71} , I_{98} , I_{129} (refer Figure 4.1 for numbering of sub-regions) as shown in Figure 4.2. At this instant there are no *OUEs* present in HIZone within a distance of 15 meters. Hence all Femtos placed at the corner of the building transmit with their peak power (0.1w) as shown in Table 4.3 (S.NO 17). So the *IUEs* inside the building get good SINR. The Figure 4.2 shows the SINR values for all users inside the building. For example, in the sub-region I_{98} , the users get SINR value of 29.9 dB as the Femto (F3) is very close to it. Similarly, the sub-regions I_6 , I_{29} , I_{79} , I_{51} inside the building have relatively good SINR values 12.9, 17.2, 5.0, 7.4 dB, respectively. But if we observe only Macro scenario where there are no Femtos inside the building

like in Figure 1.7, the sub-regions I_6 , I_{29} , I_{79} , I_{51} inside the building have relatively less SNR values of -8.2, -8.3, -9.2, -8.3 dB, respectively due to poor indoor signal strength.

As a result of Femtos, the users present inside the building get a maximum SINR up to 35 dB (as shown in SINR graph of Figure 4.2). But in this case, if some *OUEs* enters the outer sub-region (for *e.g.*, O_{48}), they will get an SINR as low as -6.0 dB. This is a consequence of the Femtos being closer to the corners of the building and hence, there being a high power leakage (interference) in HIZone. In Figure 4.4, the Femtos (F1, F2, F3, F4) are transmitting at peak power. Users in the inner sub-regions of the building, can thus connect to a certain Femto. But, the Femtos are not placed in a manner that the sub-regions spanned by their transmissions are uniform. Hence the users in some sub-regions in the neighboring rooms also can connect to another Femto based on the factors like the distance from the Femto and number of obstructing walls. For example, although the transmission power of Femto F1 (I_{30}) crosses more number of walls than Femto F2 (I_{71}) to the sub-region I_{43} , its distance from the sub-region (represented by B) is lesser. Hence, the sub-region I_{43} gets connected to the Femto F1. Similarly, the Femto located in I_{98} (F3) is closer to the sub-region I_{112} (represented by A). Hence, the sub-region I_{112} gets connected to Femto F3.

4.4.2 Scenario 2: Macro Users in HIZone

When a *OUE* enters an HIZone, the Macro BS provides users Mobility, PRS and scheduling information to Femto-GW from which we can decide if some *OUE* is present in an HIZone. At this instance the *OUEs* are present at all sides of the building, and thus all the Femtos at the corners I_{30} , I_{71} , I_{98} , I_{129} of the building have to reduce their transmission power values optimally to 0.036, 0.021, 0.027, 0.022 W as shown in (Table 4.3 S.NO 5). Now, if we observe Figure 4.3 the users in the outer sub-regions O_{48} , O_{51} , O_{36} , O_{28} , O_{20} , O_1 , O_{25} , O_{37} , O_{44} have their respective SINR values as -2.7, -2.48, -1.9, -2.3, -1.7, 3.5, 1.0, 0.1, -1.0 dB. This shows a better improvement in SINR values when compared to the method of maximum transmission power Femto as in Figure 4.2. As a result of this, the users inside the building get lesser SINR 35 dB to 30 dB as can be observed in Figures 4.2 and 4.3. The minimum $SINR_{Th}$ (-4 dB) is maintained in all sub-regions inside the building. The inner sub-region I_{98} , I_6 , I_{29} , I_{79} , I_{51} inside the building have the respective SINR values of 23.9, 9.6 14.4, 0.9, 2.3 dB, hence showing a slight degradation of SINR values when compared

Table 4.3: Optimal Femto Transmission Power

S.No	Pattern in Outer Sub-regions	$I_{30}(W)$	$I_{71}(W)$	$I_{98}(W)$	$I_{129}(W)$
1	West: $(O_1, O_2, \dots, O_{14})$	0.038	0.1	0.1	0.1
2	North: $(O_{14}, O_{16}, \dots, O_{52})$	0.1	0.0211	0.1	0.1
3	South: $(O_1, O_{15}, \dots, O_{39})$	0.1	0.1	0.0229	0.1
4	East: $(O_{39}, O_{40}, \dots, O_{52})$	0.1	0.1	0.1	0.0223
5	All Sides of Building	0.036	0.021	0.027	0.022
6	O_{18}, O_{20}	0.1	0.0344	0.1	0.1
7	O_{24}, O_{26}	0.1	0.0211	0.1	0.1
8	O_6, O_7	0.0380	0.1	0.1	0.1
9	O_2, O_3	0.0675	0.1	0.1	0.1
10	O_1, O_2	0.0828	0.1	0.1	0.1
11	O_6, O_7, O_2, O_3	0.0380	0.1	0.1	0.1
12	O_{29}, O_{31}	0.1	0.1	0.0229	0.1
13	O_{21}, O_{23}	0.1	0.1	0.0432	0.1
14	$O_{29}, O_{31}, O_{21}, O_{23}$	0.1	0.1	0.0229	0.1
15	$O_{18}, O_{20}, O_{23}, O_{24}, O_{26}$	0.1	0.0212	0.0432	0.1
16	O_{47}, O_{48}, O_{49}	0.1	0.1	0.1	0.0223
17	No Macro users	0.1	0.1	0.1	0.1

to a maximum transmission power Femto. Owing to that, the pattern of serving area of a Femto changes slightly when compared to maximum transmission power Femto connection, as shown in Figure 4.5. This is because when the transmission power of Femtos is reduced, some of the sub-regions can not maintain the minimum $SINR_{Th}$. Hence, a UE trying to get connected to a certain Femto might now connect to a neighboring Femto in such a manner that minimum $SINR_{Th}$ is maintained. As shown in Figure 4.5, the encircled regions B1, C1, D1 are the sub-regions where the threshold SINR value cannot be maintained by Femtos F2 and F3, so the users in those sub-regions will get connected to the neighboring Femto F1 to maintain an $SINR_{Th}$. Although the delay t_o is large in Algorithm 2 because for most of the combinations of Macro occupancy pattern, power values remains the same (for *e.g.*, Table 4.3 SNO 8,11), the Femto transmission power need not always be constant. All the patterns and their results in Table 4.3 are stored in the database of the Femto-GW and whenever, the pattern matches, the corresponding solution is retrieved from the database. Otherwise GAMS tool is run again. The running time of GAMS tool is less than 5 secs as shown in Figure 4.6. It would thus take even lesser time, on a machine in a Femto-GW (which has high computing resources).

Whenever the Femto power is dynamically increased (if there is no *OUE* outside

the building and close by to it), it is advantageous to an *IUE* and whenever the Femto power is dynamically decreased it is advantageous to a *HIZUE* situated in *HIZone*. Largely, this solution aims at ensuring good SINR to both indoor and outdoor users. If we observe all the outer sub-region in both Figures 1.7 and 4.3, the SINR degradation for *HIZUEs* connected to MBS is under 2 dB.

4.5 Summary

In this chapter, we designed an SON based efficient Femto placement and power control algorithm which dynamically adjusts its transmit power and guarantees $SINR_{Th}$ (-4 dB) for *IUEs* with the *HIZUEs* connected to MBS SINR degradation as lesser than 2 dB. This in turn increase the over all system throughput by reducing the impact of cross-tier interference to *HIZUEs*.

Chapter 5

Energy-efficient Femtocell Placement in LTE Networks

5.1 Introduction

Femto placement models proposed in previous chapters only addressed the problem of SNR/SINR improvement in the downlink in the LTE HetNets. As these optimization models did not consider uplink SINR improvement, in this chapter, we propose two optimization models which together guarantee a certain minimum downlink SINR threshold ($DSINR_{Th}$) and uplink SINR threshold ($USINR_{Th}$) for each user inside the building and at the same time minimize the number of Femtos to be deployed and the total uplink power spent.

In the enterprise scenario, the signal strength in cell-edge areas may be very low, and so the users in those regions may still need to spend more uplink power to connect with a Femto BS. To demonstrate the aforementioned interference problem, we considered a single-floor building with dimensions of 48 m \times 48 m \times 3 m and placed the Femtos ($N=6$ and $N=11$, where N is the number of Femtos) using center- K -means (CKM) placement. CDF of UE uplink power is plotted in Figure 5.1. We can observe from the plot that as the Femto count increases, the uplink power transmitted by the UE gets reduced. This motivates us to look into an optimization problem by choosing the optimal Femto count and reducing the uplink power. At the same time we are also considering downlink interference in the optimization because the uplink and downlink interference influences the pattern of Femto placement.

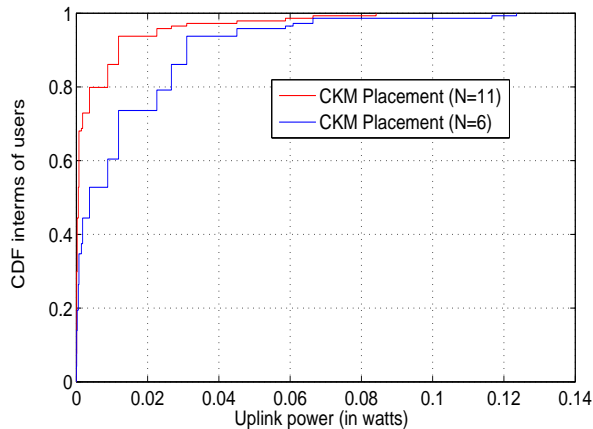


Figure 5.1: CDF of UE uplink power.

5.1.1 Organization of this Chapter

Rest of the chapter is organized as follows. Section 5.2 describes the related works. Proposed efficient uplink and downlink placement model is presented in Section 5.3. Performance results are explained in Section 5.4. Finally, Section 5.5 summarizes the work.

5.2 Related Work

Earlier mobile operators were concerned about saving power consumed by Macro BSs. This was accomplished by switching off few BSs [68] during period of less traffic, using renewable energy sources [69], cell zooming [70], etc. The concern, however, has now shifted to UEs because most of the mobile phone batteries get drained faster with the advent in increased data usage. According to 3GPP in LTE networks, the uplink transmission power [64] is tuned based on the feedback from Macro/Femto BS until desired SINR value is achieved. However, this tuning is more complex in heterogeneous networks due to cross-tier interference. In [71], the power for each frequency is tuned in an iterative manner. Since, the placement of Femtos was not optimal, high co-tier interference and a subsequent increase in power consumption would be observed.

The study [32] provided a solution to the joint optimal Femto placement and uplink power control problem. But their system model did not consider some realistic issues like uplink and downlink interference and building obstructions. In [34] the Femtos are placed inside a building to maximize the capacity of the users by con-

sidering only downlink interference. However, the placement of Femtos will change if we consider the uplink interference and obstructions in their model. In our previous chapter 4, the Femtos are placed optimally and the transmission power was dynamically adjusted to boost the SINR, by considering downlink interference and obstructions like walls and floors in the system model. To the best of our knowledge, this is the first study, where Femtos have been placed optimally by considering both uplink and downlink interference and the physical obstructions.

5.3 Proposed Work

In this section, we present system model, uplink power control and uplink & downlink placement optimization model.

5.3.1 System Model

The system model consists of an enterprise building with length (L), breadth (B), and height (H), respectively. The floor is further partitioned into several rooms by the walls. Indoor users are served by one of Femto BSs deployed inside the building. In this study, we consider an LTE HetNet system comprising of Macro and Femto BSs. They are configured to operate on same frequency (*i.e.*, reuse one), which leads to high co-channel interference. The building in which the rooms are separated by thick walls and the grids in each room depict the sub-regions of length δ_x and width δ_y to avoid complex formulation. We assume that *SINR* value does not vary within a sub-region (as the sub-regions are small). The objective of this work is to find the optimal sub-regions for placing the Femtos so that the Uplink SINR Threshold ($USINR_{Th}$) and Downlink SINR Threshold ($DSINR_{Th}$) are good for indoor UEs and the uplink power of the UE is also minimized.

The same PL models given in chapter 3 are used in this work and these PL models are applicable for both uplink and downlink transmissions.

5.3.2 Uplink Power Control

Power control refers to the exercise of optimally setting the output power levels of the UEs for uplink transmission. The 3GPP specifications [64] define this setting of the UE transmit power for Physical Uplink Shared Channel (PUSCH) by the following equation.

$$P_{tx} = \min\{P_{max}, P_x\} \quad (5.1)$$

$$P_x = P_{UE} + \alpha PL + 10\log_{10}(N') + fb(t)$$

Where, P_{max} is the maximum transmit power level of the UE in uplink, $\alpha \in \{0, 0.4, 0.5, 0.6, 0.7, 0.8, 0.9, 1\}$ is the path loss compensation factor signaled by higher RRC layers, PL is obtained from chapter 3, P_{UE} is a parameter to control UE SINR target. In LTE, the bandwidth of each Resource Block (RB) is 180 KHz. Each RB consists of 12 sub-carriers and seven OFDM symbols. N' is the number of RBs allocated in uplink and $fb(t)$ is the UE-specific correction value at TTI t , calculated from the transmit power control command in an accumulated or absolute manner. This value is transmitted by Macro/Femto BS through Downlink Control Information (DCI) channel to UEs.

5.3.3 Optimization Problem Formulations

In order to maintain good $USINR_{Th}$ and $DSINR_{Th}$ and to reduce the uplink power while guaranteeing the deployment of a minimum number of Femtos, we formulate a two-step optimization model. In the first step, we formulate a Minimize Femto and Uplink Transmission Power (MFUTP) MILP model to guarantee $USINR_{Th}$ and $DSINR_{Th}$. The objective of the above model is to minimize both, the number of Femtos required for deployment and the uplink transmission power of UEs. In the second step, we formulate a LP model with the goal to maintain Uplink SINR above a certain $USINR_{Th}$ and to reduce the total uplink transmission power. We named this model as Uplink SINR Transmission Power (USTP). Table 5.1 shows the set of notations used in this work.

Table 5.1: Glossary of MFUTP MILP Model

Notation	Definition
SR	Set of all sub-regions inside the building
U_j	Set of all users in sub-region j
x_a	1 if Femto is placed at sub-region a , zero otherwise
z_{ja}	1 if j^{th} sub-region of the building is associated with the Femto located at sub-region a , zero otherwise
G_{ja}	Channel gain between sub-regions j and a
MBS	Set of all Macro BSs
SRB	Set of all RBs

Step 1: MFUTP MILP Model

To address the optimal Femto placement problem, optimization model using MILP is formulated. The MFUTP MILP model is formulated in such a way that the $DSINR_{Th}$ is maintained. It is very difficult to determine the uplink SINR, unless the serving Femto or connectivity region is known. In order to place the Femto with both uplink and downlink constraints, the $USNR$ is considered instead of the $USINR$ and the Femtos are placed accordingly.

Our goal is to minimize the total number of Femtos deployed and total uplink power, which is expressed by Equation (5.2).

$$\min(\beta_1 \sum_{a \in SR} x_a + \beta_2 \sum_{j \in SR} \sum_{m \in U_j} P_m^u / P_{max}^u) \quad (5.2)$$

In Equation (5.2), if $\beta_1 = 0$ then the optimization problem is fully based on reduction in total uplink power consumption and if $\beta_2 = 0$ then minimizing the Femto count is the optimization problem. Thus, β_1 and β_2 can be varied depending upon the operator/customer necessity. P_m^u represents power emitted by user m at sub-region j , P_{max}^u represents the maximum power emitted by UE and P_m^u / P_{max}^u is the normalized transmit power of UE. These two objectives can be met by solving a multi-objective problem but that is beyond the scope of this work. The below constraint in Equation (5.3) ensures that every sub-region is connected to exactly one Femto.

$$\sum_{a \in SR} z_{ja} = 1 \quad \forall j \in SR \quad (5.3)$$

If a Femto is placed at a sub-region a , $x_a = 1$ else $x_a = 0$. The constraint in Equation (5.4) ensures that UE present in a sub-region j can be connected to a sub-region a only if $x_a = 1$ (*i.e.*, $z_{ja} = 1$ only if $x_a = 1$). There is no case where a UE in sub-region j can connect to a sub-region a when the Femto is non-existent there. However, there can be a case where $z_{ja} = 0$ when $x_a = 1$. This happens when there is a Femto placed at sub-region a but the sub-region j is so far away or separated by walls in such a way that the Femto at sub-region a will not be able to serve the users at sub-region j .

$$z_{ja} - x_a \leq 0 \quad \forall j, a \in SR \quad (5.4)$$

Each Femto operates at the maximum transmit power (P_{max}^f) in order to provide reasonably good signal strength to indoor UEs. Since all the Femtos use the same frequency, $DSINR$ degrades because of the adverse impact of the co-channel interference. Certain minimum $DSINR_{Th}$ needs to be guaranteed for all sub-regions of the building. $DSINR$ of a particular sub-region j due to the Femto located at sub-region a , is given by the L.H.S. of Equation (5.5). To guarantee optimum downlink coverage, $DSINR$ of sub-regions must be maintained above the predefined threshold $DSINR_{Th}(\lambda_d)$, which is given by Equation (5.5).

$$\frac{Inf * (1 - z_{ja}) + G_{ja}P_{max}^f x_a}{N_o^d + \sum_{b \in SR \setminus a} G_{jb}P_{max}^f x_b + \sum_{e \in MBS} G'_{je}P_{macro}} \geq \lambda_d \quad \forall j, a \in SR \quad (5.5)$$

Where G'_{je} and G_{ja} are the channel gain from Macro and Femto, N_o^d is the downlink system noise and PL calculated from chapter 3, respectively and P_{macro} is the power of Macro BS. In Equation (5.5), Inf is a virtual infinite value [41] (a very large value like 10^6). The reason for using $Inf * (1 - z_{ja})$ is that if $z_{ja} = 0$ then $Inf * (1 - z_{ja})$ becomes a large value and the expression can be ignored safely. Without the Virtual Infinite value, Equation (5.5) tries to ensure that all the Femtos meet the $DSINR_{Th}$ constraint to a particular sub-region. But a single Femto is enough to give $DSINR_{Th}$ for any given sub-region. The MILP will always be infeasible if the virtual infinite value is not used, as not all Femtos can meet $DSINR_{Th}$ constraint for a particular sub-region. Equation (5.5) can be rewritten as follows:

$$Inf * (1 - z_{ja}) + G_{ja}P_{max}^f x_a \geq \{(\lambda_d N_o^d + \sum_{b \in SR \setminus a} G_{jb}P_{max}^f x_b \lambda_d + \sum_{e \in MBS} G'_{je}P_{macro} \lambda_d)\} \quad \forall j, a \in SR \quad (5.6)$$

Similar to downlink, certain minimum $USNR_{Th}$ is guaranteed for all the users in the building. $USNR$ of a particular user at sub-region j due to the Femto located at sub-region a , is given by the L.H.S. of Equation (5.7). To guarantee coverage, $USNR$ of users must be maintained above the predefined threshold $USNR_{Th}(\lambda_u)$, which is given by Equation (5.7). Here Inf is used to ensure that only the users who are connected to the Femto located at sub-region a receive the threshold $USNR$.

$$\frac{Inf * (1 - z_{ja}) + G_{ja}P_m^u}{N_0^u} \geq \lambda_u \quad \forall j, a \in SR, \forall m \in U_j \quad (5.7)$$

Where N_0^u is the uplink system noise. The Equation (5.7) can be rewritten as follows,

$$Inf * (1 - z_{ja}) + G_{ja}P_m^u \geq \lambda_u N_0^u \quad \forall j, a \in SR, \forall m \in U_j \quad (5.8)$$

Finally, the *MFUTP* is formulated as follows,

$$\min(\beta_1 \sum_{a \in SR} x_a + \beta_2 \sum_{j \in SR} \sum_{m \in U_j} P_m^u / P_{max}^u) \text{ s.t.}, (5.3), (5.4), (5.6), (5.8).$$

By solving this MFUTP MILP formulation, the following values can be ascertained:

- The minimum number of Femtos needed to maintain $DSINR_{Th}$ in each sub-region of the building.
- The minimum uplink power each UE has to transmit out to maintain $USINR_{Th}$.
- The optimal locations of Femtos inside the building.
- The Femto to which the *IUEs* in any given sub-region will be associated with.

Step 2: USTP LP Model

Once the Femto co-ordinates and Femto serving region is known from step one, we can estimate the $USINR$. Further, the uplink power transmitted by UEs can be optimized by adding $USINR$ constraint. Our goal is to find the optimal value of uplink power in such a way that the $USINR_{Th}$ is guaranteed for each UE in the building. Figure 5.2 shows a building with Femtos (F1, F2, ..., F6) and UEs (U1, U2, ..., U6). The users (U1, U2, U3, U4) are connected to Femtos (F1, F2, F3, F4), respectively and are allocated the same RB1 from their respective Femtos (F1, F2, F3, F4). This will create an uplink interference as represented by the dotted lines for F1 in the diagram. If we observe UE U1, it faces interference from UEs (U2, U3, U4). This is different in the case of Femtos (F5, F6) due to allocation of different RBs.

Each Femto has N_b number of RBs and these are allocated to the users by the scheduling algorithm. For each RB, the power value can vary dynamically depending

upon the impact of interference offered by the neighboring UEs to each other. The step-two (LP) model runs (in a polynomial time [72]) for every TTI of the LTE frame and dynamically varies the transmit power of each RB in such a way that it guarantees $USINR_{Th}$ and thus the total uplink power is minimized.

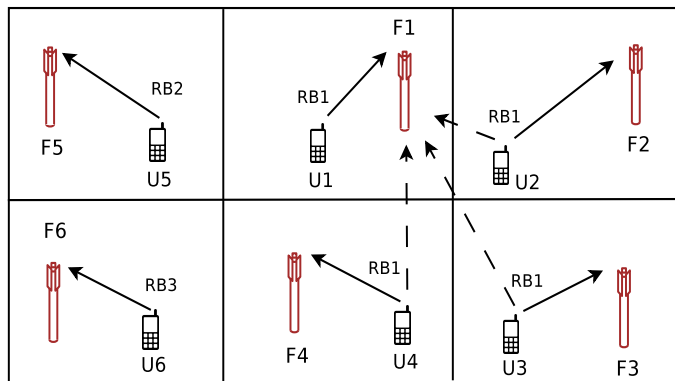


Figure 5.2: Uplink Interference Scenario in Indoor Building

$USINR$ of a particular user connected to a Femto located at sub-region a is given by the L.H.S of Equation (5.9). Depending upon $USINR$ needs of users in sub-region, $SINR_{Th}$ must be maintained above the threshold (λ_i) which is given by Equation (5.9).

$$\frac{G_{if_i} P_i^u}{N_o^u + \sum_{j \in V_r \setminus i} G_{jf_i} P_j^u} \geq \lambda_i \quad \forall i \in V_r \quad (5.9)$$

Where, V_r represents the set of users who are using RB r , where $r \in SRB$, uplink SINR threshold (λ_i) varies based on the requirement of users in sub-regions, f_i is the Femto to which user i is connected. Here, P_i^u is the power emitted by UE i to maintain the λ_i . G_{if_i} and G_{jf_i} are the channel gain from serving UE to Femto BS and interfering UE, respectively. The Equation (5.9) can be rewritten as follows,

$$G_{if_i} P_i^u \geq \lambda_i N_o^u + \lambda_i \sum_{j \in V_r \setminus i} G_{jf_i} P_j^u \quad \forall i \in V_r \quad (5.10)$$

Finally, the USTP LP model is formulated as follows,

$$\min \sum_{i \in U_r} P_i^u \quad \text{s.t., (5.10)} \quad \forall r \in SRB$$

Table 5.2: Simulation Parameters

Parameter	Value
Number of floors	One
Building dimensions	48 m \times 48 m \times 3 m
Room dimension	Non-uniform
Total number of sub-regions	144
Sub-region dimensions	4 m \times 4 m
Total number of rooms	15
Macro transmit power	46 dBm
Macro BS height	30 m
Femto transmit power	20 dBm
UE maximum transmit power	0.2 W
LTE Mode	FDD
Users distribution	One UE in each sub-region
Operating Frequency	2.6 GHz
$DSINR_{Th}$	0 dB
β_1	1
β_2	1

5.4 Experimental Setup and Numerical Results

The building setup along with Macro and Femtos BSs as elucidated in the system model given in section 6.3.2 is created in MATLAB. The Macro BS is placed at 300 m [41] Euclidean distance from the center of the sub-region 1. MFUTP is solved using GAMS CPLEX [33] solver. Femtos are then placed on the ceiling of the corresponding sub-regions. Table 5.2 contains simulation parameters.

In order to gauge the benefits of proposed MFUTP MILP model, it has been compared with CKM Placement scheme. CKM Placement scheme uses K-Means clustering algorithm which takes the mean position of each sub-region as input, forms appropriate clusters and determines the center of each cluster. In our case for each sub-region, the mean of the sub-region and the center of the sub-region are the same. Hence, the center of the sub-regions are given as input to the algorithm to form clusters. The Femtos are then placed at the centroid of each cluster.

5.4.1 Performance Results in Downlink

Center (CKM) Placement: To accurately compare CKM approach with the proposed model, we formed five clusters in the CKM placement. UE gets connected to a Femto BS which provides a good DSINR value when compared to the other Femtos.

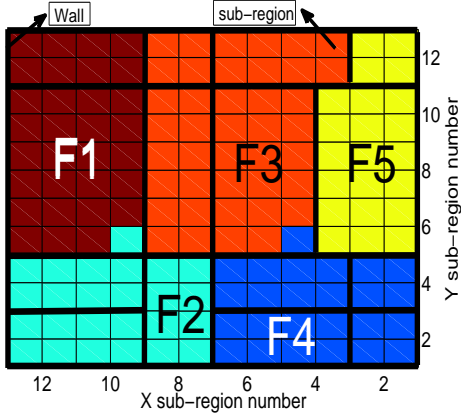


Figure 5.3: Femto sub-region association for CKM Placement

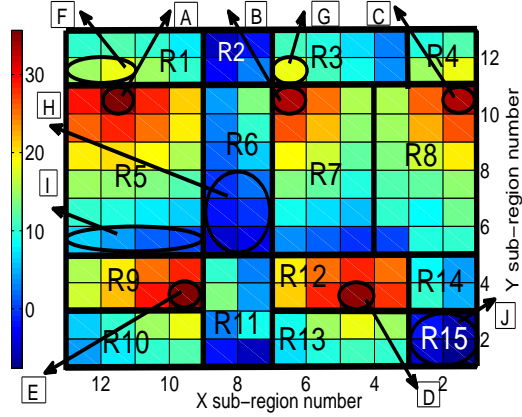


Figure 5.4: DSINR (in dB) for CKM Placement of Femtos

It is assumed that all the UEs present inside a sub-region will get connected to the same Femto. Figure 5.3 shows the Femto serving sub-regions for CKM placement of Femtos. The sub-regions marked with the same color are being served by the same Femto BS. For example, sub-regions colored in yellow as shown in Figure 5.3 are connected to the $F5$ Femto.

Figure 5.4 shows DSINR values of the sub-regions for the center placement. The color scale shown on the left side of figure maps the DSINR value pertaining to each color. The deepest shade of red in the color scale is mapped to the maximum DSINR value. The Femtos are placed in the sub-regions denoted by A to E and have deep red color. Due to path loss, the sub-regions that are farther from the position of the Femtos within the same room experience low DSINR values. For example, the region I inside room $\#R5$ has a low DSINR value as it is relatively at a greater distance from the serving Femto located at position A . The DSINR value also degrades with the increase in the number of walls that obstruct the signal from the serving Femto. This can be seen from regions (F, G) which have a DSINR value of 10 to 15 dB when compared to regions (H, J) that get a DSINR value lesser than -10 dB. This is because regions (F, G) are closer to the serving Femto and the signal strength is eroded by a single wall while regions (H, J) are deployed at relatively farther away from their serving Femtos and obstructed by two walls instead of one. Consequently, the users in the regions (H, J) cannot communicate with the Femto BS. This is the drawback of the center placement where all the users are not guaranteed a threshold DSINR value.

MFUTP MIP Model based Optimal Placement: Similar to the Femto serving sub-regions in Figure 5.3, Figure 5.5 is the Femto serving sub-regions for the

optimal positioning of Femtos. Figure 5.6 shows DSINR values in the optimal placement. From the color scale shown on the left side of figure, it can be observed that the minimum DSINR value which is guaranteed to all the users is 0 B (*i.e.*, $DSINR_{Th} = 0dB$) in contrast to the -10 dB in case of the center placement. Regions (A1, B1, C1, D1, E1) show the optimal locations of the Femtos. (F1, G1, H1) are the regions where the users get the minimum DSINR of 0 dB. The users in these regions can still communicate with the Femto BS. Based on the path loss and wall loss described earlier, the users closer to the Femtos and within the same room as the Femtos experience a better DSINR value in comparison to the users away from them. For example, the DSINR is better to the users inside the rooms (R3, R5, R8, R9, R13) because the Femtos are placed within them. Thus, the optimal placement guarantees a $DSINR_{Th}$ of 0 dB.

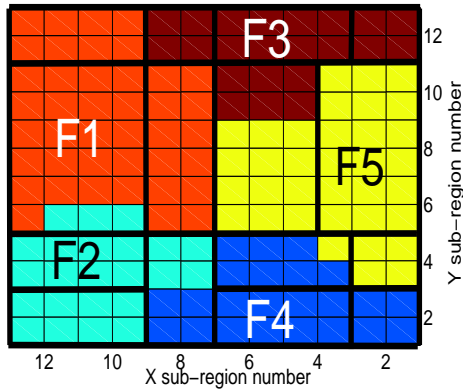


Figure 5.5: Femto sub-region association for MFUTP placement

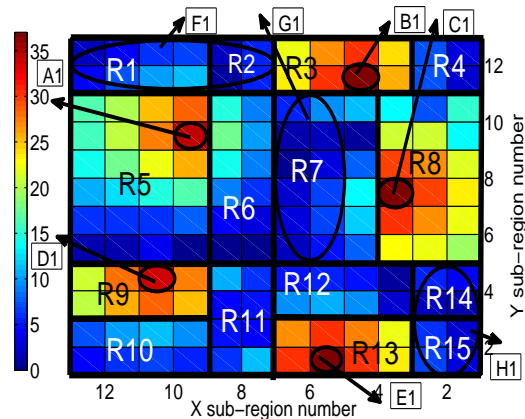


Figure 5.6: DSINR (in dB) for MFUTP Placement of Femto

5.4.2 Performance Results in Uplink

CKM-Restricted Power Control (CKM-RPC): In this case, Femtos are placed as per CKM placement with the restriction that the users have to transmit at an uplink power of at most 0.2 watt (*i.e.*, 23 dBm).

CKM-Non Restricted Power Control (CKM-NRPC): Here also Femtos are placed as per CKM placement. We allow all the users to maintain $USINR_{Th} = -2$ dB and measure the uplink power required, *i.e.*, there is no standard uplink power limit (0.2 W).

Uplink power in CKM-RPC and (MFUTP, USTP) Placement: In order to make a fair comparison, the uplink power of the every UE is to be maintained at - 2

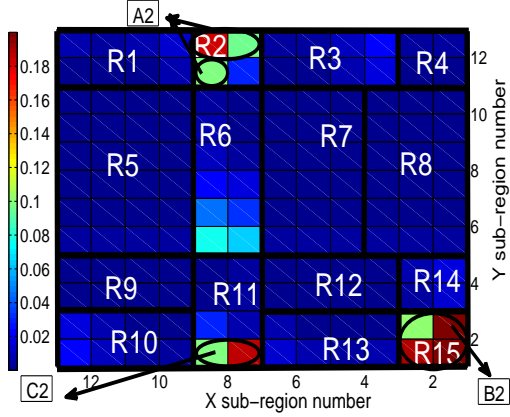


Figure 5.7: Uplink power (in Watts) for CKM-RPC Placement of Femto.

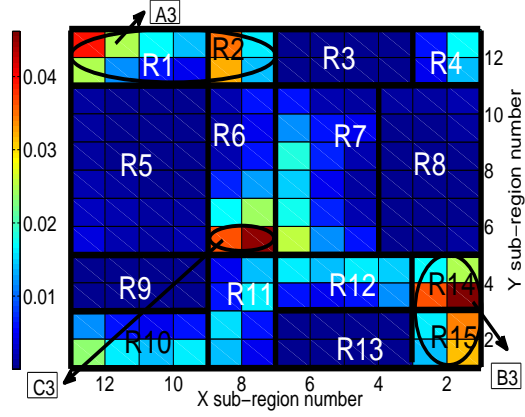


Figure 5.8: Uplink Power (in Watts) for (MFUTP, USTP) Placement of Femto.

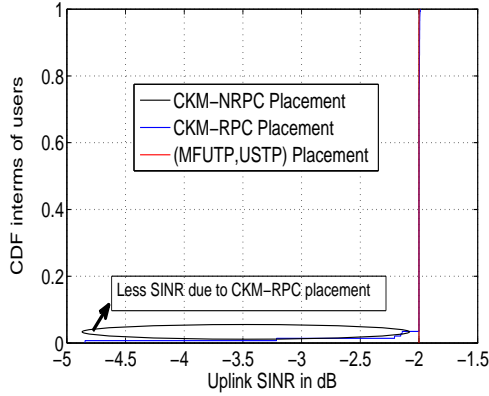


Figure 5.9: Uplink SINR (in dB) interms of users

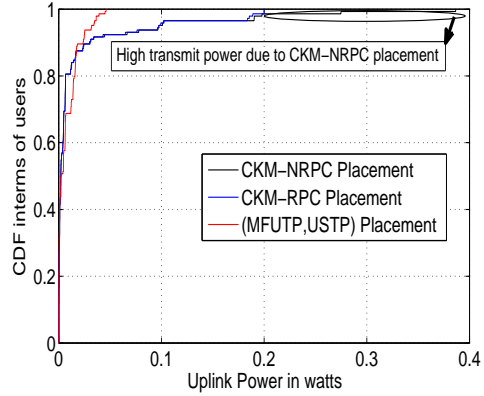


Figure 5.10: Uplink Power interms of users

dB $USINR_{Th}$ for these placements (CKM-RPC, (MFUTP, USTP)). Figure 5.7 shows the uplink power in CKM-RPC placement. We have to compare Figure 5.3, Figure 5.4 and Figure 5.7 to observe the serving sub-regions of Femtos, the placement of Femtos and uplink power metrics of the users in CKM-RPC placement. The users in the room ($R5, R7, R8, R9, R12$) transmit at low power ($0.02W$) as shown in color scale of Figure 5.7 to meet the $USINR_{Th} = -2$ dB because the Femtos are deployed in those rooms. But some users in the sub-regions ($A2, B2, C2$) must transmit at a higher power ($0.2W$) to maintain the $USINR_{Th}$ as the Femtos are farther from them (path loss) and the number of walls obstructing the signal from the Femto ($F2, F3, F4$) in Figure 5.3 is more than the former. Also, some percentage of users are not able to maintain the $USINR_{Th}$ in CKM-RPC placement. This has well explained in terms of CDF graphs.

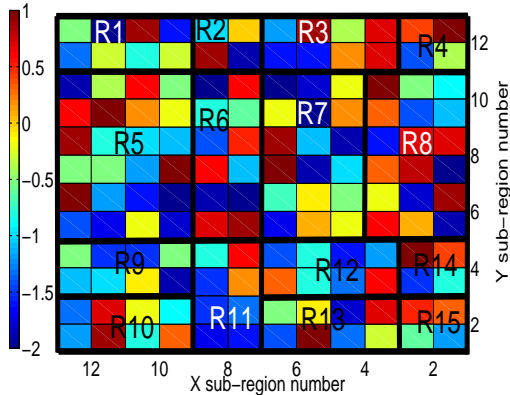


Figure 5.11: Variation of Uplink $SINR_{Th}$ (-2 to 1) dB across sub-regions in (MFUTP, USTP) placement

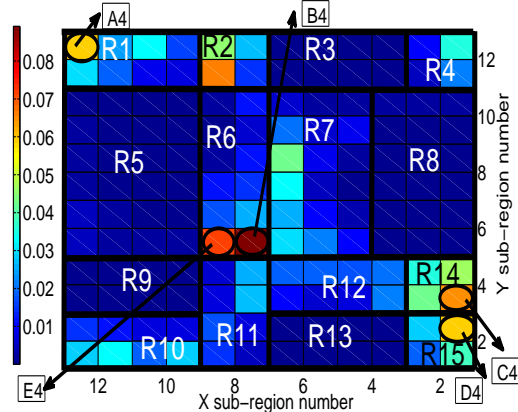


Figure 5.12: Variation of Uplink Power (in Watts) based on $SINR_{Th}$ in (MFUTP, USTP) placement

Similarly, we compare Figure 5.5, Figure 5.6 and Figure 5.8 to observe the serving sub-regions of Femto, placement of Femtos and uplink power in (MFUTP, USTP) placement. The users in the rooms ($R5, R3, R8, R9, R13$) transmit at low power ($0.005W$) as is evident from the color scale of Figure 5.8 to meet the $USINR_{Th}$. As the Femtos are deployed in those rooms, the users in the regions ($A3, B3, C3$) transmit at a higher power ($0.045W$) to maintain the $USINR_{Th}$. The (MFUTP, USTP) placement uplink power values are considerably lesser than in CKM-RPC placement.

CDF in terms of uplink power and SINR: The two graphs shown in Figure 5.9 and Figure 5.10 give an insight into the comparison of all the three placements (CKM-RPC, CKM-NRPC, (MFUTP, USTP)) with respect to the uplink power and SINR. The Figure 5.9 shows the CDF of users versus $USINR$ for all the placements. It can be seen that the $USINR$ value goes up to -5 dB in CKM-RPC, whereas the optimal (MFUTP, USTP) placement maintains the $USINR_{Th}$ at -2 dB for all the users so that there are no connectivity issues. In CKM-NRPC too, $USINR_{Th}$ is maintained at -2 dB but the transmitted uplink power is greater than 0.2 watt. It is further well explained in Figure 5.10.

In Figure 5.10, it can be perceived that the CKM-NRPC requires up to 0.4 W to achieve the $USINR_{Th}$, which is practically impossible as the UE can transmit upto a maximum of only 0.2 W. This implies that 2% of the users are in high uplink transmission power. Similarly in CKM-RPC placement, if the UEs want to maintain -2 dB $USINR_{Th}$ they have to transmit at 0.2 Watts. Whereas in optimal (MFUTP,

USTP) placement, the same threshold can be obtained with lesser power than the permitted value of 0.2 Watts for the UE. The $USINR_{Th}$ can be achieved with less than 0.05 Watts. By using optimal (MFUTP, USTP) placement, energy consumption for the entire building is 47% lesser than in CKM-RPC placement. Thus, the (MFUTP, USTP) placement saves more uplink energy and reduces CO_2 emissions in the Green HetNet system.

Variation of uplink $SINR_{Th}$ across sub-regions in (MFUTP, USTP) placement: We repeated the same experiment for random variations of $USINR_{Th}$ (-2 to 1 dB). Figure 5.11 shows the color scale variation of $SINR_{Th}$ from -2 to 1 dB across the sub-regions. Figure 5.12 shows the variation in the uplink transmission power. The circled region $A4$ should maintain roughly a $SINR_{Th}$ of -1 dB (refer Figure 5.11 as shown on the left side of color scale) but the region $A4$ is connected to the Femto $F1$, placed in room $R5$ as shown in Figure 5.5. As the signal would need to cross one wall from the Femto $F1$, the user in region $A4$ should transmit nearly at (0.06W) to maintain the $SINR_{Th}$ -1 dB. Similar is the case in regions ($B4, C4, D4, E4$).

5.5 Summary

In this work, Femtos were optimally placed considering both uplink and downlink interference in LTE Femtocell Networks. We ensured that energy consumption in uplink is 47% lesser than CKM-RPC placement. In addition to that, we also assure a reasonably good $SINRs$ for uplink and downlink.

Chapter 6

On improving SINR in LTE HetNets with D2D Relays

6.1 Introduction

In previous chapter 4, we proposed an algorithm for optimal placement and dynamic power control of the Femtos. The dynamic power control algorithm tunes the transmission power of the Femtos based on the presence of *OUEs* close to the building. By introducing dynamic power control of the Femtos, it is able to alleviate the interference issue for the *OUEs* at this *HIZone*. And at the same time it also guarantees a certain minimum $SINR_{Th}$ for the *IUEs*. Though the interference issue is addressed, fairness for *IUEs* and *HIZUEs* is not maintained. Even when there is only one *HIZUE* present at the *HIZone*, the power of the Femto which is serving *IUEs* at that side of the building has to be reduced to ensure certain minimum $SINR_{Th}$ for that *HIZUE*. This would reduce the SINR of many *IUEs* who are served by that Femto. This is clearly not fair to the *IUEs* connected to the Femtos.

In this chapter, to guarantee certain minimum SINR to both *IUEs* and *HIZUEs*, we apply the concept of D2D communication in LTE HetNets. In D2D, devices (*i.e.*, UEs) communicate directly with each other while the serving BS assists in setting up of D2D links and managing the control plane, authentication, handovers, etc. D2D helps in improving the cellular network capacity and power efficiency. In this chapter, we make use of idle *IUEs* as relays between Femtos and *HIZUEs* through D2D as an underlay to the LTE HetNet. We formulate a MILP optimization model which efficiently establishes D2D pairs between free/idle cell-edge *IUEs* and *HIZone* users by guaranteeing certain $SINR_{Th}$ for both *IUEs* and *HIZone* users. As D2D

MILP model takes more computation time, it is not usable in real-world scenarios for establishing D2D pairs on the fly. Hence, we propose a two-step D2D heuristic algorithm for establishing D2D pairs. In step one, we find the sub-optimal D2D pairs and assign the radio resources for them. In step two, a Linear Programming (*LP*) model is used to determine the transmit power for D2D pairs.

6.1.1 Organization of this Chapter

Rest of the chapter is organized as follows. Section 6.2 describes the related works. Proposed LTE HetNet system architecture with D2D links is presented in Section 6.3. In Section 6.4, proposed placement ILP model which minimizes number of Femtos to be deployed, D2D MILP model and D2D heuristic algorithm are discussed. Performance results are explained in Section 6.5. Finally, Section 6.6 summarizes the work.

6.2 Related Work

D2D is one of the most promising and challenging aspects towards 5G. In D2D communication, two UEs communicate directly with each other by means of data plane (D-plane) transmission using E-UTRA technology [73,74]. BS controls and optimizes the use of shared radio resources for cellular and D2D sessions. D2D is standardized by 3GPP in Release-12 for proximity-based services [64]. Some of the challenges in D2D include interference management, resource allocation, power control, session management, mobility management, security, location estimation and multi-hop D2D [8,75,76]. Session management [77,78] in D2D is controlled by BS. Core network is used for authentication, control channel establishment and policy control. Authors of [79] proposed a resource allocation scheme to share RBs among D2D pairs and traditional cellular users. In [80], the authors proposed an accurate model of the system and applied approximate dynamic programming model to do a fast resource scheduling in a HetNet system with D2D support. In [81] Phantom cell concept (UE-like BS) was proposed as a solution using D2D links to offload the traffic but different frequencies for the C-plane and D-plane were used. In [82], a holistic approach to efficiently offload with D2D was proposed and it incorporated a two-time scale scheduling solution with joint uplink and downlink scheduling between D2D pairs. It was shown that reuse of spectrum using Fractional Frequency Reuse (FFR) is limited but has not adapted any dynamic power control in the solution. In [83], the

authors studied different techniques to expand the cell edge coverage. They showed that using D2D for cell edge users decreases the overall power consumption. Authors of [84] proposed an optimization problem based on practical link data model with the objective of minimizing power consumption while meeting user data requirements. To solve it in a polynomial time, the authors proposed a joint mode selection, channel allocation and power assignment for D2D pairs by using a heuristic algorithm, but they predetermined and fixed the number of D2D pairs.

Multi-hop D2D communication [85–87] has applications for military communication and disaster management. The multi-hop can be applied to the problem where the UE with poor direct link to the MBS will forward data to a nearby UE over a high quality D2D link in uplink communication [88]. Here the receiving UE uploads its own data and relayed data to the MBS over its good uplink. This decreases the transmission time of the UE when compared to poor direct link to the MBS. Similarly, other work in uplink communication [89] describes the multi-hop D2D networking and resource management scheme for M2M communication to enhance end-to-end connectivity. In [90], the authors have proposed a novel distributed utility function for maximizing the D2D power control scheme which enables to balance spectral efficiency and resource allocation constraints that are essential in a given integrated cellular-D2D environment. During mode selection the impact of interference with other devices has not been considered. Also it is to be noted that the allocation of resources are random, which leads to inefficient D2D pairing.

6.2.1 Our Contributions

In this chapter, to ensure fairness and improve achievable data rates for both *IUEs* and *HIZUEs*, we apply the concept of *D2D* communication wherein *IUEs* act like UE-relays (*i.e.*, UE-like BS, forwarding data-plane traffic for some of the outdoor UEs). We first formulate a D2D *MILP* model to guarantee a certain $SINR_{Th}$ for both *IUEs* and *HIZUEs*. To reduce the computation time, we propose a two-step heuristic algorithm. In step one (called as hDPRA), we efficiently choose the potential D2D based relay pairs and allocate radio resources to them. In step two (called as hDPA), an *LP* model is formulated for power control of D2D links. We have conducted extensive evaluations to show that our proposed D2D heuristic algorithm is very close to the D2D *MILP* model.

6.3 Proposed LTE HetNet System with D2D Relays

In this section, we present architecture of LTE HetNet system with D2D relays, system model, building model and channel model.

6.3.1 HetNet Architecture with D2D Relays

In traditional cellular networks, UEs communicate with each other only through BSs (*e.g.*, Macros, Picos, and Femtos). But in D2D [76], UEs communicate directly with each other for exchanging data traffic (D-plane) and the serving BS only assists in the establishment and maintenance of D2D links as shown earlier in Figure 1.1. In our HetNet architecture with D2D relays, Femtos make use of free/idle *IUEs* (*FIUEs*) in their cells as UE-relays for forwarding downlink data traffic (D-plane) of *HIZUEs* by setting up D2D links (*i.e.*, $FIUE \rightarrow HIZUE$). Hence, *HIZUEs* are going to be served in downlink by one of Femtos deployed inside the building by using *FIUEs* (typically located at Femtocell-edge regions) as relay nodes. However, *HIZUEs* always communicate with MBS for their uplink communication. The control traffic (C-plane) for the *HIZUEs* is still delivered by the MBS [74] for better reliability and reducing the number of handovers for *HIZUEs* which are typically more mobile than indoor UEs.

The architecture of proposed HetNet system with D2D based relays is shown in Figure 6.1. The data traffic (D-plane) for the *HIZUEs* is first sent to *FIUEs* from the Femto by normal cellular communications. The *FIUEs* act as UE-relays and forward the data traffic to the *HIZUEs*. All the Femtos are connected to a F-GW over S1 interface. SON features (*e.g.*, optimally choosing D2D links and tuning their transmit power levels) can be integrated into the F-GW to automate the network operation. Broadly there are two approaches for choosing D2D links and fine tuning of their transmit power levels: distributed one which could be implemented at *FIUEs* and centralized one which could be implemented at the F-GW/SON. Both these approaches require the knowledge of distance/channel state information between *FIUEs* and *HIZUEs* for establishing D2D links with the required transmit power. But, it is very challenging and costly to acquire this information at *FIUEs* and choose D2D links by themselves in a distributed manner. Hence, in our work, we consider the centralized approach (*i.e.*, Network assisted mode [91, 92]) by implementing the proposed D2D heuristic algorithm at the F-GW/SON. MBS periodically provides the

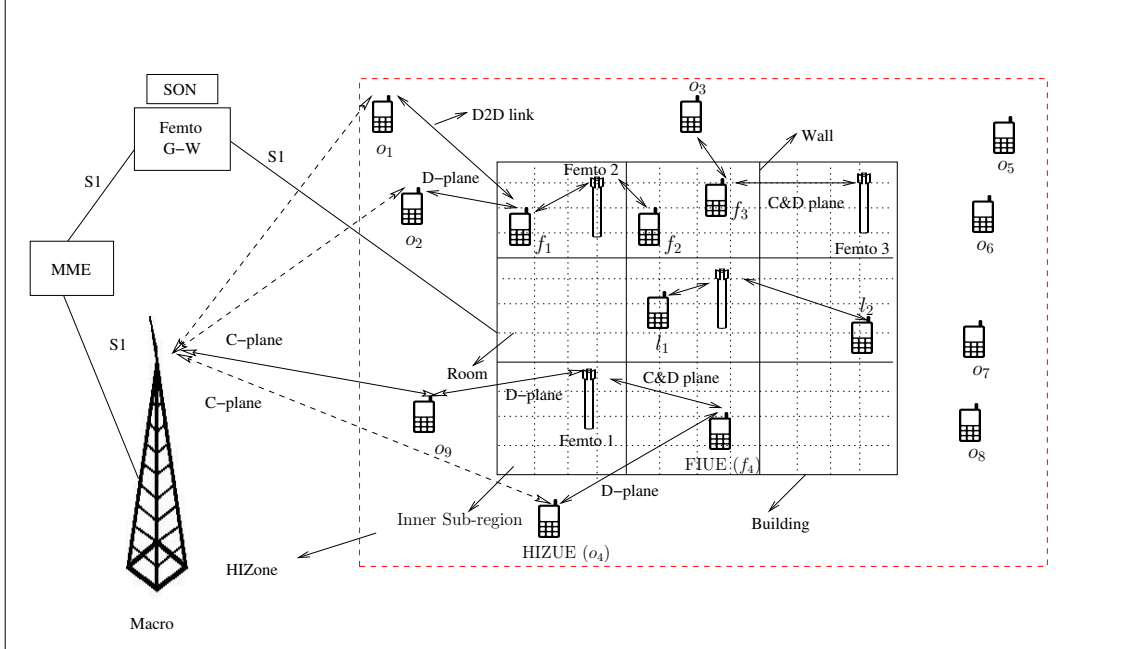


Figure 6.1: Architecture of Proposed HetNet System with D2D based Relays

list of potential *HIZUEs* (through C-plane messages) to the F-GW/SON. Femtos also provide the list of potential *FIUEs* to the F-GW/SON periodically (eg., 10 ms which is equal to one LTE frame duration). The downlink channel (from *FIUEs* to *HIZUEs*) quality can be estimated at *HIZUEs* by overhearing the uplink sounding reference signals (SRSs [64, 93–95]) of the *FIUEs*. Note that SRSs are sent periodically by *FIUEs* in the uplink to the serving Femtos for estimating uplink channel state. *HIZUEs* listening to these SRSs could estimate their downlink channel state and convey the same to F-GW/SON via MBS. If *FIUEs* are configured not to send SRSs, then the F-GW/SON needs to go for default power setting for D2D links. The D2D heuristic algorithm which is implemented at the F-GW/SON determines D2D links and their respective transmit power levels for communicating the same to respective *FIUEs* via their respective serving Femtos.

The D2D connection setup process involves choosing one of the *FIUEs* as UE-relay through *D2D candidate indication* message sent from the corresponding Femto via F-GW (refer Figure 6.2). Similarly the same *D2D candidate indication* message sent from MBS via F-GW informs the corresponding *HIZUE*. The *FIUE* and *HIZUE* then initiate the *D2D connection setup* procedure [96, 97] by sending ACK from *FIUE* to F-GW via Femto. Similarly, an ACK is sent from *HIZUE* to F-GW

via MBS. After *D2D connection setup* is established, *D2D data transfer* (D-Plane) procedure will take place.

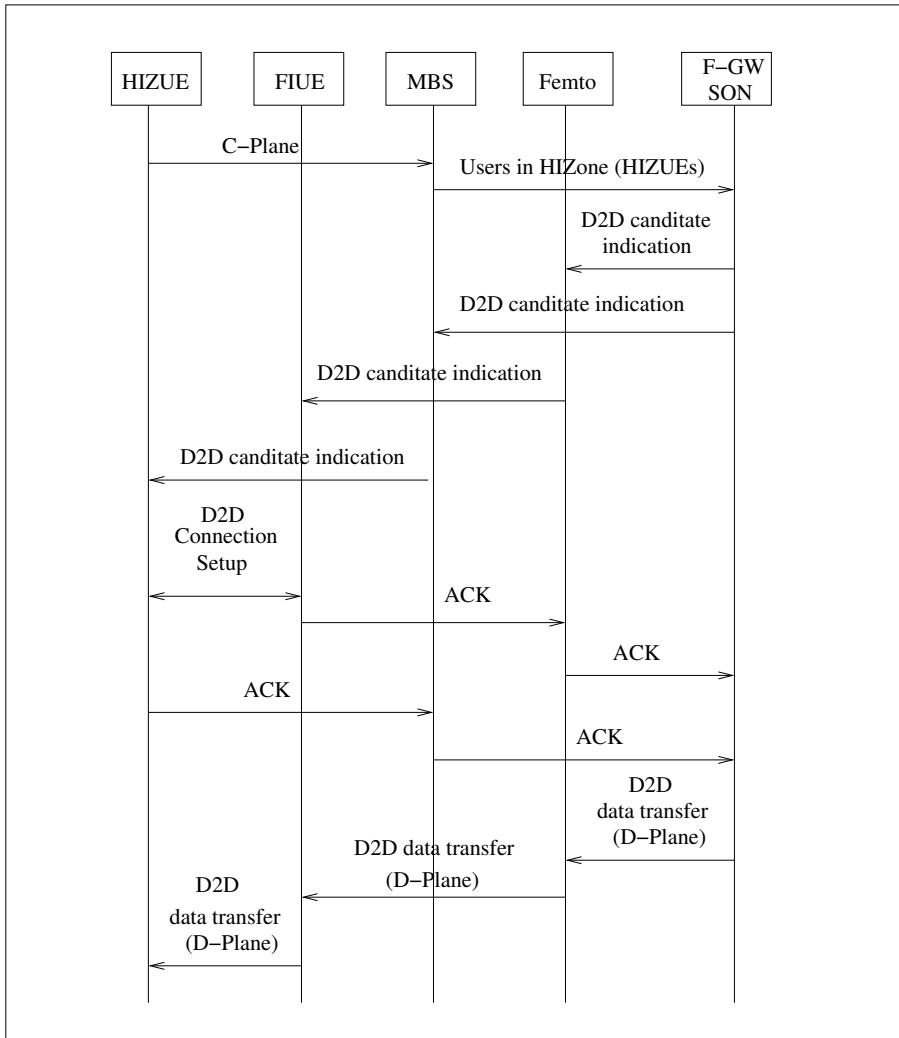


Figure 6.2: Call flow diagram for D2D based communication in proposed HetNet system

6.3.2 System Model

In this chapter, we consider an LTE HetNet system of MBSs in outdoor environment, to which the *OUEs* are associated, and Femtos inside an enterprise office building as shown in Figure 6.1. We have considered the case where Femtos and MBSs operate on the same frequency band (*i.e.*, reuse of one) to improve system's capacity. But, this can lead to high co-channel interference and affect *HIZUEs'* performance. We also assume that Femtos are all configured in open access *i.e.*, UEs are authorized to

connect with any of the Femtos of an operator. *IUEs* are connected to one of the Femtos deployed inside the building. There are two types of *IUEs*: legacy *IUEs* (*LIUEs*) represented by $l_1, l_2, l_3, \dots, l_m$ and free/idle *IUEs* (*FIUEs*) represented by $f_1, f_2, f_3, \dots, f_n$ as shown in Figure 6.1. *HIZUEs* are represented by $o_1, o_2, o_3, \dots, o_p$. *LIUEs* are *IUEs* who send/receive data to/from a Femto at a particular TTI for their own communication. *FIUEs* are *IUEs* who can act as UE-relays between their respective serving Femtos and one of *HIZUEs*. *FIUEs* can either be idle UEs or the UEs who are not going to be scheduled to receive any downlink data of their own from their serving Femtos for some TTIs. We assume that list of *FIUEs* is available at the F-GW/SON and it is updated dynamically.

The default scheduling algorithm is assumed to be running at each Femto for serving *IUEs*. The scheduling for downlink data of *HIZUEs* connected using D2D relays is also done at the Femtos. The D2D pairs are chosen such that they could be held for quiet sometime, hence they will not be changing in every TTI. This can be assured if appropriate D2D Device Discovery mechanism [98] is used for choosing the *FIUEs*. We assume that the transmission power across RBs for the Femtos are equal whereas for that of the *FIUEs* the power is varied accordingly to each RB. The D2D based relays (*FIUEs*) do not face severe battery issues because the *FIUEs* transmit at lower power. The *FIUEs* can also be provided with incentives by the operator for acting as D2D based UE-relays.

A variety of scenarios can co-exist in this HetNet system model for the D2D links as shown in Figure 6.1. A D2D link can be established by an *FIUE* to serve one or more *HIZUEs*. A single *FIUE* can also serve multiple *HIZUEs* using D2D links. In the worst case, when it is impossible to establish any D2D link due to high load at the Femto or lack of *FIUEs*, the F-GW/SON can opt for *dynamic Femto power* (OptFP) model (refer Equation (4.7) in chapter 4) in order to reduce interference to *HIZUEs* from the Femtos (explained later in Section 6.4.4). The PL model given in chapter 3 and building model given in chapter 4 are used for this work

6.4 Femto Placement and D2D Pair Selection Models in LTE HetNets

In this section, MinNF model (refer Equation 3.8 in chapter 3) is used first for optimal placement of Femto. Then we formulate D2D MILP model which establishes D2D based relay pairs between *FIUEs* and *HIZUEs* and also guarantees certain SINR

threshold ($SINR_{Th}$) for both *IUEs* and *HIZUEs*. As D2D MILP model takes more computation time, it is not usable in real-world deployments for establishing D2D pairs dynamically. To address this issue, we propose a two-step heuristic algorithm for establishing D2D pairs.

6.4.1 D2D MILP Model

In order to achieve the required $SINR_{Th}$ for both *IUEs* and *HIZUEs* in the HetNet system, we need to optimally choose D2D links, effectively allocate the RBs to the D2D links and adjust power for these links. We formulate a MILP model to address this problem. The notations used in this model are listed in Table 6.1.

Table 6.1: Glossary of D2D MILP Model

Notation	Definition
K	Set of all Resource Blocks (RBs)
F	Set of all Free Indoor UEs (<i>FIUEs</i>)
L	Set of all Legacy Indoor UEs (<i>LIUEs</i>)
O	Set of all Outdoor UEs in HIZone (<i>HIZUEs</i>)
M	Set of all MBSs
D_{fo}	A binary variable whose value is 1 if f is connected to o for D2D else 0, where $f \in F$, $o \in O$
C_{fo}^k	A binary variable whose value is 1 if f is connected to o for D2D using RB k else 0, where $f \in F$, $o \in O$, $k \in K$
h_f^k	A binary variable whose value is 1 if f is using RB k for D2D link else 0, where $f \in F$, $k \in K$
G_{xy}	Channel gain between two nodes x and y , where nodes can be <i>IUEs</i> , <i>HIZUEs</i> , MBSs or Femtos
p_f^k	Normalized power emitted by f in RB k , $0 \leq p_f^k \leq 1$, where $f \in F$, $k \in K$

In order to minimize battery drain of *FIUEs*, one of the main objectives¹ is to minimize the overall power consumed by the D2D links as expressed in Equation (6.1):

$$\min \sum_{f \in F} \sum_{k \in K} p_f^k \quad (6.1)$$

Equation (6.2) sets an upper bound on the number of *HIZUEs* that can be served by each *FIUE*. Similarly, Equation (6.3) restricts the number of *FIUEs* serving each *HIZUE*.

¹Another alternate optimization goal can be minimization of the maximum power ($\min(\max(p_f^k))$) consumed by D2D links where all the constraints are identical to the proposed D2D MILP model.

$$\sum_{o \in O} D_{fo} \leq \alpha \quad \forall f \in F \quad (6.2)$$

$$\sum_{f \in F} D_{fo} \leq \beta \quad \forall o \in O \quad (6.3)$$

$$\sum_{f \in F} \sum_{o \in O} D_{fo} = \psi \quad \forall o \in O \quad (6.4)$$

In order to limit the total number of D2D links that would be established in a TTI, we introduce Equation (6.4). The values of α , β and ψ can be fine tuned as per the requirements of the operator. The binary variable C_{fo}^k is 1 when *FIUE* f and *HIZUE* o are communicating by using RB k . Hence, C_{fo}^k can never be 1 when there is no D2D link between f and o . This is ensured by Equation (6.5). Here, η represents the maximum number of RBs that can be assigned to each D2D link.

$$\sum_{k \in K} C_{fo}^k \leq \eta \times D_{fo} \quad \forall f \in F, o \in O \quad (6.5)$$

Equation (6.6) ensures that the maximum number of times a particular RB k can be reused by an *FIUE* f is 1.

$$\sum_{o \in O} C_{fo}^k \leq 1 \quad \forall f \in F, k \in K \quad (6.6)$$

h_f^k is set to be 1 if *FIUE* f is using the RB k . This is ensured by Equation (6.7).

$$h_f^k = C_{fo}^k \quad \forall f \in F, o \in O, k \in K \quad (6.7)$$

The constraint in Equation (6.8) ensures that the normalized power emitted by *FIUE* f in a particular RB k is 0 when it is not used by f .

$$p_f^k \leq h_f^k \quad \forall f \in F, k \in K \quad (6.8)$$

The P_{max}^d is the maximum power of a D2D link. Once the MILP model is solved, transmission power of an *FIUE* f in a RB k is calculated as $p_f^k \times P_{max}^d$. G_{fl} gives the gain from the *FIUE* f to the *LIUE* l . S_l^k is an input parameter whose value is 1 when l is connected to its serving Femto (downlink) using RB k , else 0. The

constraint in Equation (6.9) ensures that the maximum interference power that is received by l is less than the allowed threshold value (I_l). I_l is computed for a given value of $SINR_{Th}$ of $IUEs$.

$$\sum_{f \in F} (G_{fl} \times S_l^k \times p_f^k \times P_{max}^d) \leq I_l \quad \forall l \in L, k \in K \quad (6.9)$$

The L.H.S. of Equation (6.10) is the SINR received by $HIZUE$ o from $FIUE$ f . To ensure good connection, the SINR of each D2D link is maintained above a predefined threshold λ_o which could vary across $HIZUEs$.

$$\frac{Inf * (1 - C_{fo}^k) + G_{fo} p_f^k P_{max}^d}{N_o + \sum_{m \in M} G_{mo} P_{macro} + \sum_{a \in B_k} G_{ao} P_{max}^f + \sum_{f' \in F \setminus f} G_{f'o} p_{f'}^k P_{max}^d} \geq \lambda_o \quad \forall f \in F, o \in O, k \in K \quad (6.10)$$

Here, B_k is the set of all Femtos using the RB k in a given TTI. Similarly, G_{ao} is the channel gain from Femto a to o , G_{fo} is the channel gain from f to o and G_{mo} is the channel gain from MBS m to o , calculated by using PL model (shown in chapter 3). The need to use $Inf * (1 - C_{fo}^k)$ is that if $C_{fo}^k = 0$ then $Inf * (1 - C_{fo}^k)$ becomes a large value and the expression can be ignored safely. Without the virtual infinite value, Equation (6.10), ensures that all the $FIUEs$ provide a minimum $SINR_{Th}$ to a particular $HIZUE$. The MILP will always be infeasible if we do not use the virtual infinite value, as not all $FIUEs$ can maintain a $SINR_{Th}$ (λ_o) for an $HIZUE$. The Equation (6.10) can be rewritten as follows,

$$Inf * (1 - C_{fo}^k) + G_{fo} p_f^k P_{max}^d \geq \{(\lambda_o N_o + \lambda_o \sum_{m \in M} G_{mo} P_{macro} + \lambda_o \sum_{a \in B_k} G_{ao} P_{max}^f + \lambda_o \sum_{f' \in F \setminus f} G_{f'o} p_{f'}^k P_{max}^d)\} \quad \forall f \in F, o \in O, k \in K \quad (6.11)$$

Finally, the D2D MILP model is formulated as follows,

$$\min \sum_{f \in F} \sum_{k \in K} p_f^k \quad s.t., (6.2), (6.3), (6.4), (6.5), (6.6), (6.7), (6.8), (6.9), (6.11).$$

By solving this MILP model, we achieve the following:

- Get best *FIUEs* as relays for establishing D2D links
- Assign RBs to each of the D2D links established
- Adjust the transmit power for each of the D2D links and minimize the overall power emitted by guaranteeing $SINR_{Th}$ for *LIUEs* and *HIZUEs* served by *FIUEs*.

As shown later in Section 6.5, the above D2D MILP model ensures fairness for both indoor and outdoor users by assuring certain minimum *SINR* for all *IUEs* and *HIZUEs*. But the computation time of this D2D MILP model is high and it may not converge in real-time for any practical usage by Femtocells. For some cases, the problem can be infeasible. To overcome this shortcoming, we propose a two-step D2D heuristic algorithm in the next sub-section.

6.4.2 D2D Heuristic Algorithm

D2D heuristic algorithm has two steps: one step for selecting D2D pairs and allocating RBs, and other step for setting the powers of D2D pairs. Below we present these two steps.

Step 1: Heuristic D2D Pair and Resource Allocation (hDPRA)

Proposed hDPRA (refer Algorithm 3) checks whether a particular *FIUE* f can connect to an *HIZUE* o using an RB k . For this we define a parameter, Win-to-Loss (W2L) Ratio (γ) for all possible (f, o, k) combinations, as expressed in Equation (6.12).

$$\gamma_{fo}^k = \frac{G_{fo}}{\sum_{o' \in O_k} G_{fo'} + \sum_{l' \in L_k} G_{fl'} + \sum_{f' \in F_k} G_{f'o}} \quad (6.12)$$

Here, $O_k (\subset O)$ represents the set of *HIZUEs* receiving data using the RB k , $L_k (\subset L)$ represents the set of *LIUEs* receiving data from Femto using the RB k and $F_k (\subset F)$ represents the set of *FIUEs* transmitting data to *HIZUEs* using the RB k . The numerator in the R.H.S. of Equation (6.12) represents the gain between f and o , hence it acts as an approximate measure (since the transmission power is not considered) for signal strength. The values $G_{fo'}$, $G_{fl'}$ and $G_{f'o}$, in the denominator represent the channel gain between f and o' , f and l' , and f' and o , respectively and they act as an approximate measure of the interference caused by the interfering links. The

Algorithm 3 Heuristic D2D Pair and Resource Allocation (hDPRA) Algorithm

Input 1 : F, O, L **Input 2** : *Optimal Femto Locations (Obtained by solving MinNF model)***Input 3** : $\bar{\gamma}, \alpha$ and β values**Output** : D_{fo}, C_{fo}^k, h_f^k

Initialization ();

- 1: $D_{fo} \leftarrow 0 \quad \forall f \in F, o \in O$
 - 2: $C_{fo}^k \leftarrow 0 \quad \forall f \in F, o \in O, k \in K$
 - 3: Compute $\gamma_{fo}^k \quad \forall f \in F, o \in O, k \in K$ and store in γ matrix
 - 4: $\alpha_f \leftarrow 0 \quad \forall f \in F$ { Count for number of *HIZUEs* connected to each *FIUE* }
 - 5: $\beta_o \leftarrow 0 \quad \forall o \in O$ { Count for number of *FIUEs* serving each *HIZUE* }
 - 6: $\sigma^* \leftarrow \{ \}$
 - 7: **while** size(γ) $\neq 0$ **do**
 - 8: $(f_{max}, o_{max}, k_{max}) \leftarrow \max(\gamma)$;
 - 9: **if** Updated W2L values of entries in $\sigma^* > \bar{\gamma}$ **then**
 - 10: $D_{f_{max}o_{max}} \leftarrow 1$
 - 11: $C_{f_{max}o_{max}}^{k_{max}} \leftarrow 1$
 - 12: $\alpha_{f_{max}} ++$
 - 13: $\beta_{o_{max}} ++$
 - 14: **if** $\alpha_{f_{max}} == \alpha$ **then**
 - 15: Remove $\gamma_{f_{max}o}^k \quad \forall o \in O, k \in K$
 - 16: **end if**
 - 17: **if** $\beta_{o_{max}} == \beta$ **then**
 - 18: Remove $\gamma_{fo}^k \quad \forall f \in F, k \in K$
 - 19: **end if**
 - 20: Remove $\gamma_{f_{max}o_{max}}^{k_{max}}$
 - 21: **if** Updated $\gamma_{fo}^{k_{max}} < \bar{\gamma}$ **then**
 - 22: Remove $\gamma_{fo}^{k_{max}}$ {Removes all f and o pairs using RB k_{max} from γ matrix }
 - 23: **end if**
 - 24: $\sigma^* \leftarrow \sigma^* \cup (f_{max}, o_{max}, k_{max})$
 - 25: **else**
 - 26: Remove $\gamma_{f_{max}o_{max}}^{k_{max}}$
 - 27: **end if**
 - 28: **end while**
-

numerator and denominator are two opposing parameters to the W2L ratio. Hence, larger the value of γ_{fo}^k , higher the possibility of the particular combination (f, o) to have a D2D link using RB k . W2L ratio will be higher in case RB k is not used by some Femtos for serving their UEs in a given TTI *i.e.*, the value of $\sum_{l' \in L_k} G_{fl'}$ will reduce in Equation (6.12).

σ^* is the set that contains the triplet (f^*, o^*, k^*) if f^* and o^* are having a D2D link using RB k^* . Every element in σ^* should have its W2L ratio greater than $\bar{\gamma}$, an operator defined parameter which gives control over the number of D2D links that can be formed. Initially σ^* is a null set. We start by computing the W2L ratio for each (f, o) pair for all possible RBs and store them in the γ matrix. From this set, the maximum W2L ratio is found and this gives the corresponding triplet $(f_{max}, o_{max}, k_{max})$. On adding this particular triplet to σ^* , there will be additional interference ($G_{f_{max}o^*}$) to the existing (f^*, o^*) pairs who are using RB k_{max} for their data transmissions. Hence, $\gamma_{f^*o^*}^{k_{max}}$ values have to be recalculated and checked whether they remain greater than $\bar{\gamma}$. If all of these values remain greater than $\bar{\gamma}$, the triplet $(f_{max}, o_{max}, k_{max})$ is added to σ^* and the recalculated $\gamma_{f^*o^*}^{k_{max}}$ values are stored in the γ matrix, otherwise triplet $(f_{max}, o_{max}, k_{max})$ is not added to σ^* . In case triplet $(f_{max}, o_{max}, k_{max})$ is added to σ^* , the $\alpha_{f_{max}}$ and $\beta_{o_{max}}$ values are incremented, where $\alpha_{f_{max}}$ is the count for the number of *HIZUEs* connected to *FIUE* f_{max} and $\beta_{o_{max}}$ is the number of *FIUEs* connected to *HIZUE* o_{max} . If $\alpha_{f_{max}}$ value reaches the maximum limit α , then all the γ_{fo}^k values for *FIUE* f_{max} are removed from the γ matrix. Similarly if $\beta_{o_{max}}$ reaches the maximum limit of β , then all the γ_{fo}^k values for *HIZUE* o_{max} are removed from the γ matrix. W2L ratio in the γ matrix is updated $\forall f, o$ which are using RB k_{max} . If any of the updated $\gamma_{fo}^{k_{max}}$ is lesser than $\bar{\gamma}$, then that value is removed from the γ matrix and is not considered during the next iteration. Finally, it removes $\gamma_{f_{max}^*o_{max}^*}^{k_{max}}$ from the γ matrix and continues to the next iteration until all the entries are removed from the γ matrix.

Step 2: Heuristic D2D Power Allocation (hDPA)

Using outputs of the hDPRA from the Step 1 Algorithm 3, namely D_{fo} , C_{fo}^k , h_f^k , as the input in the Step 2 we solve an LP model which adjusts the power for each of the D2D links. The LP model is formulated similar to D2D MILP model presented earlier but with fewer constraints as given below.

$$\min \sum_{f \in F} \sum_{k \in K} p_f^k \quad (6.13)$$

$$p_f^k \leq h_f^k \quad \forall f \in F, k \in K \quad (6.14)$$

$$\sum_{f \in F} (G_{fl} \times S_{lk} \times p_f^k \times P_{max}^d) \leq I_l \quad \forall l \in L, k \in K \quad (6.15)$$

$$\begin{aligned} Inf * (1 - C_{fo}^k) + G_{fo} p_f^k P_{max}^d \geq \{ & (\lambda_o N_o + \lambda_o \sum_{m \in M} G_{mo} P_{macro} + \lambda_o \sum_{a \in B_k} G_{ao} P_a^{fem} + \\ & \lambda_o \sum_{f' \in F \setminus f} G_{f'o} p_{f'}^k P_{max}^d) \} \quad \forall f \in F, o \in O, k \in K \end{aligned} \quad (6.16)$$

Finally, the LP model for D2D power control is formulated as follows,

$$\min \sum_{f \in F} \sum_{k \in K} p_f^k \quad s.t., (6.14), (6.15), (6.16).$$

The proposed two-step D2D heuristic algorithm is fair to both the *IUEs* and *HIZUEs* by choosing the D2D links, allocating resources to the D2D links and adjusting their transmission power levels.

6.4.3 Time Complexity

The proposed D2D MILP model takes more computation time. To reduce the running time complexity of D2D power selection, we have proposed a two-step D2D heuristic algorithm. The running time complexity for hDPRA (Step 1 of D2D heuristic algorithm) is shown below,

- The time taken to compute maximum value in the γ matrix is $O(f * o * k)$
- The running time for the while loop is $O(f * o * k)$
- The total running time is $O(f^2 * o^2 * k^2)$

Since the Step 2 of D2D heuristic algorithm (hDPA, an LP model) has a polynomial running time algorithm [72], our proposed D2D heuristic algorithm runs in polynomial time and its low running time makes it usable at F-GW/SON.

6.4.4 Optimal Femto Transmit Power (OptFP) MILP Model

Under some circumstances, when it is not possible to establish D2D links due to lack of *FIUEs* (for example: if we observe Figure 6.1, there are no *FIUEs* present in east side of the building to establish D2D link with *HIZUEs* (o_5, o_6, o_7 and o_8)),

the F-GW/SON can be directed to reduce the Femto transmission power, thereby reducing the interference to *HIZUEs* from it. The arbitrary tuning of Femto transmit power may degrade the performance of total *IUEs* connected to that Femto and also cause coverage issues. We propose a means to optimally control the Femto transmit power whenever there are *HIZUEs* present outside the building but no *FIUE* is inside, thereby guaranteeing a minimum $SINR_{Th}$ for *IUEs* and reduce the interference to *HIZUEs*. The corresponding *HIZUE* can then connect with *MBS* for D-plane communication. We used the same OptFP MILP model (explained in previous chapter 4) and by solving it we can,

- Determine the optimal power required by each Femto for maintaining the $SINR_{Th}$ in each of the inner sub-regions and maintain the SINR degradation at less than 2 dB for *HIZUEs*.
- Determine the Femto to which the users in any given inner sub-region have to be associated with.

The above OptFP model guarantees a certain minimum $SINR_{Th}$ for *IUEs* and less degradation for *HIZUEs*.

Algorithm 4 Joint D2D Heuristic and OptFP (JDHO) Algorithm

Input 1 : Set of all inner and outer sub-regions

Input 2 : Potential *HIZUEs* in *HIZone*

- 1: All Femtos are configured to transmit at their peak power by default.
 - 2: All *HIZUEs* (O) are connected to one of *MBSs* for their C-Plane.
 - 3: Find the set of all *HIZUEs*, O' , for whom it is not possible to establish *D2D based relays* by using *FIUEs*. $O' \subset O$.
 - 4: Find the set of Femtos, B' , who are causing interference to O' *HIZUEs*. $B' \subset B$.
 - 5: Apply the OptFP model [41] on B' to reduce their transmit powers so that interference to O' is reduced.
 - 6: The O' *HIZUEs* are then allowed to connect to one of *MBSs* even for their D-plane (*i.e.*, no *D2D links*, it is the traditional cellular communication).
 - 7: Apply *D2D Heuristic Algorithm* (Algorithm 3) on $(O - O')$ *HIZUEs* to establish *D2D based relays* by using *FIUEs*
-

6.4.5 Joint D2D Heuristic and OptFP (JDHO) Algorithm

In most of the cases, the F-GW/SON might not be able to establish *D2D links* in all sides of the building. It is also equally probable that *D2D links* are established

more readily in some sides of the building and not in the other sides due to lack of *FIUEs* (For *e.g.*, east and west sides of the building given in Figure 6.1). Hence, the F-GW/SON has to reduce the transmit power of Femtos optimally so as to allow the *HIZUEs* to connect with one of MBSs. This can be achieved by the combinatorial utilization of both D2D heuristic algorithm and OptFP model (called as JDHO algorithm), that would allow some HIZUEs which do not have any FIUE to get connected to one of MBSs and the remaining HIZUEs through D2D links. The proposed JDHO algorithm is given in Algorithm 4.

6.4.6 Cost Analysis

In our system model, two-hop communication cost is essentially the additional resources incurred by the proposed system over the existing traditional system. It can be classified as resource utilization, energy consumption and additional interference due to the reuse of spectrum.

1. *Resource Utilization:* In the first-hop communication (Femto to LIUEs/FIUEs), the radio resources (RBs) allocated for the data demanded by HIZUEs are the additional cost incurred by the proposed system. If the downlink scheduler at the Femto has excess resources (even after fulfilling the demand of the IUEs in a TTI) then the additional cost incurred is zero. But, if the Femto lacks excess resources, then the cost to the system is the resources allocated to the FIUEs to receive *HIZUEs* data from the Femto. These resources could have otherwise been scheduled to the LIUEs. In the second-hop (FIUE to HIZUE (D2D link)), there is reuse of radio resources which increases the interference (explained in next paragraph). Hence, the cost can be expressed as given in Equation (6.17), when the downlink scheduler at Femto does not have excess resources.

$$Radio\ Resource\ Cost = \sum_{i=1}^{N_F} No\ of\ RBs\ allocated\ to\ FIUE_i\ by\ Femto. \quad (6.17)$$

Where N_F is the number of *FIUEs* participating as *D2D based relays* for Femto to *HIZUE* communication.

2. *Interference:* In the first-hop there is no new interference source introduced to the traditional system, whereas in the second-hop (due to reuse of Femto RBs by D2D links) there is additional interference for the IUEs present in the

Table 6.2: Simulation Parameters

Parameter	Value
Building dimensions	48 m \times 48 m \times 3 m
Number of Rooms	16
Room dimensions	12 m \times 12 m \times 3 m
Number of inner Sub-regions	144
Number of outer Sub-regions	52
Inner Sub-region dimension	4 m \times 4 m \times 3 m
$SINR_{Th}$ for $IUEs$ (MinNF Model)	0 dB
Number of Floor	One
Floor and Wall loss	10 and 8 dB
Macro Transmit Power (P_{macro})	46 dBm (39.8 W)
Femto Transmit Power (P_{max}^f)	20 dBm (0.1 W)
Macro BS Height	30 m
D2D Max Transmit Power (P_{max}^d)	20 dBm (0.1 W)
Number of $IUEs$	109
$HIZUE SINR_{Th}$	-2 dB
α ($FIUE$ D2D links limit)	1
β ($HIZUE$ D2D links limit)	1
$\bar{\gamma}$ (W2L Threshold)	5

system. This could degrade SINR of $IUEs$ and this reduction in SINR is the additional cost incurred in the proposed system.

3. *Energy Consumption*: In our work, the transmission power of the Femto (first-hop communication) is kept as P_{max}^f (0.1 W) to study the system performance in the worst case scenario. In second hop communication, the power consumed for the transmission from $FIUE$ to $HIZUE$, which varies based on distance between $HIZUE$ and $FIUE$, is the cost to the system.

6.5 Performance Results

The system model described in Section 6.4 has been simulated using MATLAB. The simulation parameters are given in Table 6.2. We considered a single-floor building with a single MBS placed at a distance of 350 m from the south west side of the building. Further, we considered the scenario where all Femtos and MBS are configured to use the same 5 MHz channel (*i.e.*, 25 RBs). Femtos are allowed to be attached only to the ceiling of the building and we did not consider the user mobility

in our simulation experiments as we focused only on indoor scenarios. We show the performance of the LTE HetNet system in the worst case scenario where all RBs of all Femtos are in use in every TTI. Also we assume that channel state information of links between *FIUEs* and *HIZUEs* is available at the F-GW/SON for the fine tuning of D2D link transmission power. For the performance evaluation, we generate different topologies by varying number of UEs (*i.e.*, *IUEs* and *HIZUEs*) and their positions in such a way that in each of the topologies that we considered there always exist one or more *FIUEs* for forming D2D links for each of the *HIZUEs*.

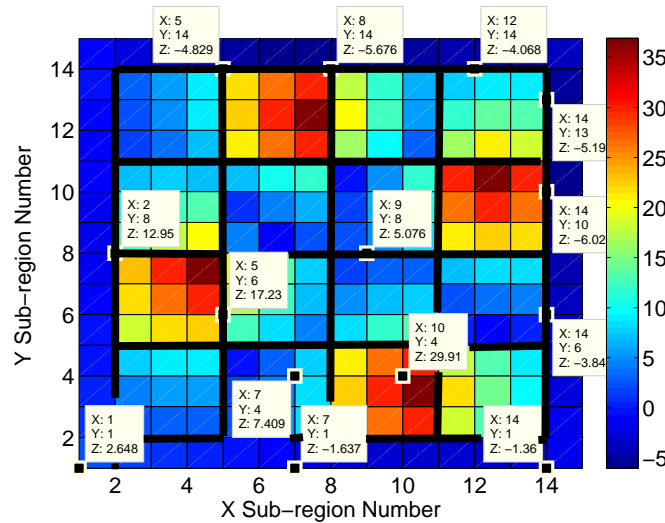


Figure 6.3: REM plot of sub-regions inside building after placing Femtos by using MinNF

6.5.1 MinNF Model: Performance Results

The four Femtos with their optimal co-ordinates are obtained by solving MinNF ILP problem with GAMS CPLEX solver [33]. The Femtos are placed in dark brown regions inside the building at sub-regions I_{30} , I_{71} , I_{98} , I_{129} (refer Figure 4.1 for numbering of sub-regions) as shown in Figure 6.3. All the Femtos transmit at their peak power (0.1 W). Figure 6.3 also shows SINR distribution for inner and outer sub-regions. For example, UEs in the sub-region I_{98} get SINR of 29.9 dB as the Femto (F3) is very close to it. Similarly, the sub-regions I_6 , I_{29} , I_{79} , and I_{51} inside the building have relatively good SINR values 12.9, 17.2, 5.0, 7.4 dB, respectively. But if we consider *Macro only scenario*, where there are no Femtos inside the building like in Figure 1.7, the sub-regions I_6 , I_{29} , I_{79} , and I_{51} inside the building have relatively less SNR values of -8.2, -8.3, -9.2, -8.3 dB, respectively due to poor indoor signal strength.

Due to addition of Femtos, the UEs present inside the building get improved SINR up to 35 dB (refer Figure 6.3). But in this case, the outer sub-regions (e.g., O_{48}), get SINR as low as -6.0 dB. This is a consequence of Femtos being closer to the corners of the building and hence there being a high power leakage (interference) in HIZone.

6.5.2 Performance Results of D2D MILP Model and D2D Heuristic Algorithm

In this section, we compare the performance of proposed D2D MILP model and D2D heuristic algorithm with the following three different schemes.

- *Macro only*: No Femtos are placed inside the building. No HIZone exists around the building, but the MBS has to serve even *IUEs* with poor signal quality.
- *Full Power Femto*: Femtos are optimally placed inside the building by MinNF model, but Femtos are configured to emit at their full transmission power. In this scheme, HIZone exists around the building and therefore affects performance of *HIZUEs*.
- *Optimal Femto Power (OptFP)*: Femtos are optimally placed inside the building by MinNF model, but transmission power of **all** the Femtos are reduced by OptFP model to decrease the interference to *HIZUEs*. Since such reduction at all the Femtos is not needed, this scheme affects performance of *IUEs*.

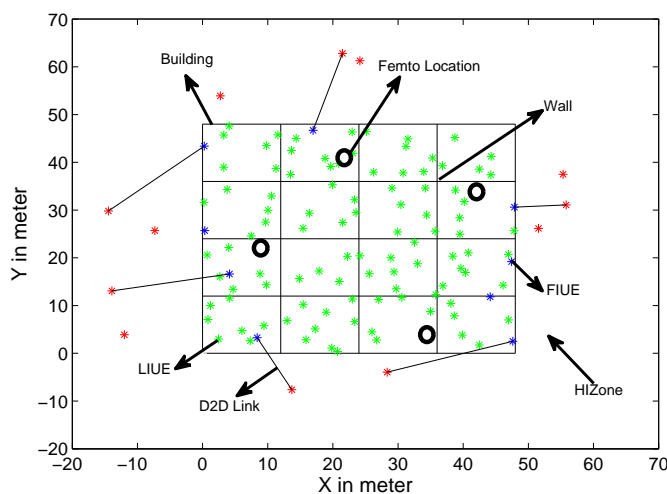


Figure 6.4: *hDPRA* D2D links in instance #1

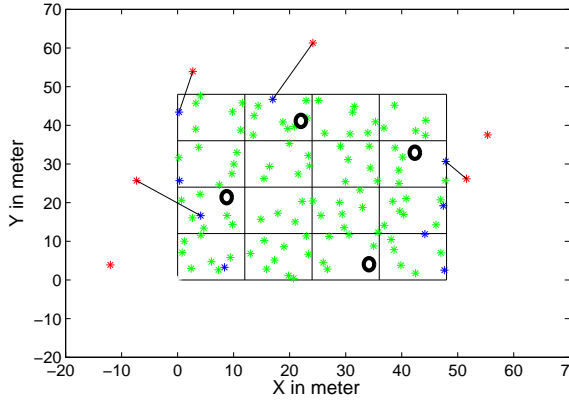


Figure 6.5: *hDPRA* D2D links in instance #2

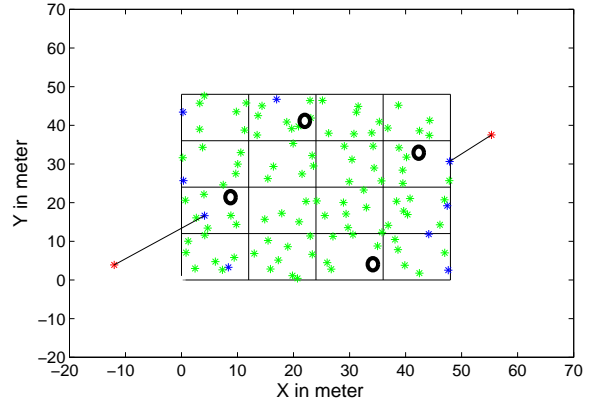


Figure 6.6: *hDPRA* D2D links in instance #3

D2D Heuristic Algorithm: Performance Results

In this section, we show the formation of efficient D2D links and SINR CDF of UEs. Also, we studied the effect of $SINR_{Th}$ on SINR of *IUEs* and effect of *IUE* density on *FIUEs* transmission power. Finally, we have shown the average performance of *D2D heuristic algorithm* by considering 500 different combinations of *IUEs* and *HIZUEs* locations.

Formation of D2D links and their effects on SINR of UEs:

In this section, we describe the *hDPRA* which efficiently chooses the potential D2D based relay pairs and allocates radio resources to them. Then we discuss about the performance of *hDPA* for power control of D2D links.

(a) *hDPRA Results:*

The optimal Femto locations given by the MinNF model are shown as the circled regions in Figure 6.4. The red, green and blue marked locations are the positions of the deployed *HIZUEs*, *LIUEs* and *FIUEs*, respectively in this topology # 1. These UEs locations at a particular instance (TTI) along with other parameters are given as input to the proposed heuristic algorithm. In Figure 6.4, D2D connectivity diagram shows the number of D2D links in the instance #1. On one hand, there are relatively less number of *HIZUEs* at the south side of the building, but on the other hand, at the east, west and north sides of the building, there are some *HIZUEs* not served by *FIUE* in a particular TTI. It has to be kept in mind that a *HIZUE* can

connect to only one *FIUE* in a given TTI as shown in all sides of the building. The reason for the other *HIZUE* to not connect is that even when there are certain free RBs that are not used by other D2D links, there is a possible interference between the *LIUEs* or the possibility of guaranteeing an SINR threshold only by increasing the transmission power for D2D links above the 3GPP standards [66,79]. Hence, the *HIZUE* that does not get paired in the given TTI, get paired in subsequent TTIs. Figures 6.5 and 6.6 show the pending D2D link connections to be made in subsequent instances. The output from hDPRA is given as the input to GAMS CPLEX solver [33] through an interface between MATLAB and GAMS to solve the hDPA LP model. Solving the hDPA model yields the transmission power for the D2D links.

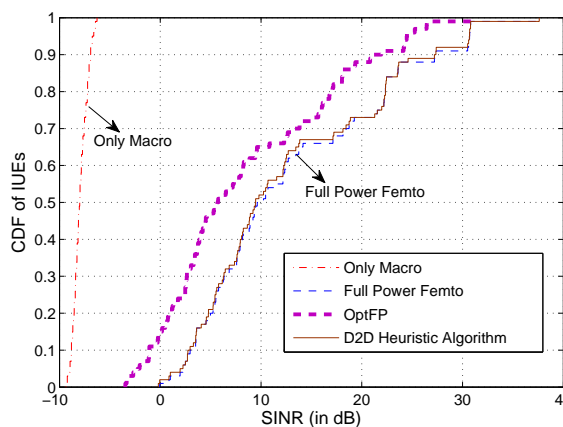


Figure 6.7: SINR CDF of *IUEs* using Heuristic Algorithm

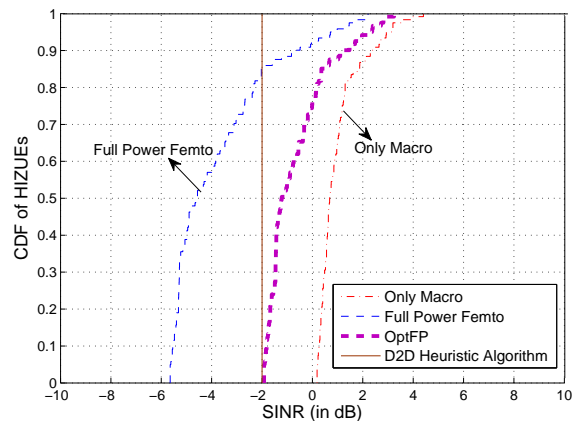


Figure 6.8: SINR CDF of *HIZUEs* using Heuristic Algorithm

(b) *hDPA Results:*

Figures 6.7 and 6.8 show the SINR CDF of *HIZUEs* and *IUEs*, respectively. In *Only Macro* scheme (shown by red curve) the *HIZUEs* receive good SINR values but the *IUEs* receive very less SINR values, less than -5 dB, which is due to the signal degradation caused by the walls. In our evaluation, we considered the worst case scenario where the *Full Power Femto* scheme (shown by blue curve) has increased SINR for the *IUEs* but at the cost of the SINR of *HIZUEs*. To overcome this issue, Femtos are made to transmit at lower power in the *OptFP* [41] *i.e.*, *OptFP* scheme (shown by purple curve) thus alleviating the interference issues of *HIZUEs*, although this declines the SINR value of *IUEs*. However in *D2D heuristic algorithm* scheme (shown by brown curve) *HIZUEs* receive good SINR values and the *IUEs* also receive SINR values close to that of *Full Power Femto* scheme (worst case scenario).

The straight line in Figure 6.8 represents the SINR value of *HIZUEs* using *D2D heuristic algorithm* maintained at -2 dB constraint (to ensure basic voice call communication for all suffering *HIZUEs*) of outdoor (HIZone) region. This is achieved by minimizing total transmit power of *FIUEs*, and thus the minimum power required to guarantee $SINR_{Th}$ ensures that all the *HIZUEs* achieve $SINR_{Th}$. The small deviation in the *IUEs* SINR values is because of the interference caused by the D2D pairs. The overall degradation in SINR for *IUEs* is 2% in the *D2D heuristic algorithm* as compared to the *Full Power Femto* scheme. But in comparison to the *OptFP* [41] scheme the SINR of *IUEs* improves by 39% for the *D2D heuristic algorithm*. Thus *D2D heuristic algorithm* is able to provide a good signal strength to the *HIZUEs* without affecting the *IUE* performance.

Effect of $SINR_{Th}$ on SINR of *IUEs*:

We studied the variation in SINR of *IUEs* by varying $SINR_{Th}$ values. We also measured the variation in average D2D transmission power for topology # 1. As shown in Table 6.3, the average transmit power of D2D links increases gradually with increasing $SINR_{Th}$. This increases the interference to the *IUEs* and hence causes a fall in average *IUE* SINR with increase in $SINR_{Th}$ of *HIZUEs*. We note that even with changes in $SINR_{Th}$ the degradation of *IUEs* SINR is not very significant. This validates the efficiency of our *D2D heuristic algorithm*.

Table 6.3: $SINR_{Th}$ vs *IUEs* SINR

Metric	$SINR_{Th} = -3$ dB	$SINR_{Th} = -2$ dB	$SINR_{Th} = -1$ dB	$SINR_{Th} = 0$ dB
Average Transmission Power of D2D links	0.03 W	0.04 W	0.05 W	0.06 W
Average <i>IUEs</i> SINR	12.78 dB	12.75 dB	12.72 dB	12.68 dB

Effect of *IUE* density on *FIUEs* transmission power:

In our work, we studied the variation in D2D transmission power. Here we consider topology # 1 as above but vary the number of *FIUEs* for a fixed *HIZUE* location (shown in Figure 6.4). Initially, the total number of *IUEs* is 110 (*i.e.*, $LIUEs = 100$ (constant) and $FIUEs = 10$) and we gradually increase only the *FIUEs* count to 15, 20, 25, 30 and 35. Table 6.4 shows that as the number of *FIUEs* increases, the average transmit power of *FIUEs* decreases. This is due to the increased possibility

of forming shorter *D2D based relay* links with increasing *FIUE* density levels. Once the *FIUEs* density level is very high, the transmission power of the *FIUEs* will get saturated due to marginal decrease in D2D relay link distance.

Table 6.4: Number of *FIUEs* vs Average D2D transmission power

S.NO	No. of <i>FIUEs</i>	Average D2D transmission power (W)
1	10	0.061
2	15	0.054
3	20	0.051
4	25	0.043
5	30	0.042
6	35	0.041

Average performance of *D2D heuristic algorithm*:

In order to obtain average performance of proposed *D2D heuristic algorithm*, we have evaluated its performance for 500 different topologies by varying the number of *IUEs* in the range of 110 to 135 and *HIZUEs* in the range of 1 to 30 and measured the SINR of *IUEs* and *HIZUEs*. Figure 6.9 shows SINR CDF of *IUEs* over various scenarios for different schemes. When compared to the *Optimal Femto Power* scheme, *D2D heuristic algorithm* improves the SINR of *IUEs* by 40% as shown in Figure 6.9. However, the degradation in SINR of *IUEs* is only 1.6% when compared to the *Full Power Femto* scheme. Similarly, Figure 6.10 shows average CDFs of *HIZUEs* over various scenarios for different schemes. If we observe Figure 6.10, the minimum $SINR_{Th}$ of -2 dB is maintained for all *HIZUEs* in the *HIZone*.

D2D MILP Model: Performance Analysis

In the proposed D2D heuristic algorithm, we cannot set the number of D2D links in each TTI. To make a fair comparison with the D2D MILP model, we have given the number of D2D links obtained from the D2D heuristic algorithm in each instance as an input for the D2D MILP model. For example, for the instance #1 shown in Figure 6.4 the number of D2D links given by the heuristic algorithm is six. Hence in the D2D MILP model the number of D2D links that have to be formed at the instance #1 is fixed to be six, *i.e.*, $\psi = 6$.

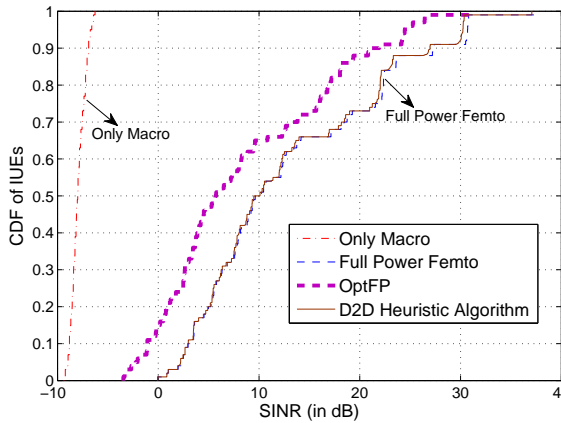


Figure 6.9: Average SINR CDF of $IUEs$ for various schemes in 500 topologies

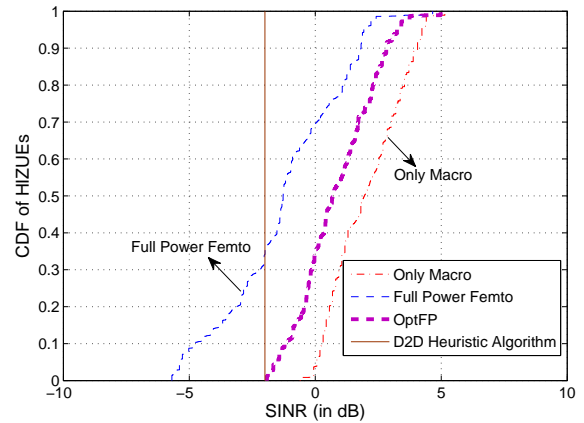


Figure 6.10: Average SINR CDF of $HIZUEs$ for various schemes in 500 topologies

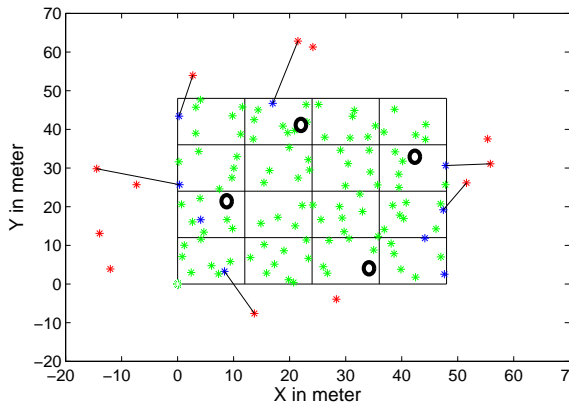


Figure 6.11: MILP D2D links in instance #1

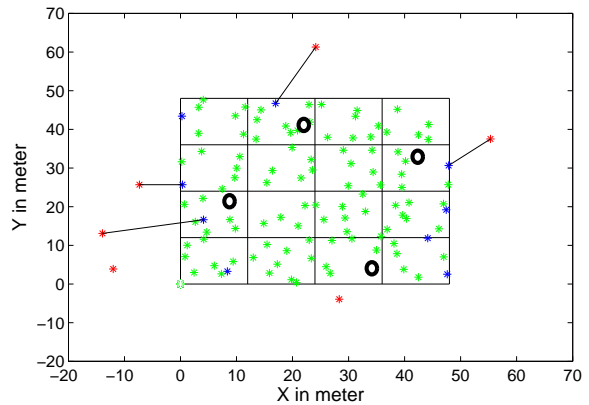


Figure 6.12: MILP D2D links in instance #2

In Figure 6.11, D2D connectivity diagram shows the number of D2D links in the instance #1. As in the heuristic algorithm, there are some $HIZUEs$ which are not served by $FIUEs$ in a particular TTI. The pending $HIZUEs$ served by $FIUEs$ based on the D2D MILP model are shown in Figure 6.12 and Figure 6.13. In the instance #1, the algorithm mostly tries to form all D2D links with the closer $HIZUEs$ to minimize the total D2D transmission power. In the next TTI, it tries to form the remaining D2D links with the farther $HIZUEs$. Hence the $FIUE$ needs to transmit high transmission power to maintain these D2D links, which increases the possibility of interference between $LIUEs$ and $HIZUEs$. Figure 6.14 shows the SINR CDF of $IUEs$. The advantage of forming optimal D2D link is that $D2D$ MILP model achieves SINR close to that of *Full Power Femto* because the power value is optimal.

Similarly, the SINR CDF of *HIZUEs* in optimal approach (D2D MILP) is also maintained $SINR_{Th} = -2dB$ as in the heuristic approach (Figure 6.8). The SINR CDF of *HIZUEs* using MILP model will be same as that of the heuristic algorithm (Figure 6.8) because the same $SINR_{Th}$ is maintained in both D2D heuristic algorithm and D2D MILP model. The overall degradation in SINR for *IUEs* is 0.5% in the *D2D MILP model* compared to the *Full Power Femto* scheme. On the other hand, when compared to *OptFP* scheme the SINR of *IUEs* improves by 52% in the *D2D MILP model*. Thus *D2D MILP model* is able to provide lesser degradation in signal strength to the *IUEs* than the *D2D heuristic algorithm* with the cost of more running time (explained further in Section 6.5.3).

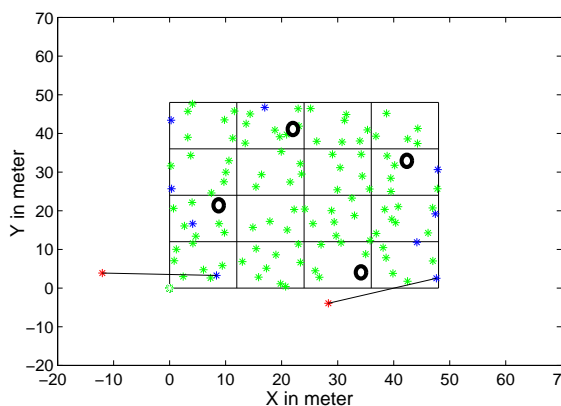


Figure 6.13: MILP D2D links in instance #3

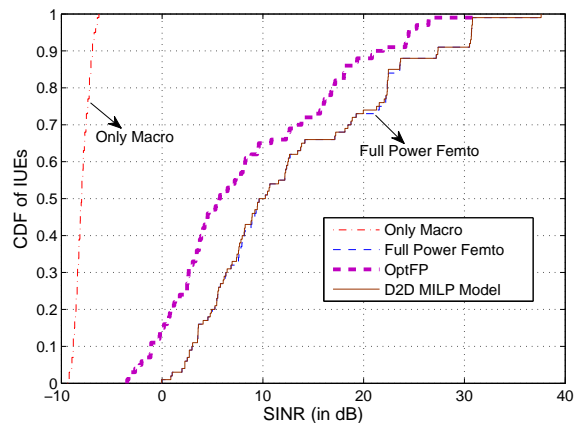


Figure 6.14: SINR CDF of *IUEs* using MILP Model

6.5.3 Comparison between D2D MILP Model and D2D Heuristic Algorithm

To compare D2D MILP model and D2D heuristic algorithm, we have taken the seven different topologies, where the *HIZUE* placement and the number of *HIZUEs* vary as shown in Figure 6.15, Figure 6.16, Figure 6.17, Figure 6.18, Figure 6.19, Figure 6.20 and Figure 6.21. Table 6.5 shows indices of outer sub-regions having *HIZUEs* in these seven topologies.

SINR of IUEs

In MILP model, the average power transmitted by the D2D links is lower than that in the heuristic algorithm. This helps to reduce the interference to *IUEs*. Figure 6.22

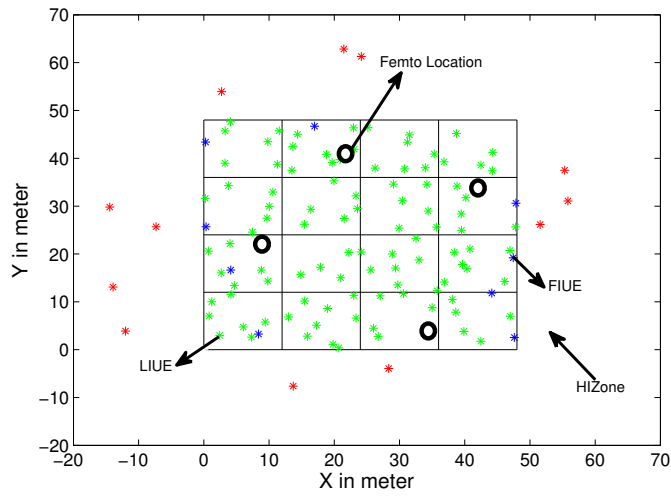


Figure 6.15: UE distribution in Topology 1

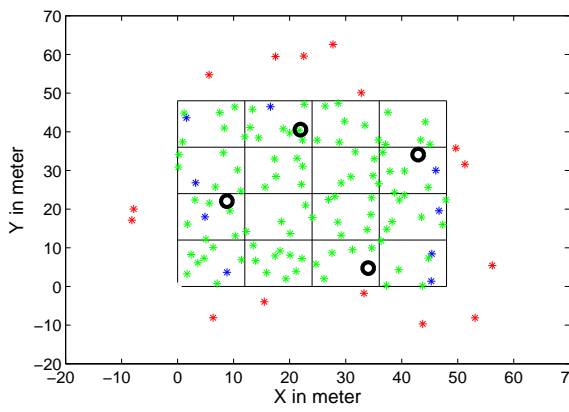


Figure 6.16: UE distribution in Topology 2

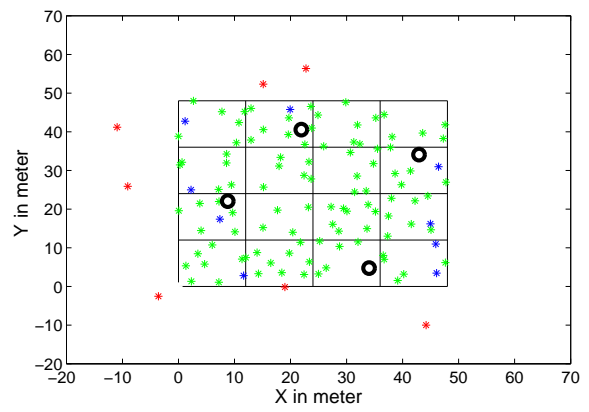


Figure 6.17: UE distribution in Topology 3

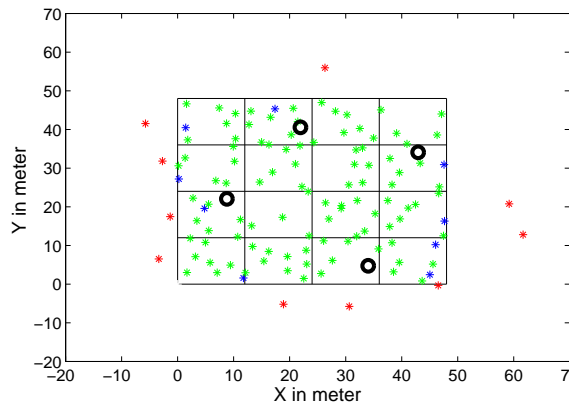


Figure 6.18: UE distribution in Topology 4

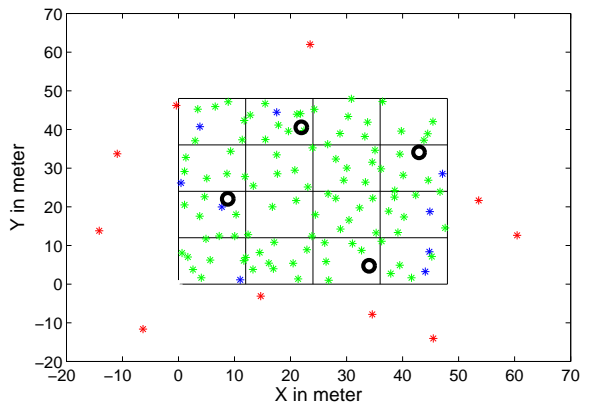


Figure 6.19: UE distribution in Topology 5

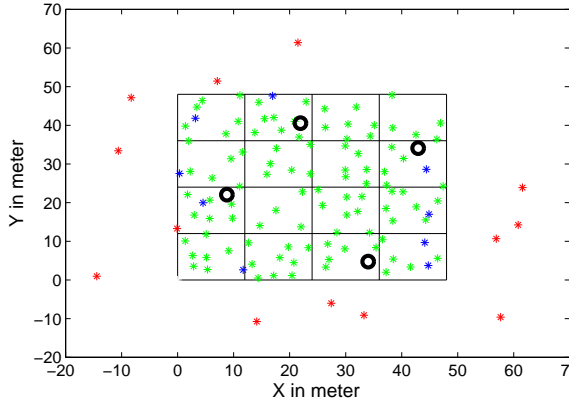


Figure 6.20: UE distribution in Topology 6

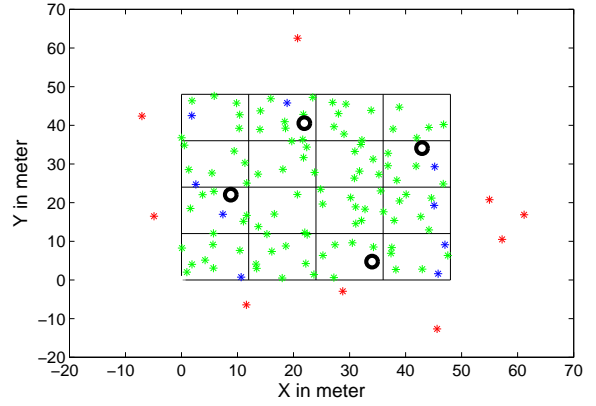


Figure 6.21: UE distribution in Topology 7

shows the average SINR achieved by *IUEs* in different topologies. The average SINR achieved in the heuristic algorithm is very close to that in the D2D MILP model.

Table 6.5: Topologies having varying distribution of *HIZUEs* in HIZone

Topology	No. of HIZUEs	Indices of Outer Sub-regions having HIZone UEs
1	12	$(O_5, O_9, O_{15}, O_{21}, O_{27}, O_{28}, O_{29}, O_{30}, O_{34}, O_{40}, O_{45}, O_{46})$
2	15	$(O_3, O_5, O_{10}, O_{12}, O_{14}, O_{18}, O_{23}, O_{25}, O_{30}, O_{32}, O_{41}, O_{44}, O_{45}, O_{46}, O_{48})$
3	7	$(O_1, O_6, O_{13}, O_{27}, O_{35}, O_{43}, O_{45})$
4	10	$(O_{17}, O_{23}, O_{29}, O_6, O_9, O_{13}, O_{22}, O_{26}, O_{35}, O_{46})$
5	10	$(O_1, O_{21}, O_{31}, O_{37}, O_{10}, O_{13}, O_{22}, O_{26}, O_{45}, O_5)$
6	13	$(O_{15}, O_{21}, O_{31}, O_{41}, O_{45}, O_8, O_{10}, O_{14}, O_{20}, O_{22}, O_{26}, O_5)$
7	9	$(O_9, O_{23}, O_{35}, O_{45}, O_{13}, O_{20}, O_{24}, O_{26}, O_4)$

Running Time

Figure 6.23 shows the average running times of D2D MILP model and D2D heuristic algorithm for different topologies. These run times are obtained on a workstation having the following configuration: 12 GB RAM, 8 Cores of 2.40 GHz each. We observe that the running time for *D2D heuristic algorithm* showed an average decrease of up to 87% when compared to *D2D MILP model* in different topologies of *HIZUE* placement. In each topology, depending on the position of the *HIZUEs*, the running time of GAMS optimization solver changed. For example, when *HIZUEs* are very close to each other it demands efficient spectrum allocation and power control between

FIUE and *HIZUE* in all instances without creating interference to *IUEs*. Therefore, on a few occasions many D2D links may not be possible within the *HIZone* at a particular TTI instance which indirectly increases the average running time. As we discussed earlier in the system model, the D2D heuristic algorithm will be running at the F-GW/SON which will have abundant computing resources to handle the load of so many Femtos [99, 100]. Therefore, the run time of *D2D heuristic algorithm* is only a few ms and usable in practical deployments of Femtos.

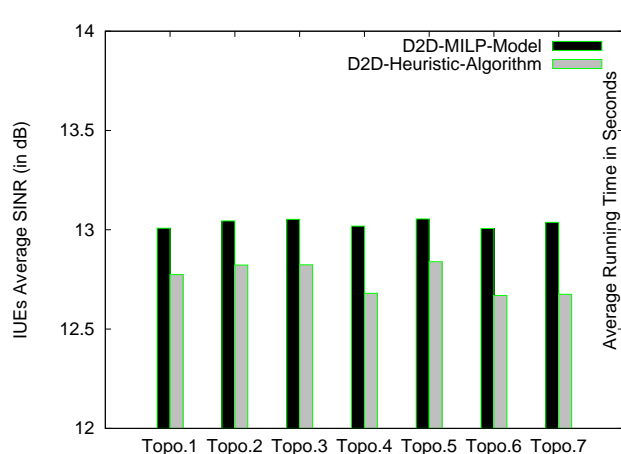


Figure 6.22: Average SINR of *IUEs*

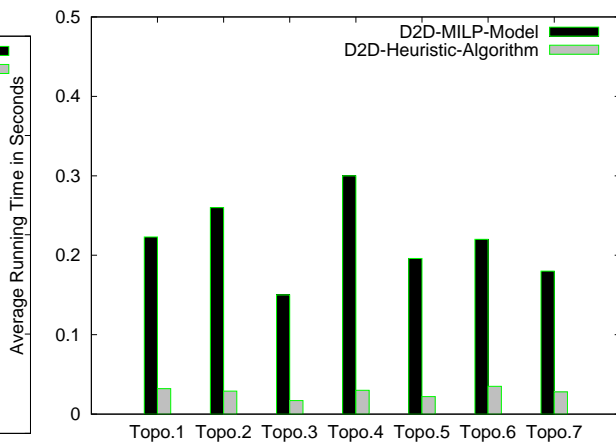


Figure 6.23: Running Time of D2D MILP and heuristic algorithm

Energy Consumption

Figure 6.24 shows the average power transmitted by the D2D links for different topologies with the $SINR_{Th}$ of -2 dB. The average power transmitted by the D2D links (for example, it is 0.043 W and 0.047 W in *D2D MILP model* and *D2D heuristic algorithm*, respectively) are lower than the maximum allowed D2D link power of 0.1 W. We can clearly observe that the average transmission power of the D2D links in the heuristic algorithm is close to that in the MILP model and the difference between them is marginal.

6.5.4 Cost Analysis

In our work we assumed that the downlink scheduling algorithm [101] (*e.g.*, proportional fair or priority set scheduler) will allocate only one RB to the selected Femto to *FIUE* links or *FIUE* to *HIZUE* links in every TTI. Using this, we have simulated

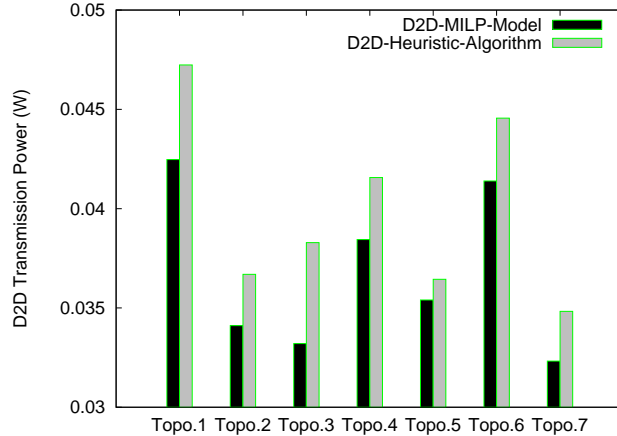


Figure 6.24: D2D Average Transmission Power

500 different possible combinations for *IUEs* and *HIZUEs* locations and observed that an average of five D2D links are formed in a TTI. Hence, five RBs will be used for the first-hop *i.e.*, Femto to FIUE link to get the data for *HIZUEs*. This means that these five RBs are the *radio resource cost*.

The *D2D based relay* links will reuse these five Femto RBs in the second-hop transmission (*FIUE* to *HIZUE*) [102–104]. The interference introduced in the system by these *D2D based relay* links leads to decrease in the SINR of IUEs by 1.6% (averaged over 500 scenarios). This is the cost of using the proposed system in terms of interference.

As shown in Figure 6.24, the transmission power of the D2D links is adjusted in order to maintain the $SINR_{Th}$ of -2 dB for *HIZUEs*. Because of power adjustment, D2D links are able to reuse the same RBs and thereby improve the spectral efficiency of the HetNet system. Hence, the total energy consumption [105] in the two-hop communication is $0.1 \text{ W} + \text{D2D based relay transmission power}$.

6.5.5 JDHO Performance Analysis

Unlike the previous Section, here we study the performance of JDHO algorithm by considering a topology where some of the *HIZUEs* could not able to make D2D links due to lack of *FIUEs*. As seen in Algorithm 4 (Step 6), these O' *HIZUEs* connect to the MBS for their D-plane communication. The remaining *HIZUEs* (*i.e.*, $(O - O')$) form D2D links with *FIUEs* by using proposed *D2D heuristic algorithm*. Consider the topology shown in Figure 6.25, where one can see that there are no *FIUEs* in the vicinity of *HIZUE A*. *D2D heuristic algorithm* which is running at F-GW cannot

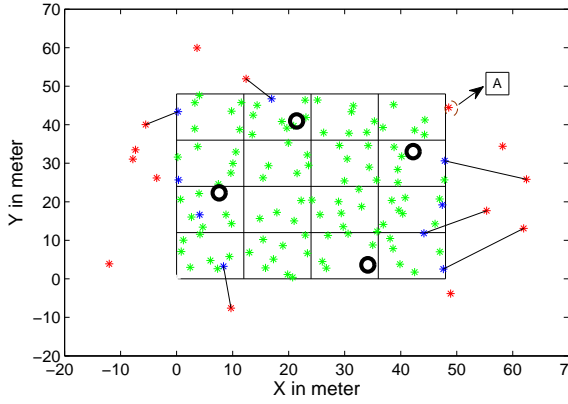


Figure 6.25: *hDPRA* D2D links in instance #1

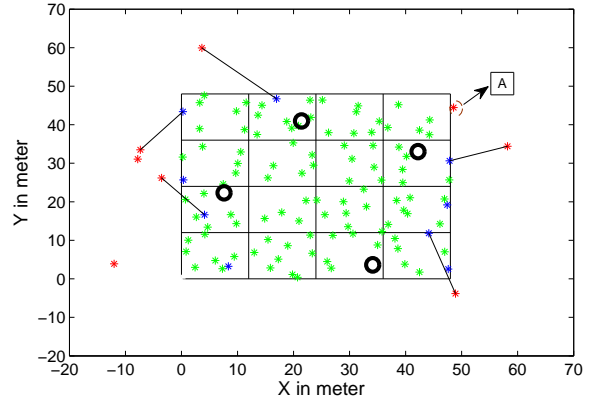


Figure 6.26: *hDPRA* D2D links in instance #2

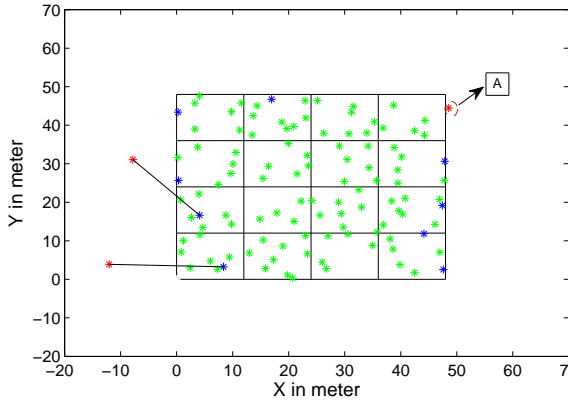


Figure 6.27: *hDPRA* D2D links in instance #3

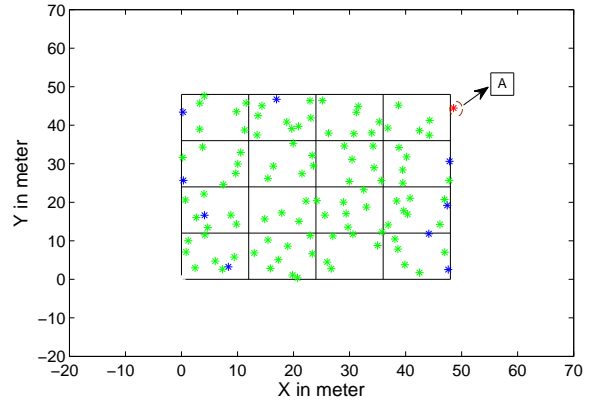


Figure 6.28: *hDPRA* D2D links in instance #4

able to form any D2D link for serving the *HIZUE* A. In order to reduce interference at this *HIZUE* in the *HIZone*, *JDHO* algorithm controls the transmit power of the Femto which is serving the parts of the building closest to this region. By doing so, the *HIZUE* A can maintain a minimum $SINR_{Th}$ in *HIZone*. Figure 6.26, Figure 6.27 and Figure 6.28 show the pending D2D links established in the subsequent instances. When compared to *Full Power Femto* scheme where the degradation of *IUEs* SINR is found to be 2% as obtained in the previous case (shown in Figure 6.7), in the current *JDHO algorithm* scenario as shown in Figure 6.29 the degradation of *IUEs* SINR was found to be 9%. This is because, to maintain the communication (D-Plane) for *HIZUE* A from MBS, the corresponding/particular Femto has to optimally decrease its transmission power further to reduce the SINR of *IUEs*. Figure 6.30 shows that *HIZUEs* maintained $SINR_{Th}$ when *JDHO algorithm* is used. In previous scenario

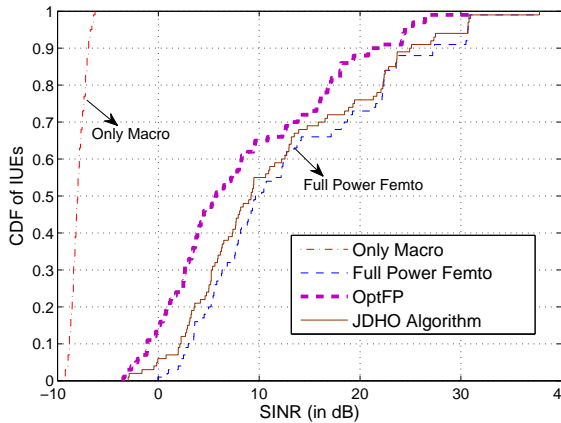


Figure 6.29: SINR CDF of $IUEs$ using JDHO algorithm

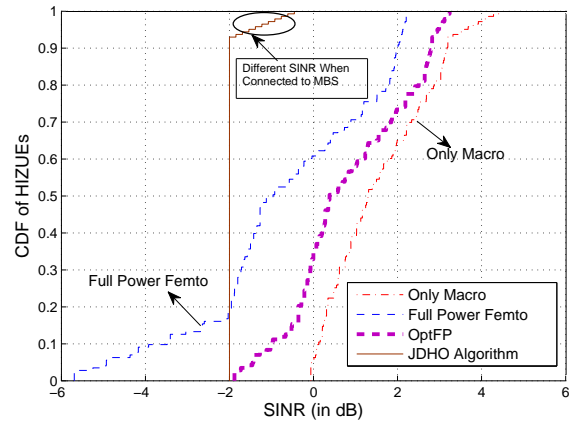


Figure 6.30: SINR CDF of $HIZUEs$ using JDHO algorithm

(shown in Figure 6.8) we maintained a constant $SINR_{Th}$ to all HIZUEs. But in the present scenario, in JDHO algorithm by using the OptFP model, the $SINR_{Th}$ for $HIZUE A$ is maintained at more than -2 dB (as shown in circle region).

6.6 Summary

In this chapter, we showed that D2D when adopted to LTE HetNets increases the spectrum efficiency by guaranteeing good $SINR_{Th}$ for all the users even when the Femtos are transmitting at their full power. By introducing Femtos, a fair distribution for both $IUEs$ and $HIZUEs$ with minimal interference can be observed. Additionally, SINR of $IUEs$ is increased by 40% when compared to the *OptFP* [41] scheme was noted in *D2D heuristic algorithm*. On the other hand, the decrease in the SINR of $IUEs$ compared to the *Full Power Femto* scheme is only 1.6%. We also observed that the average running time of the proposed *D2D heuristic algorithm* was 87% lesser when compared to *D2D MILP model*.

Chapter 7

A Novel Resource Allocation and Power Control Mechanism for Hybrid Access Femtos in LTE HetNet

7.1 Introduction

In the previous chapter, we solved the *HIZone* problem by employing *D2D based relays* for serving *HIZUEs*. Unlike in the previous chapter, in this chapter we solve the same *HIZone* problem by efficient resource allocation and power control at Femtocells which are configured in hybrid access mode of operation.

Since Femtos are deployed for offering high data rate services to indoor (paid) users in enterprise and residential buildings, each Femto is configured with a list of subscribers called Subscriber Group (SG) so that only the users in the SG can access them. The users not belonging to this list are called Non-SG (NSG) and they are served by MBSs deployed in outdoor environments even when they are in close proximity to a Femto deployed in indoors. This type of restricted access is called the closed access [106], [107] and [108]. Unlike Closed Access Femtos (CAFs), Femtos configured in open access do not distinguish between SG and NSG users and serve all users like the way MBSs serve them. Open Access Femtos (OAFs) are typically deployed in public hotspots like airports and shopping malls. If this access mechanism is employed in enterprise and residential buildings, QoS of SG users is affected as the number of NSG users increases in indoors. Hybrid access mechanism

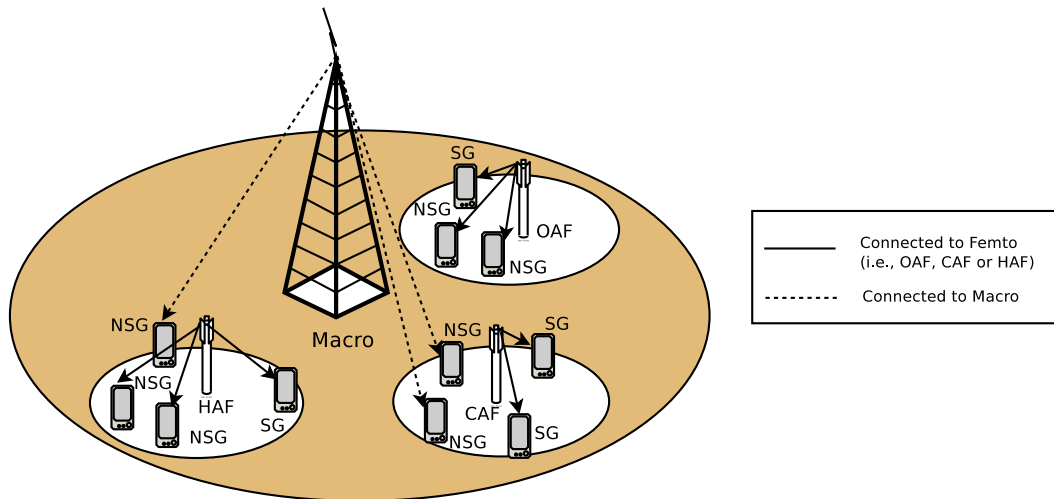


Figure 7.1: An example of LTE HetNet with MBS, OAF, CAF, and HAF Cells

integrates the principles of both closed and open access mechanisms. It lets some of NSG users in indoors to connect with Hybrid Access Femtocells (HAFs) and share its radio resources along with SG users. This mechanism provides a trade-off between maximizing overall HetNet capacity and maximizing the throughput of SG users. Figure 7.1 shows an LTE HetNet system comprising of one Macro cell and three Femtocells: one OAF, one CAF and one HAF. Here the OAF is serving both SG and NSG users located in its coverage area. But, in CAF case all of the NSG users located in the CAF's coverage area are forced to connect with the MBS. As a compromise, HAF serves two of NSG users along with SG users and rest of NSG users are served by the MBS.

HAFs partially address the issue of signal degradation faced by the NSG users in the closed access mechanism. They provide lesser throughput to SG users as compared to CAFs as they also serve the NSG users but the overall HetNet throughput improves. On the other hand, the SG throughput obtained in HAFs is better than that obtained in OAFs. Nevertheless, this is at the cost of overall HetNet throughput which is highest in the open access mechanism. Hybrid access is a compromise between the two extreme cases of closed and open access mechanisms. More importantly, HAFs provide service to NSG users when they are inside the building where they experience low signal from MBSs. And, because OAFs are not a favorite in large private buildings, HAFs are a welcome relief to the NSG users who would otherwise be deprived of even basic data rates when they are indoors in CAFs. Hybrid access mechanism needs to be effectively promoted as the SG users are usually reluctant to

share resources they have paid for, with unknown NSG users who visit their buildings. This mechanism can be made attractive by rewarding the SG users for sharing their resources with the NSG users [109], [110].

Optimal arrangement of Femtos with minimum overlapping regions is necessitated by the need to save the cost of deploying Femtos and reduce co-tier interference due to frequency reuse one in LTE HetNets. If Femtos deployment is not optimal, it increases Femtos count and so does co-tier interference. [111] deals with the optimal placement of CAFs with minimum overlapping areas and reduced co-tier interference. Optimal placement of Femtos operating in hybrid access is equally important so that users in the high interference zone *HIZone* can connect to one of HAFs for receiving good signal strength and lower cross-tier interference from MBSs. After optimally placing the HAFs, one needs to look into how to serve both SG and NSG users efficiently. Care needs to be taken to ensure QoS of SG users by dynamically splitting radio resources between SG and NSG users. Dynamic power control at HAFs reduces the cross-tier interference experienced by the *HIZone* users served by an MBS when a near-by HAF is not able to maintain the minimum QoS requirement for its users. As the interfering HAF reduces its transmission power, the *HIZone* users can connect to one of MBSs with lower SINR degradation. The reduction in transmission power may affect the *IUEs* who now get reduced signal strength but the HAF can use the additional resources, previously reserved for the *HIZone* users, to serve the *IUEs*. Having a dynamic power control mechanism also adds advantage to the *IUEs* at times when there are no users in the *HIZone*, especially at nights. During such times, HAFs may be tuned to operate at the maximum transmit power thereby serving the *IUEs* with high data rates.

7.1.1 Organization of this Chapter

The rest of this chapter is organized as follows. Related work and our contributions are given in section 7.2. Section 7.3 introduces our system model and enumerates the assumptions made in this chapter. We elaborate the proposed work in section 7.4. This section describes the optimal placement of the HAFs, the Bandwidth Allocation (BWA) and the optimal and the sub-optimal power control mechanisms. This is followed by section 7.5 where we present the simulation results and then provide insights into the working of our scheme. Finally, Section 7.6 summarizes the chapter.

7.2 Related Work

Besides scheduling, optimal placement and power control techniques improve network performance [112–114]. Optimal placement of and power control by CAFs in a two-tier LTE network overcome co-tier and cross-tier interference at the cost of reduced CAF transmission power to the SG users [111]. In order to assure minimum degradation to NSG users in outdoors, SG users suffer from lower throughput values. SG users are affected by the presence of even a single NSG user in the HIZone since the Femtos lower their transmit power to reduce cross-tier interference. [112] studies the effects of the user-deployed co-channel Femtos on the call drop probability of the macro users in residential areas. The results show that the use of co-channel Femtos is efficient but to make it financially viable the Femtos should have auto-configuration abilities. The main aspect of this auto-configuration is tuning the Femto transmit power to reduce the number of dropped calls by a NSG user. The authors of [113] provide an analysis of the co-tier interference in CAFs. They point out that coverage holes appear in the downlink of MBS cells in the vicinity of CAFs. Results show an improvement when Femtos use a transmit power adjustment mechanism and operate on an adjacent channel. The survey on transmit power control techniques in Femto networks presented in [114] discusses and compares several power control techniques focusing mainly on distributed transmit power control techniques due to decentralized nature of Femtos.

Scheduling radio resources between SG and NSG in the downlink shared access Femtos is addressed in [107]. Here the authors propose access control of Femtos depending on their distance from a MBS. Home users associate with either a Femto or MBS depending on the signal strength. Cellular users associate with a nearby Femto only when it is far away from the MBS. Packet scheduling mechanisms play an important role in cellular networks when the MBS and Femto share radio resources by operating in the same spectrum. The key features and challenges for designing a scheduler and comparison of existing popular schemes have been detailed in [101]. The main objective of a scheduler should be to achieve an optimal trade-off between spectral efficiency and throughput of user. In a particular hybrid spectrum management and interference mitigation scheme [115], the CAFs identify themselves as either inner or outer Femto depending on their distance from the MBS. Hence, they operate in either dedicated-channel or co-channel spectrum. The scheme is called hybrid because the outer Femtos (situated closer to cell edge) use the entire spectrum, the MBS operates on one part of the spectrum and the inner Femtos (closer to the MBS)

operate on the remaining part. The interference from the CAFs experienced by the NSG users closer to the cell edge is severe and of particular concern. In [116], radio resources are allocated in hybrid environment. Each Femto independently selects a mutually exclusive subset of radio resources where selection of any resource has equal probability. This decentralized mechanism which aims to reduce the cross-tier interference is not scalable. The number of radio resources that a Femto can select keeps decreasing as the Femtos count increases. The number of Femtos thus cannot be increased beyond a certain limit. Another solution to radio resource management in hybrid access is presented in [109]. The authors propose a four-stage radio resource management mechanism where base stations perform access control, radio resource allocation and channel allocation and the users perform power control. Interference mitigation is performed by maintaining dedicated channels for each Femto based on minimum QoS requirement of users and additional channels as an incentive to serve cellular users. The drawback of the proposal is that the authors consider a system with one MBS and one Femto. Channel allocation becomes a problem in practical situations when multiple Femtos are deployed, since the MBS and the Femto operate on different channels to avoid co-channel interference for the NSG.

Newer technologies focus on other aspects such as communication between proximity devices, high frequency transmission and ICIC to increase network capacity. The problem of HIZone users can be solved by device-to-device (D2D) communications [8] between nearby users in two ways. Firstly, two users can use radio resources obtained from the MBS to communicate directly without routing through the MBS. Secondly, when a MBS wants to offload a user, it transmits the data to another nearby user. The offloaded user can then receive the data via single or multi-hop D2D communication. The HIZone users may communicate with a nearby NSG user without using the Femtos radio resources. As a result the MBS has to allocate lesser radio resources than when it connects to the MBS. While [117] allows the D2D pairs in the network and sets their transmitting powers to admissible values, [118] proposes a joint mode selection (cellular and D2D modes) and radio resource allocation scheme for the D2D pairs so that network throughput is maximized. In [119], the authors propose three communication modes for D2D systems. The users can switch between cellular, dedicated and reuse modes which give a higher spectral efficiency than a single mode. While D2D solutions seem promising, the introduction of D2D pairs gives rise to new interference patterns. Moreover, D2D communication makes handover, scheduling, security of user information and interference management more complex. In D2D, apart from leasing the radio resources to two devices, the MBS does not provide any

other service. In case the number of D2D links is more than one, monitoring all D2Ds becomes difficult for MBSs. Therefore, for a network operator, designing a pricing model to support large number of D2D links becomes cumbersome. [120] talks about a relatively new technology where mobile networks make use of the untapped millimeter waves (mm-wave) in backhaul links and RAN links. Due to the small wavelength of mm-waves, penetration becomes difficult. This may prove to be a boon for the *IUEs* since there would be a very thin (1 m or 2 m) or no HIZone. But, [121] points out that in mm-wave technology, attenuation increases exponentially with link distance (more relevant for links exceeding 100 m). When the size of obstacles is of the order exceeding tens of cm, the obstacles act as reflectors causing severe losses exceeding 30 dB.

To address the dominant interference scenarios where NSG users comes close to a building having Femtos, enhanced (eICIC) techniques are developed [97]. In time domain eICIC mechanism, MBS periodically blanks its sub-frames so that the interference to the co-channel Femtos is lower. According to 3GPP, the blank sub-frames are called almost blank sub-frames (ABS) indicating that the sub-frames may still be used to transmit L1/L2 signaling messages in C-plane. In frequency domain eICIC mechanism, the C-plane messages of the Femtos are scheduled in reduced bandwidths so that the control information transmission of the Femtos is orthogonal to one another. Power control techniques in eICIC allow the MBS as well as the Femtos to operate all times but the Femtos operate at reduced transmit power levels when they interfere with the nearby NSG users.

Rewarding extra radio blocks to Femtos deployed extensively under a MBS, for serving NSG users is a new and solution for improving the network performance. The SG users who own the Femto can benefit from the extra radio blocks it receives from the MBS to serve the nearby NSG users who are far away from the MBS to receive a good signal. This Femto and MBS symbiosis strikes a balance between spectral efficiency and SG satisfaction and is discussed in [122–124]. [122] proposes an economic solution for mobile operators and SG users based on game theory by analyzing the existence of the Nash Equilibrium of the game. They use the concept of revenue sharing to provide a positive cycle to sustain the Femto service by maximizing operator’s benefits and satisfying the users’ service requirements. [123] motivates the MBSs to lease a part of their spectrum to the Femtos and the Femtos to open a part of the above obtained spectrum to serve the NSG users. The framework is modeled as a three-stack Stackelberg game where the Femtos and MBS determine the spectrum leasing ratio, its price and the open access ratio to maximize the utilities of both

Femtos and MBSs. The authors of [124] have proposed an optimal as well as a sub-optimal mechanisms to implement a reverse auction framework for a fair and efficient access permission transaction. This work further motivates SG to use HAFs. Most recent work in the area of cross-tier and co-tier interference mitigation when both Femtos and MBS operate in the same frequency is [125]. The scheme deals with CAF located at the cell edge where power control is done for each radio resource. Therefore, an interfering Femto may serve a subscriber with a radio resource R_i at higher transmit power while serving another subscriber at a lower transmit power with a radio resource R_j if MBS serves a nearby NSG user with R_j . The authors adopt static allocation of radio blocks. The power control for each radio resource is executed under the assumption that each user will have the same radio resource in the next iteration. There is a need for HAFs to serve a NSG user inside a building who receives highly degraded signal strength from the MBS or when a SG or NSG user is in the HIZone of the building.

7.2.1 Our Contributions

Our contributions in this paper are enumerated as follows.

- An *optimal placement of Femtos (OPF)* mechanism which is used for placing Femtos optimally by ensuring good SINR for both *IUEs* and *HIZUEs*.
- A decentralized *dynamic bandwidth allocation (BWA)* which divides the available bandwidth in the network between the two sets of user groups, SG and NSG.
- Dynamic power control is done by an optimal power control (OPC) mechanism which tunes the transmit power of the Femto to a reduced value whenever the users in the HIZone cannot be served by the Femtos. So that they could connect to the MBS instead. Since, the OPC is hard to solve in polynomial time we present a sub-optimal power control (SOPC) mechanism.
- An enhanced priority (EP) scheduling mechanism that uses two schedulers which implement proportional fair (PF) algorithm. While one scheduler maintains fairness among the SG users, the other fairly schedules radio blocks among the users of NSG. We justify the need of two schedulers and the use of power control in Femtos in Section 7.4.3. Our EP scheduling mechanism works better than the legacy PF scheduler as well as the legacy Priority Set (PS) sched-

uler [101] by prioritizing SG users over NSG users and maintaining fairness within both user groups.

7.3 Preliminaries and Assumptions

We describe the system model considered in this work. The building and channel models along with the associated assumptions necessary for the system setup are also detailed.

7.3.1 System Model

The system is modeled on downlink LTE HetNet consisting of MBSs in the outdoor environment and HAFs inside an enterprise building which is located in the cell edge of an MBS as shown in Figure 7.2. Frequency reuse one is employed in HetNet to improve the capacity of the system. HAFs are connected to Femto-Gateway (F-GW) over S1 interface. The F-GW has Self Organizing Network (SON) feature which makes the system self-configurable, self-optimizing and self-healing. SON helps HAFs to dynamically adjust their transmit power.

Here we assume that the radio resource requirement of SG users, R_S , can always be satisfied by the available radio resources in the HAF before power control. Otherwise, the HAF will be unable to maintain a minimum throughput for SG users at full transmit power even in the absence of NSG users. Also, a user is connected to the HAF which gives the maximum SINR. We classify the users on two parameters - priority and location. The user groups formed on basis of priority are SG and NSG where the former gets higher priority than NSG when connected to HAFs. *IUEs* and *HIZone* users are determined by their locations by using Position Reference Signal (PRS) [126–128].

The HAFs send downlink control/data plane (C/D plane) to the NSG users in the HIZone. At each periodic time interval T (comprising of a number of transmission time intervals (TTIs)), the HAFs split their radio resources between the NSG users and SG users before running the EP scheduler. When an HAF operates in full transmit power and the number of radio resources required to serve all the *HIZone* and *IUEs* at the minimum QoS exceeds the available radio resources, the F-GW tunes the HAF's transmit power. Hence, the HIZone users previously connected to the HAF are now connected to the MBS above a threshold SINR, $SINR_{Th}^{PC}$. The transmit power is tuned so that these HIZone users can connect to the MBS with

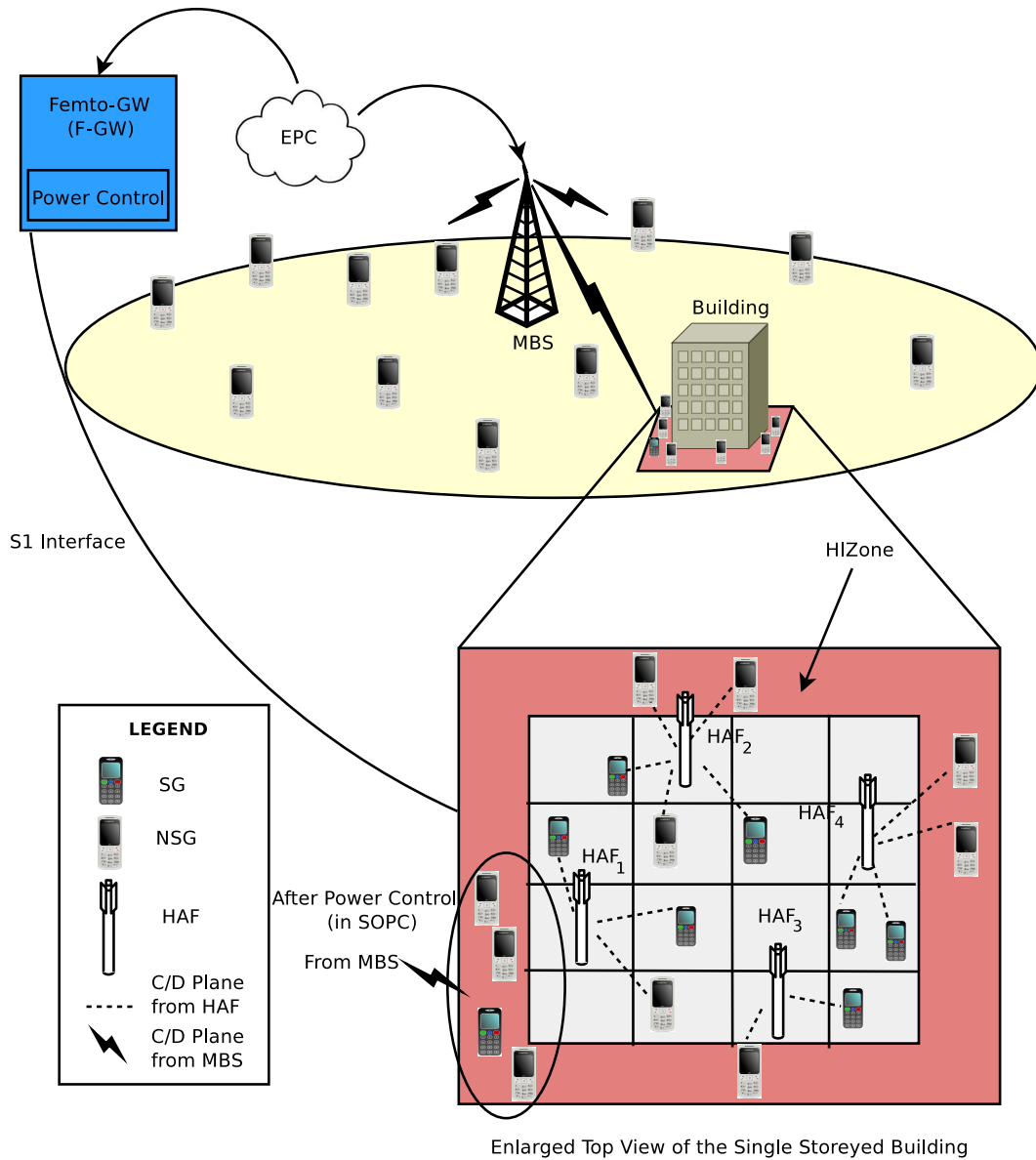


Figure 7.2: HAF based LTE HetNet System Model

minimum cross-tier interference.

For example, if HAF_1 transmits at full transmit power, there are not enough radio resources to serve with a minimum throughput all the users (both SG and NSG) with some minimum guaranteed throughput. Hence, the HAF_1 reduces its transmission power to allow the users in the HIZone to get their D-plane and C-plane from the MBS with better SINR. The radio resources of HAF_1 can then be exclusively used to serve the $IUEs$. Since the BWA is done between the two user groups, priority of the SG users is not compromised. Similarly, the SG users in the HIZone experiences

better throughput when connected to the MBS than when connected to HAF_1 which has insufficient radio resources for serving both indoor and HIZone users. The PL model given in chapter 3 and building model given in chapter 4 are used for this work.

7.4 Proposed Work

In this section, we will describe in detail the optimization problems and propose a sub-optimal mechanism which runs in polynomial time and is appropriate for dynamic scheduling. A list of notations used in this paper is presented in Table 7.1. Initially, the HAFs are placed inside the building by using an optimal placement model. This is a one time process after which the SOPC mechanism handles the SG and NSG user connections by a power control model. The set ISR has the list of all the HAFs for which $R_S + R_{NS} \leq R$ does not hold. In a situation where $ISR \neq NULL$, a new set $OCCU$ is formed which consists of all the HIZone users (SG and NSG) under the coverage of HAFs in the ISR . EP scheduler then schedules the radio blocks among all the users in each group. We describe each of the above steps, in detail, in the following subsections.

7.4.1 Optimal Placement of Femtos (OPF) Model

The first step deals with an efficient placement of HAFs inside the building by employing an optimization model. Our objective is to ensure optimal placement of the HAFs, operating at full transmit power P_{max} , inside the building so that a user situated anywhere in the building or the HIZone connects to the HAF giving highest SINR, and, is ensured a minimum SINR, $SINR_{Th}$ from the HAF.

The OPF model is formulated with the objective to minimize the number of HAFs deployed in the building, as expressed in Equation (7.1), such that the HAFs operate at P_{max} to provide good SINR to all indoor and HIZone users.

$$\min \sum_{i \in I} v_i \tag{7.1}$$

Equation (7.1) is subject to the following constraints. Since we want each indoor and HIZone sub-region to associate with only one HAF, we ensure it by adding constraints given by Equations (7.2), (7.3), (7.4) and (7.5).

Table 7.1: List of notations used in the problem formulations

Notation	Definition
F	Set of all HAFs inside a building
M	A set of MBSs
H	Set of all HIZone sub-regions
I	Set of all indoor sub-regions
T	Periodic time interval of duration equal to n TTIs
R	Number of radio resources available in a HAF in a single TTI
R_S	Number of radio resources required by SG from a HAF in a single TTI
R_{NS}	Number of radio resources required by NSG from a HAF in a single TTI
P_f	Transmitting power of a HAF, f
P_{max}	Maximum transmitting power of HAF
P_M	Transmitting power of MBS, M
N_o	System Noise
$SINR_{Th}^P$	Threshold SINR to be maintained in all indoor and HIZone sub-regions during placement of HAFs inside the building
$SINR_{Th}^{PC}$	Threshold SINR to be maintained in all indoor and HIZone sub-regions during power control of HAFs in SOPC mechanism
v_i	1 if HAF is placed in indoor sub-region i , 0 otherwise
s_{ji}	1 if indoor sub-region j is connected to HAF located in indoor sub-region i , 0 otherwise
t_{ji}	1 if HIZone sub-region j is connected to HAF located in indoor sub-region i , 0 otherwise
g'_{ja}/g''_{ja}	Channel gain between indoor sub-region or HIZone sub-region j and indoor sub-region a
g_{if}/g_{iM}	Channel gain of indoor sub-region i from HAF f or MBS M
g_{hf}/g_{hM}	Channel gain of HIZone sub-region h from HAF f or MBS M
d_i/d_h	Demand of user in indoor sub-region i or HIZone sub-region h for time interval T
$mcs(sinr_{if})$ or $mcs(sinr_{hf})$	Amount of data transmitted in one radio resource based on the MCS value of indoor sub-region i or HIZone sub-region h (a function of the sub-region's SINR value of Opt from HAF f)
x_{if}	1 if indoor sub-region i is connected to HAF f , 0 otherwise
y_{hf}	1 if HIZone sub-region h is connected to HAF f , 0 otherwise
z_h	1 if HIZone sub-region h is connected to a HAF, 0 if it is connected to MBS M
q_i/q_h	1 if indoor sub-region i or HIZone sub-region h is occupied by a user, 0 otherwise

$$\sum_{i \in I} s_{ji} = 1 \quad \forall j \in I \quad (7.2)$$

$$\sum_{i \in I} t_{ji} = 1 \quad \forall j \in H \quad (7.3)$$

$$s_{ji} - v_i \leq 0 \quad \forall j, i \in I \quad (7.4)$$

$$t_{ji} - v_i \leq 0 \quad \forall i \in I, j \in H \quad (7.5)$$

The following constraints fulfill our requirement that every indoor and HIZone sub-region should have SINR above the pre-defined threshold of $SINR_{Th}^P$. The $SINR_{Th}^P$ is set as λ_i and λ_h for indoor and HIZone sub-regions, respectively, to ensure good coverage. The L.H.S. of Equation (7.6) and Equation (7.7) are the SINR values of indoor and HIZone sub-regions, respectively obtained from HAF located at indoor sub-region, a .

$$\frac{Inf * (1 - s_{ja}) + g'_{ja} P_{max} v_a}{N_o + \sum_{b \in I \setminus a} g'_{jb} P_{max} v_b + g'_{jM} P_M} \geq \lambda_i \quad \forall j, a \in I \quad (7.6)$$

$$\frac{Inf * (1 - t_{ja}) + g''_{ja} P_{max} v_a}{N_o + \sum_{b \in I \setminus a} g''_{jb} P_{max} v_b + g''_{jM} P_M} \geq \lambda_h \quad \forall a \in I, j \in H \quad (7.7)$$

g'_{ja} and g'_{jM} are the channel gains from HAF and MBS to indoor sub-region j , respectively. Similarly, g''_{ja} and g''_{jM} are the channel gain from HAF and MBS to HIZone sub-region j , respectively. If there are multiple macro cells (the set M has more than one MBS), then summation of the channel gains from all MBSs gives the total interference. N_o is the thermal noise. Inf is a virtually infinite value (a large value like 10^6) used to ensure that the every indoor/HIZone sub-region gets at least $SINR_{Th}^P$ (λ_i for indoor sub-regions and λ_h for HIZone sub-regions), from only one HAF. Otherwise, all HAFs would try to assure the $SINR_{Th}^P$ to every sub-region and render the optimization problem infeasible.

7.4.2 Optimal Power Control (OPC) Model

After placement of the HAFs, each HAF allocates its radio blocks to every active user connected to it in every periodic time interval, T . If the radio resource demand is greater than the available radio blocks R , the F-GW performs OPC to tune transmit

powers of HAFs. The objective of OPC model is to maximize the sum of transmission powers of all HAFs so that resource demand at each HAF from its connected users can be satisfied. It chooses HIZone users (SG and NSG) who will be served by the MBS when the transmission powers of the HAFs, to whom they are connected currently, are reduced from P_{max} . In such a case, the selected HIZone users must be ensured at least a $SINR_{Th}^{PC}$ from the MBS in order to be served by it.

OPC Formulation: F is used to denote the set of all HAFs in the building and M is the set of MBSs. All the sub-regions in the HIZone and indoor form the sets H and I , respectively. D_i and D_h are the demand of i^{th} IUE and h^{th} HIZone user, respectively, in T time interval. P_M denotes the transmission power of the MBS. We use the following variables to determine the connectivity of each sub-region to an HAF and to determine whether a sub-region is occupied.

- Indoor HAF connectivity variable $x = \{x_{if} | x_{if} = \{0, 1\}; i \in I; f \in F\}$, *i.e.*, $x_{if} = 1$ if indoor sub-region i is connected to HAF f , 0 otherwise.
- HIZone HAF connectivity variable $y = \{y_{hf} | y_{hf} = \{0, 1\}; h \in H; f \in F\}$, *i.e.*, $y_{hf} = 1$ if HIZone sub-region h is connected to HAF f , 0 otherwise.
- HIZone Macro connectivity variable $z = \{z_h | z_h = \{0, 1\}; h \in H\}$, *i.e.*, $z_h = 1$ if HIZone sub-region h is connected to a HAF f , 0 if connected to M .
- Indoor sub-region occupancy $op_i = \{q_i | q_i = \{0, 1\}; i \in I\}$, *i.e.*, $q_i = 1$ if indoor sub-region i is occupied by a user, 0 otherwise.
- HIZone sub-region occupancy $op_h = \{q_h | q_h = \{0, 1\}; h \in H\}$, *i.e.*, $q_h = 1$ if HIZone sub-region h is occupied by a user, 0 otherwise.

To ensure that every HAF can serve the users connected to it with minimum number of radio resources, the OPC maximizes the total transmission power of all the HAFs, that is,

$$\max \sum_{f \in F} P_f \quad (7.8)$$

To ensure that every indoor sub-region, i , is connected to exactly one HAF and that any HIZone sub-region, h , if not connected to the MBS is associated with only a single

HAF, Equation (7.8) is subject to the connectivity constraints (7.9) and (7.10).

$$\sum_{f \in F} x_{if} = 1 \quad \forall i \in I \quad (7.9)$$

$$\sum_{f \in F} y_{hf} = z_h \quad \forall h \in H \quad (7.10)$$

We use the SINR constraint given in Equation (7.11) to make sure that all the indoor sub-regions, which are connected to HAF, f , get at least $SINR_{Th}^{PC}$ which is equal to λ_i for indoor sub-regions.

$$\frac{Inf * (1 - x_{if}) + g_{if}P_f}{N_o + \sum_{f' \in F \setminus f} g_{if'}P_{f'} + \sum_{m \in M} g_{im}P_m} \geq \lambda_i \quad \forall i \in I, f \in F \quad (7.11)$$

In order to ensure $SINR_{Th}^{PC}$, λ_h , to HIZone sub-regions from their respective HAFs, constraint given in Equation (7.12) is used.

$$\frac{Inf * (1 - y_{hf}) + g_{hf}P_f}{N_o + \sum_{f' \in F \setminus f} g_{hf'}P_{f'} + \sum_{m \in M} g_{hm}P_m} \geq \lambda_h \quad \forall h \in H, f \in F \quad (7.12)$$

where, g_{hf} and g_{hm} are the gains from HAF, f , and MBS, m , to the HIZone sub-region h , respectively. For a HAF f , Equation (7.12) uses Inf to filter the HIZone sub-regions not connected to f to prevent the problem from becoming infeasible. The constraint given in Equation (7.13) is adopted to make sure that all HIZone sub-regions connected to an MBS, $m \in M$ get SINR greater than λ_h .

$$\frac{Inf * z_h + g_{hm}P_m}{N_o + \sum_{f \in F} g_{hf}P_f} \geq \lambda_h \quad \forall h \in H \quad (7.13)$$

Like earlier, Inf filters the HIZone sub-regions not connected to the MBS.

$$\sum_{i \in I} \left[\frac{d_i q_i}{mcs(\sin r_{if})} \right] x_{if} + \sum_{h \in H} \left[\frac{d_h q_h}{mcs(\sin r_{hf})} \right] y_{hf} \leq nR \quad \forall f \in F \quad (7.14)$$

where, R is the number of radio resources available per TTI and n is the number of TTIs in the time interval T . The first summation in Equation (7.14) determines the maximum number of radio resources required by the $IUEs$ connected to HAF f which depends on the user's individual data requirement d_i for time interval T and

their MCS obtained from their SINR value ($mcs(\text{sinr}_{if})$). Similarly, the second term is the summation of the maximum number of radio resources required by the HIZone users connected to f . The constraint gives an upper bound of nR to the net required radio resources obtained from both the summation terms for the time interval T .

Thus, the OPC takes care of BWA for any combination of SG and NSG user locations by tuning the transmit power of HAFs whenever the demand in a HAF exceeds R . The demand from the *IUEs* (SG and NSG) itself can exceed R in a HAF operating at P_{max} due to presence of large number of indoor NSG users. Then the BWA is in proportion of the radio resource demand between the SG and NSG (refer Equation (7.15) and Equation (7.16)) as the OPC is not feasible in such a situation.

$$R'_S = \frac{R_S}{R_S + R_{NS}} R \quad (7.15)$$

$$R'_{NS} = \frac{R_{NS}}{R_S + R_{NS}} R \quad (7.16)$$

The OPC problem (refer Equation 7.8) is a Mixed Integer Non-linear Programming (MINLP) problem and is very hard to solve in polynomial time. Hence, we propose an effective heuristic power control mechanism to solve the above MINLP power control problem in polynomial time.

7.4.3 Sub-Optimal Power Control (SOPC) Mechanism

The flowchart in Figure 7.3 provides a basic idea of our proposed SOPC mechanism. The first step is the optimal placement of the HAFs which takes as input the layout of the building and gives the co-ordinates where the HAFs are to be placed. This placement is such that a minimum $SINR_{Th}^P$ is guaranteed to all indoor and HIZone sub-regions. At the start of each time interval, T , the demand of the SG and NSG in terms of R_S and R_{NS} is computed in each HAF transmitting at P_{max} (refer Algorithm 5) and the radio resources are split between the two user groups (SG and NSG). A set ISR is maintained which lists all the HAFs for which the constraint $R_S + R_{NS} \leq R$ does not hold. When $R_S + R_{NS} < R$ (*i.e.*, when $ISR = NULL$), the excess radio resources are used by the SG to further improve their throughput (refer Algorithm 6). After this the BWA is performed where the available bandwidth is divided between the two groups (SG and NSG).

When one or more HAFs have insufficient resources to meet the minimum throughput requirement of all connected users (*i.e.*, when $ISR \neq NULL$), a new set $OCCU$ is formed. $OCCU$ comprises all the HIZone users (SG and NSG) connected to HAFs

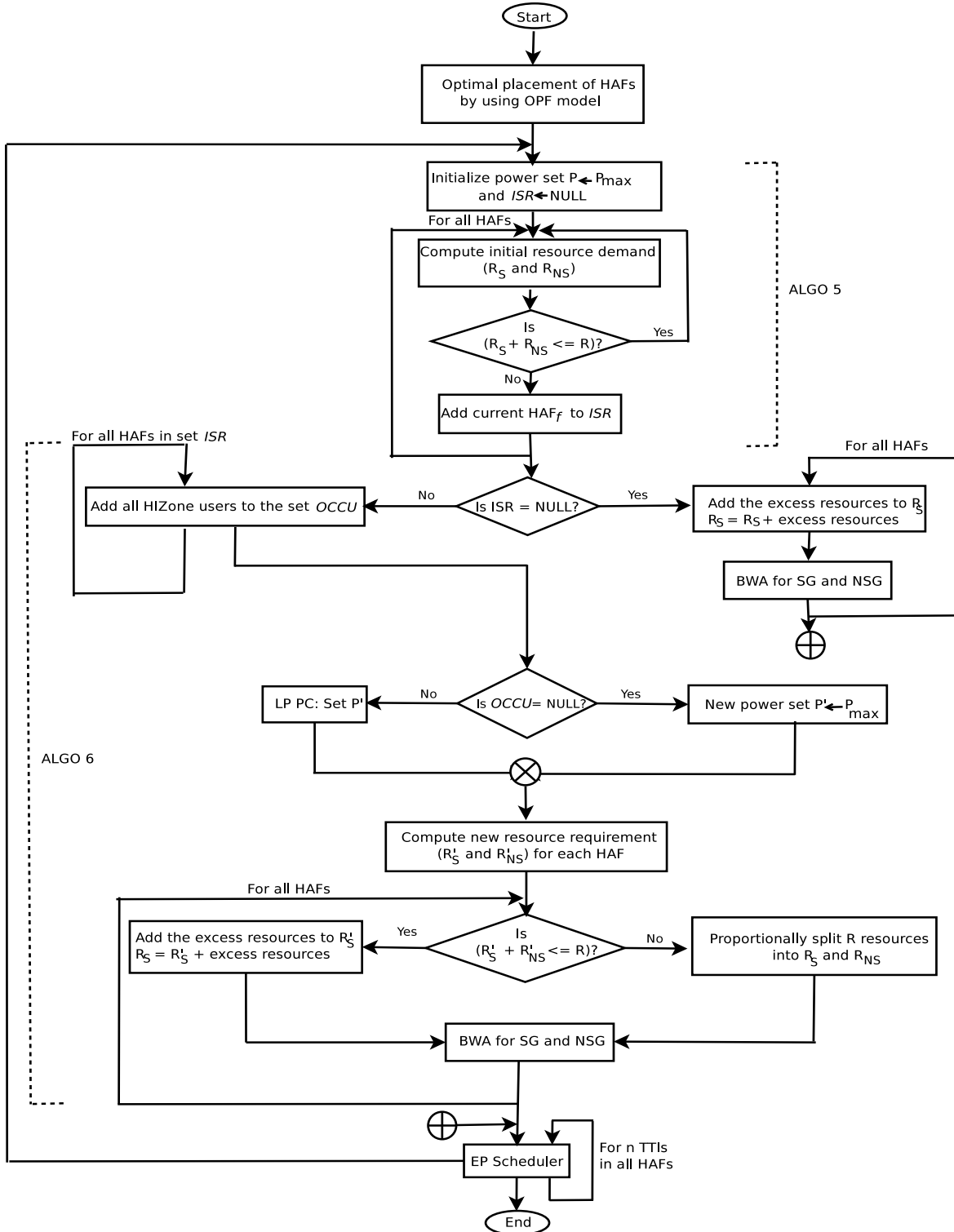


Figure 7.3: Flowchart of the proposed SOPC mechanism

belonging to the set ISR (refer Algorithm 6). The F-GW then tunes the power of the HAFs such that the total transmission power is maximized. Hence, the HIZone users in the set $OCCU$ connect to the MBS with a signal strength greater than or equal to the threshold SINR, $SINR_{Th}^{PC}$. The radio resource requirement in each HAF is computed for the new transmit power values P' . If the new resource requirement can be fulfilled by R , the radio resources are split in the same way as it is done when $ISR = NULL$. Otherwise the radio resources are divided in proportion of the radio resource demand of SG and NSG in each HAF. Thereafter the BWA is performed where the entire bandwidth is divided between the SG and the NSG in each HAF in proportion to R_S and R_{NS} . The EP scheduler then schedules the radio resources among all the users in each group.

Algorithm 5 Radio Resource Demand Computation at P_{max}

Input: List of SG and NSG users in each HAF, list of indoor and HIZone users. Let ISR be the set of all HAFs with insufficient radio resources.

Output: R_S and R_{NS} for each HAF before power control.

```

1: Initialize  $ISR \leftarrow NULL$ 
2: for each HAF  $f \in F$  do
3:   Compute  $R_S$  {  $R_S$  : Radio resources required by SG users connected to HAF  $f$ 
   at  $P_{max}$  for the current time interval  $T$  }
4:   Compute  $R_{NS}$  {  $R_{NS}$  : Radio resources required by NSG users connected to
   HAF  $f$  at  $P_{max}$  for the current time interval  $T$  }
5:   if  $R_S + R_{NS} > R$  then
6:      $ISR \leftarrow ISR \cup f$ 
7:   end if
8: end for

```

The SOPC mechanism is comprised of two algorithms which are outlined as follows:

- Algorithm 5: Computation of radio resource demand at P_{max} .
- Algorithm 6: BWA when HAFs can satisfy the user demand with the R radio resources available at each HAF and BWA when the radio resource demand by users exceeds the radio resources available at HAF.

At the beginning of each time interval T , the set of active users is determined by the PRS and fed as input to Algorithm 5. This algorithm computes the radio resource demand of SG and NSG under each HAF operating at P_{max} . If for a HAF f , the total radio resources required by SG and NSG in a TTI exceeds R , then f is added

Algorithm 6 BWA Algorithm

Input: ISR , initial R_S and R_{NS} for each HAF obtained from Algorithm5

Output: Final R_S and R_{NS} for each HAF

Let P' be the set of new transmit powers of HAFs & $OCCU$ be set of $HIZUE$ s connected to MBS

```
1: if  $ISR = NULL$  then
2:   for each HAF  $f \in F$  do
3:      $R_S \leftarrow R_S + (R - R_S - R_{NS})$  {The leftover radio resources are given to the SG users}
4:     Perform Bandwidth Allocation (BWA) for  $f$ 
5:   end for
6: else
7:   { $ISR \neq NULL$ }
8:    $OCCU \leftarrow NULL$ 
9:   for each HAF  $f \in ISR$  do
10:    for each NSG user in  $f$  do
11:      if NSG user is in HIZone then
12:         $OCCU \leftarrow OCCU \cup NSG$ 
13:      end if
14:    end for
15:    for each SG user in  $f$  do
16:      if a SG user is in HIZone then
17:         $OCCU \leftarrow OCCU \cup SG$ 
18:      end if
19:    end for
20:  end for
21:  if  $OCCU \neq NULL$  then
22:    {There is at least one HIZone user}
23:    Initiate PC (i.e., Equation (7.17)) and obtain new power values,  $P'$  {PC problem is solvable in polynomial time}
24:    Compute new SINR REM and connectivity map
25:    for each HAF  $f \in F$  do
26:      Compute  $R'_S$  and  $R'_{NS}$  {with the new SINR values}
27:    end for
28:  else
29:     $P' \leftarrow P_{max}$  {New transmit power values remain same as maximum values}
30:     $R'_S \leftarrow R_S$ 
31:     $R'_{NS} \leftarrow R_{NS}$  {Radio resource count is same as that obtained at  $P_{max}$ }
32:  end if
33:  for each HAF  $f \in F$  do
34:    if  $R'_S + R'_{NS} \leq R$  then
35:       $R_S \leftarrow R'_S + (R - R'_S - R'_{NS})$  {The leftover radio resources are given to the SG users of  $f$ }
36:       $R_{NS} \leftarrow R'_{NS}$ 
37:    else
38:      Compute radio resource requirement at reduced transmit power by proportional split
39:       $R'_{S_{reduced}} \leftarrow \lfloor \frac{R'_S}{R'_S + R'_{NS}} R \rfloor$  {We take floor so that atleast one radio resource is given to the NSG}
40:       $R_S \leftarrow R'_{S_{reduced}}$ 
41:       $R_{NS} \leftarrow R - R_S$ 
42:      Perform Bandwidth Allocation (BWA) for  $f$ 
43:    end if
44:  end for
45: end if
```

to the set ISR . The output of this algorithm is the set ISR which forms the input of Algorithm 6.

After Algorithm 5, Algorithm 6 is performed in each time interval T . If $ISR = NULL$, Algorithm 6 performs BWA after the final R_S and R_{NS} counts for the SG and NSG in each HAF are computed. If the total demand is less than R , the R_S is recomputed by adding the remaining radio resources to it.

Algorithm 6 also performs the BWA in accordance with the final count of radio resources required by the SG and NSG in each HAF if $ISR \neq NULL$. In this case, first the $OCCU$ set is formed by adding all the HIZone users (consisting of both SG and NSG users) who are connected to the HAFs in the set ISR . If the insufficiency in bandwidth is due to the presence of at least one HIZone user, that is, if $OCCU \neq NULL$, the linear programming (LP) power control (PC) is performed.

This PC has the following objectives:

- To maximize the total transmission power of all HAFs
- To maintain $SINR_{Th}^{PC}$ for HIZone users in the set $OCCU$ who are connected to the MBS

The PC in SOPC mechanism maximizes the sum of transmission power of all HAFs given by Equation (7.17).

$$\max \sum_{f \in F} P_f \quad (7.17)$$

where, P_f is the transmitting power of each HAF, such that Equation (7.18) is satisfied.

$$\frac{Inf * z_h + g_{hM} P_M}{N_o + \sum_{f \in F} g_{hf} P_f} \geq \lambda_h \quad \forall h \in H \quad (7.18)$$

This constraint maximizes the total transmission power by selecting only those HIZone users to be connected to the MBS who if connected to a HAF increase the radio resource demand to greater than the available radio resources, that is, $z_h = 0$ for all HIZone sub-regions to which the SG and NSG in $OCCU$ belong, where, $OCCU$ is the set of all HIZone users initially connected to HAFs belonging to the set ISR when operating at P_{max} .

The values P_f obtained from the above optimization problem form the set P' . This problem is a LP optimization problem with the set P' containing P_f , the variables, and the $SINR_{Th}^{PC}$ being the constraint and can be solved in polynomial time [72].

The new SINR REM and connectivity maps are determined with the new transmit power values. The radio resource requirements of SG, R'_S , and NSG, R'_{NS} , are

computed with the new SINR values. If the new radio resource demand of SG and NSG connected to a HAF can be satisfied by R , the process similar to the case where $ISR = NULL$ is performed. After the power control co-tier interference from neighboring HAFs reduces allowing the HAF edge users to receive better signal thereby requiring lesser radio resources. The demand for radio resources for the users situated closer to a HAF increases when its transmission power is reduced. However, after power control, a HAF allocates the radio resources previously reserved for the HIZone users, to the *IUEs*. Thus, the total demand from a HAF may still be satisfiable even if the HAF reduces its transmit power. The power control may not necessarily reduce the demand for radio resources. There may arise a situation where on reducing the transmission power of a HAF, a significant number of the HAF cell edge users shift their connectivity to a neighboring HAF. If this increase is such that the radio resource demand from the neighboring HAF exceeds R , the algorithm divides R between SG and NSG so that the allotted radio resources are in proportion to the actual requirement.

If $OCCU = NULL$, it means that there are no HIZone users and the radio resource requirement of the *IUEs* itself is very high. Thus, the HAFs continue to operate at P_{max} and the radio resource requirement remains same for SG and NSG. The BWA is done by proportionally splitting the the spectrum with respect to the radio resource demand of the SG and NSG users in the building.

We now justify the need for the Enhanced Priority (EP) scheduler. A legacy PF scheduler maintains fairness among all users. The scheduler dynamically selects the active users in the current time interval of T with priority based on traffic characteristics. The PF scheduler cannot distinguish between SG and NSG users which may be unacceptable to the SG. A legacy PS scheduler might serve as an alternative, but, a PS scheduler gives the NSG users extra radio blocks which ought to be given to the SG.

We make use of two PF schedulers to serve the SG and NSG jointly by dividing the radio resources between the two groups. The schedulers maintain the required minimum throughput for both group of users when available resources in a HAF are sufficient to satisfy the total radio resource demand of all users of the HAF. The throughput of the SG users is maximized by allocating NSG users with the exact radio resource needed to meet their minimum throughput and using the rest for the SG users. We name this two-scheduler scheme as an EP scheduling scheme since it enhances the priority of the SG over NSG at the same time maintaining fairness among users of the individual groups.

We analyze the time complexity of the SOPC mechanism to determine its polynomial nature. In Algorithm 5 the radio resource requirement for every SG and NSG is calculated and added to R_S and R_{NS} , respectively. This process is repeated for all HAFs. If the total number of SG users and NSG users are S and NS , then the radio resource computation takes $(O(S)+O(NS))$ time. The ISR is formed in $O(|f|)$ time, where $|f|$ is the cardinality of the set of HAFs. Since $|f|$ is very less compared to S and NS , the time complexity of Algorithm 5 is dominated by the time taken for radio resource computation, that is, $(O(S) + O(NS))$.

If Step 1 (if $ISR = NULL$) of Algorithm 6 is true, the R_S and R_{NS} for each HAF is recomputed by adding extra radio resources to R_S . The radio resources required by individual user, however, need not be recomputed. Here time complexity is $O(|f|)$

If Step 1 of Algorithm 6 is false, to form the $OCCU$ set, the *for* loop takes $(O(S) + O(NS))$ time to check every SG and NSG user. The power control is a LP optimization problem which will take $O(n^{3.5}L)$ time, where n is the number of variables (here, $|f|$) and L is the number of bits needed to store the input. The radio resource computation from the new SINR values will take $(O(S) + O(NS))$ time. The final radio resource computation runs once for each HAF thereby taking time $O(|f|)$. Thus, the total running time is $(O(S) + O(NS) + O(n^{3.5}L))$.

Thus, summing up, the total running time of the SOPC is:

- $O(S) + O(NS)$ if Algorithm 5 and Step 1 of Algorithm 6 is true.
- $O(S) + O(NS) + O(n^{3.5}L)$ if Algorithm 5 and Step 1 of Algorithm 6 is false with LP PC due to *HIZone* UEs.
- $O(S) + O(NS)$ if Algorithm 5 and Step 1 of Algorithm 6 is false with out LP PC due to lack of *HIZone* UEs.

7.4.4 Analysis of Occupant Locations

The different combinations of occupant locations are given in Table 7.2, where, PC is the power control optimization adopted in Algorithm 6 of the SOPC mechanism. An entry with value 1 in Table 7.2 represents the scenario where SG/NSG users are present in Indoor/*HIZone*. The first four row entries are the scenarios without any *HIZone* users. These scenarios occur in reality especially during the night time. The *IUEs* can take benefit of HAFs operating at P_{max} by being served at higher data rates. Here power control is not required since there are no *HIZone* users. Even if there is a spike in the radio resource demand from the *IUEs*, the HAF continues

Table 7.2: Truth table showing combinations of user occupant locations

	HIZone		Indoor	
	SG	NSG	SG	NSG
PC not re-quired	0	0	0	0
	0	0	0	1
	0	0	1	0
	0	0	1	1
PC may be re-quired	0	1	0	0
	0	1	0	1
	0	1	1	0
	0	1	1	1
	1	0	0	0
	1	0	0	1
	1	0	1	0
	1	0	1	1
	1	1	0	0
	1	1	0	1
	1	1	1	0
	1	1	1	1

to operate at P_{max} but the *IUEs* are served at a lower data rate. This may occur in three cases. First, when the building is occupied by NSG users only (refer to the second entry of Table 7.2) and say, everyone is simultaneously making a voice call or downloading a video. Since NSG users are not subscribed, the HAFs may be designed to either provide no service at all or provide best-effort service. Second case is when the building has only SG users. As mentioned in the system model, we assumed that the HAFs can handle all types of demands from indoor SG users. If however, the demand shoots up, it can be taken care of by load balancing between HAFs as has been done in [129, 130] to solve localized congestion problems or D2D communication which improves spectral efficiency as devices use lower radio resources in direct communication [76, 80, 81, 84, 96]. The third case is when the indoor demand increases due to increase in demand of both SG and NSG users. This may also be solved by load balancing or D2D communication.

Power control may be required however in the next 12 scenarios when the radio resource requirement in a HAF exceeds R and the HAF tunes its transmit power in order to revoke the radio resources initially set aside for the HIZone users and use them to serve the *IUEs*. This ensures that the HIZone users can get service at least

from the MBS while the HAFs serve the *IUEs*. In worst cases, for example, where the indoor radio resource requirement itself exceeds R , then, even after power control and shifting of HIZone users to the MBS, the SG users will not receive their minimum required throughput even after power control. Here, the HAFs may be allowed to operate at P_{max} by proportionally splitting the radio resources between the SG and NSG if the SG get more radio resources than they get when the HAFs operate at reduced transmit power.

7.5 Simulation Setup and Performance Results

The system model described in Section 7.3 is simulated using MATLAB. First, we describe the simulation parameters used for setting up the environment. Then we present the performance of our model under different use cases.

7.5.1 Simulation Environment

We have enumerated the simulation parameters in Table 7.3. The network topology in our simulation consists of a single MBS with one building (dimensions specified in Table 7.3) having multiple HAFs. The lower leftmost indoor sub-region of the building is at a distance of 350 m from the MBS. The HIZone around the building is chosen to be 10 m wide. The SG and NSG users in and around the building are uniformly randomly positioned without any mobility. The power control optimization (refer Equation (7.17)) which is used to obtain the new tuned transmit power values runs is solved using GAMS CPLEX solver. For simplicity we have considered minimum data rate to be same among all users in SG and NSG, respectively, that is, 400 kbps for SG and 200 kbps for NSG. All the users have infinite traffic demand and the HAFs with R radio resources try to guarantee at least the above mentioned data rates to the SG and the NSG. For the user locations in indoor and HIZone sub-regions, we have considered one user in each sub-region.

The number of HAFs and their co-ordinates inside the building are determined by the OPF model (refer Equation (7.1)) solved using GAMS CPLEX solver [33]. All the HAFs are placed on the ceiling of the building. The minimum number of HAFs required and their optimal locations inside the building when all the HAFs are operating at P_{max} as obtained from the OPF model are depicted in Figure 7.4. The dark red colored indoor sub-regions which are encircled and marked are the sub-regions where the HAFs are positioned on the ceiling. The co-ordinates of the HAFs

Table 7.3: Simulation Parameters

Parameter	Value
Building dimensions	$48m \times 48m \times 3m$
Number of rooms	16
Room dimensions	$12m \times 12m \times 3m$
HIZone width	10m
Number of indoor sub-regions	144
Number of HIZone sub-regions	52
Indoor sub-region dimensions	$4m \times 4m \times 3m$
Number of floors	One
$SINR_{Th}^P$	-2 dB
$SINR_{Th}^{PC}$	-4 dB
Floor and wall loss	8 and 10 dB
HAF transmit power (P_{max})	0.2W (23 dBm)
Macro transmit power (P_M)	39.8W (46 dBm)
MBS height	30m
Transmission time interval (TTI)	1 ms
Simulation time (T)	100s
Number of RBs (R)	25
Minimum average data rate of SG users	400 Kbps
Minimum average data rate of NSG users	200 Kbps

are the center of the encircled sub-regions. This placement ensures that every indoor and HIZone sub-region gets above $SINR_{Th}^P$. As can be seen from the figure, the weakest signal received by a sub-region is above -2 dB. Here, some sub-regions, like sub-regions at co-ordinates (3,2) and (2,7) named $SR_{(3,2)}$ and $SR_{(2,7)}$, are lighter than the others like $SR_{(12,2)}$, $SR_{(8,8)}$, $SR_{(4,13)}$ and $SR_{(13,12)}$ because these sub-regions with lighter shade experience greater co-tier interference than the others.

The connectivity map in Figure 7.5 shows the coverage area of each HAF inside the building and in the HIZone when operated in P_{max} . The sub-regions in the cell edge of the HAFs are the ones which receive lower SINR values. This occurrence can be observed by comparing an indoor sub-region $SR_{(2,8)}$ and HIZone sub-regions $SR_{(2,14)}$ and $SR_{(5,14)}$ in Figure 7.4. Sub-regions which receive direct interference from the MBS (*i.e.*, those situated outside the building) have lower SINR values than those inside the building. This is illustrated as follows. The signal from HAF_3 has to cross just one wall to reach the sub-region $SR_{(2,8)}$. The same holds for the signal coming from HAF_6 to the sub-regions $SR_{(2,14)}$ and $SR_{(5,14)}$. However, the cross-tier interference from the MBS to the sub-region $SR_{(2,8)}$ is lower when compared

to the sub-regions $SR_{(2,14)}$ and $SR_{(5,14)}$. This is because the signal from the MBS has to penetrate through the building wall to reach sub-region $SR_{(2,8)}$. The sub-region $SR_{(4,13)}$, above which HAF_6 is located is darker compared to $SR_{(2,7)}$ above which HAF_3 is located, that is, sub-regions close to HAF_6 experience lower co-tier interference than the ones near to HAF_3 . But, still, the SINR of $SR_{(2,8)}$ is higher than that of both $SR_{(2,14)}$ and $SR_{(5,14)}$. This shows that the cross-tier interference is dominant over co-tier interference outside the building yet, the $SINR_{Th}^P$ is maintained in indoor and HIZone which reinforces the need for using OPF model for placement of HAFs. Optimally placed HAFs reduce not only co-tier interference but also cross-tier interference inside the building and as well as in HIZone.

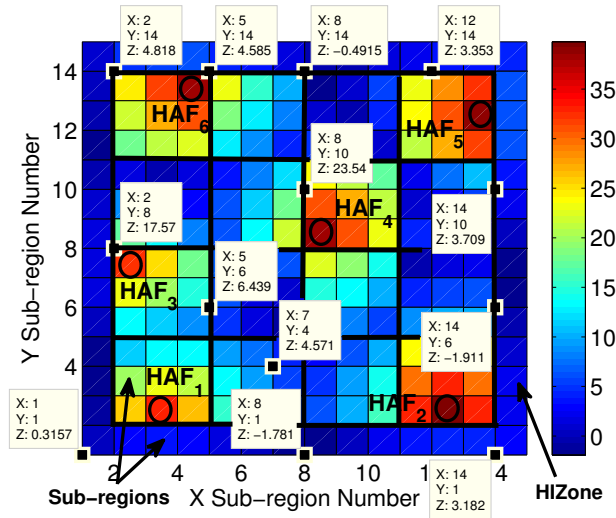


Figure 7.4: REM across sub-regions for HAFs at P_{max}

7.5.2 Performance Analysis

We provide a detailed assessment of the SOPC mechanism and how it handles different situations with the help of four scenarios. The scenarios are selected from Table 7.2. We first consider a simple scenario where the SG users are indoors and NSG users are in the HIZone (seventh entry in Table 7.2). Another scenario is where SG and NSG users occupy both indoors and the HIZone (last entry in Table 7.2). Our objective is to study how the SOPC works in both the scenarios like when all HAFs can serve their users and when most of the HAFs cannot serve the HIZone users. The fate of the HIZone users who connected to the MBS after power control is also discussed later.

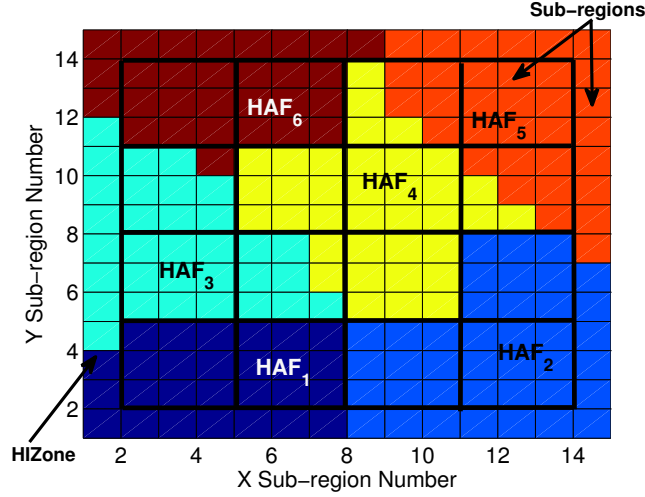


Figure 7.5: Connectivity of sub-regions to HAFs, where same coloured sub-regions are connected to a single HAF, HAF_i

The PF metric is obtained from Equation (7.19).

$$Metric_i^{PF}(t) = \frac{T_i(t)}{TP_i^{PF}(t-1)} \quad (7.19)$$

where, $T_i(t)$ is the achievable throughput of the i^{th} user in a particular TTI t in the simulation interval of T and $TP_i^{PF}(t-1)$ is the throughput at time $(t-1)$. The Priority Set (PS) Scheduler discussed in [101] can be used to distinguish between SG and the NSG. We altered the PF metric so that a user is prioritized on the basis of its past average throughput as well as its minimum required data rate per T , that is, d_{SG} for SG user and d_{NSG} for NSG user. The altered PF metrics for SG and NSG users are given by Equation (7.20) and Equation (7.21), respectively.

$$Metric_{SG_i}^{PSS}(t) = \frac{T_i(t)}{TP_i^{PSS}(t-1)} d_{SG} \quad (7.20)$$

$$Metric_{NSG_j}^{PSS}(t) = \frac{T_j(t)}{TP_j^{PSS}(t-1)} d_{NSG} \quad (7.21)$$

Scenario I

In this case we look into the performance of the SOPC mechanism when the SG users are present indoors and NSG users are present in the HIZone and all the HAFs can serve its users at the minimum data rate with R resource blocks. To explain this case, we arbitrarily place as many SG and NSG users as possible such that the resource

requirement for all HAFs remain within R . There are 43 SG users in the building and 16 NSG users in the HIzone in this case as illustrated in Figure 7.6. Since all the HAFs have sufficient radio resources and are operating at P_{max} , the REM plot and UE connectivity are same as in Figures 7.4 and 7.5, respectively.

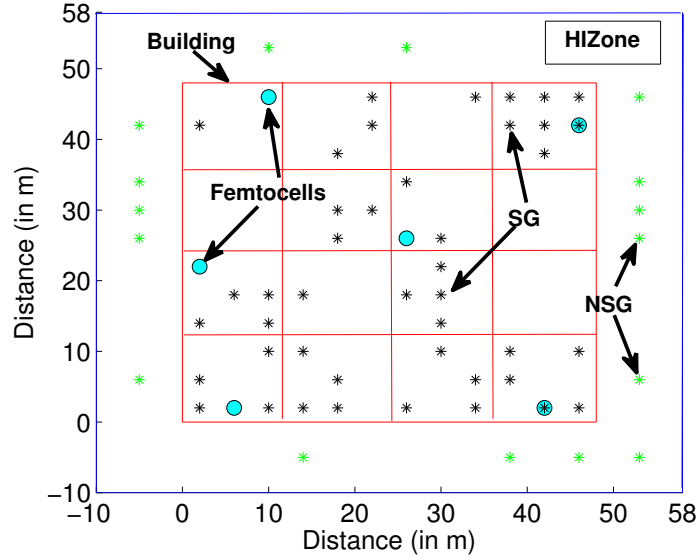


Figure 7.6: Scenario I: Building with SG users in indoor sub-regions and NSG users in HIzone sub-regions

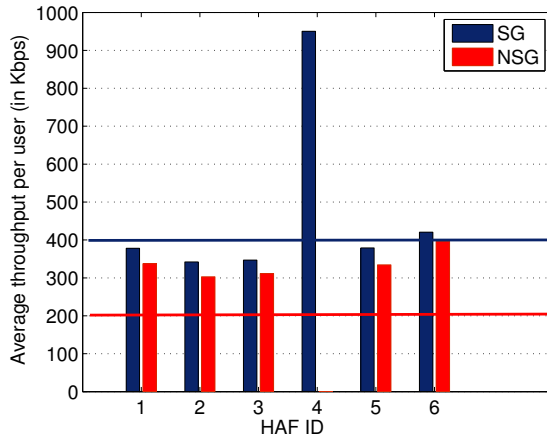


Figure 7.7: Average throughput per user in each HAF using a legacy PF scheduler

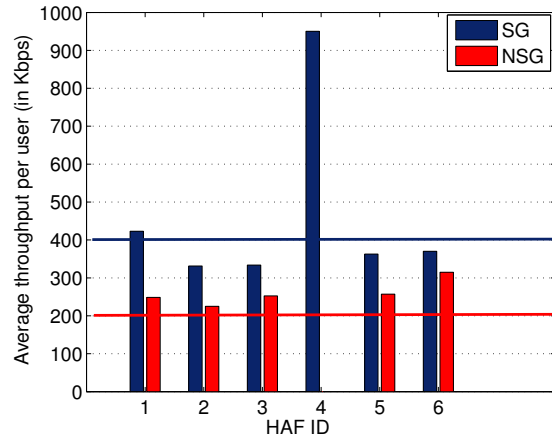


Figure 7.8: Average throughput per user in each HAF using a legacy PS scheduler

From Figures 7.7, 7.8 and 7.9 we can compare the performance of proposed EP scheduler with respect to legacy PF and PS schedulers. The PF scheduler if used to

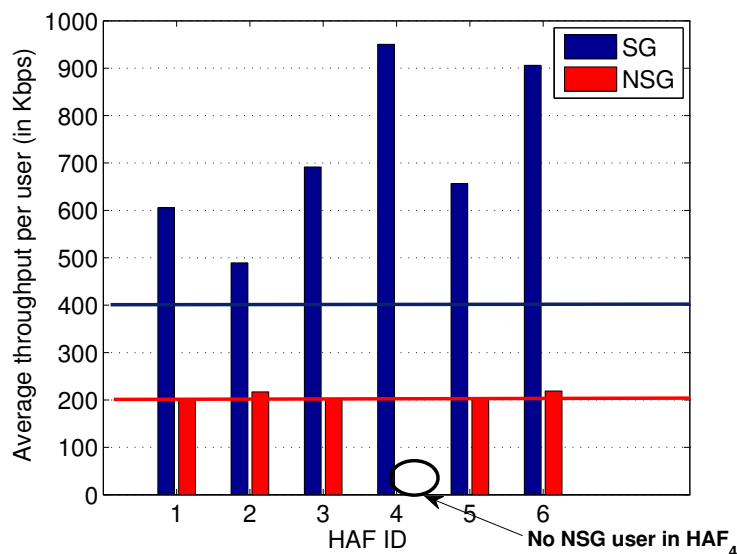


Figure 7.9: Average throughput per user in each HAF using EP scheduler

schedule the available radio resources among all users does not distinguish between the SG and NSG users and every user is treated with equal fairness. We can conclude from Figure 7.7 that the scheduler in each HAF is almost equally fair to both groups. The throughput of the SG is slightly better than the NSG because the NSG users are located far away from the HAF and are served at a weaker signal strength as compared to the indoor SG users.

Though PS scheduler serves the purpose of providing differentiated service, it does not limit the radio resource allocation to the NSG users. As a result, NSG users receive radio resources even after their required throughput is met. These radio resources could be used to serve only the SG users to maximize their throughput. We can see in Figure 7.8 that the NSG users get a throughput above their minimum requirement. Even though the difference of average throughput per user for SG and NSG in each HAF is greater than that in Figure 7.7, it is still quite small. This in realistic cases will not be appreciated by the SG users who would want to have as many radio resources at their disposal as possible. Therefore, we use EP scheduler in such a way that the PF scheduler for NSG is configured with minimum of RBs required to guarantee their required data rate. The PF scheduler of SG on the other hand is configured with remaining radio resources. For instance, in a HAF with 25 RBs in a TTI, the SG and NSG demand is 17 and 5 RBs, respectively in a TTI. The SOPC mechanism would give 20 (3 excess radio resources in addition to the required

17) radio resources to the scheduler of the SG while the scheduler of NSG would schedule only 5 radio resources among its users. We observe from Figures 7.7, 7.8 and 7.9 that the average throughput per user of all the SG users under HAF_4 remains constant. This is because there are no NSG users under HAF_4 and the number of users served in each case remains the same.

Our use of two separate PF schedulers for the two groups in the EP scheduler gives the SG users a higher throughput whenever there are excess RBs. The percentage gain in throughput for the SG with EP scheduler over the legacy PF and PS scheduler for the building scenario in this case is greater than 40%. The throughputs achieved by SG users improve significantly with the lowest being 500 Kbps (as shown in Figure 7.9). This is a striking contrast to throughputs obtained from PF or PS schedulers where the maximum average throughput achieved by a SG user is just above 400 Kbps. The values of per user average throughput is different for all HAFs because of the fact that the number of SG users and NSG users served by a HAF differs from one HAF to another. From Figure 7.9, we can interpret that the average throughput per user of SG is lowest in HAF_2 because it has the highest number of users, 13. The throughput of the users is also dependant on the number of users being served, *i.e.*, more number of users brings down the average throughput of each user. Therefore, we analyzed the performance of the EP scheduler using the Jain's fairness index. The Jain's fairness index is a well-known indicator used to measure the level of throughput fairness among users [131]. The value of the Jain's fairness index ranges from 0 to 1, where value close to 1 means that the radio resources are fairly allocated to the users. Results showed that the EP scheduler maintains fairness index above 0.99 for both the SG and NSG.

In order to maintain the QoS for different traffic classes of SG, the PS scheduling algorithm can be incorporated in the EP scheduler. We use PF scheduler for simplicity. We have considered all SG users to have the same minimum data requirement and similarly for the NSG users. From here on, all the scheduling is performed by the EP scheduler.

Figure 7.10 gives an idea of how the throughput per user for SG and NSG changes with increasing NSG users in the HIZone for as long as all HAFs have sufficient radio resources to serve all its users above or at their minimum data rate. The result shown here is for 24 SG users inside the building with the number of NSG users ranging from 5 to 35. We have taken an average of 4 SG users per HAF because we want to study the effect of increasing HIZone users on the otherwise lightly loaded HAF. The HAFs have only 25 RBs and the SG and NSG users have infinite buffers. As the number of

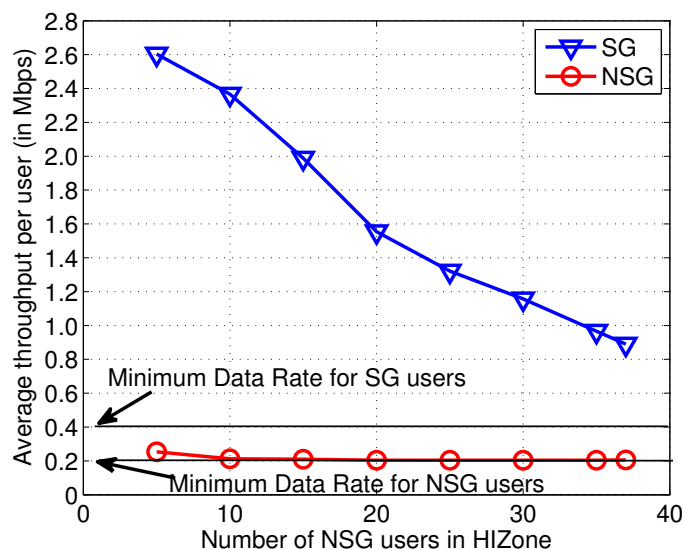


Figure 7.10: Average throughput per user connected to HAF as a function of NSG users in the HIZone

NSG users goes above 37 there is one HAF which has insufficient radio resources. We can derive from the figure that the NSG users always get just the required minimum data rate. In the first case, the throughput of the SG users is slightly above 200 Kbps because the users might have required only a fraction of the radio resources. But, radio resources are not allotted in fractions therefore the throughput is slightly better. The SG users enjoy high data rates when the NSG users are very less in number. The achieved data rate keeps decreasing as more NSG users occupy the HIZone. Since the HAFs have sufficient radio resources at all instances the average throughput remains well above the minimum required rate.

Scenario II

As in the previous scenario here also the SG users are located indoors and the NSG users are located in the HIZone sub-regions as shown in Figure 7.11. The number of SG and NSG users are 51 and 18, respectively. The number of SG and NSG users are chosen so that at least one HAF has insufficient radio resources for serving the required demand. The NSG users in the HIZone sub-regions connected to the MBS (red circle marker) after power control in SOPC are differentiable from those who are connected to the HAFs (green star marker).

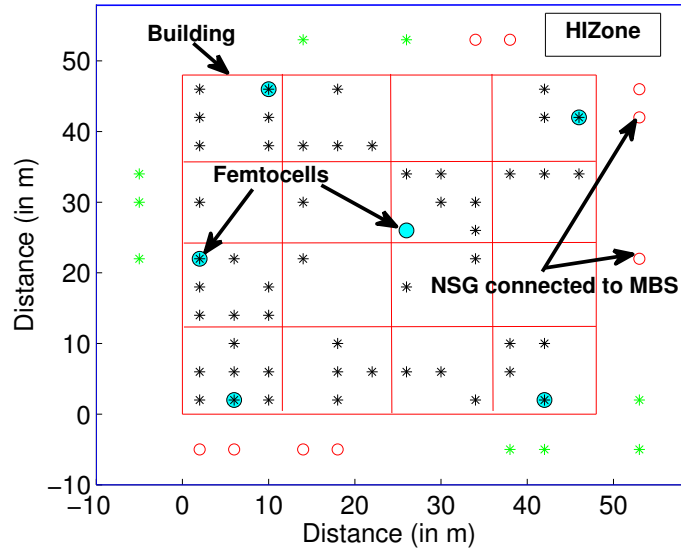


Figure 7.11: Scenario II: Building with SG in indoor sub-regions and NSG in HIZone sub-regions

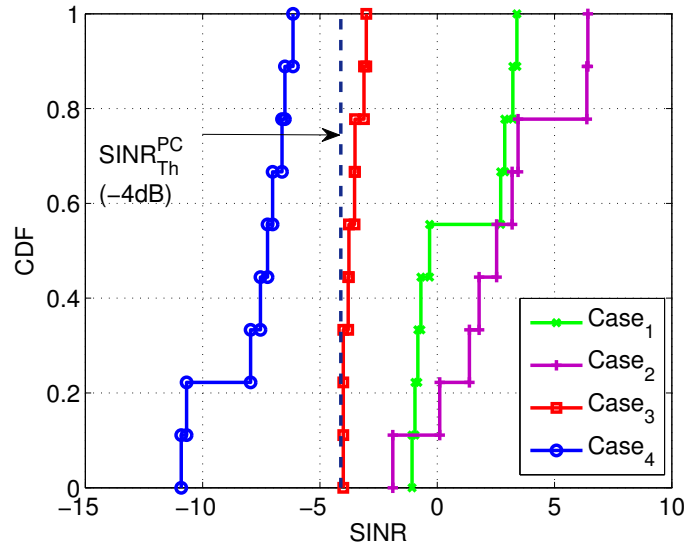


Figure 7.12: CDF plot for Scenario II; $Case_1$: When the HIZone users are connected to the MBS and there are no HAFs in the building, $Case_2$: When the HIZone users are connected to HAFs operating at P_{max} , $Case_3$: When the HIZone users connect to MBS after the HAFs tune their transmit power to P' , $Case_4$: When the HIZone users connect to MBS with the HAFs operating at P_{max} in closed access mode for the HIZone users

Since HAF_1 and HAF_5 have radio resource demand greater than what is available, according to the SOPC mechanism, Algorithm 6 is executed. The power control ensures that all the HIZone users which were previously connected to HAF_1 (4 NSG users) and HAF_5 (5 NSG users) can now connect to the MBS. The new transmit power values of the set P' are as given in Table 7.4. Even though HAF_1 and HAF_5 are the ones which needed to reduce their transmit power in order to reduce interference to the HIZone users, we observe that HAF_2 and HAF_4 also reduce their transmit powers. HAF_2 reduces its transmit power in order to reduce the cross-tier interference to the nearby HIZone users who are now trying to connect to the MBS. HAF_4 reduces its transmit power to reduce the co-tier interference to the $IUEs$ located close to HAF_5 which is now operating at a very low transmit power. If HAF_4 was to operate at P_{max} , the $IUEs$ connected to HAF_5 would experience high co-tier interference from HAF_4 . The signal from HAF_4 at P_{max} would be strong enough to create interference but not strong enough to serve them.

Table 7.4: New transmit power values after power control

HAF_1	HAF_2	HAF_3	HAF_4	HAF_5	HAF_6
0.0853W	0.11798W	0.2W	0.18722W	0.02W	0.2W

Figure 7.12 compares four CDF plots of SINR received by the victim HIZone users. The victim HIZone users are those users who if connected to the HAFs, will bring down the minimum data rate of all the users of that HAF. $Case_1$ assumes that there are no HAFs in the building. The HIZone users receive good SINR from the MBS without any cross-tier interference. $Case_2$ is the ideal case where the HIZone users receive signal from the nearby HAFs. Though the cross-tier interference is absent in $Case_1$, the CDF plot of $Case_2$ is better because the HAFs are located close to the HIZone users as compared to the MBS and therefore the signal strength received from the HAF is higher than that received from MBS in the absence of HAFs. The CDF plot for $Case_3$ is obtained from the SINR values that the HIZone users receive when connected to the MBS after power control. This in comparison with the CDF plot in $Case_4$, where the HIZone users connect to MBS as HAFs operating at P_{max} in closed access mode, shows that the HIZone users can now at least make a connection. In $Case_4$ all victim HIZone users would be unable to connect to the MBS because none of the users receive SINR greater than -4 dB. The CDF plot in $Case_1$ seems better than the plot in $Case_3$. But, in the former the HIZone users get throughputs lower than the minimum required rate even with better SINR values due to insufficiency

of radio blocks in the HAF. Also, the HIZone bring down the throughput of the SG users connected to the same HAF like them.

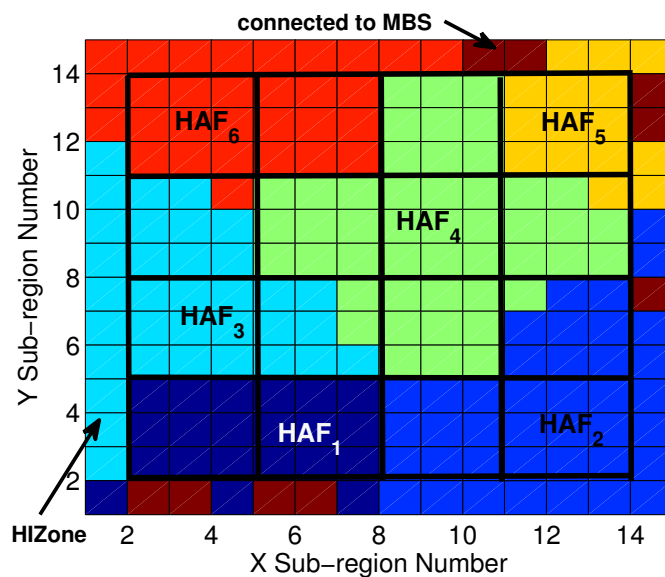


Figure 7.13: Connectivity of sub-regions to HAFs, where same colored sub-regions are connected to a single HAF, HAF_i

The connectivity of sub-regions (indoor and HIZone) to the HAFs changes (refer Figure 7.13) from what is observed when all the HAFs operate at P_{max} . While the HAFs which have reduced transmit power now have smaller coverage areas, the HAFs operating at relatively higher transmit power spread their coverage areas to neighboring sub-regions. As the coverage area of the HAFs change after power control, some HAF cell edge users may reconnect to a neighboring HAF offering better signal strength. The HAFs reducing their transmit power may thus lose some of their edge users to a neighboring HAF. The radio resource demand of users closer to a HAF increases if the HAF operate at reduced transmission power. Since it does not have to serve the HIZone users any more, the said HAF has extra radio resources at its disposal which can be used by the *IUEs*. Some HAFs which serve more users because of the shift in user connectivity, experience increased radio resource demand. If the number of users shifting connectivity is high or an edge user is connected to a HAF with relatively low transmit power, then the radio resource requirement goes up. If this demand becomes greater than R then the HAF splits R between SG and NSG in proportion to their demands. For HAFs with less number of HAF cell edge users, the users experience higher SINR than before. This is apparent in the HAFs which are still operating at P_{max} . As the neighboring HAFs decrease their transmit power,

the co-tier interferences experience by all the HAFs reduce and the users experience better signal strength from the closest HAFs.

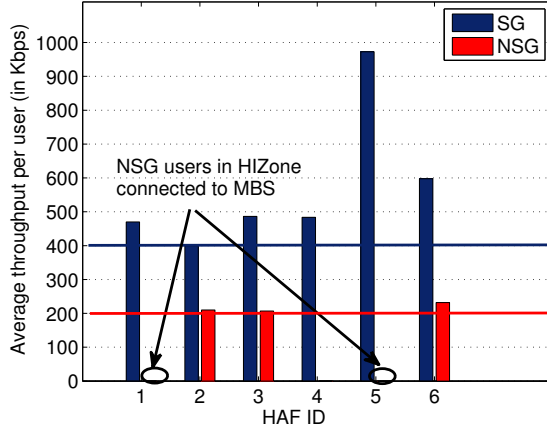


Figure 7.14: Average throughput per user in each HAF after power control in SOPC mechanism

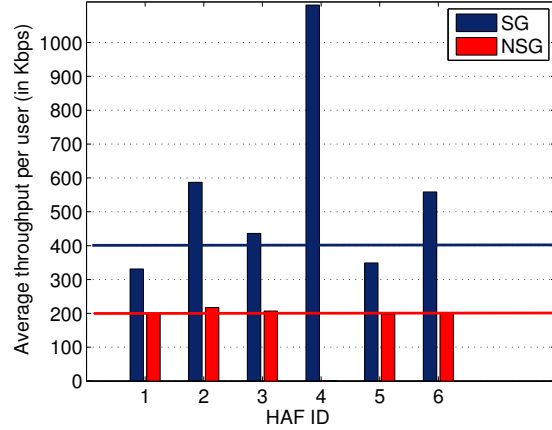


Figure 7.15: Average throughput per user in each HAF without power control

Figure 7.14 shows the per user average throughput in each HAF after the power control. Figure 7.15 on the other hand shows the per user average throughput in each HAF for the situation when the power control is not employed. If the power control is not employed, a HAF will try to serve all users in its coverage area even if it cannot guarantee the minimum data rate thereby lowering the average throughput of all its users. This will be unacceptable to the SG users who are unwilling to share radio resources with NSG users at the expense of their own throughput. Instead of making all SG users belonging to HAF_1 and HAF_5 suffer lower throughputs (less than 400 Kbps), the SOPC assures a minimum of 400 Kbps to all SG users and a minimum of 200 Kbps to all NSG users connected to the HAFs. The average throughput of SG users in HAF_4 is lesser in SOPC mechanism because the number of users under the HAF increases by 2, but it remains above 400 Kbps. On the other hand, the average throughput of SG users in HAF_5 increases by almost 180% as the number of users to be served drops from 6 SG users and 5 NSG users to only 4 SG users after doing power control by the SOPC mechanism.

Scenario III

Here, the indoor and HIZone users are a mix of SG and NSG users. All the HAFs have sufficient radio resources to serve all the users, they operate at P_{max} and maintain at least the minimum data rate for all the users. This scenario resembles the first

scenario in terms of meeting the minimum data requirements with the difference being in the user distribution. While previously we restricted the location of SG and NSG to indoor and HIZone sub-regions respectively, here we allow NSG users to access the HAFs from inside the building and the SG users to enjoy the HAFs' service from the HIZone. We select the number of SG and NSG users such that the total radio resource demand in each HAF is at most R resources. The SINR REM and connectivity maps of the building and the surrounding HIZone are similar to Figures 7.4 and 7.5, respectively as all the HAFs operate at P_{max} .

Scenario IV

The users are located in a fashion similar to Scenario III in Subsection 7.5.2 - a mix of SG and NSG users occupy the indoor and HIZone sub-regions. This scenario differs from the previous in the transmitting power of the HAFs. For all the HAFs R radio resources per TTI may not be enough to serve all the users at their minimum data rate due to presence of more HIZone users or more NSG users inside the building. Refer to Figure 7.16 for the user location setup that we shall consider for this scenario. In total there are 41 indoor SG users, 10 indoor NSG users, 5 HIZone SG users and 17 HIZone NSG users. The number of users are chosen arbitrarily so that they satisfy the resource demand. The figure also shows the location of each user and their status after power control, that is, whether the user is connected to a HAF or the MBS. As can be discerned from the figure, HAF_1 , HAF_2 , HAF_5 and HAF_6 have high radio resource demand due to which the HAF service to the HIZone users is cut off.

We provide the CDF plot which shows that the $SINR_{Th}^{PC}$ is maintained for all the HIZone users closer to HAF_1 , HAF_2 , HAF_5 and HAF_6 but are to be served by the MBS. The CDF plot for $Case_3$ in Figure 7.17 shows that all HIZone users connected to the MBS after the power control in the SOPC mechanism get SINR value of at least -4 dB from the MBS. Though $Case_2$, where the HIZone users connect to HAFs operating at P_{max} , is the best choice (with 85% of users getting a positive non-zero SINR), it is not opted during situations when the radio resource demand in HAF is more than what is available otherwise the throughput of the $IUEs$ will be degraded. $Case_4$ is the worst case which occurs when the HAFs operate at P_{max} and do not serve the HIZone users. $Case_1$ is the base case where there are no HAFs in the MBS cell and the users experience no cross-tier interference.

The SINR REM and connectivity maps are shown in Figures 7.18 and 7.19, respectively, for the new power values which can be referred from Table 7.5. Unlike HAF_4 in Scenario II (refer 7.5.2), in this case both HAF_3 and HAF_4 (having radio

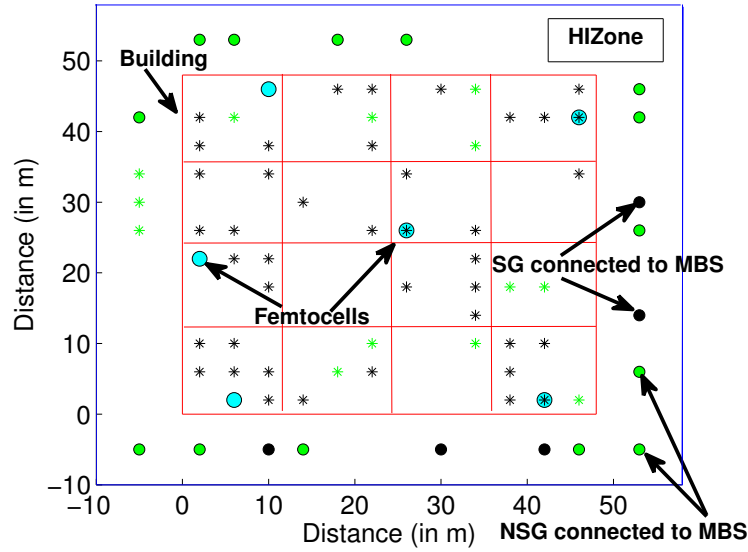


Figure 7.16: Scenario IV: Building with SG and NSG users in indoor as well as HIZone sub-regions

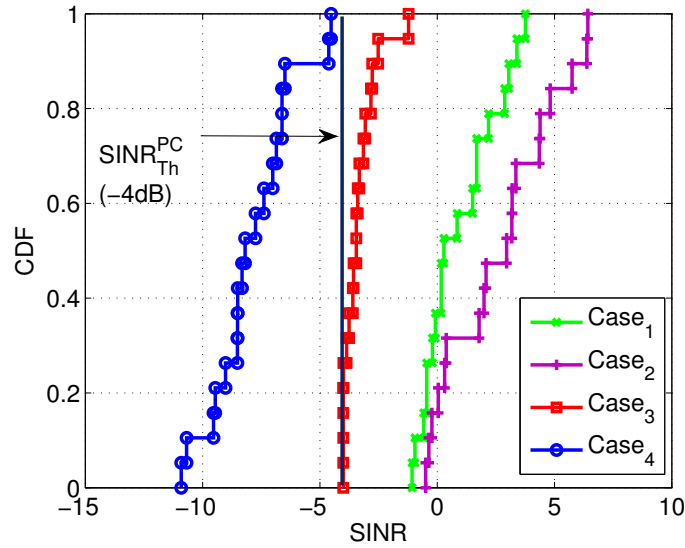


Figure 7.17: CDF plot for Scenario IV; $Case_1$: When the HIZone users are connected to the MBS and there are no HAFs in the building, $Case_2$: When the HIZone users are connected to HAFs operating at P_{max} , $Case_3$: When the HIZone users connect to MBS after the HAFs tune their transmit power to P' , $Case_4$: When the HIZone users connect to MBS with the HAFs operating at P_{max} in closed access mode

Table 7.5: New transmit power values after power control

HAF_1	HAF_2	HAF_3	HAF_4	HAF_5	HAF_6
0.09134W	0.05436W	0.2W	0.2W	0.02042W	0.03896W

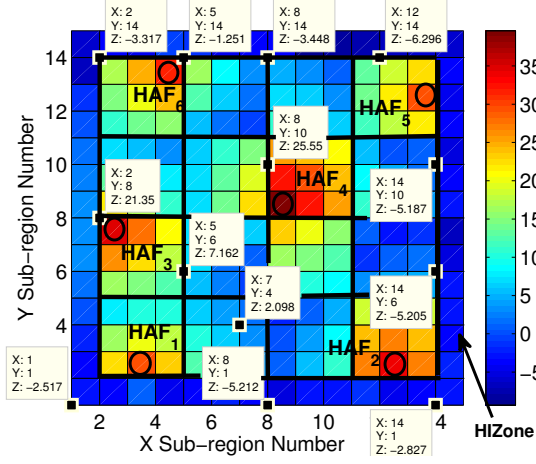


Figure 7.18: REM across sub-regions for HAFs after power control

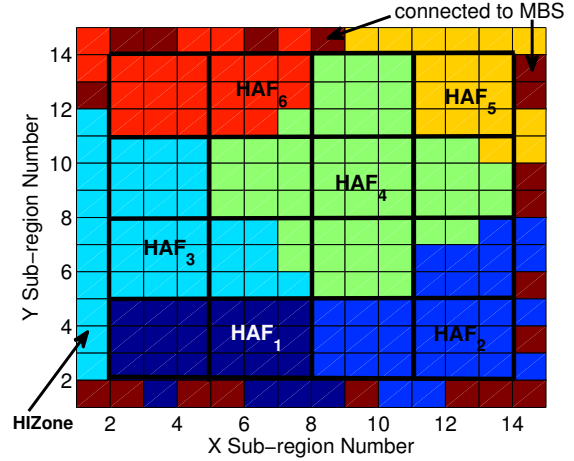


Figure 7.19: Connectivity of sub-regions to HAFs, where same colored sub-regions are connected to a single HAF, HAF_i

resource demand less than R) operate at P_{max} . This may be explained by the presence of lesser number of indoor cell edge users. Cell edge users are more affected by the co-tier interference from neighboring HAFs after reduced power transmissions. With the new power values we can now compare the REM plots in Figures 7.4 and 7.18. The signal values from the HAFs are very low in the HIZone sub-regions. For sub-regions like $SR_{(8,1)}$, $SR_{(12,14)}$, $SR_{(14,6)}$ and $SR_{(14,10)}$, the SINR from the nearest HAF is below $SINR_{Th}^{PC}$ (-4 dB threshold). However, for those connected to the MBS, marked in brown in Figure 7.19, like the sub-regions $SR_{(1,1)}$ and $SR_{(14,1)}$, the SINR is lower than that received from HAF but is above $SINR_{Th}^{PC}$. The SINR for indoor sub-regions increases due to lower co-tier interference from the neighboring HAFs operating at reduced power. This can be seen by comparing the SINR values of sub-regions $SR_{(2,8)}$, $SR_{(5,6)}$ and $SR_{(8,10)}$ in Figures 7.4 and 7.18. The coverage areas of HAF_1 , HAF_2 , HAF_5 and HAF_6 reduce on power control with the effect more prominent in HAF_5 which has the least transmit power. The HIZone sub-regions not occupied by any users are shown to be connected to a HAF. However, from the REM map we can observe that some of these sub-regions, especially those near to HAFs operating at low transmit power, have SINR lower than $SINR_{Th}^{PC}$ (sub-regions $SR_{(8,1)}$, $SR_{(12,14)}$,

$SR_{(14,6)}$ and $SR_{(14,10)}$). This simply means that, in the event that sub-regions were occupied by users, they would be connected to the MBS to receive improved signal strength.

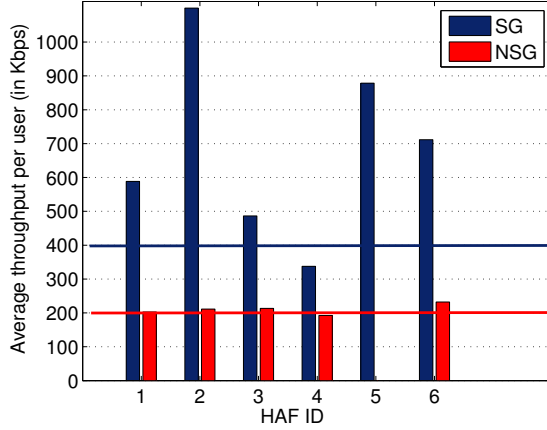


Figure 7.20: Average throughput per user in each HAF after power control in SOPC mechanism

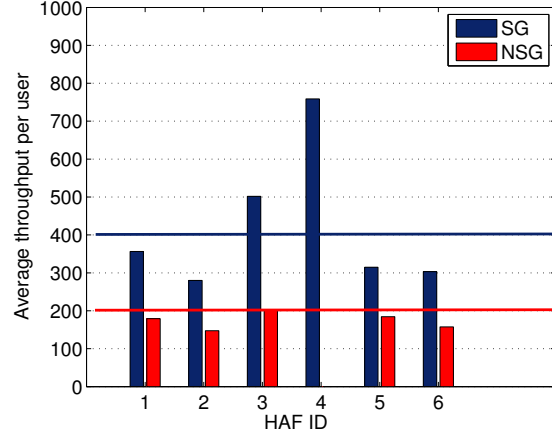


Figure 7.21: Average throughput per user in each HAF without power control

Table 7.6: Radio resource requirement in each HAF before power control

Number of SG users	Radio resource demand R_S	Number of NSG users	Radio resource demand R_{NS}	Total demand
9	1608700	5	1236300	2845000
8	2420500	7	1245100	3665600
6	1053200	3	1190700	2243900
9	1335200	0	0	1335200
7	1853000	5	1204100	3057100
7	1772700	7	1566500	3339200

The radio resource demand shown is for $T = 100sec$

Figures 7.20 and 7.21 compare the per user throughput of all the users connected to the HAFs with and without power control, respectively. The average throughput of each user is way below the minimum data rate for those connected to HAFs HAF_1 , HAF_2 , HAF_5 and HAF_6 if no power control is employed. After the power control, the throughput of the users connected to these HAFs improve. HAF_2 gives highest average throughput since it now has to serve only 9 users (5 SG and 4 NSG users) as

Table 7.7: Radio resource requirement in each HAF after power control

Number of SG users	Radio resource demand R_S	Number of NSG users	Radio resource demand R_{NS}	Total demand
8	1452500	2	395300	1847800
5	436300	4	1268100	1704400
7	1258600	3	938000	2196600
11	2474300	2	521500	2995800
5	1173200	0	0	1173200
5	1137500	2	439800	1577300

The radio resource demand shown is for $T = 100sec$

opposed to 15 users (8 SG and 7 NSG users) prior to the power control. But, as seen in Figure 7.20 the users connected to HAF_4 suffer from low throughput values. This can be explained from Tables 7.6 and 7.7 by comparing the radio resource requirement of each HAF before and after the power control. The combined radio resource demand from SG and NSG in HAF_1 , HAF_2 , HAF_5 and HAF_6 is greater than the available 2500000 RBs in a HAF for 100 seconds of simulation interval. After the power control, the total demand decreases as the number of users under these HAFs decrease and the average throughput gain for the SG users in each of these HAFs is almost 65%, 294%, 179% and 135%, respectively. The decrease in the number of users can be due to two reasons. Firstly, it can be because of handovering the HIZone users to the MBS and secondly because of handovers as a result of change in the HAF coverage areas. The radio resource demand of NSG users in HAF_2 increases. This can be explained by the fact that some NSG users connected to HAF_2 are situated at the HAF cell edge and need more radio resources as the HAF reduces its transmission power. There is a handover of one SG user to HAF_3 as a result of which the radio resource demand of SG users in HAF_3 increases. But, the minimum throughput for the SG as well as NSG users is maintained with the average throughput per user for the SG reducing by only 3% when compared to that obtained without any power control. The average throughput in HAF_4 reduces by 55% after doing power control using SOPC. The number of users in HAF_4 increases by 4. Since the new users joining HAF_4 were cell edge users of neighboring HAFs, they are located at the cell edge of HAF_4 . In order to serve these new users, the HAF experience an insufficiency in radio resources and is therefore unable to maintain the minimum data rate for the users connected

to it. Henceforth, it may be possible that a HAF initially having sufficient radio resources before the power control has insufficient radio resources after it. This may be because the HAF now has to accommodate some cell edge users of neighboring HAFs or because the HAF which reduced its power has all or most of its users near its cell edge. If in an extreme case we find that even after power control the insufficiency in most of the HAFs is increasing, we may allow the HAFs to operate at P_{max} if that provides the SG users with greater number of radio resources.

Analysis of throughput of Macro users

Here, we provide an analysis of the throughput of the Macro users, that is, any SG or NSG user connected to the MBS from outside the building (including the HIZone), by varying the number of Macro users in the system and compare the average throughput curves thus obtained for the following four cases:

- *Case₁*: When the HIZone users are connected to the MBS and there are no HAFs. All the users in the system connect to the MBS.
- *Case₂*: When the HIZone users are connected to HAFs operating at P_{max} . The MBS provides service to all the outdoor users in the cell except those in the HIZone and inside the building.
- *Case₃*: When the HIZone users connect to the MBS after the HAFs tune their transmit power by using the SOPC mechanism. Here the MBS may also serve some users in the HIZone, that is, those HIZone users who cannot be served by the nearest HAF.
- *Case₄*: When the HIZone users try to connect to the MBS with the HAFs operating at P_{max} . The HAFs act as closed access points for the HIZone users. The MBS serves those HIZone users who have SINR greater than a threshold value. The other HIZone users get no service from either the HAFs or MBS due to high cross-tier interference.
- *Case₅*: When time domain eICIC technique based on Almost Blank Subframe (ABS [132, 133]) is used. Here, the HAFs mute their transmissions for 1/8 of each time interval, T (simulation time), so that the MBS can schedule the HIZone users experiencing strong interference from HAFs.

In Figure 7.22, *Case₂* apparently seems the best choice as all the HIZone users are always served by the HAFs which transmit at P_{max} such that the number of

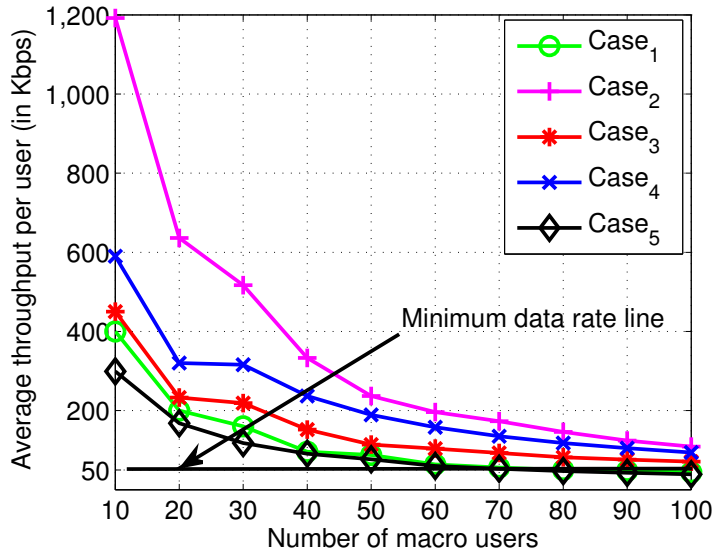


Figure 7.22: Average throughput plot for users connected to the MBS for video sessions

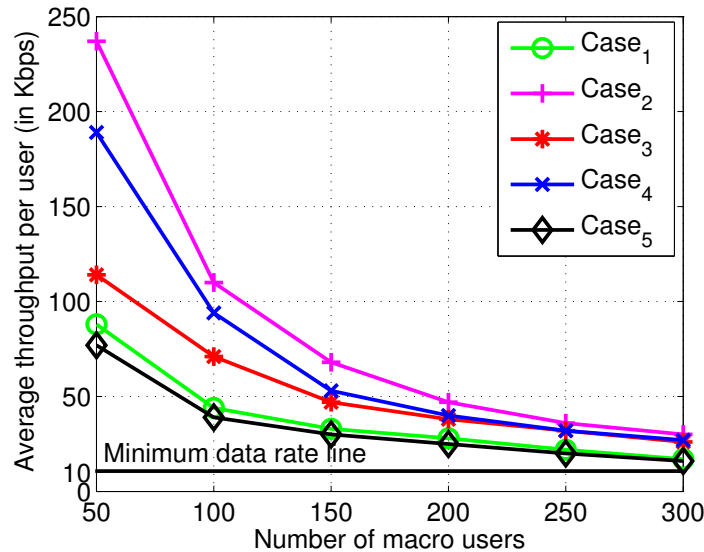


Figure 7.23: Average throughput plot for users connected to the MBS for voice sessions

users that the MBS has to serve goes down and their throughput is boosted. A point worth noting is that though the Macro users enjoy high throughput values, the throughput of the HIZone users connected to the HAFs degrades since, the minimum data requirements are not met. The performance of the Macro users under

the proposed SOPC mechanism is recorded in *Case₃*. The curve in *Case₄* also shows a better performance than the SOPC mechanism but, *Case₄* has the possibility of having some HIZone users with zero throughput. *Case₄* is when the HIZone users are denied access to the HAFs. As a result they try to connect to the MBS. Since the HAFs operate at P_{max} in this particular case, the HIZone users experience very strong cross-tier interference and almost 40% of the sub-regions cannot connect to the MBS due to the received SINR being lower than $SINR_{Th}$. Although the *IUEs* enjoy high throughput values from HAFs operating at P_{max} , there may be users in the HIZone with zero throughput. *Case₃* provides a trade-off between the *Case₄* (where *IUEs* have a high priority at the cost of no signal to around 40% HIZone sub-regions) and *Case₂* (where the Macro users enjoy uninterrupted service at the cost of degraded service to the *IUEs*). In *Case₂*, if all the HAFs are able to meet the minimum user data rate, then the MBS does not have to serve the HIZone users. If, however, any HAF is unable to meet the minimum data rate, the power control allows the HIZone users of these HAFs to be served by the MBS. As a result, all users are served at all times without greatly affecting any particular group of users. The curve obtained for *Case₁* is lower than the one obtained from the SOPC mechanism, *Case₃*, because, in the former, the MBS has to serve all the users irrespective of their locations. *Case₃* improves over *Case₁* by almost 30% when there are 50 Macro users and 61% in case of 100 Macro users in the system. There is no interference from any HAFs and all users are served fairly in *Case₁* and unlike in previous cases, the HIZone users cannot be offloaded to the nearby HAFs. The curve in *Case₅* shows the average throughput per user when eICIC is employed. Our SOPC mechanism performs better than eICIC offering a gain of almost 48% and 82% in case of 50 and 100 Macro users, respectively. The curve obtained in the SOPC mechanism provides a per user average throughput greater than 50 Kbps with 100 Macro users and can therefore could support flows requiring higher guaranteed data rates. The curves become flatter and come closer to each other as the number of users increase because the user density served by the Macro increases at a much faster rate than the user density in the HIZone. As voice calls can be made with low data rate requirements, in Figure 7.23 we vary the number of Macro users till 300. The average throughput per user obtained in our SOPC mechanism in *Case₃* is at an acceptable data rate of 26 Kbps, which is almost 62% greater than that obtained in eICIC mechanism in *Case₅*.

7.6 Summary

In this chapter, we motivated the hybrid access control in Femtos so that the SG users can benefit from the re-use of spectrum by the HAFs and in return the NSG users can get a minimum service when they are in the HIZone of buildings. The importance of optimal placement of HAFs in the building was explained and an optimal placement model was formulated. We proposed an optimal and a sub-optimal power control mechanisms that split radio resources between the SG and NSG and tune the transmit power of the HAFs whenever the radio resources available are insufficient to serve all the users connected to them. Simulation results showed that our use of power control and EP scheduler not only improved the throughput of the SG users but also provided service to NSG when they were in the HIZone or inside the building where the signal from the MBS was insufficient to obtain any service. The SOPC mechanism provides a gain of almost 82% over the eICIC mechanism when there are 100 Macro users in the system. Dynamic transmit power control in hybrid access mode is shown to be advantageous for both SG and the NSG with the MBS throughput being comparable to the MBS throughput in CAFs with fixed transmission power.

Chapter 8

Comparison of Proposed Solutions

Over the last few chapters, various solutions that can be used to improve the data rates of IUEs without much affecting the data rates of HIZUEs have been proposed. In this chapter, we compare the performance of different solutions, and highlight their merits and demerits. More specifically, we analyze the throughput variation of *IUEs* and *HIZUEs* in each of the solutions. In the following, we briefly describe each of the solutions.

- ***CKM placement:*** The co-ordinates of the every center sub-region of the building are given as the input. By K-Means clustering algorithm [63], the required number of clusters are formed using these co-ordinates of sub-regions. The Femtos are then placed at centroid of each cluster inside the building.
- ***MinNF Model:*** In this solution, the *MinNF* model minimizes the number of Femtos by determining optimal locations for their deployment inside the building. The Femtos transmit with full/ transmit power. The model is formulated as an ILP problem (chapter 3).
- ***OptFP Model:*** In this solution, the Femtos which are optimally placed using *MinNF* model transmit with optimal power obtained using *OptFP* model. The *OptFP* model is formulated as an MILP problem which tries to reduce interference to *HIZone* users who are connected to an MBS (chapter 4).
- ***D2D MILP Model:*** In this solution, the *IUEs* serve as *D2D based relays* and provide downlink connectivity to the *HIZUEs*. The selection, resource block allocation and power control of the D2D links are performed with the help of MILP optimization model (chapter 6).

- **D2D Heuristic Algorithm:** In this solution, the *IUEs* serve as *D2D based relays* and provide connectivity to the *HIZUEs*. The selection, resource block allocation and power control of the D2D links are performed with the help of two-step *D2D heuristic algorithm*. The *D2D heuristic algorithm* is formulated as an LP problem (chapter 6).
- **JDHO:** This can be achieved by the combinatorial utilization of both *D2D heuristic algorithm* and *OptFP* model (called as JDHO algorithm), that would allow some *HIZUEs* which do not have any *FIUE* to provide downlink access to get connected to one of MBSs and the remaining *HIZUEs* through D2D links (chapter 6).
- **OPF & OPC:** In this solution, the *HIZUEs* connect to the nearby hybrid access Femtos instead of the Macro BS. The RB allocation and user selection are performed using HAF Optimal model (chapter 7).
- **OPF & SOPC:** In this solution, the *HIZUEs* connect to the nearby hybrid access Femtos instead of the Macro BS. The RB allocation and user selection are performed using HAF sub-optimal PC algorithm (chapter 7).
- **DUD:** In this solution, to reduce the battery drain from UEs and to improve the downlink data rate, we use the *DUD* access method *i.e.*, uplink connected to the closest Femto and downlink to a less loaded Femto (chapter 2).
- **VR:** In this solution, to reduce the co-tier interference between neighboring Femtos, Femtos dynamically increase or decrease the cell edge/non-cell edge region of Femtos and efficiently allocate the radio resources among cell edge/non-cell edge region of Femtos (chapter 9).

The characteristics of above mentioned proposed solutions are compared in Table 8.1.

8.1 Scheduling Algorithms

In *No Femto*, *MinNF*, and *OptFP* models, the MBS and Femto schedule the users using PF scheduling algorithm. In each TTI t , the PF algorithm determines the PF metric for all the UEs using Equation (8.1).

$$PFmetric_i^t = \frac{IAT_i^t}{AAT_i^{t-1}} \quad (8.1)$$

Table 8.1: Characteristic of Proposed Solutions

Solutions	Optimal Placement	Power Control	Femto Access Mode	Load Balance	DL/UL	Interference Management
CKM	✗	✗	Open	✗	DL	✓
MinNF Model	✓	✗	Open	✗	DL	✓
OptFP Model	✓	✓	Open	✓	DL	✓
D2D MILP Model	✗	✓	✗	✓	DL & UL	✓
D2D Heuristic Algorithm	✗	✓	✗	✓	DL & UL	✓
JDHO Algorithm	✓	✓	Open	✓	DL	✓
OPF & OPC	✓	✓	Hybrid	✓	DL	✓
OPF & SOPC	✓	✓	Hybrid	✓	DL	✓
DUD	✓	✗	Open	✓	DL & UL	✗
VR Algorithm	✗	✗	Open	✗	DL	✓

In above equation, $PFmetric_i^t$ and IAT_i^t are the PF metric and Instantaneous Achieved Throughput of UE i at TTI t , respectively. AAT_i^{t-1} is the Average Achieved Throughput of UE i till TTI $(t - 1)$. The calculation of IAT_i^t and AAT_i^{t-1} is shown below.

$$IAT_i^t = B_i^t * SE(SINR_i^t) \quad (8.2)$$

$$AAT_i^{t-1} = \beta * AAT_i^{t-2} + (1 - \beta) * IAT_i^{t-1} \quad (8.3)$$

where, B_i^t is the RBs assigned to UE i at TTI t , $SE(SINR_i^t)$ is the Spectral Efficiency corresponding to the SINR of UE i at TTI t . The SE can be calculated using the LTE/CQI table [134]. IAT_i^t will be 0 if the UE i is not scheduled in TTI t . β is a weighting factor which lies between 0 and 1. In our simulation, we set the value of β as 0.99.

In *D2D heuristic algorithm*, the Femto and MBS use PF scheduling algorithm. For scheduling the D2D links, PF algorithm cannot be used, because the D2D selection is done as part of our D2D heuristic algorithm. But proposed *D2D heuristic* algorithm does not perform time domain scheduling of D2D links (*i.e.*, from the potential HIZUEs set our algorithm only selects the D2D links, assigns resources and allocates power to each of the link, but it does not update the set as time progresses). For example, the set of *HIZUEs* which are scheduled at TTI t should be removed from the potential *HIZUE* set in TTI $(t + 1)$, otherwise, the heuristic algorithm may keep choosing the same D2D pairs repeatedly and hence the other D2Ds will not receive any data. Our *D2D heuristic* algorithm does not update the potential *HIZUE* set continuously. We have used a Round Robin (RR) scheduling algorithm to schedule the D2Ds. The RR algorithm keeps removing those *HIZUEs* which are

already scheduled and maintains a list of those *HIZUEs* which are not scheduled yet. Once all the *HIZUEs* receive data from the *FIUEs*, RR adds all *HIZUEs* back to the potential *HIZUE* set and repeats the scheduling process. Of course, unlike PF algorithm, RR does not guarantee throughput fairness among the D2Ds. Also the Femto must send the *HIZUE* data to the FIUE before D2D scheduling takes place which is not considered in PF scheduling algorithm. In future, we consider developing a scheduling algorithm which accounts for the above stated challenges.

The scheduling algorithm (*i.e.*, EP scheduler) used by the *OPF and SOPC* has already been discussed in Section 7.4. In each scenario, UE scheduling occurs for 100000 TTIs (*i.e.*, 100 seconds).

8.2 Experimental Setup and Comparison Results

The LTE HetNet system model is simulated using MATLAB as given in chapter 6.3. A single floor building is considered where one MBS is located at a distance of 350 m from the south-west side of the building of dimensions 48 m \times 48 m \times 3 m. The transmission power of MBS and Femto are 46 dBm and 20 dBm, respectively. The MBS and the Femtos share the same 5 MHz spectrum (*i.e.*, frequency reuse one). 200 UEs are uniformly distributed around the MBS. Out of this 200 OUEs, 20 UEs are *HIZUEs* and 100 UEs are uniformly distributed inside the building. For the D2D based relays, 15 UEs out of 100 IUEs, act as FIUEs. We assume that the UEs have infinitely backlogged data. The results provided in this chapter show the performance of different solutions over 50 different UE placement scenarios. Other important simulation parameters are same as in Table 7.3. In the rest of the chapter, we discuss the throughputs of *IUEs* and *HIZUEs* obtained using different solutions.

8.2.1 Throughput Comparison

Figures 8.1 and 8.2 show the throughput CDF *IUEs* and *HIZUEs* in different solutions. In both the figures, the legend name is associated with $SINR_{Th}$ for *IUEs* and *HIZUEs*, respectively (for example -4 dB and 0 dB in case of *D2D heuristic algorithm*). In *No Femto* method, since there is no cross-tier interference from Femtos, the throughput of *HIZUEs* is high. Since the MBS is not able to maintain a minimum $SINR_{Th}$ inside the building, most of the IUEs will experience negligible throughput in *No Femto* method. In *CKM placement* method, the Femtos are deployed inside the centroid (the building) of each cluster hence, it does not create any interference to

the *HIZUES* in *HIZone*. Thus it is more similar to *No Femto* method. But at the same time the *IUEs* performance got degraded due to non-optimal way of placement of Femtos inside the building.

Figure 8.1 shows that *MinNF* model provides high data rate for the *IUEs*. This is mainly because of the high SINR guaranteed by the Femtos which are optimally placed inside the building. In *MinNF* model, no $SINR_{Th}$ is set for the *HIZUES*, only the *IUEs* have $SINR_{Th}$ (-2 dB). Since the Femtos transmit at their full power in *MinNF* model, *HIZUES* experience cross-tier interference, leading to their SINR degradation. This SINR degradation leads to decrease in throughput of *HIZUES* in *MinNF* model. Also, we can observe that 18% of *HIZUES* receive zero throughput from the MBS.

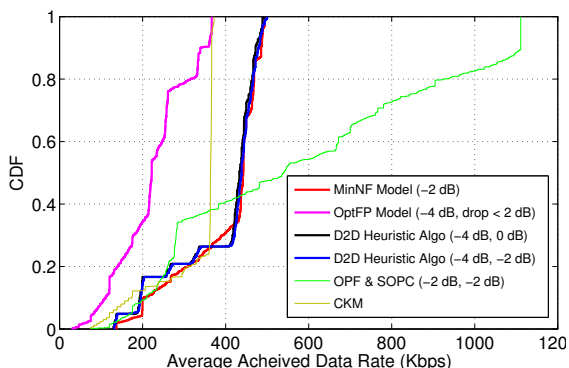


Figure 8.1: CDF of *IUEs* Throughput in Different Solutions

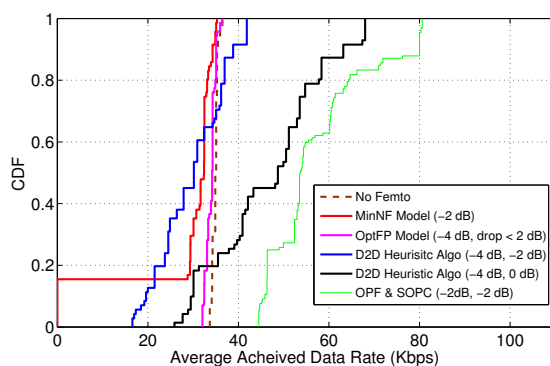


Figure 8.2: CDF of *HIZUES* Throughput in Different Solutions

OptFP model reduces the transmission power of the Femtos to ensure that the SINR degradation of the *HIZUES* (compared to the value obtained when there were no Femtos) is not more than 2 dB. Since the Femto power is reduced in *OptFP* model, the $SINR_{Th}$ of *IUEs* is reduced to -4 dB. Figure 8.2 shows the improvement in *HIZUES* throughput in *OptFP* model when compared to *MinNF* model. Also, it is closer to the throughput obtained in *No Femto* method. Due to decrease in Femto transmit power, the SINR of *IUEs* decreases. This leads to a drastic decrease of *IUEs* throughput (*i.e.*, 44%) in the *OptFP* model. Note that setting a higher SINR, drop value for the *HIZUES* increases the Femto transmit power, and thereby SINR and throughput of *IUEs* can be improved but it can affect the *HIZUES* performance.

Using *D2D heuristic algorithm*, Femtos can transmit with peak power without affecting the *HIZUES* performance. To compensate for the D2D interference, $SINR_{Th}$ of *IUEs* is set as -4 dB. Since the performance of the *HIZUES* highly depends on the $SINR_{Th}$, we have analysed the throughput of *IUEs* and *HIZUES* by fixing two

different thresholds for *HIZUE* (*i.e.*, - 2 dB and 0 dB). From Figure 8.1, we can observe that the throughput of *IUE* obtained in *D2D heuristic algorithm* is close to the throughput obtained in *MinNF* model. A slight decrease in the throughput is due to the additional D2D interference. From Figure 8.2, we can observe that for higher $SINR_{Th}$, the throughput of *HIZUEs* is higher. This is because of the increase in MCS as the SINR increases. The narrowness of the throughput of *HIZUEs* CDF lines in *No Femto*, *MinNF*, and *OptFP* show that the MBS which uses PF scheduling algorithm has indeed ensured throughput fairness to all its UEs. Since *D2D heuristic algorithm* uses RR algorithm, the throughput fairness is not guaranteed.

Table 8.2: $SINR_{Th}$ vs Average D2D Transmission Power

Metric	$SINR_{Th} =$ - 2dB	$SINR_{Th} =$ 0dB	$SINR_{Th} =$ 2dB
Average D2D Tx Power (W)	0.026 W	0.048 W	0.076 W
Data received by <i>HIZUEs</i>	3.42%	5.41%	7.49%

Table 8.2 shows the variation in average D2D transmission power (*i.e.*, transmission power of the *FIUEs*) with change in *HIZUEs* $SINR_{Th}$. As expected, the average D2D transmission power increases with increasing $SINR_{Th}$. One would expect the throughput of *IUEs* to decrease with increase in D2D transmission power because of the increased D2D interference. But we can clearly see from Figure 8.1 that the throughput of *IUEs* has not decreased much (only 0.84%) for $SINR_{Th}$ of 0 dB case when compared to $SINR_{Th}$ of -2 dB case. Even though the power has increased significantly with increasing $SINR_{Th}$, the interference to the *IUEs* is not significant. This explains the efficiency of our proposed D2D pairing and resource allocation algorithm (hDPRA) (chapter 6.4.2). Table 8.2 shows the percentage of the data received by *HIZUE* as compared to the total received data by *FIUEs*. Since the D2Ds operate in higher MCS in higher SINR, the amount of data received by the *HIZUEs* increases with increasing $SINR_{Th}$. Comparison of different solutions is done in Table. 8.3.

Remarks: In order to compensate for this loss of data (*i.e.*, when the number of *IUEs* traffics are high and in that case if some RBs are used for *HIZUEs* data transfer we call this state as loss of data) for the *FIUEs*, the Femto scheduler has to increase the scheduling (resource allocation) frequency for the *FIUEs*. As mentioned earlier, a future approach could be designing such a scheduler which compensates for the data loss in *FIUEs*, ensures fairness to all the *HIZUEs*, and provides required

Table 8.3: Comparison of different solutions

Solution	No. of Femtos	Avg. data rate of <i>IUEs</i> (in Kbps)	Avg. data rate of <i>HIZUEs</i> (in Kbps)	Remarks
No Femto	0	0	34	Coverage hole inside the building
CKM	4	327	34	Coverage hole inside the building
MinNF (-2 dB)	4	397	27	No coverage hole but huge throughput degradation for <i>HIZUEs</i>
OptFP (-4 dB, drop < 2 dB)	4	224	33	Less degradation for <i>HIZUEs</i> at the cost of decrease in more <i>IUEs</i> throughput.
D2D Heuristic Algorithm (-4 dB, 0 dB)	4	384	46	No coverage hole but additional overhead for operators to monitor more D2D pairs
D2D Heuristic Algorithm (-4 dB, -2 dB)	4	387	29	No coverage hole but additional overhead for operators to monitor more D2D pairs
OPF and SOPC (-2 dB, -2 dB)	6	577	57	No coverage hole but increase in Femto count (<i>i.e.</i> , CAPEX)

HIZUE data to the *FIUE* before the D2D transmission (data transmission between *HIZUE* and *FIUE*) begins.

Compared to all other solutions, the throughput of *IUEs* is very high in *OPF and SOPC*. This is mainly due to the increased Femto count in *OPF and SOPC*. Six *HAFs* are required to provide coverage to the entire building (including the *HIZone*) in *OPF and SOPC* based solution whereas in all other solutions only four Femtos are required. Also the throughput of *HIZUEs* is higher in *OPF and SOPC*, because the *HAFs* use dedicated resources to schedule the *HIZUEs*.

8.2.2 Operators' Revenue: An estimate

In large scale planned deployments, usually for a building of 10 floors, we require approximately 60-70 Femtos (each Femto BS costs around \$100) and it incurs huge investment cost for operators. But, they can save 20-30% of money (*i.e.*, CAPEX) by adapting *MinNF* model. To further improve the capacity, operators may think of solutions based on *D2D based relay* model. Operators could provide incentives (like free call service, discount in data plan, free SMS service) for the *FIUEs* to act as *D2D based relays*. For a single building, it will cost around \$0.33 per year. And this cost is not fixed as it will not come as direct investment from the operator side because of infra structureless communication (*i.e.*, D2D communication). Hence, depending upon the scenarios or *UEs* demand operators can decide efficient schemes to achieve more revenues.

Another alternative to increase the operators revenue could be by deploying Fem-

tos based on *OPF and SOPC* model. This model will increase the overall system performance by allocating more dedicated spectrum compared to *D2D heuristic algorithm* at the cost of increased Femto count.

Chapter 9

Enhanced Distributed Resource Allocation and Interference Management in LTE Femtocell Networks

9.1 Introduction

In above chapters, placement of Femtos is optimized to reduce co-channel co-tier interference among neighboring Femtos and transmit power of Femtos is optimized to reduce cross-tier interference between MBSs and Femtos. But, for arbitrary deployed Femtos, Inter Cell Interference Coordination (ICIC) techniques could be employed to address co-tier interference problem among Femtos which are connected with each other over X2 interface. Hence, in this chapter, we propose an ICIC technique, Variable Radius (VR) algorithm which dynamically increases or decreases the cell edge/non-cell edge regions of Femtos and efficiently allocates radio resources among cell edge/non-cell edge regions of Femtos so that the interference between neighboring Femtos can be avoided.

9.1.1 Organization of this Chapter

Rest of the chapter is organized as follows: Section 9.2 describes the related work. Proposed VR algorithm is discussed in Section 9.3. The simulation methodology and results are presented in Section 9.4. Finally, Section 9.5 summarizes the work.

9.2 Related Work

In this section, we review existing works addressing the interference issues due to incorporation of Femtos into LTE systems. In Release 8 [64], X2 was introduced for direct communication between Macro BSs. This X2 could be used by ICIC mechanisms to reduce inter cell interference due to reuse one. In Release 11 [64], X2 interface is introduced between Femtos of enterprise femtocell networks to avoid interference and directly route the data and signaling messages among Femtos, thereby reducing the load on MME of LTE core network and offers better coordination among Femtos. Cross-tier interference can be avoided by dividing the spectrum between macro and Femtocells orthogonally [135,136]. In these schemes, radio resources are shared between Femtos in a distributed manner by using F-ALOHA scheme, which introduces slotting and contention amongst Femtos. In [137], three cross-tier interference management schemes are proposed. First scheme divides spectrum between macros and Femtos, but as number of Femtos increases the spectrum allocated to macros decreases considerably. Second scheme allocates the whole spectrum to both macros and Femtos which can lead to high interference. In third scheme, some part of the spectrum is shared by Femtos and macros. The remaining spectrum is divided between macros and Femtos. But, this scheme is efficient only if UEs count is low.

Two types of frequency reuse techniques can be applied to reduce co-tier interference. Fractional Frequency Reuse (FFR) [138] has *frequency reuse three*, which means that only one third of the spectrum is used in a particular cell and therefore leads to inefficient usage of spectrum resource. The other approach is Soft Frequency Reuse (SFR) [139,140]. In SFR, the cell area is divided logically into two regions based on spectrum allocation: an inner region where major portion of spectrum is available and a cell edge area where a small fraction of the spectrum is available. Since the capacity at cell edge may be low, it can be increased by allocating higher power carriers to UEs in this region, where as lower power carriers are allocated to UEs in the inner region. But, SFR was studied only for Macros. To improve the spectrum efficiency and throughput of the indoor UEs, SFR technique can also be adapted to enterprise Femto networks. But the drawback of implementing SFR in Femtos is that it can lead to high interference due to overlap of coverage regions of Femtos. Hence, we propose an efficient interference management technique (VR: Variable Radius algorithm) which dynamically increases or decreases the width of cell edge region inside the Femto coverage area to overcome the drawback of SFR for Femtos.

9.3 Proposed VR Algorithm

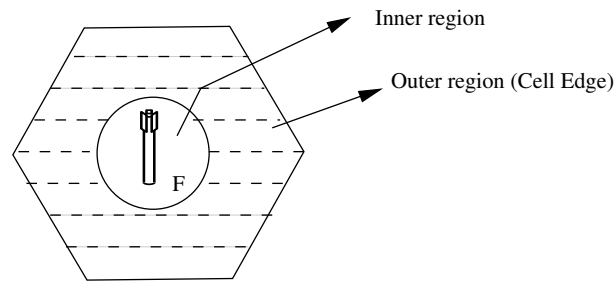


Figure 9.1: Regions inside Femto coverage area

Every Femto communicates about the RBs allocated to its cell edge UEs with neighboring Femtos through X2 interface. Femto allocates RBs to its UEs in outer region such that same RBs are not allocated in the outer regions of its neighboring Femtos, thus avoiding the interference. Such an allocation is known as restricted RB allocation. But, since the delay to get the required number of RBs increases, the average throughput of cell edge UEs decrease. For the UEs of inner region, there is no such restriction on RB allocation, unlike cell edge users. Any free RB can be allocated to them by respective Femtos without any coordination with neighboring Femtos through X2 interface.

Let us consider an enterprise Femto deployment scenario with six Femtos namely F1-F6 randomly placed UEs as shown in Figure 9.3 for describing the proposed VR algorithm. The two scenarios of it are given below.

9.3.1 Interference Scenario 1

Initially, the width of outer region is zero for all of the Femtos as shown in Figure 9.2. In this case, interference occurs if the cell edge UEs in overlapping regions of neighboring Femtos use the same RBs. This results in decrement of CQI due to poor SINR and hence leads to low data rates. According to 3GPP TS [36.301], the CQI values vary from 1 to 15 [142] gives the mapping of SINR to CQI. Active UEs provide CQI feedback to Femto at regular intervals. Femto transmits data with higher modulation scheme like 64-QAM if the UE has higher CQI value. In consummate circumstances caused by very high interference, CQI becomes very low and the UE may not able to transmit any data.

Algorithm 7 Variable Radius Algorithm

Input $CQI_Threshold$: Handover CQI threshold**Input** $FR_Threshold$: Threshold Fail Ratio**Input** R : Radius of Femto

```
1:  $r \leftarrow R$  {Initialize Radius of Inner Region}
2: while true do
3:    $CQI \leftarrow CalculateCQIInnerRegion()$ ; {Calculates average CQI for a given inner region }
4:   if (  $CQI < CQI\_Threshold$  ) then
5:     DecreaseRadius  $\leftarrow$  true;
6:   else
7:     DecreaseRadius  $\leftarrow$  false;
8:   end if
9:    $FR \leftarrow CalculateFRUEsOuterRegion()$ ; {Calculates Fail Ratio of UEs in cell edge region }
10:  if (  $FR > FR\_Threshold$  ) then
11:    IncreaseRadius  $\leftarrow$  true;
12:  else
13:    IncreaseRadius  $\leftarrow$  false;
14:  end if
15:  if ((IncreaseRadius) && (DecreaseRadius)) || ((!IncreaseRadius) && (!DecreaseRadius)) then
16:    Continue;
17:  else
18:    if ( DecreaseRadius && !IncreaseRadius ) then
19:       $CQI\ array \leftarrow Sort(CQI\ inner\ region)$ 
20:       $\gamma \leftarrow Search(CQI\ array)$  {finds threshold distance  $\gamma$  of the first UE whose AVG CQI along circumference of circle with radius  $d > CQI\_Threshold$  }
21:       $r \leftarrow (r + \gamma)/2$  ; { where  $\delta$  is the width of the region containing users whose AVG CQI  $< CQI\_Threshold$ }
22:       $PFScheduling()$ ; {Proportional Fair Algorithm}
23:    else
24:       $r \leftarrow r + \delta'$  ; { (where  $\delta'$  will bring  $RR-(AR/2)$  unsatisfied users of outer region nearest to the boundary between inner and outer regions into inner region)}
25:       $PFScheduling()$ ;
26:    end if
27:  end if
28: end while
```

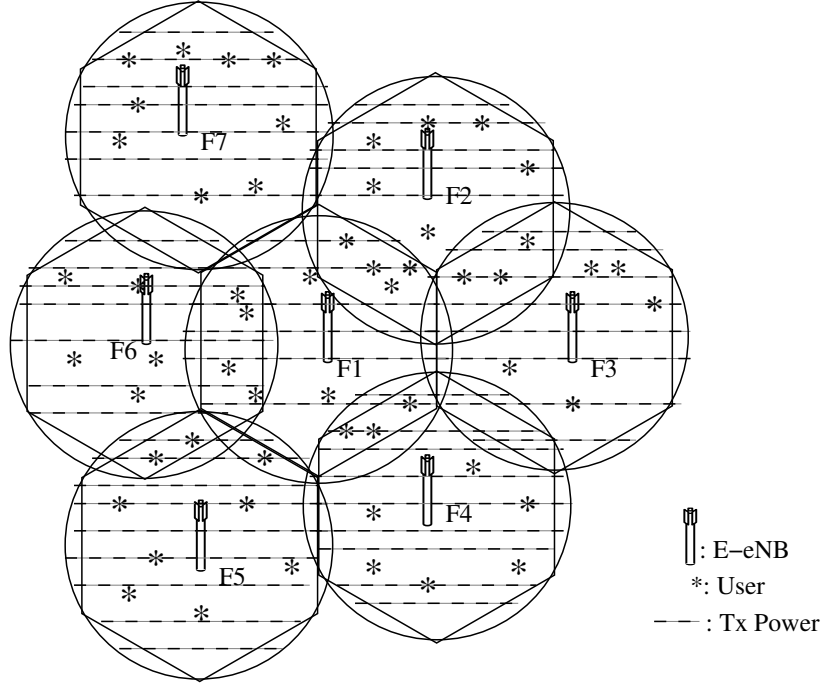


Figure 9.2: Initial inner regions of Femtos

To reduce this interference, the radius of the inner region is decreased which in turn increases the width of the outer region as shown in Figure 9.3. To determine the average CQI of a UE at a distance d from the Femto center, firstly an inner and an outer circle are drawn with the radius as $(d - \delta)$ and $(d + \delta)$, respectively as shown in Figure 9.4. The width of the resultant strip is 2δ . Secondly, the average of the CQI of all UEs within this strip is calculated and this value is assigned to the UE at distance d . The average CQI is calculated and assigned similarly to every UE at any distance from the Femto within the radius of inner region. Thirdly, the average CQI of all UEs is sorted in increasing order. Fourthly, the first UE whose average CQI value is greater than a threshold CQI value is identified. The distance of this identified UE from the Femto is the threshold distance and is named γ . Finally, bisection method is used to calculate the mean of the inner region radius r and the threshold distance γ as $r = (r + \gamma)/2$.

This mean value (r) is the radius of the inner region. By using X2 interface the interference is avoided in the outer regions by exchanging signaling messages between neighboring Femtos for restricted RB allocation. Bisection method is used in general to find the roots of a polynomial. Here bisection method is used to find the approximate radius value for which the average CQI value at the given radius is

equivalent to the threshold value.

Using mean value helps us to decrease the effective inner radius of the Femto from R (cell radius) to r . The advantage of calculating the mean over considering the threshold distance γ , as radius, is that when the threshold distance is very small, a large number of UEs reside in outer region which may lead to unfair allocation of RBs to the cell edge UEs, as very less amount of RBs are catered to cell edge UEs, due to restricted allocation. The threshold CQI value for contraction is the CQI used for indoor data traffic handover *i.e.*, less than -3 dB in terms of SINR.

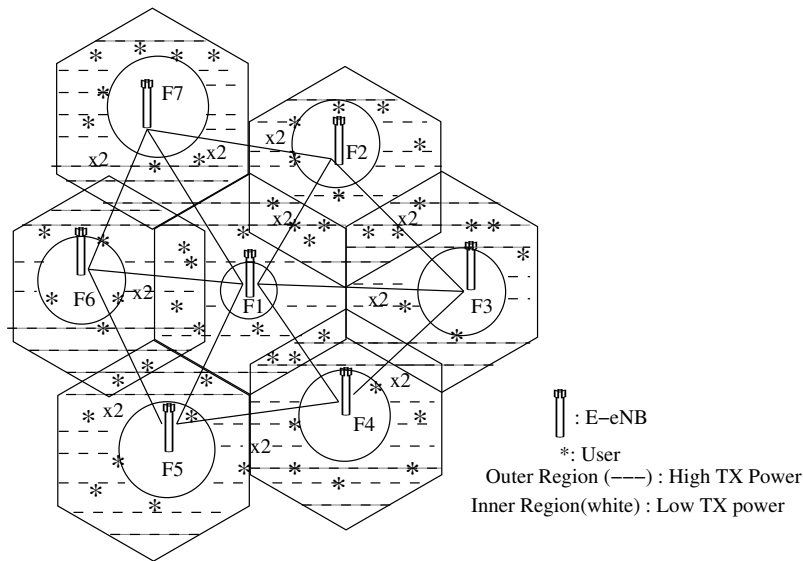


Figure 9.3: Reducing the inner regions of Femtos

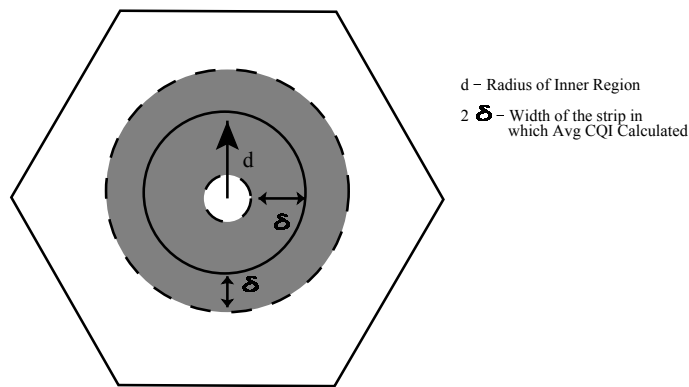


Figure 9.4: Calculating Avg CQI value in the strip

9.3.2 Interference Scenario 2

When the number of UEs in the outer region increases drastically, due to restricted RB allocation, many RB requests from UEs of the outer region may not get satisfied. This leads to dramatic decrease in the system throughput. In order to overcome this problem, the inner region has to be expanded to accommodate the excess UEs of the outer region as shown in Figure 9.5.

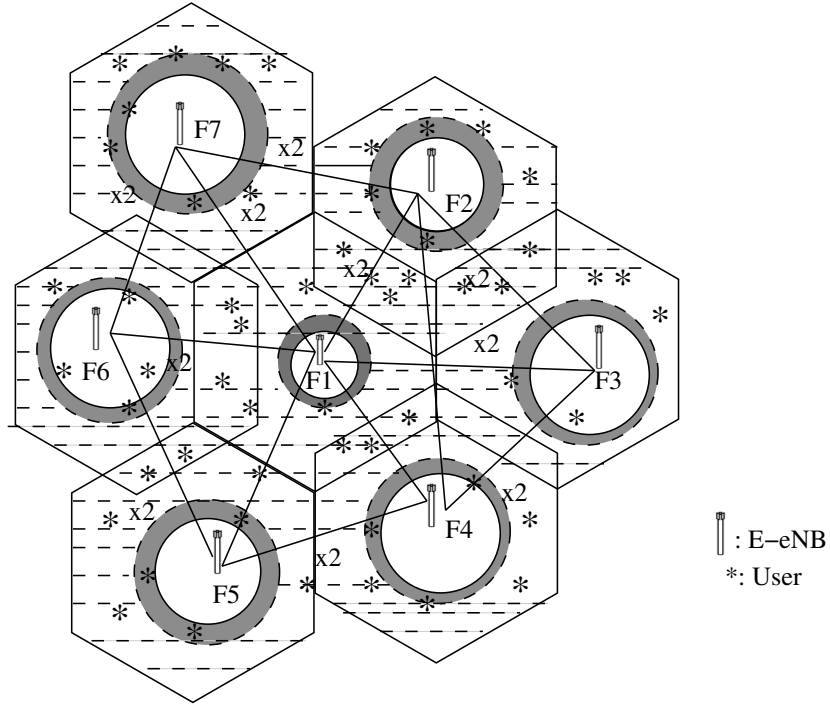


Figure 9.5: Increasing the Inner regions of Femtos

Depending upon the Fail Ratio (FR) the radius increases, where FR is defined as, $FR = \frac{RejectedRequests(RR)}{AcceptedRequests(AR)}$, where RR is the number of unsatisfied requests coming from outer region due to restricted RB allocation and AR is the number of requests coming from outer region that can be satisfied in some subframe. Due to unavailability of RBs certain requests cannot be satisfied in a particular subframe and these requests are excluded in AR . The radius of inner region will remain the same if FR is less than or equal to the threshold value (FR-Threshold) and this value can be set by the network operator. If FR is greater than threshold value, the radius of inner region is increased. The radius is incremented by δ' such that $RR - (AR/2)$ unsatisfied UEs from outer region are brought into the inner region. Thus, the excess UEs of outer region are brought into the inner region and the FR reduces below $FR.Threshold$. Hence, the UE load in the outer region reduces and the throughput increases. The

Table 9.1: Simulation Parameters

Parameter	Value
Number of Femtocells	6
Number of UEs per Femto	10, 15
UE Deployment	Random
Femto coverage range	70 m
Femto Bandwidth	5 MHz (25 RBs)
Duplexing Mode	FDD
Scheduling Algorithm	PF, VR+PF
Simulated Traffic	Downlink (Video)
Mobility of Mobile UEs	1m/s
Mobility of Static UEs	0.1m/s
Mobility Model	Building Mobility Model
δ	0.5 m
CQI threshold	4
UDP Application Data Rate	4 Mbps

proposed VR algorithm (refer Algorithm 7) will therefore reduces the interference efficiently in a large scale deployment of Femto networks.

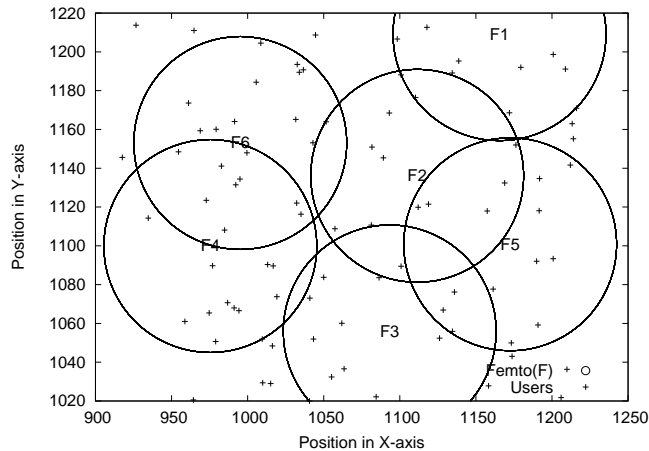


Figure 9.6: Positions of six Femtos and 90 UEs inside a building

9.4 Simulation Setup and Performance Results

In NS-3 simulator six apartment buildings scenario is created and in each apartment one Femto is placed randomly. Figure 9.7 shows the REM plot for the Femto placement. Simulation parameters are given in the Table 9.1. The VR algorithm

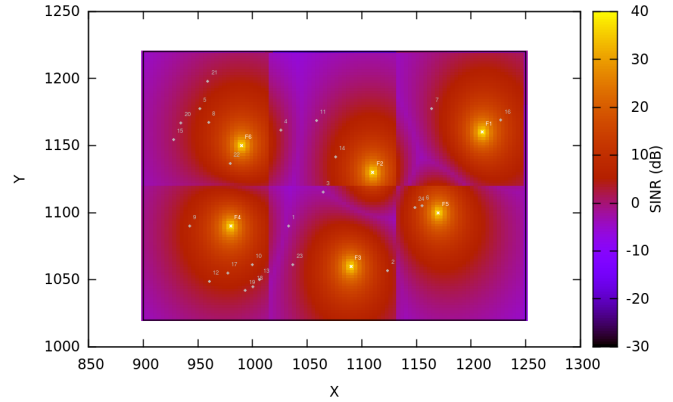


Figure 9.7: REM for Femto Locations

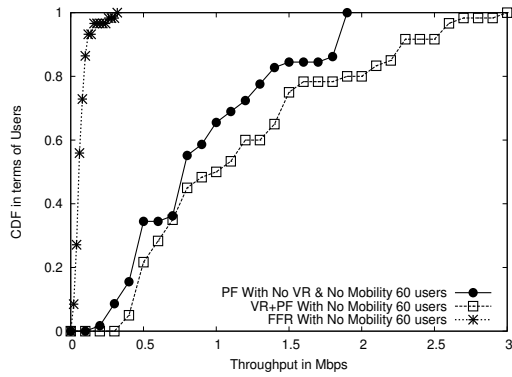


Figure 9.8: CDF of throughput of UEs: Static, 60 UEs

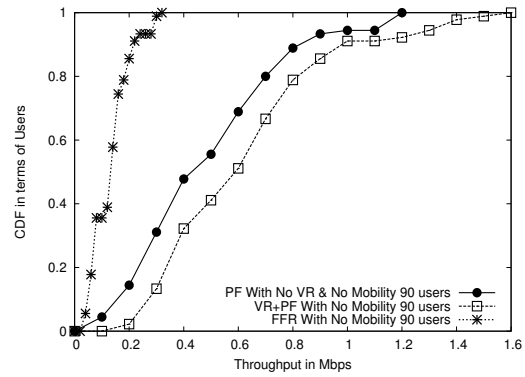


Figure 9.9: CDF of throughput of UEs: Static, 90 UEs

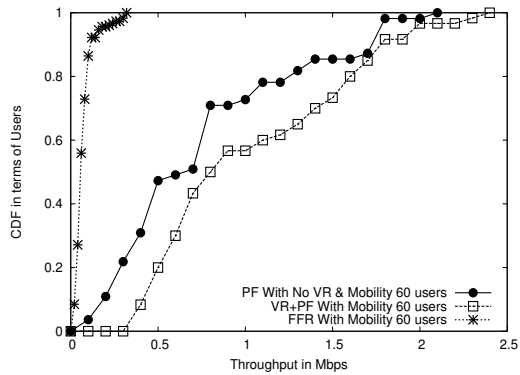


Figure 9.10: CDF of throughput of UEs: Mobile, 60 UEs

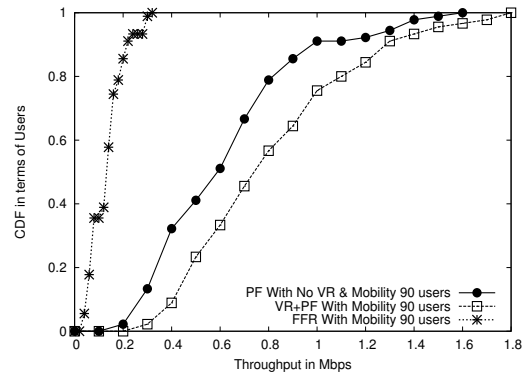


Figure 9.11: CDF of throughput of UEs: Mobile, 90 UEs

is implemented in NS-3 on top of the Proportional Fair (PF) scheduling algorithm to ensure fairness to all the UEs. We modified the building mobility model in NS-3 to introduce limited mobility for indoor UEs. We restrict the users from entering

into the other room, as we are not dealing with handovers in this chapter. In real life, even static users will have some mobility. In order to replicate the same scenario in the simulator, we assigned the mobility rate as 0.1 m/s even for the static users. In our scenario, there is no cross-tier interference hence no Macro considered in these experiments. Each UE has single downlink flow from its connected Femto. The $CQI_Threshold$ is the CQI value used for indoor data traffic handover. It varies between 4 and 6 and it is less than -3 dB in terms of SINR. The $FR_Threshold$ is set as 0.5. The metrics used for performance evaluation are area spectrum efficiency in b/s/hz/m² and system throughput in Mbps. The results shown in this chapter are the averaged values after running simulations for 10 different seed values. Figure 9.6 shows the positions of 90 indoor UEs (6 Femtos and 15 UEs in each Femto).

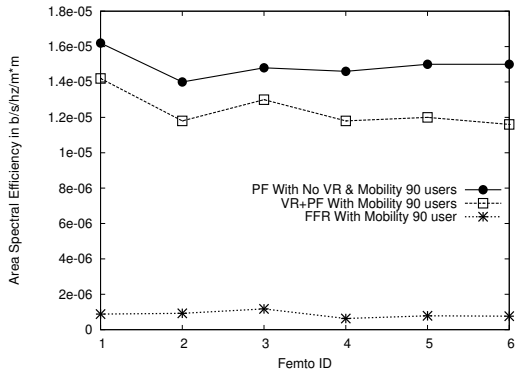


Figure 9.12: Area Spectrum Efficiency of Femtos with 60 static UEs

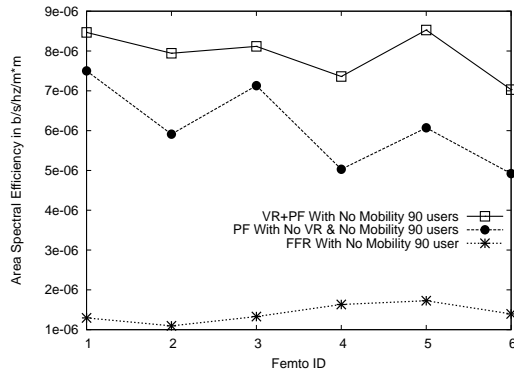


Figure 9.13: Area Spectrum Efficiency of Femtos with 90 static UEs

9.4.1 Throughput Results

In Figures 9.8 and 9.9, average throughput of VR+PF algorithm is compared against classic PF scheduling and FFR for 60 and 90 static UEs (*i.e.*, one flow per UE), respectively. Average throughput of 60 static UEs is increased by 27% when VR algorithm is employed with PF. For 90 static indoor UEs, the average throughput is increased by 29% when VR algorithm is employed with PF. In Figures 9.10 and 9.11, achieved throughput of VR+PF algorithm is compared against PF and FFR for 60 and 90 mobile UEs, respectively. Average throughput of 60 mobile UEs is increased by 37% when VR+PF algorithm is used. For 90 UEs the average throughput is increased by 38% when VR+PF algorithm is used. Since the inner region radius changes dynamically more number of UEs can be served by the inner region and thus

it increases the average throughput. Bisection method makes sure that UEs who are supposed to be in the outer region will come inside the inner region, even though they have interference with neighboring Femtos. It is observed that proposed VR algorithm also performs better in mobile scenarios because of UEs mobility there is enough potential for interference management and load balancing in outer regions and the average CQI values of UEs with high mobility vary at much faster rate when compared to UEs with low mobility.

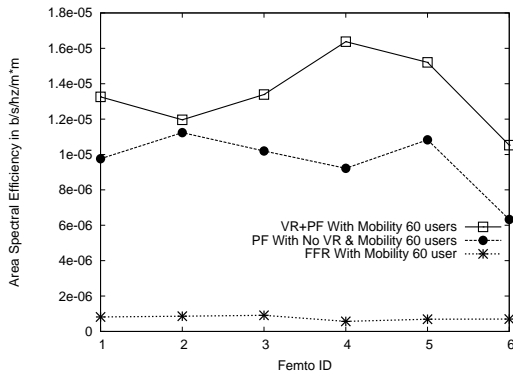


Figure 9.14: Area Spectrum Efficiency of Femtos with 60 mobile UEs

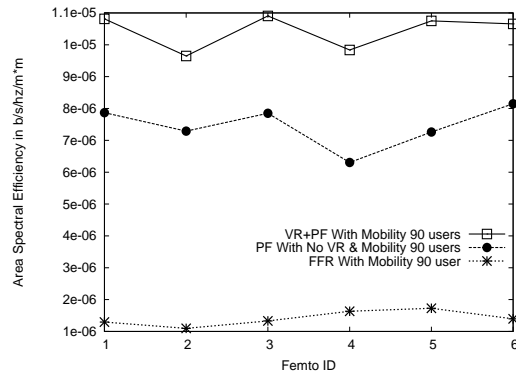


Figure 9.15: Area Spectrum Efficiency of Femtos with 90 mobile UEs

9.4.2 Area Spectrum Efficiency Results

In Figures 9.12 and 9.13, area spectral efficiency of VR+PF, PF and FFR are compared for 60 and 90 static UEs, respectively. In Figures 9.14 and 9.15, area spectral efficiency of VR+PF and PF are compared for 60 and 90 mobile UEs, respectively. In order to be more precise, area spectral efficiency of each of six Femto is plotted separately in the graphs. Area spectral efficiency of Femtos for 60 and 90 static UEs is increased by 20% and 30%, respectively when VR algorithm is employed with PF because the interference is avoided in the outer overlapping regions of Femtos by restricted RB allocation with the help of communication over X2 interface.

9.5 Summary

In this chapter, we proposed an VR algorithm on top of PF scheduler in NS-3 simulator which dynamically increase or decrease the radius of inner regions to avoid co-tier

interference among Femto BSs. Our experiment shows for 90 UEs the proposed technique (VR +PF) achieved 29% and 38% improvement in average throughput for static and mobile scenarios, respectively when compared to classic PF algorithm without any interference management. Also all Femtos need not increase/decrease their inner region radius by same amount at the same time as VR algorithm depends on the user count and overlap with neighboring Femtos.

Chapter 10

Conclusions and Future Work

10.1 Conclusions

Advent of smart phones and applications led to drastic increase in data demand from telecom networks. Small cells could address this challenging but suffers from co-tier and cross-tier interference problem. One of the main solutions to tackle this is optimal placement of Femtos in HetNets. In this thesis, we performed a planned Femto placement with DUD connections based on the shortest path loss Femto for the uplink access and the less loaded neighboring Femtos for the downlink access. We proposed an OptHO placement model to reduce the number of unnecessary handovers in enterprise building environments. To reduce battery drain at UEs a two-step optimization model was formulated which guarantees $USINR_{Th}$ and minimizes the total uplink transmit power. We developed an efficient Femto placement and power control algorithm which dynamically adjusts the transmit power levels at Femtos in order to reduce the *HIZone* interference to *HIZUEs*. We showed that D2D communication when adopted to LTE HetNets increases the spectrum efficiency by guaranteeing good $SINR_{Th}$ for all the users in LTE HetNet even when the Femtos are transmitting at their peak power. We also addressed various challenges involved in deployment and operation of HAFs in indoor environments by proposing an OPF model, a dynamic BWA scheme for splitting radio resources between SG and NSG users, a dynamic *power control* mechanism to mitigate co-tier and cross-tier interference in HetNets and an *EP* scheduling mechanism. Finally, to reduce co-tier interference in dense HetNet scenarios, we proposed a VR algorithm which dynamically increases or decreases the radius of inner regions of Femtos.

10.2 Future Research Directions

In the following, we enumerate some potential topics for further study:

- In our current system model we have not incorporated scheduling algorithm for *IUEs* and *HIZUEs*. In order to analyze the fairness for both *IUEs* and *HIZUEs*, we plan to design a centralized scheduling algorithm for *D2D based relay* in LTE HetNet system.
- Optimization of the *HIZone* are based on the upcoming D2D standards (*i.e.*, maximum D2D link distance and transmit power) is also a future task.
- We would like to study Dual-strip model of 3GPP [143] the effects on the *HIZone* users by introducing another building very close to the first. As the *HIZone* between the two closely placed buildings will be prone to high interference both co-tier and cross-tier and the optimal placement of the HAFs in the buildings will be independent of each other, the power control will become more complex. The SOPC mechanism proposed in chapter 7 dynamically adjusts power in every time interval. This may lead to ping-pong effects. We would like to subject our SOPC mechanism to extra constraints so that the handover is minimum and there is proper load balancing within the building.
- The proposed VR algorithm can be further extend to determine the optimal value of FR. We also have to define a function to vary δ based on UE density.
- In Full Duplex (FD) communications, a BS is capable of transmitting (in the DL to users) and receiving (in the UL from users) signals at the same time on the same channel. Theoretically the FD communication is capable of reducing the spectrum demand by half when the BSs perform FD operation in each transmission time interval (TTI) in LTE/LTE-A. Hence, optimal power control and scheduling in full-duplex small cell networks is an important problem. In our work, we plan to design a efficient user selection and power control algorithm which in turn boost the system capacity.
- Adapting the eICIC mechanism in LTE HetNets, wherein instead of muting the whole sub-frame of an LTE frame we sub-mute it (*i.e.*, Femto transmits in the sub-frame with very minimal power). To boost the capacity of HetNet system, we plan to establish D2D communication links during these sub-muted intervals.

List of Publications

Published Journal Papers

1. V. Sathya, V. Venkatesh, R. Ramji, A. Ramamurthy, and B. R. Tamma, "Handover and SINR optimized deployment of LTE femtocells in enterprise environments", *Springer Wireless Personal Communications*, vol. 88, pp. 619-643, June 2016.

2. V. Sathya, A. Ramamurthy, S. Kumar, and B. R. Tamma, "On improving SINR in LTE HetNets with D2D relays", *Elsevier Computer Communications*, vol. 83, pp. 27-44, June 2016.

3. V. Sathya, A. Ramamurthy, M. Tahalani, and B. R. Tamma, "On femto placement and decoupled access for downlink and uplink in enterprise environments", *EAI Endorsed Transactions on Ubiquitous Environments*, November 2015.

Published Conference Papers

1. A. Ramamurthy, V. Sathya, V. Venkatesh, R. Ramji, and B. R. Tamma, "Energy-efficient Femtocell Placement in LTE Networks", in *Proc. of IEEE CONECCT*, July 2015, Bangalore, India.

2. V. Sathya, A. Ramamurthy, and B. R. Tamma, "Joint placement and power control of LTE Femto base stations in enterprise environments", in *Proc. of IEEE ICNC*, pp. 1029–1033, February 2015, Anaheim, California, USA.

3. V. Sathya, A. Ramamurthy, and B. R. Tamma, "On placement and dynamic power control of Femtocells in LTE HetNets", in *Proc. of IEEE GLOBECOM*, pp. 4394–4399, December 2014, Texas, Austin, USA.

4. M. Tahalani, V. Sathya, A. Ramamurthy, U. Suhas, M. K. Giluka, and B. R. Tamma, "Optimal placement of Femto base stations in enterprise Femtocell networks", in *Proc. of IEEE ANTS*, December 2014, New Delhi, India.

5. R. Chaganti, V. Sathya, S. Ahammed, R. Rex, and B. R. Tamma, "Efficient SON handover scheme for enterprise Femtocell networks", in *Proc. of IEEE ANTS*,

December 2013, Bangalore, India.

6. V. Sathya, H. V. Gudivada, H. Narayanam, B. M. Krishna, and B. R. Tamma, "Enhanced distributed resource allocation and interference management in LTE Femtocell networks", in *Proc. of IEEE WiMob*, pp. 553–558, October 2013, Lyon, France.

Paper Under Review

1. V. Sathya, S. Gosh, A. Ramamurthy, and B. R. Tamma, "A novel resource allocation and power control mechanism for hybrid access femtocells", *submitted to IEEE Transactions on Vehicular Technology*, May 2016.

Publications (Other supporting work)

1. V. Sathya, Anil Kumar, A. Ramamurthy, and B. R. Tamma, "Maximizing dual cell connectivity opportunities in LTE smallcell deployment", in *Proc. of NCC*, March 2016, Guwahati, Assam, India.

2. H. Lokhandwala, V. Sathya, and B. R. Tamma, "Phantom Cell Architecture for LTE and its Application in Vehicular IoT Environments", *EAI Endorsed Transactions on Future Internet*, July 2015.

3. H. Lokhandwala, V. Sathya, and B. R. Tamma, "Phantom cell realization in LTE and its performance analysis", in *Proc. of IEEE ANTS*, December 2014, New Delhi, India.

4. M. Tahalani, V. Sathya, U. Suhas, R. Chaganti, and B. R. Tamma, "Optimal femto placement in enterprise building", in *Proc. of IEEE ANTS*, December 2013, Bangalore, India.

References

- [1] R. Prasad and T. Ojanperä, “A survey on CDMA: evolution towards wideband cdma”, in *Proc. of IEEE 5th International Symposium on Spread Spectrum Techniques and Applications*, vol. 1, pp. 323–331, 1998.
- [2] T. Hwang, C. Yang, G. Wu, S. Li, and G. Y. Li, “OFDM and its wireless applications: a survey”, *IEEE Transactions on Vehicular Technology*, vol. 58, no. 4, pp. 1673–1694, 2009.
- [3] H. Bölcskei, “MIMO-OFDM wireless systems: basics, perspectives, and challenges”, *IEEE Wireless Communications*, vol. 13, no. 4, pp. 31–37, 2006.
- [4] E. Dahlman, S. Parkvall, and J. Skold, *4G: LTE/LTE-advanced for mobile broadband*, Academic press, 2013.
- [5] Z. Shen, A. Papasakellariou, J. Montojo, D. Gerstenberger, and F. Xu, “Overview of 3gpp LTE-advanced carrier aggregation for 4G wireless communications”, *IEEE Communications Magazine*, vol. 50, no. 2, pp. 122–130, 2012.
- [6] D. Lee, H. Seo, B. Clerckx, E. Hardouin, D. Mazzaresse, S. Nagata, and K. Sayana, “Coordinated multipoint transmission and reception in LTE-advanced: deployment scenarios and operational challenges”, *IEEE Communications Magazine*, vol. 50, no. 2, pp. 148–155, 2012.
- [7] M. Sawahashi, Y. Kishiyama, A. Morimoto, D. Nishikawa, and M. Tanno, “Coordinated multipoint transmission/reception techniques for LTE-advanced coordinated and distributed MIMO”, *IEEE Wireless Communications*, vol. 17, no. 3, pp. 26–34, 2010.
- [8] A. Asadi, Q. Wang, and V. Mancuso, “A survey on device-to-device communication in cellular networks”, *IEEE Communications Surveys & Tutorials*, vol. 16, no. 4, pp. 1801–1819, 2014.

- [9] A. Zakrzewska, D. López-Pérez, S. Kucera, and H. Claussen, “Dual connectivity in LTE HetNets with split control-and user-plane”, in *Proc. of IEEE Globecom Workshops*, pp. 391–396, 2013.
- [10] G. I. Naik, “LTE WLAN interworking for wi-fi hotspots”, in *Proc. of 2nd international conference on Communication systems and NETWORKS*, pp. 462–463, Press, 2010.
- [11] L. Atzori, A. Iera, and G. Morabito, “The Internet of things: A survey”, *Computer networks*, vol. 54, no. 15, pp. 2787–2805, 2010.
- [12] H. Kim, K. Kim, Y. Han, and S. Yun, “A proportional fair scheduling for multicarrier transmission systems”, in *Proc. of IEEE VTC2004-Fall*, vol. 1, pp. 409–413, 2004.
- [13] “CISCO” http://www.cisco.com/c/en/us/solutions/collateral/service-provider/visual-networking-index-vni/white_paper_c11-520862.html.
- [14] “White Paper-Enterprise multi-femtocell deployment guidelines”, Qualcomm Inc., 2011.
- [15] Y. Wang, Y. Chang, and D. Yang, “An efficient inter-cell interference coordination scheme in heterogeneous cellular networks”, in *Proc. of IEEE VTC Fall*, 2012.
- [16] X. Zhang, C. He, L. Jiang, and J. Xu, “Inter-cell interference coordination based on softer frequency reuse in OFDMA cellular systems”, in *Proc. of IEEE International Conference on Neural Networks and Signal Processing*, pp. 270–275, 2008.
- [17] Z. Bakhti and S. S. Moghaddam, “Inter-cell interference coordination with adaptive frequency-reuse for VOIP and data traffic in downlink of 3GPP-LTE”, in *Proc. of IEEE AICT*, 2010.
- [18] X. Mao, A. Maaref, and K. H. Teo, “Adaptive soft frequency reuse for inter-cell interference coordination in SC-FDMA based 3GPP LTE uplinks”, in *Proc. of IEEE GLOBECOM*, 2008.
- [19] K. Koutlia, J. Perez-Romero, and R. Agustí, “On enhancing almost blank subframes management for efficient eICIC in HetNets”, in *Proc. of IEEE VTC Spring*, 2015.

- [20] J. Wang, L. Liu, K. Takeda, and H. Jiang, “Time domain inter-cell interference coordination for dense small cell deployments”, in *Proc. of IEEE VTC Fall*, 2014.
- [21] A. Lobinger, S. Stefanski, T. Jansen, and I. Balan, “Coordinating handover parameter optimization and load balancing in LTE self-optimizing networks”, in *Proc. of IEEE VTC Spring*, 2011.
- [22] I. Siomina and D. Yuan, “Load balancing in heterogeneous LTE: Range optimization via cell offset and load-coupling characterization”, in *Proc. of IEEE ICC*, pp. 1357–1361, 2012.
- [23] F. Boccardi, J. Andrews, H. Elshaer, M. Dohler, S. Parkvall, P. Popovski, and S. Singh, “Why to decouple the uplink and downlink in cellular networks and how to do it”, *arXiv preprint arXiv:1503.06746*, 2015.
- [24] K. Smiljkovikj, P. Popovski, and L. Gavrilovska, “Analysis of the decoupled access for downlink and uplink in wireless heterogeneous networks”, *Wireless Communications Letters*, vol. 4, no. 2, pp. 173–176, 2015.
- [25] G. Gódor, Z. Jakó, Á. Knapp, and S. Imre, “A survey of handover management in LTE-based multi-tier femtocell networks: Requirements, challenges and solutions”, *Computer Networks*, vol. 76, pp. 17–41, 2015.
- [26] D. Xenakis, N. Passas, L. Merakos, and C. Verikoukis, “Mobility management for femtocells in LTE-advanced: key aspects and survey of handover decision algorithms”, *IEEE Communications Surveys & Tutorials*, vol. 16, no. 1, pp. 64–91, 2014.
- [27] “White Paper-3gpp femtocells: Architecture and protocols”, *Qualcomm Inc.*, Sept. 2010.
- [28] Z. Shen, A. Khoryaev, E. Eriksson, and X. Pan, “Dynamic uplink-downlink configuration and interference management in TD-LTE”, *IEEE Communications Magazine*, vol. 50, no. 11, pp. 51–59, 2012.
- [29] T. Nakamura, S. Nagata, A. Benjebbour, Y. Kishiyama, T. Hai, S. Xiaodong, Y. Ning, and L. Nan, “Trends in small cell enhancements in LTE advanced”, *IEEE Communications Magazine*, vol. 51, no. 2, pp. 98–105, 2013.

- [30] H. Wang, L. Ding, P. Wu, Z. Pan, N. Liu, and X. You, “Dynamic load balancing in 3gpp LTE multi-cell networks with heterogenous services”, in *Proc. of 5th International ICST Conference on CHINACOM*, 2010.
- [31] H. Wang, L. Ding, P. Wu, Z. Pan, N. Liu, and X. You, “QOS-aware load balancing in 3GPP long term evolution multi-cell networks”, in *Proc. of IEEE ICC*, 2011.
- [32] J. Liu, Q. Chen, and H. D. Sherali, “Algorithm design for femtocell base station placement in commercial building environments,” in *Proc. of IEEE INFOCOM*, pp. 2951–2955, 2012.
- [33] “GAMS”, <http://www.gams.com/>.
- [34] W. Guo, S. Wang, X. Chu, J. Zhang, J. Chen, and H. Song, “Automated small-cell deployment for heterogeneous cellular networks”, *IEEE Communications Magazine*, vol. 51, no. 5, pp. 46–53, 2013.
- [35] W. Guo and S. Wang, “Interference-aware self-deploying femto-cell”, *IEEE Wireless Communications Letters*, vol. 1, no. 6, pp. 609–612, 2012.
- [36] R. Liu, I. J. Wassell, and K. Soga, “Relay node placement for wireless sensor networks deployed in tunnels”, in *Proc. of IEEE WiMob*, pp. 144–150, 2010.
- [37] S. S. Dhillon, K. Chakrabarty, and S. Iyengar, “Sensor placement for grid coverage under imprecise detections”, in *Proc. of Fifth International Conference on Information Fusion*, vol. 2, pp. 1581–1587, 2002.
- [38] A. Capone, M. Cesana, D. De Donno, and I. Filippini, “Optimal placement of multiple interconnected gateways in heterogeneous wireless sensor networks”, in *NETWORKING 2009 (Springer)*, pp. 442–455, 2009.
- [39] J. Zhang, X. Jia, Z. Zheng, and Y. Zhou, “Minimizing cost of placement of multi-radio and multi-power-level access points with rate adaptation in indoor environment”, *IEEE Transactions on Wireless Communications*, vol. 10, no. 7, pp. 2186–2195, 2011.
- [40] J. Liu, T. Kou, Q. Chen, and H. D. Sherali, “Femtocell base station deployment in commercial buildings: A global optimization approach”, *IEEE Journal on Selected Areas in Communications*, vol. 30, no. 3, pp. 652–663, 2012.

- [41] V. Sathya, A. Ramamurthy, and B. R. Tamma, “On placement and dynamic power control of femtocells in LTE HetNets”, in *Proc. of IEEE GLOBECOM*, pp. 4394–4399, 2014.
- [42] Z. Li, H. Wang, Z. Pan, N. Liu, and X. You, “Joint optimization on load balancing and network load in 3gpp LTE multi-cell networks”, in *Proc. of WCSP Conference*, 2011.
- [43] H. Elshaer, F. Boccardi, M. Dohler, and R. Irmer, “Downlink and uplink decoupling: a disruptive architectural design for 5G networks”, *arXiv preprint arXiv:1405.1853*, 2014.
- [44] J. Liu, J. Liu, and H. Sun, “An enhanced power control scheme for dual connectivity”, in *Proc. of IEEE VTC Fall*, 2014.
- [45] A. Hooshmand, A. Nallanathan, and H. Aghvami, “Joint inter-cell interference coordination and forced cooperative scheduling for the downlink of LTE systems”, in *Proc. of IEEE WCNC*, pp. 1880–1884, 2014.
- [46] M. Chiang, “Non-convex optimization of communication systems”, in *Proc. of Advances in Mechanics and Mathematics*, vol. 3, pp. 137–196, 2008.
- [47] T. Yang, J. P. Ignizio, and H.-J. Kim, “Fuzzy programming with nonlinear membership functions: piecewise linear approximation”, in *Proc. of Fuzzy sets and systems*, vol. 41, no. 1, pp. 39–53, 1991.
- [48] M. T. Kawser, N. I. B. Hamid, M. N. Hasan, M. S. Alam, and M. M. Rahman, “Downlink SINR to CQI mapping for different multiple antenna techniques in lte”, *International Journal of Information and Electronics Engineering*, vol. 2, no. 5, 2012.
- [49] H.-D. Bae, B. Ryu, and N.-H. Park, “Analysis of handover failures in lte femtocell systems”, in *Proc. of IEEE ATNAC, 2011*, 2011.
- [50] H. Zhang, W. Ma, W. Li, W. Zheng, X. Wen, and C. Jiang, “Signaling cost evaluation of handover management schemes in lte-advanced femtocell”, in *Proc. of IEEE VTC Spring*, 2011.
- [51] A. Ulvan, R. Bestak, and M. Ulvan, “Handover scenario and procedure in LTE-based femtocell networks”, in *Proc. of UBICOMM*, pp. 213–218, 2010.

- [52] M. Tahalani, V. Sathya, A. Ramamurthy, U. Suhas, M. K. Giluka, and B. R. Tamma, “Optimal placement of femto base stations in enterprise femtocell networks”, in *Proc. of IEEE ANTS*, 2014.
- [53] Y. Lin, W. Yu, and Y. Lostanlen, “Optimization of wireless access point placement in realistic urban heterogeneous networks”, in *Proc. of IEEE GLOBECOM*, pp. 4963–4968, 2012.
- [54] K. Han, Y. Choi, D. Kim, M. Na, S. Choi, and K. Han, “Optimization of femtocell network configuration under interference constraints”, in *Proc. of IEEE WiOPT*, 2009.
- [55] V. Sathya, A. Ramamurthy, and B. Tamma, “Joint placement and power control of LTE femto base stations in enterprise environments”, in *Proc. of IEEE ICNC*, pp. 1029–1033, 2015.
- [56] R. Chaganti, V. Sathya, S. A. Ahammed, R. Rex, and B. R. Tamma, “Efficient SON handover scheme for enterprise femtocell networks”, in *Proc. of IEEE ANTS*, 2013.
- [57] L. Wang, Y. Zhang, and Z. Wei, “Mobility management schemes at radio network layer for LTE femtocells”, in *Proc. of IEEE VTC Spring*, 2009.
- [58] H. Zhang, X. Wen, B. Wang, W. Zheng, and Y. Sun, “A novel handover mechanism between femtocell and macrocell for LTE based networks”, in *Proc. of ICCSN’10*, pp. 228–231, 2010.
- [59] Z. Becvar and P. Mach, “Adaptive hysteresis margin for handover in femtocell networks”, in *Proc. of ICWMC*, pp. 256–261, 2010.
- [60] P. Munoz, R. Barco, and I. de la Bandera, “On the potential of handover parameter optimization for self-organizing networks”, *IEEE Transactions on Vehicular Technology*, vol. 62, no. 5, pp. 1895–1905, 2013.
- [61] A. Awada, B. Wegmann, I. Viering, and A. Klein, “A SON-based algorithm for the optimization of inter RAT handover parameters”, *IEEE Transactions on Vehicular Technology*, , vol. 62, no. 5, pp. 1906–1923, 2013.
- [62] D. Xenakis, N. Passas, L. Merakos, and C. Verikoukis, “Energy-efficient and interference-aware handover decision for the LTE-advanced femtocell network”, in *Proc. of IEEE ICC*, pp. 2464–2468, 2013.

- [63] T. Kanungo, D. M. Mount, N. S. Netanyahu, C. D. Piatko, R. Silverman, and A. Y. Wu, “An efficient k-means clustering algorithm: Analysis and implementation”, *IEEE Transactions on Pattern Analysis and Machine Intelligence*, vol. 24, no. 7, pp. 881–892, 2002.
- [64] “3GPP Releases”, <http://www.3gpp.org/releases>.
- [65] B. Tastan and G. Sukthankar, “Leveraging human behavior models to predict paths in indoor environments”, *Pervasive and Mobile Computing*, vol. 7, no. 3, pp. 319–330, 2011.
- [66] “3GPP, ”3GPP: LTE;E-UTRA; UE radio transmission and reception”, *3GPP, Tech.Rep. TR 25.101*, 2015.
- [67] I. E. Ahmed, B. R. Qazi, and J. M. Elmighani, “Base stations locations optimization in an airport environment using genetic algorithms”, in *Proc. of IWCMC*, pp. 24–29, 2012.
- [68] A. Bousia, E. Kartsakli, L. Alonso, and C. Verikoukis, “Energy efficient base station maximization switch off scheme for LTE-advanced”, in *Proc. of International Workshop on CAMAD*, pp. 256–260, 2012.
- [69] G. Piro, M. Miozzo, G. Forte, N. Baldo, L. A. Grieco, G. Boggia, and P. Dini, “HetNets powered by renewable energy sources: Sustainable next-generation cellular networks”, *Internet Computing*, vol. 17, no. 1, pp. 32–39, 2013.
- [70] Z. Niu, Y. Wu, J. Gong, and Z. Yang, “Cell zooming for cost-efficient green cellular networks”, *IEEE Communications Magazine*, vol. 48, no. 11, pp. 74–79, 2010.
- [71] Y. Wang and S. Venkatraman, “Uplink power control in LTE heterogeneous networks”, in *Proc. of Globecom Workshop*, pp. 592–597, 2012.
- [72] N. Karmarkar, “A new polynomial-time algorithm for linear programming”, in *Proc. of the sixteenth annual ACM symposium on theory of computing*, pp. 302–311, 1984.
- [73] H. Ishii, Y. Kishiyama, and H. Takahashi, “A novel architecture for LTE-B: C-plane/U-plane split and phantom cell concept”, in *Proc. of Globecom Workshop*, pp. 624–630, 2012.

- [74] H. Lokhandwala, V. Sathya, and B. R. Tamma, “Phantom cell realization in LTE and its performance analysis”, in *Proc. of IEEE ANTS*, 2014.
- [75] L. Wei, R. Q. Hu, Y. Qian, and G. Wu, “Enable device-to-device communications underlying cellular networks: challenges and research aspects”, *IEEE Communications Magazine*, vol. 52, no. 6, pp. 90–96, 2014.
- [76] P. Phunchongharn, E. Hossain, and D. I. Kim, “Resource allocation for device-to-device communications underlying LTE-advanced networks”, *IEEE Wireless Communications*, vol. 20, no. 4, 2013.
- [77] L. Lei, Z. Zhong, C. Lin, and X. Shen, “Operator controlled device-to-device communications in LTE-advanced networks”, *IEEE Wireless Communications*, vol. 19, no. 3, 2012.
- [78] B. Raghothaman, E. Deng, R. Pragada, G. Sternberg, T. Deng, and K. Vanganuru, “Architecture and protocols for LTE-based device to device communication”, in *Proc. of ICNC*, pp. 895–899, 2013.
- [79] M. Zulhasnine, C. Huang, and A. Srinivasan, “Efficient resource allocation for device-to-device communication underlying LTE network”, in *Proc. of IEEE WiMob*, pp. 368–375, 2010.
- [80] F. Malandrino, C. Casetti, C.-F. Chiasserini, and Z. Limani, “Fast resource scheduling in HetNets with d2d support”, *arXiv preprint arXiv:1311.6837*, 2013.
- [81] H. Ishii, X. Cheng, S. Mukherjee, and B. Yu, “An LTE offload solution using small cells with d2d links”, in *Proc. of IEEE ICC*, pp. 1155–1160, 2013.
- [82] T. Bansal, K. Sundaresan, S. Rangarajan, and P. Sinha, “R2d2: Embracing device-to-device communication in next generation cellular networks”, in *Proc. of IEEE INFOCOM*, vol. 50, no. 3, pp. 3–9, 2014.
- [83] k. E. sambo, sahir and Muhammad, “Expanding cellular coverage via cell-edge deployment in heterogeneous networks: spectral efficiency and backhaul power consumption perspectives”, *IEEE Communications Magazine*, vol. 52, no. 6, pp. 140–149, 2014.
- [84] C. Gao, X. Sheng, J. Tang, W. Zhang, S. Zou, and M. Guizani, “Joint mode selection, channel allocation and power assignment for green device-to-device communications”, in *Proc. of IEEE ICC*, pp. 178–183, 2014.

- [85] H. Nishiyama, M. Ito, and N. Kato, “Relay-by-smartphone: realizing multihop device-to-device communications”, *IEEE Communications Magazine*, vol. 52, no. 4, pp. 56–65, 2014.
- [86] M. Alam, D. Yang, J. Rodriguez, and R. Abd-Alhameed, “Secure device-to-device communication in LTE-A”, *IEEE Communications Magazine*, vol. 52, no. 4, pp. 66–73, 2014.
- [87] N. Bhushan, J. Li, D. Malladi, R. Gilmore, D. Brenner, A. Damnjanovic, R. Sukhavasi, C. Patel, and S. Geirhofer, “Network densification: the dominant theme for wireless evolution into 5G”, *IEEE Communications Magazine*, vol. 52, no. 2, pp. 82–89, 2014.
- [88] A. Orsino, L. Militano, G. Araniti, A. Molinaro, and A. Iera, “Efficient data uploading supported by D2D communications in LTE-A systems”, *arXiv preprint arXiv:1503.09076*, 2015.
- [89] G. Rigazzi, F. Chiti, R. Fantacci, and C. Carlini, “Multi-hop D2D networking and resource management scheme for M2M communications over LTE-A systems”, in *Proc. of IEEE IWCMC*, pp. 973–978, 2014.
- [90] J. M. B. da Silva, G. Fodor, and T. F. Maciel, “Performance analysis of network-assisted two-hop D2D communications”, in *Proc. of IEEE Globecom Workshop*, pp. 1050–1056, IEEE, 2014.
- [91] S. Doumiati, H. Artail, and D. M. Gutierrez-Estevez, “A framework for LTE-A proximity-based device-to-device service registration and discovery”, in *Proc of Computer Science*, vol. 34, pp. 87–94, 2014.
- [92] G. Fodor, E. Dahlman, G. Mildh, S. Parkvall, N. Reider, G. Miklós, and Z. Turányi, “Design aspects of network assisted device-to-device communications”, *IEEE Communications Magazine*, vol. 50, no. 3, pp. 170–177, 2012.
- [93] “Sounding Reference Signal”, http://www.sharetechnote.com/html/Handbook_LTE_SRS.html.
- [94] K. Lee, W. Kang, and H.-J. Choi, “A practical channel estimation and feedback method for device-to-device communication in 3GPP LTE system”, in *Proc. of ACM 8th International Conference on Ubiquitous Information Management and Communication*, 2014.

- [95] J. Jang, H. Cho, Y. Kwon, and H. Lee, “Communication method between terminals, and terminal”, *EP Patent App*, Jan. 30 2013.
- [96] M. J. Yang, S. Y. Lim, H. J. Park, and N. H. Park, “Solving the data overload: Device-to-device bearer control architecture for cellular data offloading”, *IEEE Vehicular Technology Magazine*, vol. 8, no. 1, pp. 31–39, 2013.
- [97] “3GPP, ”3GPP TSGSA: Feasibility Study for Proximity Services (ProSe) (Release 12)”, *3GPP, Tech.Rep. TR 22.803*, Aug 2013.
- [98] X. Lin, J. G. Andrews, A. Ghosh, and R. Ratasuk, “An overview of 3GPP device-to-device proximity services”, *IEEE Communications Magazine*, vol. 52, no. 4, pp. 40–48, 2014.
- [99] “White Paper- radisys: SCTP Fast Path Optimization for 3G/LTE Networks.”
- [100] “White Paper-Continuous Computing: Trillium Femtocell Gateway.”
- [101] F. Capozzi, G. Piro, L. A. Grieco, G. Boggia, and P. Camarda, “Downlink packet scheduling in LTE cellular networks: Key design issues and a survey”, *IEEE Communications Surveys & Tutorials*, vol. 15, no. 2, pp. 678–700, 2013.
- [102] T. D. Hoang, L. B. Le, and T. Le-Ngoc, “Resource allocation for d2d communications under proportional fairness”, in *Proc. of IEEE GLOBECOM*, pp. 1259–1264, 2014.
- [103] R. L. Batista, J. M. B. da Silva, T. F. Maciel, F. R. P. Cavalcanti, *et al.*, “What happens with a proportional fair cellular scheduling when D2D communications underlay a cellular network”, in *Proc. of IEEE WCNC*, pp. 260–265, 2014.
- [104] F. Malandrino, C. Casetti, C.-F. Chiasserini, and Z. Limani, “Fast resource scheduling in hetnets with D2D support,” in *Proc. of IEEE INFOCOM*, pp. 1536–1544, 2014.
- [105] Q. Wang, M. Hempstead, and W. Yang, “A realistic power consumption model for wireless sensor network devices”, in *Proc. of IEEE SECON*, vol. 1, pp. 286–295, 2006.
- [106] J. G. Andrews, H. Claussen, M. Dohler, S. Rangan, and M. C. Reed, “Femto-cells: Past, present, and future”, *IEEE Journal on Selected Areas in Communications*, vol. 30, no. 3, pp. 497–508, 2012.

- [107] H.-S. Jo, P. Xia, and J. G. Andrews, “Open, closed, and shared access femtocells in the downlink”, *EURASIP Journal on Wireless Communications and Networking*, vol. 2012, no. 1, 2012.
- [108] G. De La Roche, A. Valcarce, D. López-Pérez, and J. Zhang, “Access control mechanisms for femtocells”, *IEEE Communications Magazine*, vol. 48, no. 1, pp. 33–39, 2010.
- [109] B. Niu and V. W. Wong, “The design of resource management mechanism with hybrid access in a macro-femto system”, in *Proc. of IEEE Globecom Workshops*, pp. 4679–4685, 2013.
- [110] N. Zhang, N. Cheng, A. T. Gamage, K. Zhang, J. Mark, and X. Shen, “Cloud assisted hetnets toward 5G wireless networks”, *IEEE Communication Magazine*, vol. 53, no. 6, pp. 59-65, 2015.
- [111] V. Sathya, A. Ramamurthy, and B. R. Tamma, “On placement and dynamic power control of femtocells in LTE HetNets”, in *Proc. of IEEE GLOBECOM*, pp. 4394–4399, 2014.
- [112] L. T. Ho and H. Claussen, “Effects of user-deployed, co-channel femtocells on the call drop probability in a residential scenario”, in *Proc. of IEEE PIMRC*, 2007.
- [113] J. Espino and J. Markendahl, “Analysis of macrofemtocell interference and implications for spectrum allocation”, in *Proc. of IEEE PIMRC*, pp. 2208–2212, 2009.
- [114] S. A. Saad, M. Ismail, and R. Nordin, “A survey on power control techniques in femtocell networks”, *Journal of Communications*, vol. 8, no. 12, pp. 845-854, 2013
- [115] Y. Bai and L. Chen, “Hybrid spectrum arrangement and interference mitigation for coexistence between LTE macrocellular and femtocell networks”, *EURASIP Journal on Wireless Communications and Networking*, vol. 2013, no. 1, 2013.
- [116] X. Chu, Y. Wu, L. Benmesbah, and W.-K. Ling, “Resource allocation in hybrid macro/femto networks”, in *Proc. of IEEE WCNC*, 2010.
- [117] D. Feng, L. Lu, Y. Yuan-Wu, G. Y. Li, G. Feng, and S. Li, “Device-to-device communications underlying cellular networks”, *IEEE Transactions on Communications*, vol. 61, no. 8, pp. 3541–3551, 2013.

- [118] G. Yu, L. Xu, D. Feng, R. Yin, G. Y. Li, and Y. Jiang, “Joint mode selection and resource allocation for device-to-device communications”, *IEEE Transactions on Communications*, vol. 62, no. 11, pp. 3814–3824, 2014.
- [119] D. Feng, G. Yu, Y. Yuan-Wu, G. Y. Li, G. Feng, and S. Li, “Mode switching for device-to-device communications in cellular networks”, *in Proc. of IEEE GlobalSIP*, pp. 1291–1295, 2014.
- [120] T. S. Rappaport, S. Sun, R. Mayzus, H. Zhao, Y. Azar, K. Wang, G. N. Wong, J. K. Schulz, M. Samimi, and F. Gutierrez, “Millimeter wave mobile communications for 5G cellular: It will work!”, *IEEE Access*, vol. 1, pp. 335–349, 2013.
- [121] R. J. Weiler, M. Peter, W. Keusgen, E. Strinati, A. Domenico, I. Filippini, A. Capone, I. Siaud, A. Ulmer-Moll, A. Maltsev, *et al.*, “Enabling 5G backhaul and access with millimeter-waves”, *in Proc. of EuCNC*, 2014.
- [122] Y. Shih, A. Pang, M. Tsai, and C. Chai, “A rewarding framework for network resource sharing in co-channel hybrid access femtocell networks”, *IEEE Transactions on Computers*, vol. 64, no. 11, pp. 3079–3090, 2015.
- [123] Y. Yi, J. Zhang, Q. Zhang, and T. Jiang, “Spectrum leasing to femto service provider with hybrid access”, *in Proc. of IEEE INFOCOM*, pp. 1215–1223, 2012.
- [124] Y. Chen, J. Zhang, Q. Zhang, and J. Jia, “A reverse auction framework for access permission transaction to promote hybrid access in femtocell network”, *in Proc. of IEEE INFOCOM*, pp. 2761–2765, 2012.
- [125] R. Kurda, L. Boukhatem, and M. Kaneko, “Femtocell power control methods based on users context information in two-tier heterogeneous networks”, *EURASIP Journal on Wireless Communications and Networking*, vol. 2015, no. 1, 2015.
- [126] S. Fischer, “Observed time difference of arrival (otdoa) positioning in 3GPP lte”, *Tech. rep.*, 2014.
- [127] C. Gentner, E. Muñoz, M. Khider, E. Staudinger, S. Sand, and A. Dammann, “Particle filter based positioning with 3GPP-LTE in indoor environments”, *in Proc. of IEEE PLANS*, pp. 301–308, 2012.

- [128] I. Sharp and K. Yu, “Enhanced least-squares positioning algorithm for indoor positioning”, *IEEE Transactions on Mobile Computing*, vol. 12, no. 8, pp. 1640–1650, 2013.
- [129] J. M. R. Avilés, S. Luna-Ramirez, M. Toril, F. Ruiz, I. De la Bandera-Cascales, and P. Munoz-Luengo, “Analysis of load sharing techniques in enterprise LTE femtocells”, in *Proc. of WiAd*, pp. 195–200, 2011.
- [130] Z. Liu, P. Hong, K. Xue, and M. Peng, “Conflict avoidance between mobility robustness optimization and mobility load balancing”, in *Proc. of IEEE GLOBECOM*, 2010.
- [131] R. Jain, D.-M. Chiu, and W. Hawe, “A quantitative measure of fairness and discrimination for resource allocation in shared computer systems”, *Eastern Research Laboratory, Digital Equipment Corporation Hudson*, vol 38, 1984.
- [132] Z. Chen, T. Lin, and D. Din, “Multi-tone almost blank subframes for enhanced inter-cell interference coordination in LTE HetNets”, in *Proc. IEEE ICNC*, pp. 1014–1018, 2015.
- [133] X. Wang, C. Wang, R. Cai, S. Huang, C. Wang, and W. Wang, “Reduced power centralized eICIC for LTE-advanced heterogeneous networks”, in *Proc. of IEEE ICC*, pp. 743–747, 2014.
- [134] 3GPP, “Evolved universal terrestrial radio access (E-UTRA); Physical layer procedures”, *Tech. Rep. TS 36.213*, Feb 2013.
- [135] V. Chandrasekhar and J. Andrews, “Spectrum allocation in tiered cellular networks”, *IEEE Transactions on Communications*, vol. 57, no. 10, pp. 3059–3068, 2009.
- [136] J. Yoon, M. Y. Arslan, K. Sundaresan, S. V. Krishnamurthy, and S. Banerjee, “A distributed resource management framework for interference mitigation in OFDMA femtocell networks”, in *Proc. of ACM MOBIHOC*, pp. 233–242, 2012.
- [137] M. Andrews, V. Capdevielle, A. Feki, and P. Gupta, “Autonomous spectrum sharing for mixed LTE femto and macro cells deployments”, in *Proc. of IEEE INFOCOM*, 2010.
- [138] P. Lee, T. Lee, J. Jeong, and J. Shin, “Interference management in LTE femtocell systems using fractional frequency reuse”, in *Proc. of ICACT*, vol. 2, pp. 1047–1051, 2010.

- [139] Y. Yu, E. Dutkiewicz, X. Huang, M. Mueck, and G. Fang, “Performance analysis of soft frequency reuse for inter-cell interference coordination in LTE networks”, *in Proc. of ISCIT 2010*, pp. 504–509, 2010.
- [140] M. Al-Shalash, F. Khafizov, and Z. Chao, “Interference constrained soft frequency reuse for uplink icic in lte networks”, *in Proc. of IEEE PIMRC*, pp. 1882–1887, 2010.
- [141] J. A. del Peral-Rosado, J. A. López-Salcedo, G. Seco-Granados, F. Zanier, and M. Crisci, “Joint channel and time delay estimation for LTE positioning reference signals”, *in Proc. of NAVITEC*, 2012.
- [142] M. T. Kawser, N. I. B. Hamid, M. N. Hasan, M. S. Alam, and M. M. Rahman, “Downlink SINR to CQI mapping for different multiple antenna techniques in lte”, *in Proc. of ICFIT*, 2010.
- [143] 3GPP, “Technical specification group radio access network (E-UTRA)); Physical layer procedures”, *Tech. Rep. TR 36.814*, 2010.

DOCTORAL COMMITTEE

1. Chairperson: Dr. Bheemarjuna Reddy Tamma

2. Guide: Dr. Bheemarjuna Reddy Tamma

3. Members:

Dr. M. V. Panduranga Rao (Dept. of CSE)

Dr. Subrahmanyam Kalyanasundaram (Dept. of CSE)

Dr. Mohammed Zafar Ali Khan (Dept. of EE)

Dr. Kiran Kumar Kuchi (Dept. of EE)